Universidade do Minho
Escola de Engenharia

Daniela Sofia Dias Ferreira

Molecularly Designed Self-assembling Matrices for Applications in Regenerative Medicine

novembro de 2014

Universidade do Minho
Escola de Engenharia

Daniela Sofia Dias Ferreira

Molecularly Designed Self-assembling Matrices for Applications in Regenerative Medicine

Programa Doutoral em Engenharia de Tecidos, Medicina Regenerativa e Células Estaminais

Trabalho realizado sob a orientação do
Professor Doutor Rui L. Reis
e da
Doutora Helena S. Azevedo

novembro de 2014

STATEMENT OF INTEGRITY

I hereby declare having conducted my thesis with integrity. I confirm that I have not used plagiarism or any form of falsification of results in the process of the thesis elaboration.

I further declare that I have fully acknowledged the Code of Ethical Conduct of the University of Minho.

Universidade do Minho, 14 de Novembro de 2014

Full name: Daniela Sofia Dias Ferreira

Signature:

_____

Aos meus pais

(To my parents)

If you are reading these words, it means that in the end everything went well, and I finally succeeded to have a thesis. The work presented in this thesis results from the combination of dedication, commitment, joy, frustration, enthusiasm, mentoring, and frustration again, happiness, friendship, and it would not be possible without all the people that during these years somehow contributed to its development. As such, I would like to express my deepest gratitude towards them.

First and foremost, I am truly thankful to my supervisor and director of the 3B's Research Group, Professor Rui Reis, for giving me the opportunity to be part of his multidisciplinary and internationally recognized lab; for allowing me to pursue my PhD work in a new field in the group and for providing the necessary research conditions. His accomplishments are an inspiration for any student and an example, that great things can be achieved with hard work and dedication.

I also would like to acknowledge Dr Helena Azevedo for being more than just a mentor throughout the years. This thesis would never been possible without her mentoring, guidance and friendship. Her enthusiasm, strength and dedication motivated me to become a better researcher and always give the best of myself. Her inspiration greatly contributed to who I have become today. Thank you for introducing me to the "peptide synthesis world", for giving me the opportunity to go to Queen Mary University of London (QMUL), for the freedom to explore new ideas, and mostly, for your honesty. For all of that I am deeply grateful.

My gratitude is also extended to Professor Jeffrey Hubbell, for allowing me to work in his lab at École Polytechnique Fédérale de Lausanne. I am profoundly grateful for his guidance and for being a constant source of inspiration. During my year in his research group, I always felt welcome; this experience greatly contributed to improve my research skills and influenced the direction of my research.

I would like to thank Dr Alexandra Marques for the support in the first years of my PhD. I really appreciate her contribution to increase my knowledge about skin cells and her input on my first publication.

I am also grateful to the co-authors of my research papers described in this thesis. Their contribution was crucial for me to succeed in achieving this milestone. In particular, to Professor Honggang Cui and

his student Yi-An Lin from the Institute for NanoBioTechnology at The Johns Hopkins University, for the extraordinary TEM images of the peptides, and Dr Ronit Bitton from the Ben-Gurion University of the Negev for the SAXS analysis. These results greatly improved the quality of the research papers.

I would also like to acknowledge the Foundation for Science and Technology (FCT) for my personal doctoral grant (SFRH/BD/44977/2008) and for providing funding (grant PTDC/EBB-BIO/114523/2009) that supported most of the research described in this thesis.

To my dear colleagues and friends at 3B's, including some that have already left the group, for all the support, good moments and laughs. You are so many that it is not possible to acknowledge you all individually. I am truly grateful to all of you that somehow contributed to this thesis or to my personal development. To Ricardo Silva, for the help with the HPLC in the beginning of my PhD. To Mariana Cerqueira, for bringing the samples from Porto and for teaching me how to isolate the cells from the skin samples. To Ana Rita Pinto and Wojteck, for teaching me how to isolate Wharton jelly stem cells and endothelial cells, respectively. To the technicians, Liliana, Claudia, Ana, Adriano and Filipe, I am deeply grateful for your efforts on having all the necessary tools to carry out my work. A special thanks to Belinha, for your friendship and for having such an important role on keeping me balanced when I needed. There are not enough words to express my gratitude for your actions.

To the members of the "Clube Alegria no Coração", we are all in different cities now (countries for some) but I still smile when I remember our times together. Thank you for the great moments, especially for the laughs and support during these years. I miss our coffee breaks and nonsense conversations. A special thanks to Catarina, for being always there, for the support and motivation in the last months, and for always making me feel close, even when I was living in another country.

To my colleagues at Hubbell's lab, Jennifer, Laura and Evan, thank you for the knowledge you shared and also for the cheerful disposition. A special thanks to Diana and Jeffrey for making me feel welcome in Lausanne.

To all the people at QMUL that supported me in the last year of the PhD. To Filipe ("mafia tuga"), thank you for your expertise on AFM and for the good laughs. To Alvaro Mata's lab, for adopting me and making me feel welcome in London. A special thanks to Estelle, I know you only for a short time, but it

is so simple to be friend with you. I am deeply grateful for your support in the last months (and for the cakes too).

To Vânia and Luís, thank you for your friendship and support, and for making me feel welcome and part of the family. My days after work were much happier with you at home.

To all my friends outside the "research world", thank you for keeping my balance outside of the lab and for being there no matter how long it has passed since the last time we saw each other.
A special thanks to Teresa, my dearest friend. Thank you for making my first year in Braga so memorable and for being always present, no matter what.

To my family,
Ao Filipe, pelo apoio incondicional e pela paciência. Por literalmente me levares ao céu e me mostrares o mundo de outra perspectiva, somos tão pequeninos a dois mil pés de altitude...
Aos meus irmãos, Ana e Guito, por serem tão diferentes e complementarem a minha personalidade com um bocadinho de cada um de vós. Pelas palavras de incentivo, pelos beijos e abraços estrafegados nas horas certas.
Aos meus pais, a quem dedico esta tese. A vós devo tudo o que sou, pelos valores que me transmitiram, pelos exemplos de força e superação que me deram. Não existem palavras suficientes para descrever a minha gratidão. Obrigada!

Abstract

The exquisite field of molecular self-assembly (SA) offers numerous opportunities to fabricate biomaterials with increased level of precision and complexity. Peptide molecules have been widely used as building blocks in biomaterial SA as they provide the possibility to form nanofibers that resemble the filamentous structure of the natural extracellular matrix (ECM). Peptide amphiphiles (PAs) were used throughout the work described in this thesis to develop new biomaterials (membranes and capsules) by SA. To develop bioactive membranes recapitulating some features of the skin ECM, positively charged PAs were combined with hyaluronan (HA). Membranes were obtained by SA and presented a nanofibrillar morphology resembling the ECM architecture. The cell-adhesive sequence (RGDS) was then integrated into the PA structure and was shown to increase the adhesion of human dermal fibroblasts (hDFbs). To further expand the versatility of these membranes, and recreate some of the aspects of the ECM remodeling, a cleavable sequence (GPQGIWGQ, octapeptide) sensitive to matrix metalloproteinase-1 (MMP-1) was incorporated into the PA structure. Enzymatic degradation studies with exogenous enzymes (hyaluronidase and MMP-1) revealed that membranes containing the MMP-1 substrate exhibited enhanced enzymatic degradation, being completely degraded after 7 days. Cell culture studies using hDFbs showed that the presence of MMP-1 cleavable sequence stimulated the secretion of MMP-1 by hDFbs and interfered with matrix deposition, particularly the deposition of collagen. A notable observation from this work was the spontaneous formation of well-defined micro-groove-like patterns on the membrane surface during the SA process. The micro-pattern formation was then investigated by varying the conditions (experimental set up, incubation time, concentration of the building blocks, HA molecular weight and nature of polyelectrolyte) during SA. These studies revealed that the presence of an air-liquid interface at the PA side and the nature of the underneath polyelectrolyte played a key role on the formation of the micro-grooved patterns. hDFbs cultured on the patterned membranes were shown to align in a parallel direction with the micro-grooves, suggesting the possibility of using the self-patterned membranes for guided-tissue regeneration. The role of the octapeptide domain on the membrane topography was also investigated using a peptide library containing 15 PAs with variations on the central octapeptide segment, in terms of length and amino acid composition. Membranes with very distinct surface morphologies, from well-defined micro-grooves to micro-sized aggregates, were obtained by simply manipulating the PA structure. The results from site-direct mutations suggest that the size of the central domain, including the presence of isoleucine in the middle, and existence of β-sheet structures are determinant for the formation of micro-groove patterns. In a distinct work, electrostatic self-assembly of PAs of opposite charge was combined with microfluidics to develop soft peptide-based capsules for cell encapsulation. The resulting capsules exhibited regular shape and size, and a gelled core made of a dense nanofibrillar network. Their properties (nanofibrillar density, permeability) were able to be modulated by changing the PAs concentration. These properties were also shown to influence the morphology of hDFbs encapsulated within the microcapsules. On less dense capsules, hDFbs exhibited their typical elongated morphology and organized cytoskeleton. In addition, the developed microcapsules allowed the co-culture of two cell types (hDFbs and keratinocytes). The research work described in this thesis highlights the use of molecular engineering strategies to design peptides, integrating SA ability and specific biochemical functionalities, for the bottom-up fabrication of novel biomaterials. The developed biomaterials exhibited intrinsic bioactivity and hierarchical structure, enabling their application as artificial matrices for probing cell behavior in defined microenvironments that recapitulate critical aspects of native tissues and thus develop novel therapeutic strategies for tissue regeneration.

Matrizes Biomiméticas com Estrutura Organizada a Nível Molecular para Aplicações em Medicina Regenerativa

Resumo

Avanços na área da química supramolecular oferecem inúmeras oportunidades para o desenvolvimento de novos biomateriais com elevado nível de precisão e complexidade. Péptidos têm sido amplamente utilizados para o desenvolvimento de biomateriais por processos de auto-organização, uma vez que permitem a formação de estruturas fibrilares semelhantes às existentes na matriz extracelular. Na presente tese foram utilizados péptidos anfifílicos (PAs) para desenvolver novos biomateriais (membranas e microcápsulas) por processos de auto-organização. Para desenvolver membranas bioactivas que mimetizem alguns aspectos da matriz extracelular da pele, PAs com carga positiva foram combinados com um polímero de carga oposta (ácido hialurónico). As membranas foram obtidas por processos de auto-organização, apresentando uma estrutura fibrilar. A sequência peptídica de adesão celular (RGDS) foi integrada na estrutura do PA, para promover a adesão de fibroblastos nas membranas. Para recriar outras funcionalidades da matriz extracelular, nomeadamente o processo de remodelação, a sequência peptídica (GPQGIWGQ, octapéptido) sensível à degradação pela enzima metaloproteinase-1 (MMP-1) foi incorporada na estrutura do PA. Ensaios de degradação enzimática, na presença de hialuronidase e MMP-1, mostraram que as membranas contendo o substrato da MMP-1 apresentaram sinais evidentes de degradação, tendo sido completamente degradadas após 7 dias. Estudos celulares com fibroblastos mostraram que a presença do substrato da MMP-1 nas membranas estimulou a secreção de MMP-1 pelas células e afectou a deposição de matriz extracelular, particularmente a deposição de colagénio. Uma observação notável resultante deste trabalho, foi a formação espontânea de topografias organizadas à microescala na forma de canais. Análises de microscopia revelaram um alinhamento das células (fibroblastos) ao longo dos microcanais quando cultivadas nas membranas.

Através de um dispositivo de microfluidicos, uma solução de péptido foi emulsionada num óleo a fim de gerar gotas esféricas. Estas gotas foram posteriormente gelificados quando em contacto com uma outra solução de péptido de carga oposta, formando capsulas de forma e tamanho regular, e interior gelificado. De forma a controlar as propriedades das capsulas (densidade fibrilar, permeabilidade) variou-se a concentração dos péptidos usados. Estudos celulares feitos com fibroblastos no interior das cápsulas revelaram que as células mantiveram-se viáveis. No entanto, a sua morfologia mostrou depender da densidade nanofibrillar das cápsulas. Além disso, este sistema permitiu também a co-cultura de dois tipos de células, fibroblastos e queratinócitos.

Os estudos descritos nesta tese realçam a vantagem de manipular a estrutura de biomateriais à escala molecular. Os biomateriais desenvolvidos (membranas e microcápsulas) apresentam estruturas hierarquicamente organizadas e bioactividade intrínseca, permitindo a sua aplicação no desenvolvimento de novas estratégias terapêuticas para a regeneração de tecidos.

Table of contents

A

Ala or A	Alanine
AFM	Atomic force microscopy
Arg or R	Arginine
Asn or N	Asparagine
ANOVA	Analysis of variance

B

BMP-2	Bone morphogenetic protein-2
BMHP-1	Bone marrow homing peptide-1

C

Calcein-AM	Calcein acetomethyl
CD	Circular dichroism
CNS	Central nervous system
Cys or C	Cysteine

D

DAPI	4',6-diamidino-2-phenylindole dihydrochloride
Dex	Dexamethasone
DMEM	Dulbeccco's Modified Eagle's Medium
DMF	Dimethylformamide
DNA	Deoxyribonucleic acid
DPSCs	Dental pulp stem cells
dsDNA	Double stranded DNA
DIEA	N,N-Diisopropylethylamine
DPSCs	Dental pulp stem cells

E

ECM	Extracellular matrix
EGF	Epidermal growth factor
ESI-MS	Electrospray ionization mass spectrometry

F

FBS	Fetal Bovine Serum
FGF-2	Fibroblast growth factor-2
FITC	Fluorescein isothiocyanide
Fmoc	9-fluorenylmethoxycarbonyl

G

Gln or Q	Glutamine
Glu or E	Glutamic acid
Gly or G	Glycine
GFP	Green fluorescent protein

H

H5V	Mouse endothelial cells
HA	Hyaluronic acid
HAase	Hyaluronidase
HBTU	O-(benzotriazol-1-yl)-N,N,N',N'-tetramethyluronium
Hep	Heparin
His or H	Histidine
HMDS	Hexamethyldisilazane

HPLC	High performance liquid chromatography
hDFb	Human dermal fibroblasts
hMSCs	Human mensenchymal stem cells
hKc	Human epidermal keratinocytes
hNSCs	Human neural stem cells
HUVECS	Human umbilical vein endothelial cells
HAECs	Human aortic endothelial cells
I	
Ile or I	Isoleucine
IGF-1	Insuline-like growth fator-1
L	
Leu or L	Leucine
LDL	Low density lipoprotein
Lys or K	Lysine
M	
MBHA	4-methylbenzhydrylamine rim amide resin
MSCs	Mesenchymal stem cells
Met or M	Methionine
MMP	Matrix metalloproteinase
mNSCs	Mouse neural stem cells
Mw	Molecular weight
N	
NAG	N-acetyl glucosamine
P	
PA	Peptide amphiphile
PBS	Phosphate buffer saline
Phe or F	Phenylalanine
PI	Propidium iodide
Pro or P	Proline
Q	
QCM-D	Quartz crystal microbalance with dissipation
R	
rMSCs	Rat mesenchymal stem cells
S	
SA	Self-assembly
SAXS	Small-angle X-ray scattering
SCI	Spinal cord injury
SEM	Scanning electron microscopy
Ser or S	Serine
SHED	Stem cells from human exfoliated deciduous teeth
SPPS	Solid phase peptide synthesis
T	
TCPS	Tissue culture polystyrene
TEM	Transmission electron microscopy
TFA	Trifluoroacetic acid
TGF-β1	Transforming growth factor

	β1
Thr or T	Threonine
TIS	Triisopropylsilane
Trp or W	Tryptophan
Tyr or Y	Tyrosine

U

UV	Ultraviolet

V

Val or V	Valine
VEGF	Vascular endothelial growth factor

W

Wt%	Weight percentage
w/v	Weight/ volume

Others

3D	Three-dimensional

The present thesis is divided into four sections, containing a total of eight chapters, and is based on the format adopted by the 3B´s Research Group, which consist on the compilation of scientific papers published or submitted for publication in international peer-reviewed journals, as identified in the first page of each chapter. The contents of each section and chapters are summarized below.

The first section (**Section 1 - Introduction**) provides a brief introduction of the work performed under the scope of the present thesis, including the main objectives of the PhD work, followed by an independent chapter that consists of a review paper on the application of peptides in tissue engineering (**Chapter I**). This chapter aims to provide the background for the topic presented in the PhD thesis.

Section 2 (**Experimental**) includes a detailed description of the materials and methods used within the experimental work. This section aims to complement the information given in each of the experimental chapters and justify the adopted methodology.

The following five chapters in **Section 3** describe original research corresponding to manuscripts either published or submitted to international journals. In **Chapter III**, a bioactive membrane, obtained by self-assembly between peptide amphiphiles and hyaluronan, was investigated as a biomimetic matrix to reconstruct the skin extracellular environment. Peptides were further engineered to include a cleavable site for matrix metalloproteinase 1 and develop membranes that are responsive to cell secreted enzymes (**Chapter IV**). **Chapter V** describes the formation of a membrane with ordered patterns through self-assembly, without a physical template, when a specific peptide amphiphile is combined with hyaluronan. The effect of different peptide sequences on membrane topography was further explored in **Chapter VI**.

Chapter VII reports the development of peptide-based capsules formed by electrostatic self-assembly of peptides with opposite charge in combination with microfluidics and the co-culture of cells within and on the microcapsules.

The last section of the thesis (**Section 4 - Conclusions**) includes **Chapter VIII**, which summarizes the significant findings in the experiments presented in the previous section and highlights the possibilities for further research.

Six chapters presented in this thesis are based on the following articles:

Chapter I

Daniela S. Ferreira, Rui L. Reis, Peptides in tissue engineering: from decorating molecules to complex nanostructured scaffolds, 2014, submitted

Chapter III

Daniela S. Ferreira, Alexandra P. Marques, Rui L. Reis, Helena S. Azevedo, Hyaluronan and self-assembling peptides as building blocks to reconstruct the extracellular environment in skin tissue, Biomaterials Science, 1 (9): 952-964, 2013.

Chapter IV

Daniela S. Ferreira Yi-An Lin, Honggang Cui, Jeffrey A. Hubbell, Rui L. Reis, Helena S. Azevedo, Molecularly engineered self-assembling membranes for cell-mediated degradation, Advanced Healthcare Materials, 2014, DOI: 10.1002/adhm.201400586

Chapter V

Daniela S. Ferreira, Oliver Picot, Yi-An Lin, Honggang Cui, Ronit Bitton, Rui L. Reis, Helena S. Azevedo, Single-step self-assembly of micro-patterned membranes: from solution to higher-ordered supramolecular structures, 2014, submitted

Chapter VI

Daniela S. Ferreira, Yi-An Lin, Honggang Cui, Rui L. Reis, Helena S. Azevedo, Specific amino acid sequences and their localization in the structure of peptide amphiphiles modulate the surface topography of self-assembled peptide-hyaluronan membranes, 2014, submitted

Chapter VII

Daniela S. Ferreira, Rui L. Reis, Helena S. Azevedo, Peptide-based microcapsules obtained by self-assembly and microfluidics as controlled environments for cell culture, Soft Matter, 9: 9237-9248, 2013

Section 1

INTRODUCTION

Background

The extracellular matrix (ECM) of tissues is a dynamic and hierarchically organized nanocomposite that regulates essential cell functions such as adhesion, migration, proliferation and differentiation. Engineering complex tissues requires biomaterial scaffolds that recapitulate the structure and composition of ECM to provide cells with physical and biochemical signals that are important for tissue development and organization (functional tissue). 3D scaffolds, in which cells are randomly distributed, offer limited control over spatial cell organization and tissue architecture. Microscale control over cell position and ECM composition may enable improved regulation of biochemical signaling, interactions between cells and ECM and cell-cell contacts.

Peptides have received great attention in tissue engineering and regenerative medicine due to their well-known diverse biochemical functions (specific recognition by cells, enzymes or other macromolecules). They have been used primarily in the functionalization of scaffold biomaterials, but advances in the chemical synthesis of peptides has expanded the use of these small molecules in self-assembly (SA) approaches to construct more biomimetic scaffolds. Self-assembly is a nanofabrication technique that is based on the spontaneous organization of individual building blocks into ordered and stable nanostructures by noncovalent interactions.

Peptides offer numerous advantages as self-assembling units, as the information required for their self-assembly is encoded within their sequence; their self-assembly is usually spontaneous (simple method to develop nanostructured materials), instantaneous (milliseconds) and reproducible (defined stable structures). Furthermore, by varying systematically the chemical structure (e.g. sequence size and nature of the amino acid side groups) during synthesis it is possible to adjust the self-assembling properties of the building blocks, as well as to produce ECM-like nanostructures (e.g. nanofibers). Self-assembling peptides can also be designed to include specific epitopes to promote cell-matrix interactions at the molecular level.

Hypotheses

The work presented in this PhD thesis was based on the following hypotheses:

(i) Hyaluronan and peptide amphiphiles (PAs) can be used as building blocks to reconstruct the extracellular environment of skin ECM;

(ii) Self-assembly can be used to develop membranes and capsules, using the above mentioned building blocks, to recreate the nano-architectural features of natural ECMs;

(iii) Molecular engineering can be used to introduce specific biochemical functionalities into PA structures and affect their self-assembly behavior;

(iv) SA and molecular engineering can be combined to develop new biomaterials with increased level of control over physical and chemical functionalities.

Research objectives

The general aim of the PhD work was to integrate self-assembly principles with biological building blocks (hyaluronan and peptides) to develop self-assembling matrices (membranes and capsules) with specific biochemical functionalities for potential applications in regenerative medicine. The specific aims of this PhD work were:

(i) develop self-assembling membranes with cell adhesive properties for wound healing applications by integrating structural components of skin ECM (HA) with bioactive peptide sequences (RGDS);

(ii) develop self-assembling membranes with programmable degradation by incorporating enzymatic sensitive components into the membrane formulation;

(iii) understand the effects of SA conditions on the formation of micropatterns on the surface of HA-PA membranes;

(iv) investigate how amino acid mutations in specific domains of PA structures affect their self-assembly behavior and the micro/nanotopography of HA-PA self-assembled membranes;

(v) expand the application of PA self-assembly to develop 3D microenvironments with tunable properties for cell (co)-culture.

Chapter I

Peptides in tissue engineering: from decorating molecules to complex nanostructured scaffolds

Chapter I*

Peptides in tissue engineering: from decorating molecules to complex nanostructured scaffolds

Abstract

Peptides present a unique starting platform for designing biomimetic biomaterials. Their versatility, conferred by the amino acids in the sequence, leads to diverse sequence combinations, resulting in different physical properties and interaction with biological systems. Despite their chemical simplicity, numerous peptide motifs have been coupled to biomaterials as extracellular matrix (ECM) mimetics to recapitulate the functional and structural features of ECM proteins.

Current efforts have been made to engineer biomimetic materials that resemble essential features of the natural ECM, such as its hierarchical architecture and biological functions. Self-assembling peptides have undergone rapid development in the last two decades. These molecules can self-assemble into fibrillar networks that mimic the nanostructure of the native ECM. In addition, their ability to incorporate biological active motifs gives further control over the function of these networks. This review provides an overview of the application of peptides in tissue engineering, starting from conventional biomaterials functionalization to more complex self-assembling peptide-based systems incorporating biological motifs of natural ECM.

.

* This chapter is based on the following publication:

Daniela S. Ferreira, Rui L. Reis, Peptides in tissue engineering: from decorating molecules to complex nanostructured scaffolds, 2014, submitted

1. Introduction

The extracellular matrix (ECM) of tissues is an intricate and hierarchically organized network of multifunctional macromolecules (such as proteoglycans, collagens, laminins, fibronectin and sequestered growth factors), which modulates cell behavior and directs tissue morphogenesis through biophysical and biological cues.[1] Progress in biomaterials design is converging to design instructive materials that resemble key molecular features of the ECM as candidates for biomedical applications.[2] The design of functional biomaterials that can regulate cell behavior (e.g. adhesion, proliferation and differentiation), as well as eliciting specific cellular responses and directing new tissue formation when implanted in vivo, is a key component in regenerative medicine therapies.

The early work on the surface modification of biomaterials (fibers, sponges, foams, films) with bioactive molecules has long used as strategy a simple coating procedure with solutions of ECM proteins via non covalent interactions.[3] Although this method has showed improvements in cell adhesion and proliferation, it requires the adsorption of a high density of protein, once the protein can denature on the surface or adopt a random conformation, which would significantly reduce the active binding domains available and decrease cell affinity.[4] The use of short peptide motifs for biomaterials functionalization presents several advantages over the use of full ECM proteins.[5] Short peptide motifs are relatively more stable during modification processes for surface functionalization. In addition, peptides are chemically defined and can be easily synthesized in chemistry laboratories. Peptides have an additional appeal for applications in tissue engineering, due to their inherent biocompatibility and biodegradability. The most widely studied peptide for surface functionalization is the sequence Arg-Gly-Asp (RGD).[6, 7] RGD is the principal integrin-binding domain found in many ECM proteins, including fibronectin, laminin, vitronectin, collagen type IV, tenascin and fibrinogen.[8, 9] Since the early 90s, RGD has been widely used to enhance cell adhesion to biomaterial surfaces.[10, 11] Meanwhile, thanks to the development of viral phage display technologies, peptides that bind specifically certain cell receptors have been identified, providing a vast library of receptor-binding peptides for use in tissue engineering among other applications.[12] Some peptides sequences that have been investigated for biomaterial functionalization are presented in Table I.I.

These bioactive motifs can be further combined to yield biomaterials that recreate multiple cues of the ECM. Another strategy for the incorporation of bioactive peptide motifs into biomaterials includes the covalent binding of the peptides into the material during its assembly.[13-15] Several biopolymers, such as poly(ethylene glycol) (PEG),[13, 15-17] alginate,[18-20] and hyaluronan,[21, 22] have been have been routinely combined with bioactive peptide sequences to gain functionalization.

In addition to providing cells with biological signals, ECM remodeling is itself a process that highly affects cell response. In recent years, researchers have made efforts to engineer biomaterials that resemble this feature of the ECM. For this, peptides have been incorporated into biomaterials to modulate their proteolytic susceptibility. In particular, enzyme-degradable peptide sequences such as matrix metalloproteinases (MMPs)[23, 24] or plasmin[25] sensitive peptides have received particular interest, enabling the tailored degradation of the material. In a work pioneered by the Hubbell group, the coupling of a peptide that carries both a cell-adhesive sequence and a domain that is a substrate for enzymatic crosslinking by the transglutaminase factor XIIIa has also been used to engineer ECM mimetics for tissue engineering applications.[26]

Peptides can also be designed to self-assemble, forming three-dimensional networks that mimic the nanofibrillar structure of the natural ECM. Several classes of peptide motifs that favor self-assembly to nanostructured scaffolds have been designed. These include, α-helical peptides,[27, 28] and β-sheet forming peptides, such as ionic-self complementary peptides, [29] glutamine rich peptides,[30] peptide amphiphiles,[31, 32] and short aromatic peptides.[33, 34] These self-assembling peptides and their application in tissue engineering will be further discussed in this review.

2. Peptides

Peptides result from the successive linkage of series of amino acids by amide bonds. In nature, there are 20 natural amino acids that are used for peptide synthesis (Fig. I.1). All the natural amino acids only exist in the L-form, and all, except glycine (G), are chiral. Amino acids share the same basic structure, a central α carbon (Cα) atom to which a hydrogen atom, an amino group, a carboxyl group and side chain (R-group) are attached. Depending on which R-groups are in the amino acids neighborhood, peptides can adopt specific configuration affecting their structure. Considering the number of amino acids and the possible combinations, the number of possible sequences that can be formed are close to infinite.

Peptide immobilization into materials (biomolecules, polymers, surfaces and nanoparticles) is generally accomplished by formation of covalent bonds via functional groups in the peptides (Fig. I.1).[6] Various chemical immobilization schemes can be utilized to create stable covalent linkages, the most simple involves reacting the N-terminus amine group of the peptide molecule with the material surface. Peptides have been immobilized by reacting the N-terminus amine groups (-NH_2) with biomaterial surface carboxyl, hydroxyl, epoxyde and aldehyde groups. In alternative, peptides can be immobilized through the C-terminus carboxyl group (-COOH), which offers less chemical options, as carboxyl groups can react only with amine and hydroxyl groups. These immobilization techniques, although widely

employed, are not suitable for all the peptide sequences, due to the presence of reactive groups in the side-chain of some amino acids, such as $-NH_2$ (Arg, Lys, His), -COOH (Asp, Glu) and –SH (Cys). If not protected, these functional groups can also react. Additionally, these groups can also be used for conjugation with biomaterials (Fig. I.1).[6] The thiol (-SH) containing side chain of cysteine is the most reactive specie present in naturally occurring amino acids. Peptides containing a single cysteine can form dimers by oxidation of the cysteine side chain thiols, linking two chains together by a disulfide bond. Peptides containing two or more cysteine residues can form intramolecular disulfide bridges. N-terminal cysteine peptides can also be used for selective conjugation of peptides into biomaterials, the unique reactivity of the cysteine side chain allows various useful chemistries to be undertaken (Fig. I.1)

.

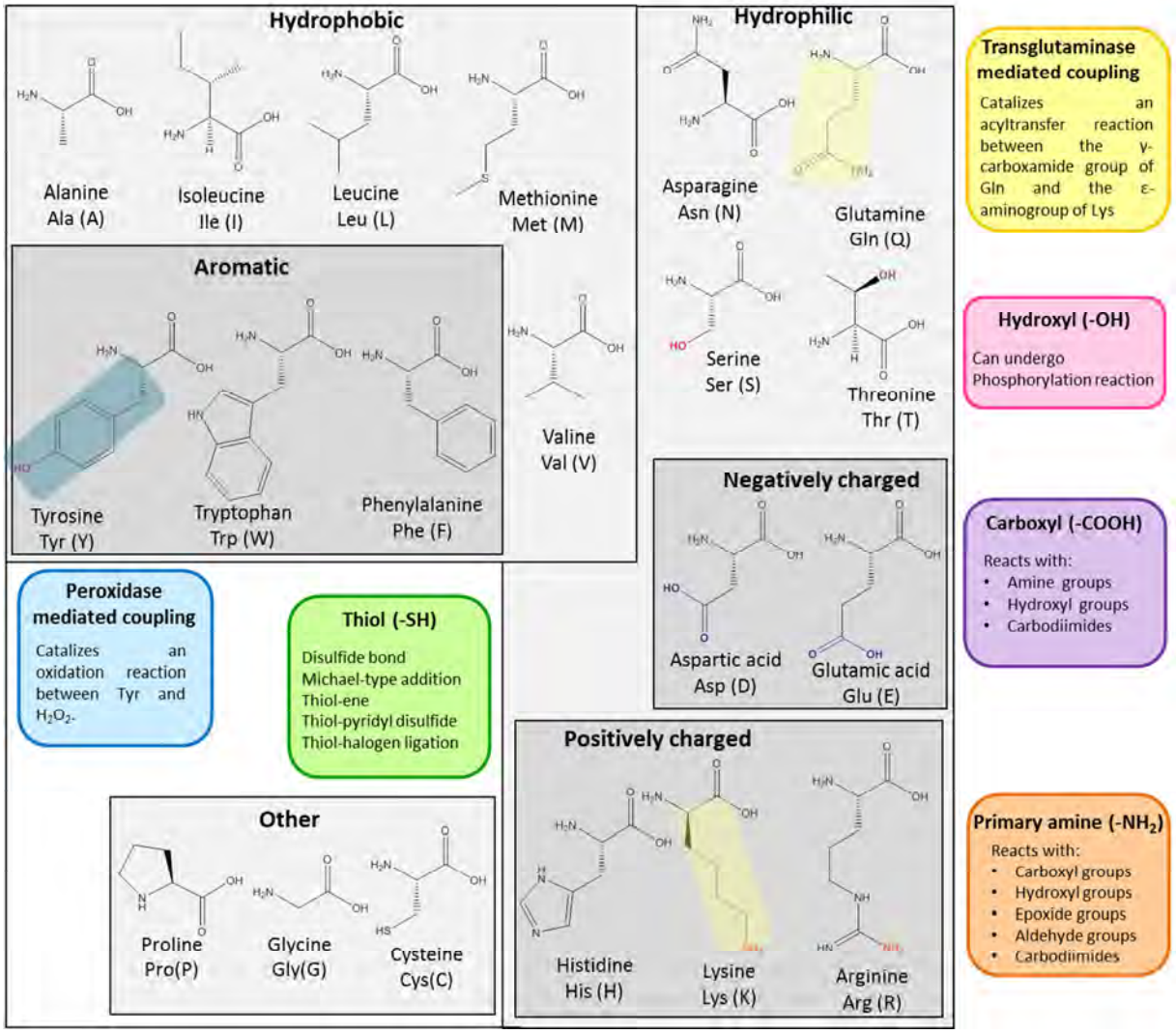

Figure I.1 – Chemical structure of the 20 amino acids highlighting the available functionalities to react with other groups present in conventional materials used as tissue engineering scaffolds.

2.1. Peptide structure and properties

The sequence of amino acids, normally written as one or three letter codes, confers the primary structure. The chemical designed flexibility conferred by amino acids results in a variety of possible secondary, tertiary and quaternary structures. Peptide-adopted secondary structures (e.g. β-sheet, α-helix, and collagen like triple helix) contribute to the design and fabrication of biomaterials with hierarchical organization (e.g. synthetic membranes, multilamellar structures, micelles, tubules).[35-37] Peptides are versatile building blocks for the design of supramolecular assemblies with controllable structural features at the nanoscale. Peptide self-assembly can result from the interaction of a single peptide with another complementary peptide via non-covalent interactions (hydrogen bonding, hydrophobic, electrostatic interactions, van der Waals forces and π-π stacking). These interactions between adjacent peptides can be modulated through engineering the primary sequence (amino acids) and thus the secondary structure of the peptides.[38, 39]

2.2. Peptide synthesis

Peptides can be obtained either from natural or synthetic sources. The isolation of peptides from natural sources is a highly demanding process and hardly originates high purity peptides. The most advantageous property of chemical synthetic peptides is that they are chemically defined, thus avoiding the impurities that can result from genetic engineering techniques. Chemical peptide synthesis enables the systematic refinement of their structure and parallel experimental designs to discover novel peptides. Peptide synthesis includes a large range of techniques and procedures that enable the preparation of materials ranging from small peptides up to 50 residues. Peptides can be synthesized in solution or by solid phase. Solid phase peptide synthesis (SPPS) has become a method of choice to produce peptides, this method allows the preparation of monodispersed peptides with precise control of the primary structure and high yields.[40, 41] The general process for synthesizing peptides by SPPS starts by attaching the first amino acid via its carboxyl group to a resin (hydroxyl: Wang, 2-Chlorotrityl chloride, Rink acid resin or amino: Rink amide (MBHA)) to yield respectively an ester or amide linked peptide that ultimately produce a C-terminal acid or a C-terminal amide peptide (Fig. I.2). To prevent the polymerization of the amino acid, the alpha amino group and the reactive side chains are protected with a temporary protecting group. This is an orthogonal protection system, since the side chain protecting groups can be removed without displacing the N-terminal protection. Once the amino acid is attached to the resin, the excess of reactants is removed by filtration and washings. Next, the N-terminal protecting group is removed (deprotection) allowing the addition of the next N-protected amino acid by activation of its alpha-carboxylic acid (coupling). During these processes, side-chain functional groups of amino acids

must be masked with protecting groups that are stable in the reaction conditions used during peptide elongation.

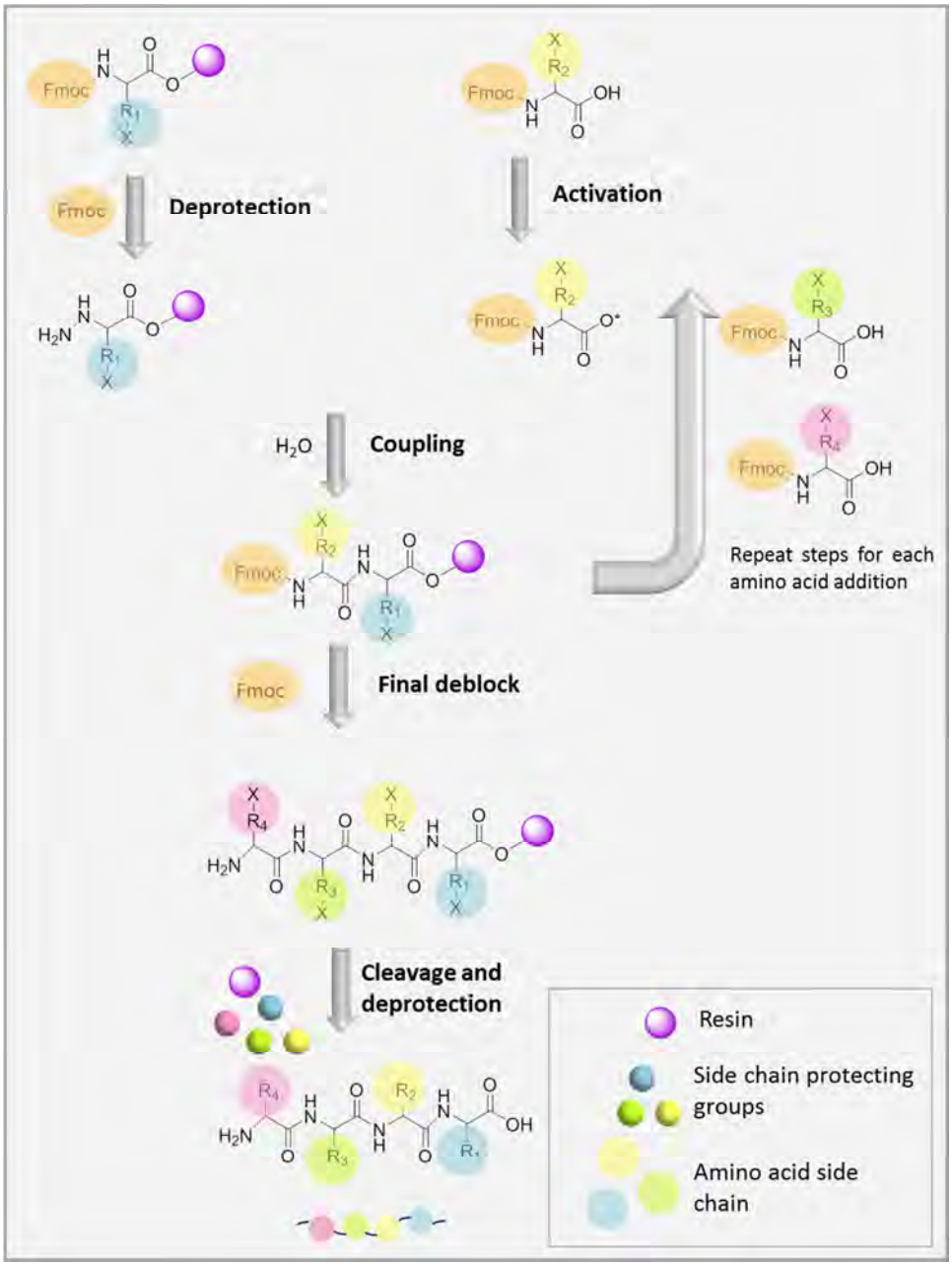

Figure I.2 – Diagram showing the steps in solid phase peptide synthesis (SPPS).

The peptide is assembled from the C-terminus to the N-terminus (C→N) by repetitive cycles (deprotection/coupling) until the desired sequence of amino acids is obtained (Fig. I.2). At the end, the peptide is cleaved from the resin and the side-chain protecting groups concomitantly removed. As peptide synthesis involves numerous repetitive steps, the use of a solid support has obvious advantages. Excess reagents and side products can be separated from the growing and insoluble peptide simply by filtration and washings, and all the synthesis steps can be performed in the same vessel without any transfer of material. Using commercially available resins, activating agents, amino

acid derivatives, and solvents, peptides of up to 30-50 residues can be routinely prepared by SPPS with good yields.[41, 42]

2.3. Bioactive peptides for scaffold surface functionalization

2.3.1 Linear bioactive peptides

The addition of short biologically active peptide motifs to material surfaces is the simplest way to render them functionality. Short simple linear peptides have been extensively used as ECM mimics to recapitulate the biological functions and structural features of ECM proteins. The most widely employed and studied sequence for biomaterials functionalization is RGD, a fibronectin derived epitope, first reported by Pierschbacher.[43] Since its discovery, numerous materials have been functionalized with RGD for tissue engineering applications.[6, 9, 11, 44] There are many different ways in which an RGD motif can be presented towards cells and the manner in which the peptide is immobilized on a surface can affect the peptide concentration, density, retention, accessibility, arrangement, conformation and activity. In the early 90s, Massia and Hubbell have studied covalent surface immobilization of RGD-containing peptides on a variety of surfaces.[11, 45, 46] These peptides were shown to improve cell-adhesion, and in addition, authors have observed that a spacing of 400 nm was enough for integrin-mediated fibroblast proliferation.[10] RGD has been copolymerized with PEG-diacrylates (PEGDA) to form hydrogels that promote cell adhesion and survival.[13, 16] Additionally, the combination of both the RGD and the heparin-binding motifs from bone sialoprotein (FHRRIKA) was shown to synergistically improve cell adhesion and mineralization in osteoblast culture.[47]

Other peptide sequences, such as REDV,[45, 49] YIGSR,[46, 71] and IKVAV[72] have also been immobilized on various biomaterials to improve cell adhesion. Peptides can possess a diversity of functions beyond cell-adhesion through integrin-binding, such as specific proteolytic susceptibility,[23, 73-78] collagen mimetics[79, 80] and growth factor binding.[60, 81] Some of the most commonly used peptide sequences to functionalize biomaterials for tissue engineering applications are summarized in Table I.I.

Table I.I – Peptide sequences commonly used in the functionalization of biomaterial scaffolds.

Peptide sequence	Source	Biological function	References
RGD PHSRN	Fibronectin	Integrin binding	43, 48
REDV	Fibronectin		49
IKVAV YIGSR RYVVLPR	Laminin		50-52
GFOGER	Collagen I		53
TAGSCLRKFSTM	Collagen IV		52
GPQGIAGQ	Collagen I	MMP-1 substrate	23
PVGLIG	Osteonectin	MMP-2 substrate	54
VLK, EKK	-	Plasmin substrate	55
FKGG, NQEQVSPL	α2-plasmin inhibitor	Transglutaminase substrate	26
FAKLAARLYRKA RPKAKAKAKAKDQTK	Antithrombin III	Heparin binding	56, 57
FHRRIKA	Bone sialoprotein		47
LRKKLGKA	Proteins with heparina binding site		58
VFDNFVLKK	Tenascin-C	Tenascin mimetic	59
K$^{(S)}$	-	Heparin mimetic	60
DGEA GTPGPQGIAGQRGVV	-	Collagen mimetic	61
KRTGQYKL	FGF-2	FGF-2 binding	62
HSNGLPL	-	TGF-β1 binding	63
PFSSTKT SKPPGTSS	-	BMHP1	64
KIPKASSVPTELSAISTLYL	BMP-2	Growth factor mimetic	65-67
S$^{(P)}$KIPKASSVPTELSAISTLYLDDD	BMP-2		68
STGSKQRSQNRSKTPKNQEA AISVLYFDDSSNVILKKYRN	BMP-7		69
KLTWQELYQLKYKGI	VEGF		70

MMP: matrix metalloproteinases, FGF-2: fibroblast growth factor 2, TGF-β1: transforming growth factor β1, VEGF: vascular endothelial growth factor, BMP-2: bone morphogenetic protein 2, BMHP1: bone marrow homing peptide 1, S$^{(P)}$: phosphorylated serine, K$^{(S)}$: sulfonated lysine

2.3.2 Cyclic peptides

Authors have pointed out that the conformation of the peptides when presented to the cells does influence the way they interact and the binding affinity.[82, 83] Various conformations and lengths have been proposed for RGD ligands, its activity decreases in the following order: GRGDSP > RGDS > RGD amide terminal > RGD carboxyl terminal.[84] Cyclic analogues of RGD are more active in promoting attachment if compared with linear sequences.[82] Pakalns and co-workers have investigated the effects of orientation and conformation of RGD peptides on cellular responses.[85] Two conformations were designed, one linear and one cyclic, and two orientations of the linear RGD, N- and C- grafted, which were independently presented to cells. Results demonstrated that membranes of cyclic RGD supported adhesion and spreading of M14 human melanoma cells in a dose-dependent manner. The cyclization of these peptides may act to increase their stability and make them less susceptible to chemical and enzymatic degradation. This conformational stability of the cyclic RGD peptides arises from backbone rigidity. Gandavarapu and co-workers have incorporated the cyclic RRETAWA peptide, known to bind to $\alpha 5\beta 1$ integrin, into PEG hydrogels to study osteogenic differentiation of human mesenchymal stem cells (MSCs).[86] Results showed that the combination of $\alpha 5\beta 1$ integrin signaling stimulated by the cyclic peptide with high substrate stiffness was sufficient to induce osteogenic differentiation of MSCs without requiring the addition of soluble factors.

2.4. Peptide building blocks for self-assembling scaffolds

2.4.1. Concept of self-assembly

Molecular self-assembly (SA) is the spontaneous organization of molecules into hierarchical ordered structures, mediated by weak, non-covalent bonds, such as hydrogen bonds, hydrophobic interactions, electrostatic interactions, π-π stacking and van der Waals interactions.[87] This strategy is very attractive to create nanoscale materials for application in regenerative medicine due to both its simplicity in application and its unique capacity to produce a variety of diverse nanostructures.[87-89] Designing and synthesizing molecules that self-assemble into well-ordered nanostructures is an attractive bottom-up approach for developing new functional biomaterials.[35] In nature, peptides and proteins interact and self-organize to form well-defined structures that are associated with important physiological and biochemical functions. Peptides are a unique platform for the design of self-assembled materials with controllable structural features at the nanoscale.[90-92] Significant research over the past decade has been devoted to the design and fabrication of novel biomimetic materials through peptide self-assembly.[27] Self-assembling peptides have been designed to form different nanostructures, such as fibers, vesicles

and nanotubes.[93-95] The chemical design versatility afforded by amino acid sequences leads to a variety of possible secondary structures through folding and hydrogen bonding.[96]

2.4.2. Classes of self-assembling peptides

Different peptide sequences have been designed to yield peptides with self-assembling properties (Fig. I.3). The most widely applied in tissue engineering are discussed below.

2.4.2.1. Alpha helical peptides

The α-helical coiled-coil peptide motifs are excellent starting building blocks for the design of self-assembled constructs, due to their richness in structure and function.[27, 28] Most coiled coils are based on the heptad sequence repeat, which has seven residues (abcdefg). The first and fourth positions (a and d) are usually hydrophobic (H) amino acids, with the remaining sites largely polar (P). The resulting pattern (HPPHPPP) sets up the potential for an amphipathic α-helix. In water, two or more helices can associate to bury their hydrophobic faces and originate helical rope-like structures that measures 1 nm per heptad.[97] Most notably, α-helical coiled-coil peptides that self-assemble into hydrogelating self-assembling fibers (hSAFs) have been extensively studied and developed by Woolfson and colleagues.[98-100] Banwell and co-workers have shown that hSAFs were able to support cell growth and differentiation, similar to cells cultured in collagen and Matrigel, which is very encouraging due to their simplicity when compared these complex matrices.[98] Variations of self-assembling coiled-coil proteins containing RGD motifs have been designed, and the production of additional variants may provide an excellent platform for producing multi-component biomaterials.[101] A detailed description of these systems and can be found in several other recent reviews.[27, 99]

Collagen is the most abundant protein in the human body. It is a triple helical polypeptide that self-assembles in multiple level hierarchical structures and plays a major role in the structural integrity of the ECM. Due to its potential for biomedical applications in tissue engineering, strong efforts have been made to replicate the helical structure of this remarkable molecule.[102, 103] Hartgerink and co-workers have reported the synthesis of collagen mimetic peptides $(PKG)_4(POG)_4(DOG)_4$ that were shown to form sticky-ended collagen-like triple helix nanofibers.[102] These nanofibers self-assemble to originate a hydrogel with triple helical packing similar to that of natural collagen.

2.4.2.2. β-sheet forming peptides

The β-sheet motif, commonly present in self-assembling systems in biology, has been widely explored for the design of oligopeptides that self-assemble into organized structures.[30] Several β-sheet forming peptides incorporating alternating hydrophobic and hydrophilic motifs have been designed (Fig. I.3)

.

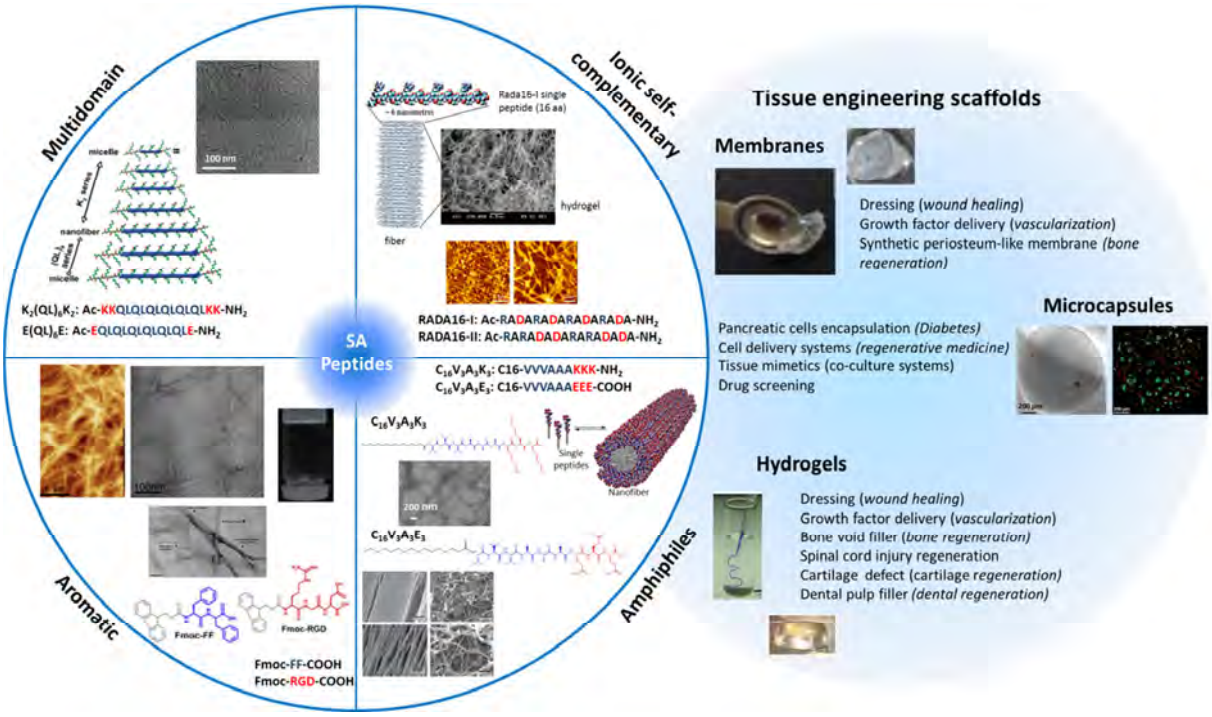

Figure I.3 – Examples of the most widely used self-assembling peptides as tissue engineering scaffolds.

Ionic self-complementary peptides

In the early 1990s, the group of Zhang has reported the use of β-sheet peptide motifs to produce hydrogels.[29] The first member of this class of peptides, AEAK16-II (AEAEAKAKAEAEAKAK), was derived from the yeast protein, Zuotin.[29] Peptides were designed to contain alternating hydrophobic and hydrophilic residues that commonly form β-sheets, owing to the placement of all hydrophobic residues on one face of the sheet and all hydrophilic residues on the opposite face. The β-sheets stack to form nanofibers of approximately 10 nm in diameter. Messersmith and co-workers[104] also studied 16-amino-acid peptide, FEK-16 ($(FEFEFKFK)_2$), containing alternating hydrophobic and hydrophilic residues. This peptide self-assembled into highly crosslinked, fibrillar, β-sheet hydrogels in the presence of inorganic salts. Additional β-sheet self-assembling peptides have been designed (RADA16-I and RADA16-II), in which arginine and aspartate residues substitute lysine and glutamate (in AEK16), and were shown to form hydrogels in the presence of salts. [29, 105-108]

Multi-domain short peptides

Hartgerink's group designed a series of ABA multi-domain short peptides, in which the B block is composed of alternating hydrophilic and hydrophobic amino acids (glutamine or serine and leucine, respectively), surrounded by the A block with flanking charged residues (lysine or glutamate), such as Ac-K_2(QL)$_6$$K_2$-$NH_2$, Ac-E(QL)$_6$E-$NH_2$, Ac-$K_2(SL)_6$$K_2$-$NH_2$, Ac-E(SL)$_6$E-$NH_2$ and Ac-E(CLSL)$_3$E-NH_2.[109] When the flanking charged residues are neutralized the hydrophobic interactions in the β-sheet B-domain induce self-assembly.[110] Different variations of these peptides have been synthesized, were bioactive motifs such as metalloproteinase cleavage sites and cell adhesion sequences were incorporated, for tissue engineering applications.[74, 111, 112] Some of these applications will be further explored in the next section.

Glutamine-rich peptides

Aggeli and co-workers developed a class of fibrillizing peptides that form β-sheet nanotapes. [30] These amphiphilic peptides undergo self-assembly from random coil monomers to nanotapes of anti-parallel β-sheets.[113] Members of this class of β-sheet nanotapes contain between seven and eleven amino acids, of which the 11-mers P_{11} (Q_2RFQWQFEQ_2), $P_{11\text{-}2}$) are the most extensively studied. The design is based on alternating hydrophilic (R, Q, E) and hydrophobic (F, W) residues in the core which favored a β-strand conformation. The terminal glutamine residues are uncharged, and can thus facilitate hydrogen bonding and hydrophobic interactions between adjacent antiparallel β-sheets. The positively charged arginine and the negatively charged glutamic acid residues are positioned such that the complementary charges of arginine and glutamic acid on neighboring strands are adjacent to each other if the peptide is in an antiparallel β-sheet configuration. $P_{11\text{-}4}$ (Q_2RFEWEFEQ2) adopts β-sheet conformation when the pH is lowered to less than 2, due to the net positive charge of arginine.[114] By substituting aromatic with aliphatic hydrophobic residues, shorter sequences of 7-9 amino acids could still produce fibril networks that trap water to form hydrogels. Yu and co-workers[115] used a system composed from a pair of peptides with opposite charges. The modular design strategy based on mutual attraction but self-repulsion prevents spontaneous gelation or aggregation. Gelation may be triggered by mixing two peptides (WKVKVKVKVK and EWEVEVEVEV) or by suppressing ionization by changes in pH and/or ionic strength. Using the same strategy, Collier and co-workers have designed other glutamine-rich peptides (Q_2KFQFQFEQ_2, Q11).[116, 117] Q11 peptides with N-terminal IKVAV and RGDS sequences were shown to co-assemble into fibrils presenting the biological signals on their surface, and to influence endothelial cell growth.[117]

Peptide amphiphiles

Peptide amphiphiles are characterized by a peptide sequence which is covalently bond to an alkyl tail. These peptides were first reported by Tirrell and co-workers, in which a dialkyl ester tail was covalently bond onto a peptide sequence from collagen, forming a self-assembled monolayer at the air-liquid interface.[32] The Stupp laboratory has later reported a novel PA structure, in which an hydrophobic domain, typically a palmitic acid molecule, was appended to the N terminal of a hydrophilic peptide sequence.[31] The peptide sequence, the hydrophilic domain, can comprise three structural domains.[31, 118] The first domain, adjacent to the hydrophobic segment, consists of short peptide sequence designed to promote β-sheet formation resulting from intermolecular hydrogen bonding, which induces the assembly of PAs into high aspect ratio cylindrical nanofibers instead of micelles.[119] The second domain contains charged amino acids to enhance solubility in aqueous solutions. The net charge also enables the design of PAs for pH or salt-induced self-assembly. The last domain is optional, and can be used for the inclusion of biological epitopes, to generate functional biomaterials. Driven by the hydrophobic collapse of the alkyl tail and the intermolecular hydrogen formation, these PAs self-assemble in aqueous solution into high aspect ratio nanofibers.[119] This assembly mechanism allows the biological epitopes to be displayed on the surface of the nanofibers, readily available to interact with cells or other molecules.[120] These nanofibers can further organize into 3D networks, and form self-supporting gels that resemble the natural ECM fibrils.[121, 122] A different assembly strategy has been explored by Stupp and co-workers, to produce hybrid hierarchical structures by mixing PAs with polymers (hyaluronan, alginate, heparin) with opposite charge. Authors have shown that mixing a solution of high molecular weight hyaluronic acid (HA) with a solution containing a positively charged PA ($C_{16}O$-$V_3A_3K_3$) resulted in the immediate formation of a membrane at the interface.[123] Robust sacs were made instantly by injecting HA solution directly into the PA solution. These hierarchical structures were shown to support the growth and differentiation of human mesenchymal stem cells (MSCs) for up to 4 weeks. Using the same approach, our group has developed bioactive membranes, that result from the self-assembly between HA and $C_{16}O$-$V_3A_3K_3$ PA for wound healing applications.[124] To foster cell adhesion, the cell-adhesive sequence RGDS was integrated on the membranes ($C_{16}O$-$V_3A_3K_3$RGDS). To further expand the versatility of these self-assembled membranes, and recreate some of the aspects of the ECM remodeling, an enzymatic cleavable sequence (GPQGIWGQ) sensitive to matrix metalloproteinase-1 (MMP1) was incorporated into the PA structure.[125]

Aromatic peptides

The smallest self-assembled peptide sequence identified is the diphenylalanine (FF). This aromatic dipeptide is derived from the core recognition motif of Alzheimer's disease β-amyloid polypeptide and is self-assembled into hollow tubular assemblies.[126] Researchers have shown that short peptide sequences, containing just two or three amino acids with aromatic functionality (either provided by amino acid side chains, or by appended aromatic ligands) can form self-supporting nanostructured hydrogels.[33, 34, 127] In these systems, aromatic interactions as well as hydrogen bonding play key roles.[128] One example is the addition of the 9-fluorenylmethoxycarbonyl (Fmoc) group, which is widely used as a protecting group in peptide synthesis, to diphenylalanine peptide (Fmoc-FF) that originated biocompatible macroscopic hydrogels, with order at the nano-scale.[33, 127] These self-supporting hydrogels were able to sustain cell growth and the release of small molecules in a controlled manner.

Zhou et al.[129] have observed that the co-assembly of two aromatic short peptides, Fmoc-FF and Fmoc-RGD, resulted on the formation of a nanofibrous hydrogel through π-π stacking of the Fmoc groups, leaving the RGD groups outside the nanofiber surfaces. By inserting the cell-adhesive epitope (RGD), this approach aimed to mimic certain essential features of the ECM, and investigate their potential for applications in skin tissue engineering. The display of RGD signals within the hydrogels is tunable and was shown to have the ability to support attachment, spreading and proliferation of encapsulated human dermal fibroblasts.[129, 130]

Orbach et al.[131] have shown that similar peptides having different configurations of aromatic residues exhibited significantly different hydrogel formation kinetics. In addition, they also observed that aromatic groups had a critical role in the regulation of the self-assembly process and, consequently, influence the structural and physical properties of the formed hydrogels.

3. Applications of self-assembled peptide scaffolds in tissue engineering

Since the early 1990s it has been accepted that peptide-based biomaterials, provide valuable matrices for cell culture and tissue regeneration.[29] Self-assembling peptides are attractive as they mimic the nanofibrillar microarchitecture of the natural ECM.[35, 132] Further, the ability to incorporate peptide-based signaling sequences confers control over the function of these networks. In addition to these features, peptides have an added appeal because of their inherent biocompatibility and biodegradability.

This section of the review describes self-assembled peptide systems that have been currently designed for tissue engineering applications.

Table I.II – Examples of self-assembling biomaterials obtained from peptide building blocks designed for target applications in regenerative medicine

Biomaterial	*Composition/Formulation*	*Cells*	*Application*	*Refs*
Membranes	$C_{16}O$-$V_3A_3K_3CONH_2$, $C_{16}V_3A_3K_3$RGDS-$CONH_2$ + HA	hDFBs	Wound healing	124
	$C_{16}O$-V_3A_3GPQGIWGQK_3CONH_2 + HA			125
	NH_2-$K_2(QL)_6K_2$-$CONH_2$ + HA	rMSCs	Stem cell culture	133
	$C_{16}O$-A_4G_3LRK_2LGKA-$CONH_2$ + Hep + HA + VEGF + FGF-2	hMSCs	Angiogenesis	134
Capsules	$C_{16}O$-$V_3A_3K_3$-$CONH_2$ + $C_{16}O$-$V_3A_3E_3$-COOH	hDFbs hKc	Cell encapsulation Co-culture	135
	$C_{16}O$-$V_3A_3K_3$-$CONH_2$ + Alginate	-	Protein delivery	136
Hydrogels	$C_{16}O$-AGERGD-$CONH_2$ + BMP-2	-	Bone regeneration	137
	$C_{12}O$-VFDNFVLKK-$CONH_2$	rMSCs		59
	$C_{16}O$-$C_4G_3S^{(P)}$RGD-COOH	-	Biomineralization/Bone regeneration	31
	Ac-QQRFEWEFEQ-$CONH_2$	-	Dental tissue regeneration	138, 139
	Ac-K$(SL)_3$RG$(SL)_3$KGRGDS-$CONH_2$ + TGF-β1+ FGF-2 + VEGF)	Mesenchymal human DPSCs	Dental pulp regeneration	111
	$C_{16}O$-GTAGLIGQERGDS-$CONH_2$	SHED, DPSC	Dental tissue regeneration	112
	Ac-$(KLDL)_3$-$CONH_2$	Bovine chondrocytes	Cartilage regeneration	108
	Ac-$(KLDL)_{12}$-$CONH_2$ + TGF-β1 + IGF + dex	BMSCs		140
	Ac-$(RADA)_4$-$CONH_2$ +TGF-β3	Bovine chondrocytes		141
	Ac-HSNGLPLGGGSEEEAAAVVV(K)-$CO(CH_2)_{10}CH_2$ + TGF-β1	hMSCs		63
	Ac-$(RADA)_4$-$CONH_2$ + EGF	Fibroblasts Keratinocytes	Wound healing	142, 143
	Ac-ILVAGK-$CONH_2$ Ac-LIVAGK-$CONH_2$	-		144
	Ac-$(RADA)_4$-$CONH_2$ Ac-$(RARADADA)_2$-$CONH_2$	Rat PC12, mouse neurons, Schwann cells	Spinal cord injury/acute injured brain	107, 145, 146
	Ac$(RADA)_4$-$CONH_2$ Ac$(RADA)_4$-GG-SKPPGTSS-$CONH_2$ Ac$(RADA)_4$-GG-PFSSTKT-$CONH_2$ Ac$(RADA)_4$-GG-RGDS-$CONH_2$	mNSCs hNSCs	3D culture of neural stem cells	64, 147, 148
	$C_{16}O$-A_4G_3EIKVAV-$CONH_2$	Murine neural progenitor cells	Inhibit glial scar formation	120, 149
	Ac$(RADA)_4$- $CONH_2$ Ac-YIGSR-GG-$(RADA)_4$-$CONH_2$ Ac-RYVVLPR-GG-$(RADA)_4$-$CONH_2$ Ac-TAGSCLRKFSTM-GG-$(RADA)_4$-$CONH_2$	HAECs	Angiogenesis/ Vascularization	52
	Ac-$(RADA)_4G_4$KLTWQELYQLKYKGI-$CONH_2$ Ac-$(RADA)_4$GPRGDSGYRGDS-$CONH_2$	HUVECs		150
	Ac-$(RARADADA)_2$-$CONH_2$ + VEGF	rBMCs		151
	$C_{16}O$-A_4G_3LRKKLGKA-$CONH_2$ + Hep	mMSCs		152, 153

	$C_{16}O$-A_4G_3LRKKLGKA-$CONH_2$ + Hep + VEGF + FGF-2	mouse pancreatic islets		
	$C_{12}O$-V_2AGEGDK$^{(S)}$S-$CONH_2$	H5V, HUVECs		60
	Ac-QQKFQFQFEQQ-$CONH_2$ Ac-GGRGDSGGG- QQKFQFQFEQQ -$CONH_2$ Ac-GGIKVAVGGG- QQKFQFQFEQQ -$CONH_2$	HUVECs		154

hDFBs: human dermal fibroblasts, hKc: human epidermal keratinocytes, rMSCs: rat mensenchymal stem cells, hMSCs: human mesenchymal stem cells, mNSCs: mouse neural stem cells, hNSCs: human neural stem cells, HUVECs: human umbilical vein endothelial cells, DPSCs: dental pulp stem cells, rBMSCs: rat bone-marrow mesenchymal stem cells, mMSCs: mouse mesenchymal stem cells, SHED: stem cells from human exfoliated deciduous teeth, H5V: mouse endothelial cells, HAECs: human aortic endothelial cells, BMP-2: bone morphogenetic protein 1, TGF-β1: transforming growth factor β1, IGF: insulin growth factor, EGF: epidermal growth factor, VEGF: vascular endothelial growth factor, HA: hyaluronan, Hep: heparin, dex: dexamethasone, $S^{(P)}$: phosphorylated serine, $K^{(S)}$: sulfonated lysine

Bone

Self-assembling peptide amphiphiles have great potential as biomaterials for bone regeneration. They can originate diverse hierarchical structures, such as hydrogels for bone void filling or membranes to mimic the periostium (Fig.I.3). Hosseinkhani and co-workers developed a self-assembling peptide hydrogel to induce ectopic bone formation, by mixing a peptide amphiphile (Ac-AGERGD-COOH) with BMP-2.[137] When injected subcutaneously in the back of rats, peptide hydrogels were shown to induce ectopic bone formation by the release of BMP-2. When the same amount of BMP-2 was injected without the hydrogel, no induction in ectopic bone was observed, showing the importance of the hydrogel in the controlled release of BMP-2. Zhang and co-workers investigated the application of self-assembling peptide hydrogels of RADA16-I, commercially available as PuraMatrix™, for in vivo bone regeneration.[155, 156] When implanted in small bone defects in mice calvaria, RADA16-I, promoted bone regeneration by inducing the expression of bone-related genes such as alkaline phosphatase, Runx2, and Osterix in adjacent tissue cells.[155] Horii and co-workers have also studied the potential of RADA16-I hydrogels for bone tissue regeneration.[156] RADA16-I peptides were designed to include biological active motifs such as an osteogenic growth peptide (ALKRQGRTLYGF), an osteopontin cell adhesion motif (DGRGDSVAYG) and 2-unit RGD binding sequence (PRGDSGYRGDS). The resulting self-assembling peptide scaffolds promoted mouse pre-osteoblast MC3T3-E1 cell proliferation and an increase in alkaline phosphatase (ALP) activity and osteocalcin secretion, which are early and late markers for osteoblastic differentiation. In 2001, the Stupp laboratory designed a peptide amphiphile for biomineralization.[31] The hydrophilic domain of the PA contained four cysteines, three glycines, a single phosphorylated serine and the cell adhesion signal RGD ($C_{16}C_4G_3S^{(P)}$RGD). The PAs self-assembled into nanofibers, and were designed to direct mineralization of hydroxyapatite to form a composite material in which the crystallographic axes of hydroxyapatite are aligned with the long axes of the formed nanofibrillar structure. The intermolecular disulfide bonds formed by the crosslinking of the cysteine residues improved nanofibers robustness, increasing their resistance to pH variations. The hydroxyapatite nucleated on the surface of the nanofibers and its crystals grew with their C axes oriented along the long axes of the nanofibers.[31] Aggeli

and co-workers investigated the use of P_{11-4} peptides as injectable scaffolds for restorative treatment of bone defects, dentinal hypersensitivity and dental decay.[157] Peptides self-assembled, forming a fibrillar network within the pores of the lesion, where the anionic groups of the side chains could attract calcium ions, leading to the nucleation of hydroxyapatite, slowing down the demineralization process. The P_{11-4} peptide had been recently tested in a clinical trial as a dental filler for the treatment of early caries, and shown beneficial results in respect of enamel regeneration.[158]

Cartilage

Cartilage has limited self-healing ability because of the lack of vascular networks, the reduced availability and proliferation of chondrocytes and the formation of protease inhibitors and growth inhibitor.[159, 160] One approach widely used for cartilage regeneration, is the delivery of chondrocytes into the defect site, by using injectable systems. These systems allow the simultaneous delivery of cells and other molecules, such growth factors, to assist regeneration and stimulate cells to produce ECM. Zhang and co-workers have developed a series of ionic self-complementary peptides (Fig. I.3) that form stable hydrogels at low peptide concentrations (0.1-1%).[29, 35, 106] This peptide-based systems show great potential for use in the repair of cartilage tissue.[160-162] Peptides were composed by an alternating sequence of hydrophobic and hydrophilic residues, in which the hydrophilic residues alternate between positively and negatively charged, such as $(KLDL)_n$, $(EAKA)_n$ and $(RADA)_n$. Self-assembling peptide hydrogels, $(KLDL)_3$, were shown to maintain differentiated chondrocytes and to stimulate ECM production.[108] In addition, $(KLDL)_{12}$ peptide hydrogels loaded with growth factors (transforming growth factor β1 (TGF-β1), insulin-like growth factor-1 (IGF-1)), were shown to enhance the production of cartilage ECM macromolecules (aggrecan, type II collagen), when implanted in a critical size defect in a rabbit model.[140] The controlled release of growth factors from RADA16-I peptide hydrogels, implanted in vivo in a bovine model, has resulted in extensive synthesis of ECM macromolecules and good integration with native cartilage tissue.[141] In a different approach, Shah and co-workers have designed a self-assembling peptide hydrogel that results from the co-assembly of PAs, one displaying a binding epitope to TGF-β1 ($HSNGLPLG_3SE_3A_3V_3(K)$-$CO(CH_2)_{10}CH_3$ (Table I.II).[63] These hydrogels were able to support the survival and promote the chondrogenic differentiation of human mesenchymal stem cells (MSCs). When implanted in a full thickness chondral defect treated with microfracture in a rabbit model they were able to promote the regeneration of articular cartilage.

Wound healing

Loss of skin integrity and function due to wound injury has led to increased efforts to better design biomaterials that can optimize wound repair.[163] Schneider and co-workers developed self-assembling peptide nanofiber gels of RADA16-I combined with epidermal growth factor (EGF) as a bioactive wound dressing.[142] Human skin equivalents (HSEs) were used to study the capacity of these nanofiber gels combined with EGF, to modulate the wound healing rate in tissues that closely mimic the human wound response in vivo. Peptides underwent molecular self-assembly originating nanofibers gels that covered the surface of the wound. EGF was released from the hydrogel only when in contact with the wound and the release of EGF increased the rate of wound closure by more than 3.5 fold, when compared to hydrogels without EGF. Kao and co-workers developed a biocompatible skin mimetic system using RADA16-I peptide hydrogels.[143] Human fibroblasts were shown to proliferate within the hydrogel and to secrete collagen type I. The epidermis was stratified with three to five layers of keratinocytes, and it showed desquamation of the superficial layers. This study demonstrated that the designer self-assembling peptide nanofiber gel supported human fibroblast cell proliferation and differentiation in the three-dimensional scaffold and established fibroblast keratinocyte interactions in the scaffold.

Central nervous system

Strategies for regenerating the central nervous system (CNS) remain a significant challenge within regenerative medicine, as neurons have very limited potential for healing. Different self-assembled peptide hydrogels have been investigated for CNS repair, as they can be injected and facilitate minimally surgery. Preliminary studies using peptide hydrogels, formed by self-assembly of ionic self-complementary peptides, RAD16-I $(RADA)_4$ and RADA16-II $(RARADADA)_2$ were shown to support neuronal cell attachment, extensive neurite outgrowth, and promote active and functional synapse formations when neural cells were plated on the surface of pre-formed peptide hydrogel matrices.[107] Using the same approach, $(RADA)_4$ peptide hydrogels were shown to support the transplantation of neural progenitor cells and Schwann cells into the transected dorsal column of spinal cord of rats.[145] Both cell types were able to survive, migrate and differentiate within these hydrogels. Furthermore, there was both robust migration of host cells and growth of blood vessels into the scaffolds, showing the potential of these hydrogels to repair damaged tissue and to bridge the injured axons across the lesion site after spinal cord injury (SCI). These hydrogels were further studied for the reconstruction of acutely injured brain.[146] In hydrogel-treated animals the graft integrated well with the host tissue with no obvious gaps, showing that this matrix may help to reconstruct the acutely injured brain. Koutsopoulos and Zhang have developed a series of modified self-assembling peptide hydrogels ($(RADA)_4$) carrying the

functional motifs SKPPGTSS and PFSSTKT, which are important cellular signaling molecules with a vital role in the development of the nervous system and mediating neurotransmission, and RGDS, known to improve cell adhesion and sprouting of hippocampal mouse neurons.[148] These peptide-based matrices were able to support the culture of encapsulated adult stem cells for up to 5 months in serum-free medium conditions. Peptide functionalization with cell adhesion and cell differentiation motifs showed superior survival and differentiation properties compared to non-modified peptide hydrogels. Neural stem cells were able to differentiate into progenitor neural cells, neurons, astrocytes and oligodendrocytes, providing a platform to study neural cell proliferation and differentiation in long-term studies. In another approach, negatively charged PAs were designed to present the neurite-promoting laminin epitope, IKVAV, to mediate cell attachment and guidance.[120] Neural progenitor cells were encapsulated within the self-assembled PA hydrogel and were shown to induce very rapid differentiation of cells into neurons, while discouraging the development of astrocytes, enhancing neural attachment, migration and neurite outgrowth.[120] This model has been further used as a therapy in a mouse model of SCI.[149] The animal model used mice treated with an injection of IKVAV PA solution 24 h following SCI, forming a hydrogel by self-assembly through electrolyte screening of the molecules. When injected in vivo, the PA-based hydrogel reduced astrogliosis, reduced cell death, and increased the number of oligodendroglia at the site of injury. In addition, the PA-based hydrogel promoted the regeneration of both descending motor fibers and ascending sensory fibers through the lesion site and resulted in significant behavioral improvement.

Vascularization

The process of angiogenesis, that encompasses the formation of new blood vessels from existing vasculature, holds great potential for the treatment of several disorders, such as ischemic disease, peripheral vasculature and chronic wounds.164, 165 In regenerative medicine, an adequate blood vessel supply to the newly formed tissue and within the implanted biomaterial is critical for the success of the tissue regeneration. Genové and co-workers have developed RADA16-I self-assembling peptide hydrogels with further potential as synthetic basement membrane analogs.52 Functionalized hydrogels were developed by the inclusion of peptide motifs that are present in two major protein components of the basement membrane, laminin 1 (YIGSR, RYVVLPR), which is known to induce cell adhesion and formation of endothelial cell tubules and collagen IV (TAGSCLRKFSTM), which also promotes cell adhesion. These tailor-made hydrogels enhanced the formation of confluent cell monolayers of human aortic endothelial cells (HAEC) in culture when compared with non-functionalized hydrogels. In parallel experiments, HAECs cultured in collagen I gels or Matrigel (natural basement membrane) showed a

similar growth, suggesting that the functionalized hydrogels present potential as synthetic basement membrane mimetics. Additional assays designed to evaluate endothelial cell function indicated that HAEC monolayers not only maintain low density lipoprotein (LDL) uptake activity but also enhanced nitric oxide release and elevated laminin 1 and collagen IV deposition. Wang and co-workers have developed two functionalized self-assembling peptide hydrogels designed specifically for angiogenesis, through directly coupling pure RADA16-I with short biologically angiogenic motifs ((RADA)4G4KLTWQELYQLKYKGI and (RADA)4GPRGDSGYRGDS).150 The functionalized peptide-based hydrogels were shown to enhance endothelial cell survival, proliferation, migration, and morphological tubulogenesis compared with non-functionalized hydrogels. Interestingly, by placing functionalized and non-functionalized RADA16-I hydrogels in contact with each other, the authors observed that functionalized hydrogel could induce cell migration towards it and away from the non-functionalized hydrogel, highlighting the importance of the additional peptide motifs. Davis and co-workers injected RADA16-II peptide hydrogels into the left ventricle of mice, to create an injectable microenvironment within the myocardium, that recruit endothelial cells and promote their survival and organization.166 These self-assembling hydrogels were shown to recruit progenitor cells that express endothelial markers and vascular smooth muscle cells, which appear to form functional vascular structures. When labeled green fluorescent protein (GFP)-positive cardiomyocytes encapsulated in the hydrogel were transplanted into the mice, cells survived in the peptide microenvironment and also augmented endogenous cell recruitment. Lin and co-workers developed RADA16-II peptide based hydrogels combined with vascular endothelial growth factor (VEGF) to improve post-infarct neovascularization in rats.151 These hydrogels were shown to support the sustain delivery of VEGF within the myocardium for up to 14 days, and to create a favorable microenvironment that recruited endogenous myofibroblasts and assisted revascularization.

Heparin, a highly sulfated glycosaminoglycan that is known to bind angiogenic growth factors including VEGF167 and fibroblast growth factor-2 (FGF-2)168 through their heparin binding domain, was used to trigger the self-assembly of heparin-binding PAs.169 In vivo, these heparin-PA complexes stimulated extensive new blood vessel formation using very small amounts of growth factors in a rat corneal assay. These heparin-binding peptide amphiphile (HBPA) that self-assemble into nanofibers gels were injected into the heart following coronary artery ligation in a mouse ischemia-reperfusion model of acute myocardial infarction, with significant preservation of haemodynamic function.152 When applied in a chronic rat ischemic hind limb these HBPA nanofibers contributed to extensive limb revascularization. Chow and co-workers have used these HBPA nanofiber gels to deliver VEGF and FGF-2 into pancreatic islets.153 These hydrogels were found to be necessary to retain FGF-2 within the islet for 48 h and to

increase cell viability and insulin secretion for at least 7 days in culture. The delivery of growth factors in conjunction with the HBPA/heparin nanofibers also induced a significant amount of islet endothelial cell sprouting from the islets into the hydrogel. This approach may have significant impact on islet transplantation to treat diabetes type I. In a similar approach, these HBPA were combined with another glycosaminoglycan, hyaluronan, to create self-assembled membranes.134 Using an in vivo assay, these membranes were shown to promote rapid angiogenesis, when heparin-binding growth factors were used.

4. Conclusions

The key for developing functional biomaterials for tissue engineering applications is to understand the participating factors and to work on the design at the molecular level. Although, short peptide sequences derived from natural ECM proteins have been widely used to functionalize biomaterials, they are limited in terms of affinity and specificity, as they typically possess only one function. In contrast, natural ECM proteins are multifunctional, conferring both, biological and structural functions. Self-assembling peptides offer the possibility to integrate multiple functions within ECM mimetic matrices. These peptides can self-assemble and form hierarchical networks that mimic the nanostructure of the natural ECM. In addition, these peptides can incorporate several biological (cell adhesion and differentiation) and physical (fibrils formation and proteolytic susceptibility) functions. Unlike natural the natural ECM, these hierarchical nanostructures are chemically defined, with known amounts of each component. The tailorable nature of peptides leaves much room for the discovery and development of additional functions in the future.

References

1. W. P. Daley, S. B. Peters and M. Larsen, Extracellular matrix dynamics in development and regenerative medicine, *Journal of Cell Science*, 2008, 121, 255-264.

2. M. P. Lutolf and J. A. Hubbell, Synthetic biomaterials as instructive extracellular microenvironments for morphogenesis in tissue engineering, *Nat Biotech*, 2005, 23, 47-55.

3. A. J. Garcia, M. D. Vega and D. Boettiger, Modulation of cell proliferation and differentiation through substrate-dependent changes in fibronectin conformation, *Mol Biol Cell*, 1999, 10, 785-798.

4. K. Vallieres, P. Chevallier, C. Sarra-Bournet, S. Turgeon and G. Laroche, AFM imaging of immobilized fibronectin: does the surface conjugation scheme affect the protein orientation/conformation?, *Langmuir*, 2007, 23, 9745-9751.

5. J. H. Collier and T. Segura, Evolving the use of peptides as components of biomaterials, *Biomaterials*, 2011, 32, 4198-4204.

6. U. Hersel, C. Dahmen and H. Kessler, RGD modified polymers: biomaterials for stimulated cell adhesion and beyond, *Biomaterials*, 2003, 24, 4385-4415.

7. S. L. Bellis, Advantages of RGD peptides for directing cell association with biomaterials, *Biomaterials*, 2011, 32, 4205-4210.

8. M. A. Arnaout, B. Mahalingam and J. P. Xiong, Integrin structure, allostery, and bidirectional signaling, *Annu Rev Cell Dev Biol*, 2005, 21, 381-410.

9. E. Ruoslahti and M. Pierschbacher, New perspectives in cell adhesion: RGD and integrins, *Science*, 1987, 238, 491-497.

10. S. P. Massia and J. A. Hubbell, An RGD spacing of 440 nm is sufficient for integrin alpha-v-beta-3-mediated fibroblast spreading aad 140 nm for focal contact and stress fiber formation, *J. Cell Biol.*, 1991, 114, 1089-1100.

11. S. P. Massia and J. A. Hubbell, Human endothelial interactions with surface-coupled adhesion peptides on a nonadhesive glass substrate and 2 polymeric biomaterials, *J. Biomed. Mater. Res.*, 1991, 25, 223-242.

12. G. P. Smith and V. A. Petrenko, Phage Display, *Chemical Reviews*, 1997, 97, 391-410.

13. D. L. Hern and J. A. Hubbell, Incorporation of adhesion peptides into nonadhesive hydrogels useful for tissue resurfacing, *J Biomed Mater Res*, 1998, 39, 266-276.

14. X. Z. Shu, K. Ghosh, Y. Liu, F. S. Palumbo, Y. Luo, R. A. Clark and G. D. Prestwich, Attachment and spreading of fibroblasts on an RGD peptide-modified injectable hyaluronan hydrogel, *J Biomed Mater Res A*, 2004, 68, 365-375.

15. S. Q. Liu, P. L. Ee, C. Y. Ke, J. L. Hedrick and Y. Y. Yang, Biodegradable poly(ethylene glycol)-peptide hydrogels with well-defined structure and properties for cell delivery, *Biomaterials*, 2009, 30, 1453-1461.

16. J. A. Burdick and K. S. Anseth, Photoencapsulation of osteoblasts in injectable RGD-modified PEG hydrogels for bone tissue engineering, *Biomaterials*, 2002, 23, 4315-4323.

17. A. H. Zisch, M. P. Lutolf, M. Ehrbar, G. P. Raeber, S. C. Rizzi, N. Davies, H. Schmokel, D. Bezuidenhout, V. Djonov, P. Zilla and J. A. Hubbell, Cell-demanded release of VEGF from synthetic, biointeractive cell ingrowth matrices for vascularized tissue growth, *FASEB J*, 2003, 17, 2260-2262.

18. E. Alsberg, K. W. Anderson, A. Albeiruti, J. A. Rowley and D. J. Mooney, Engineering growing tissues, *Proceedings of the National Academy of Sciences*, 2002, 99, 12025-12030.

19. J. A. Rowley, G. Madlambayan and D. J. Mooney, Alginate hydrogels as synthetic extracellular matrix materials, *Biomaterials*, 1999, 20, 45-53.

20. E. Alsberg, K. W. Anderson, A. Albeiruti, R. T. Franceschi and D. J. Mooney, Cell-interactive alginate hydrogels for bone tissue engineering, *Journal of Dental Research*, 2001, 80, 2025-2029.

21. X. Z. Shu, K. Ghosh, Y. C. Liu, F. S. Palumbo, Y. Luo, R. A. Clark and G. D. Prestwich, Attachment and spreading of fibroblasts on an RGD peptide-modified injectable hyaluronan hydrogel, *J. Biomed. Mater. Res. Part A*, 2004, 68A, 365-375.

22. L. M. Bian, M. Guvendiren, R. L. Mauck and J. A. Burdick, Hydrogels that mimic developmentally relevant matrix and N-cadherin interactions enhance MSC chondrogenesis, *Proceedings of the National Academy of Sciences of the United States of America*, 2013, 110, 10117-10122.

23. M. P. Lutolf, J. L. Lauer-Fields, H. G. Schmoekel, A. T. Metters, F. E. Weber, G. B. Fields and J. A. Hubbell, Synthetic matrix metalloproteinase-sensitive hydrogels for the conduction of tissue regeneration: Engineering cell-invasion characteristics, *Proceedings of the National Academy of Sciences*, 2003, 100, 5413-5418.

24. M. P. Lutolf, F. E. Weber, H. G. Schmoekel, J. C. Schense, T. Kohler, R. Muller and J. A. Hubbell, Repair of bone defects using synthetic mimetics of collagenous extracellular matrices, *Nat Biotech*, 2003, 21, 513-518.

25. J. Patterson and J. A. Hubbell, SPARC-derived protease substrates to enhance the plasmin sensitivity of molecularly engineered PEG hydrogels, *Biomaterials*, 2011, 32, 1301-1310.

26. M. Ehrbar, S. C. Rizzi, R. Hlushchuk, V. Djonov, A. H. Zisch, J. A. Hubbell, F. E. Weber and M. P. Lutolf, Enzymatic formation of modular cell-instructive fibrin analogs for tissue engineering, *Biomaterials*, 2007, 28, 3856-3866.

27. E. H. C. Bromley, K. Channon, E. Moutevelis and D. N. Woolfson, Peptide and Protein Building Blocks for Synthetic Biology: From Programming Biomolecules to Self-Organized Biomolecular Systems, *ACS Chemical Biology*, 2008, 3, 38-50.

28. J. M. Mason and K. M. Arndt, Coiled Coil Domains: Stability, Specificity, and Biological Implications, *ChemBioChem*, 2004, 5, 170-176.

29. S. Zhang, T. Holmes, C. Lockshin and A. Rich, Spontaneous assembly of a self-complementary oligopeptide to form a stable macroscopic membrane, *Proceedings of the National Academy of Sciences*, 1993, 90, 3334-3338.

30. A. Aggeli, M. Bell, N. Boden, J. N. Keen, P. F. Knowles, T. C. B. McLeish, M. Pitkeathly and S. E. Radford, Responsive gels formed by the spontaneous self-assembly of peptides into polymeric [beta]-sheet tapes, *Nature*, 1997, 386, 259-262.

31. J. D. Hartgerink, E. Beniash and S. I. Stupp, Self-Assembly and Mineralization of Peptide-Amphiphile Nanofibers, *Science*, 2001, 294, 1684-1688.

32. P. Berndt, G. B. Fields and M. Tirrell, Synthetic lipidation of peptides and amino acids: monolayer structure and properties, *Journal of the American Chemical Society*, 1995, 117, 9515-9522.

33. V. Jayawarna, M. Ali, T. A. Jowitt, A. F. Miller, A. Saiani, J. E. Gough and R. V. Ulijn, Nanostructured Hydrogels for Three-Dimensional Cell Culture Through Self-Assembly of Fluorenylmethoxycarbonyl–Dipeptides, *Advanced Materials*, 2006, 18, 611-614.

34. Y. Zhang, H. Gu, Z. Yang and B. Xu, Supramolecular Hydrogels Respond to Ligand–Receptor Interaction, *Journal of the American Chemical Society*, 2003, 125, 13680-13681.

35. S. Zhang, Fabrication of novel biomaterials through molecular self-assembly, *Nat Biotech*, 2003, 21, 1171-1178.

36. Y. Loo, S. Zhang and C. A. E. Hauser, From short peptides to nanofibers to macromolecular assemblies in biomedicine, *Biotechnology Advances*, 2012, 30, 593-603.

37. H. Hosseinkhani, P.-D. Hong and D.-S. Yu, Self-Assembled Proteins and Peptides for Regenerative Medicine, *Chemical Reviews*, 2013, 113, 4837-4861.

38. X. Zhao and S. Zhang, Molecular designer self-assembling peptides, *Chemical Society Reviews*, 2006, 35, 1105-1110.

39. X. Zhao, F. Pan, H. Xu, M. Yaseen, H. Shan, C. A. E. Hauser, S. Zhang and J. R. Lu, Molecular self-assembly and applications of designer peptide amphiphiles, *Chemical Society Reviews*, 2010, 39, 3480-3498.

40. R. B. Merrifield, Solid Phase Peptide Synthesis. I. The Synthesis of a Tetrapeptide, *Journal of the American Chemical Society*, 1963, 85, 2149-2154.

41. I. Coin, M. Beyermann and M. Bienert, Solid-phase peptide synthesis: from standard procedures to the synthesis of difficult sequences, *Nat. Protocols*, 2007, 2, 3247-3256.

42. M. Amblard, J. A. Fehrentz, J. Martinez and G. Subra, Fundamentals of modern peptide synthesis, *Methods Mol Biol*, 2005, 298, 3-24.

43. M. D. Pierschbacher and E. Ruoslahti, Cell attachment activity of fibronectin can be duplicated by small synthetic fragments of the molecule, *Nature*, 1984, 309, 30-33.

44. M. O. Guler, L. Hsu, S. Soukasene, D. A. Harrington, J. F. Hulvat and S. I. Stupp, Presentation of RGDS Epitopes on Self-Assembled Nanofibers of Branched Peptide Amphiphiles, *Biomacromolecules*, 2006, 7, 1855-1863.

45. J. A. Hubbell, S. P. Massia, N. P. Desai and P. D. Drumheller, Endothelial cell-selective materials for tissue engineering in the vascular graft via a new receptor, *Bio-Technology*, 1991, 9, 568-572.

46. S. P. Massia and J. A. Hubbell, Covalent surface immobilization of Arg-Gly-Asp-containing and Tyr-Ile-Gly-Ser-Arg-containing peptides to obtain well-defined cell-adhesive substrates, *Anal. Biochem.*, 1990, 187, 292-301.

47. K. E. Healy, A. Rezania and R. A. Stile, Designing biomaterials to direct biological responses, *Ann N Y Acad Sci*, 1999, 875, 24-35.

48. Y. Feng and M. Mrksich, The Synergy Peptide PHSRN and the Adhesion Peptide RGD Mediate Cell Adhesion through a Common Mechanism†, *Biochemistry*, 2004, 43, 15811-15821.

49. S. P. Massia and J. A. Hubbell, Vascular endothelial-cell adhesion and spreading promoted by the peptide REDV of the IIICs region of plasma fibronectin is mediated by integrin-4-beta-1, *J. Biol. Chem.*, 1992, 267, 14019-14026.

50. K. Tashiro, G. C. Sephel, B. Weeks, M. Sasaki, G. R. Martin, H. K. Kleinman and Y. Yamada, A synthetic peptide containing the IKVAV sequence from the A chain of laminin mediates cell attachment, migration, and neurite outgrowth, *J. Biol. Chem.*, 1989, 264, 16174-16182.

51. J. Graf, R. C. Ogle, F. A. Robey, M. Sasaki, G. R. Martin, Y. Yamada and H. K. Kleinman, A pentapeptide from the laminin-B1 chain mediates cell-adhesion and binds the 67000-laminin receptor, *Biochemistry*, 1987, 26, 6896-6900.

52. E. Genové, C. Shen, S. Zhang and C. E. Semino, The effect of functionalized self-assembling peptide scaffolds on human aortic endothelial cell function, *Biomaterials*, 2005, 26, 3341-3351.

53. C. G. Knight, L. F. Morton, D. J. Onley, A. R. Peachey, A. J. Messent, P. A. Smethurst, D. S. Tuckwell, R. W. Farndale and M. J. Barnes, Identification in Collagen Type I of an Integrin $\alpha 2\beta 1$-binding Site Containing an Essential GER Sequence, *J. Biol. Chem.*, 1998, 273, 33287-33294.

54. B. E. Turk, L. L. Huang, E. T. Piro and L. C. Cantley, Determination of protease cleavage site motifs using mixture-based oriented peptide libraries, *Nat Biotech*, 2001, 19, 661-667.

55. H. Kato, N. Adachi, Y. Ohno, S. Iwanaga, K. Takada and S. Sakakibara, New fluorogenic peptide substrates for plasmin, *J Biochem*, 1980, 88, 183-190.

56. R. Tyler-Cross, R. B. Harris, M. Sobel and D. Marques, Heparin binding domain peptides of antithrombin III: Analysis by isothermal titration calorimetry and circular dichroism spectroscopy, *Protein Science*, 1994, 3, 620-627.

57. S. H. Kim and K. L. Kiick, Heparin-mimetic sulfated peptides with modulated affinities for heparin-binding peptides and growth factors, *Peptides*, 2007, 28, 2125-2136.

58. A. D. Cardin and H. J. Weintraub, Molecular modeling of protein-glycosaminoglycan interactions, *Arteriosclerosis, Thrombosis, and Vascular Biology*, 1989, 9, 21-32.

59. M. Sever, B. Mammadov, M. O. Guler and A. B. Tekinay, Tenascin-C Mimetic Peptide Nanofibers Direct Stem Cell Differentiation to Osteogenic Lineage, *Biomacromolecules*, 2014.

60. R. Mammadov, B. Mammadov, S. Toksoz, B. Aydin, R. Yagci, A. B. Tekinay and M. O. Guler, Heparin Mimetic Peptide Nanofibers Promote Angiogenesis, *Biomacromolecules*, 2011, 12, 3508-3519.

61. A. M. Wojtowicz, A. Shekaran, M. E. Oest, K. M. Dupont, K. L. Templeman, D. W. Hutmacher, R. E. Guldberg and A. J. Garcia, Coating of biomaterial scaffolds with the collagen-mimetic peptide GFOGER for bone defect repair, *Biomaterials*, 2010, 31, 2574-2582.

62. C.-C. Lin and K. S. Anseth, Controlling Affinity Binding with Peptide-Functionalized Poly(ethylene glycol) Hydrogels, *Advanced Functional Materials*, 2009, 19, 2325-2331.

63. R. N. Shah, N. A. Shah, M. M. Del Rosario Lim, C. Hsieh, G. Nuber and S. I. Stupp, Supramolecular design of self-assembling nanofibers for cartilage regeneration, *Proceedings of the National Academy of Sciences*, 2010, 107, 3293-3298.

64. F. Gelain, D. Silva, A. Caprini, F. Taraballi, A. Natalello, O. Villa, K. T. Nam, R. N. Zuckermann, S. M. Doglia and A. Vescovi, BMHP1-derived self-assembling peptides: hierarchically assembled structures with self-healing propensity and potential for tissue engineering applications, *ACS Nano*, 2011, 5, 1845-1859.

65. A. Saito, Y. Suzuki, S.-I. Ogata, C. Ohtsuki and M. Tanihara, Accelerated bone repair with the use of a synthetic BMP-2-derived peptide and bone-marrow stromal cells, *J. Biomed. Mater. Res. Part A*, 2005, 72A, 77-82.

66. A. Saito, Y. Suzuki, S.-i. Ogata, C. Ohtsuki and M. Tanihara, Activation of osteo-progenitor cells by a novel synthetic peptide derived from the bone morphogenetic protein-2 knuckle epitope, *Biochimica et Biophysica Acta (BBA) - Proteins and Proteomics*, 2003, 1651, 60-67.

67. J. S. Lee, J. S. Lee, A. Wagoner-Johnson and W. L. Murphy, Modular Peptide Growth Factors for Substrate-Mediated Stem Cell Differentiation, *Angewandte Chemie International Edition*, 2009, 48, 6266-6269.

68. Z. Duan, Q. Zheng, X. Guo, Q. Yuan and S. Chen, Experimental research on ectopic osteogenesis of BMP2-derived peptide P24 combined with PLGA copolymers, *J. Huazhong Univ. Sc. Technol.*, 2007, 27, 179-182.

69. K. Kirkwood, B. Rheude, Y. J. Kim, K. White and K. C. Dee, In Vitro Mineralization Studies with Substrate-immobilized Bone Morphogenetic Protein Peptides, *Journal of Oral Implantology*, 2003, 29, 57-65.

70. L. D. D'Andrea, G. Iaccarino, R. Fattorusso, D. Sorriento, C. Carannante, D. Capasso, B. Trimarco and C. Pedone, Targeting angiogenesis: Structural characterization and biological properties of a de novo engineered VEGF mimicking peptide, *Proceedings of the National Academy of Sciences of the United States of America*, 2005, 102, 14215-14220.

71. S. P. Massia, S. S. Rao and J. A. Hubbell, Covalently immobilized laminin peptide Tyr-Ile-Gly-Ser-Arg (YIGSR) supports cell spreading and co-localization of the 67-kilodalton laminin receptor with alpha-actinin and vinculin, *J Biol Chem*, 1993, 268, 8053-8059.

72. M. Nomizu, B. S. Weeks, C. A. Weston, W. H. Kim, H. K. Kleinman and Y. Yamada, Structure-activity study of a laminin $\alpha 1$ chain active peptide segment Ile-Lys-Val-Ala-Val (IKVAV), *FEBS Letters*, 1995, 365, 227-231.

73. Y. Chau, Y. Luo, A. C. Y. Cheung, Y. Nagai, S. Zhang, J. B. Kobler, S. M. Zeitels and R. Langer, Incorporation of a matrix metalloproteinase-sensitive substrate into self-assembling peptides – A model for biofunctional scaffolds, *Biomaterials*, 2008, 29, 1713-1719.

74. K. M. Galler, L. Aulisa, K. R. Regan, R. N. D'Souza and J. D. Hartgerink, Self-Assembling Multidomain Peptide Hydrogels: Designed Susceptibility to Enzymatic Cleavage Allows Enhanced Cell Migration and Spreading, *Journal of the American Chemical Society*, 2010, 132, 3217-3223.

75. K. B. Fonseca, F. R. Maia, F. A. Cruz, D. Andrade, M. A. Juliano, P. L. Granja and C. C. Barrias, Enzymatic, physicochemical and biological properties of MMP-sensitive alginate hydrogels, *Soft Matter*, 2013, 9, 3283-3292.

76. D. Seliktar, A. H. Zisch, M. P. Lutolf, J. L. Wrana and J. A. Hubbell, MMP-2 sensitive, VEGF-bearing bioactive hydrogels for promotion of vascular healing, *J. Biomed. Mater. Res. Part A*, 2004, 68A, 704-716.

77. Y. A. Lin, Y. C. Ou, A. G. Cheetham and H. G. Cui, Rational Design of MMP Degradable Peptide-Based Supramolecular Filaments, *Biomacromolecules*, 2014, 15, 1419-1427.

78. A. B. Pratt, F. E. Weber, H. G. Schmoekel, R. Müller and J. A. Hubbell, Synthetic extracellular matrices for in situ tissue engineering, *Biotechnology and Bioengineering*, 2004, 86, 27-36.

79. A. M. Wojtowicz, A. Shekaran, M. E. Oest, K. M. Dupont, K. L. Templeman, D. W. Hutmacher, R. E. Guldberg and A. J. García, Coating of biomaterial scaffolds with the collagen-mimetic peptide GFOGER for bone defect repair, *Biomaterials*, 2010, 31, 2574-2582.

80. C. D. Reyes and A. J. García, Engineering integrin-specific surfaces with a triple-helical collagen-mimetic peptide, *J. Biomed. Mater. Res. Part A*, 2003, 65A, 511-523.

81. R. Mammadov, B. Mammadov, M. O. Guler and A. B. Tekinay, Growth Factor Binding on Heparin Mimetic Peptide Nanofibers, *Biomacromolecules*, 2012, 13, 3311-3319.

82. R. M. Scarborough and D. D. Gretler, Platelet glycoprotein IIb-IIIa antagonists as prototypical integrin blockers: novel parenteral and potential oral antithrombotic agents, *J Med Chem*, 2000, 43, 3453-3473.

83. P. R. Patel, R. C. Kiser, Y. Y. Lu, E. Fong, W. C. Ho, D. A. Tirrell and R. H. Grubbs, Synthesis and Cell Adhesive Properties of Linear and Cyclic RGD Functionalized Polynorbornene Thin Films, *Biomacromolecules*, 2012, 13, 2546-2553.

84. M. D. Pierschbacher and E. Ruoslahti, Influence of stereochemistry of the sequence Arg-Gly-Asp-Xaa on binding specificity in cell adhesion, *J. Biol. Chem.*, 1987, 262, 17294-17298.

85. T. Pakalns, K. L. Haverstick, G. B. Fields, J. B. McCarthy, D. L. Mooradian and M. Tirrell, Cellular recognition of synthetic peptide amphiphiles in self-assembled monolayer films, *Biomaterials*, 1999, 20, 2265-2279.

86. N. R. Gandavarapu, D. L. Alge and K. S. Anseth, Osteogenic differentiation of human mesenchymal stem cells on [small alpha]5 integrin binding peptide hydrogels is dependent on substrate elasticity, *Biomaterials Science*, 2014, 2, 352-361.

87. B. A. Grzybowski, C. E. Wilmer, J. Kim, K. P. Browne and K. J. M. Bishop, Self-assembly: from crystals to cells, *Soft Matter*, 2009, 5, 1110-1128.

88. G. M. Whitesides and B. Grzybowski, Self-Assembly at All Scales, *Science*, 2002, 295, 2418-2421.

89. G. Whitesides, J. Mathias and C. Seto, Molecular self-assembly and nanochemistry: a chemical strategy for the synthesis of nanostructures, *Science*, 1991, 254, 1312-1319.

90. L. C. Palmer and S. I. Stupp, Molecular self-assembly into one-dimensional nanostructures, *Acc Chem Res*, 2008, 41, 1674-1684.

91. L. C. Palmer, Y. S. Velichko, M. O. d. l. Cruz and S. I. Stupp, Supramolecular Self-Assembly Codes for Functional Structures, *Philosophical Transactions: Mathematical, Physical and Engineering Sciences*, 2007, 365, 1417-1433.

92. R. V. Ulijn and A. M. Smith, Designing peptide based nanomaterials, *Chemical Society Reviews*, 2008, 37, 664-675.

93. W. S. Childers, R. Ni, A. K. Mehta and D. G. Lynn, Peptide membranes in chemical evolution, *Current Opinion in Chemical Biology*, 2009, 13, 652-659.

94. E. Gazit, Bioinspired chemistry: Diversity for self-assembly, *Nat Chem*, 2010, 2, 1010-1011.

95. E. Gazit, Self-assembled peptide nanostructures: the design of molecular building blocks and their technological utilization, *Chemical Society Reviews*, 2007, 36, 1263-1269.

96. S. Zhang, Emerging biological materials through molecular self-assembly, *Biotechnology Advances*, 2002, 20, 321-339.

97. D. N. Woolfson, in *Advances in Protein Chemistry*, eds. A. D. P. David and M. S. John, Academic Press, 2005, vol. Volume 70, pp. 79-112.

98. E. F. Banwell, E. S. Abelardo, D. J. Adams, M. A. Birchall, A. Corrigan, A. M. Donald, M. Kirkland, L. C. Serpell, M. F. Butler and D. N. Woolfson, Rational design and application of responsive [alpha]-helical peptide hydrogels, *Nat Mater*, 2009, 8, 596-600.

99. D. N. Woolfson, Building fibrous biomaterials from α-helical and collagen-like coiled-coil peptides, *Peptide Science*, 2010, 94, 118-127.

100. C. Gribbon, K. J. Channon, W. Zhang, E. F. Banwell, E. H. C. Bromley, J. B. Chaudhuri, R. O. C. Oreffo and D. N. Woolfson, MagicWand: A Single, Designed Peptide That Assembles to Stable, Ordered α-Helical Fibers†, *Biochemistry*, 2008, 47, 10365-10371.

101. V. Villard, O. Kalyuzhniy, O. Riccio, S. Potekhin, T. N. Melnik, A. V. Kajava, C. Ruegg and G. Corradin, Synthetic RGD-containing alpha-helical coiled coil peptides promote integrin-dependent cell adhesion, *J Pept Sci*, 2006, 12, 206-212.

102. L. E. R. O'Leary, J. A. Fallas, E. L. Bakota, M. K. Kang and J. D. Hartgerink, Multi-hierarchical self-assembly of a collagen mimetic peptide from triple helix to nanofibre and hydrogel, *Nat Chem*, 2011, 3, 821-828.

103. S. Rele, Y. Song, R. P. Apkarian, Z. Qu, V. P. Conticello and E. L. Chaikof, D-Periodic Collagen-Mimetic Microfibers, *Journal of the American Chemical Society*, 2007, 129, 14780-14787.

104. J. H. Collier, B. H. Hu, J. W. Ruberti, J. Zhang, P. Shum, D. H. Thompson and P. B. Messersmith, Thermally and Photochemically Triggered Self-Assembly of Peptide Hydrogels, *Journal of the American Chemical Society*, 2001, 123, 9463-9464.

105. S. Zhang, C. Lockshin, R. Cook and A. Rich, Unusually stable beta-sheet formation in an ionic self-complementary oligopeptide, *Biopolymers*, 1994, 34, 663-672.

106. S. Zhang, T. C. Holmes, C. M. DiPersio, R. O. Hynes, X. Su and A. Rich, Self-complementary oligopeptide matrices support mammalian cell attachment, *Biomaterials*, 1995, 16, 1385-1393.

107. T. C. Holmes, S. de Lacalle, X. Su, G. Liu, A. Rich and S. Zhang, Extensive neurite outgrowth and active synapse formation on self-assembling peptide scaffolds, *Proceedings of the National Academy of Sciences*, 2000, 97, 6728-6733.

108. J. Kisiday, M. Jin, B. Kurz, H. Hung, C. Semino, S. Zhang and A. J. Grodzinsky, Self-assembling peptide hydrogel fosters chondrocyte extracellular matrix production and cell division: Implications for cartilage tissue repair, *Proceedings of the National Academy of Sciences*, 2002, 99, 9996-10001.

109. H. Dong, S. E. Paramonov, L. Aulisa, E. L. Bakota and J. D. Hartgerink, Self-Assembly of Multidomain Peptides: Balancing Molecular Frustration Controls Conformation and Nanostructure, *Journal of the American Chemical Society*, 2007, 129, 12468-12472.

110. L. Aulisa, H. Dong and J. D. Hartgerink, Self-Assembly of Multidomain Peptides: Sequence Variation Allows Control over Cross-Linking and Viscoelasticity, *Biomacromolecules*, 2009, 10, 2694-2698.

111. K. M. Galler, J. D. Hartgerink, A. C. Cavender, G. Schmalz and R. N. D'Souza, A Customized Self-Assembling Peptide Hydrogel for Dental Pulp Tissue Engineering, *Tissue Engineering Part A*, 2011, 18, 176-184.

112. K. M. Galler, A. Cavender, V. Yuwono, H. Dong, S. Shi, G. Schmalz, J. D. Hartgerink and R. N. D'Souza, Self-Assembling Peptide Amphiphile Nanofibers as a Scaffold for Dental Stem Cells, *Tissue Engineering Part A*, 2008, 14, 2051-2058.

113. A. Aggeli, I. A. Nyrkova, M. Bell, R. Harding, L. Carrick, T. C. B. McLeish, A. N. Semenov and N. Boden, Hierarchical self-assembly of chiral rod-like molecules as a model for peptide β-sheet tapes, ribbons, fibrils, and fibers, *Proceedings of the National Academy of Sciences*, 2001, 98, 11857-11862.

114. A. Aggeli, M. Bell, L. M. Carrick, C. W. G. Fishwick, R. Harding, P. J. Mawer, S. E. Radford, A. E. Strong and N. Boden, pH as a Trigger of Peptide β-Sheet Self-Assembly and Reversible Switching

between Nematic and Isotropic Phases, *Journal of the American Chemical Society*, 2003, 125, 9619-9628.

115. S. Ramachandran, Y. Tseng and Y. B. Yu, Repeated rapid shear-responsiveness of peptide hydrogels with tunable shear modulus, *Biomacromolecules*, 2005, 6, 1316-1321.

116. J. H. Collier and P. B. Messersmith, Enzymatic modification of self-assembled peptide structures with tissue transglutaminase, *Bioconjug Chem*, 2003, 14, 748-755.

117. J. P. Jung, A. K. Nagaraj, E. K. Fox, J. S. Rudra, J. M. Devgun and J. H. Collier, Co-assembling peptides as defined matrices for endothelial cells, *Biomaterials*, 2009, 30, 2400-2410.

118. M. J. Webber, J. A. Kessler and S. I. Stupp, Emerging peptide nanomedicine to regenerate tissues and organs, *Journal of Internal Medicine*, 2010, 267, 71-88.

119. Y. S. Velichko, S. I. Stupp and M. O. de la Cruz, Molecular Simulation Study of Peptide Amphiphile Self-Assembly, *The Journal of Physical Chemistry B*, 2008, 112, 2326-2334.

120. G. A. Silva, C. Czeisler, K. L. Niece, E. Beniash, D. A. Harrington, J. A. Kessler and S. I. Stupp, Selective Differentiation of Neural Progenitor Cells by High-Epitope Density Nanofibers, *Science*, 2004, 303, 1352-1355.

121. J. C. Stendahl, M. S. Rao, M. O. Guler and S. I. Stupp, Intermolecular Forces in the Self-Assembly of Peptide Amphiphile Nanofibers, *Advanced Functional Materials*, 2006, 16, 499-508.

122. E. Beniash, J. D. Hartgerink, H. Storrie, J. C. Stendahl and S. I. Stupp, Self-assembling peptide amphiphile nanofiber matrices for cell entrapment, *Acta Biomaterialia*, 2005, 1, 387-397.

123. R. M. Capito, H. S. Azevedo, Y. S. Velichko, A. Mata and S. I. Stupp, Self-Assembly of Large and Small Molecules into Hierarchically Ordered Sacs and Membranes, *Science*, 2008, 319, 1812-1816.

124. D. S. Ferreira, A. P. Marques, R. L. Reis and H. S. Azevedo, Hyaluronan and self-assembling peptides as building blocks to reconstruct the extracellular environment in skin tissue, *Biomaterials Science*, 2013, 1, 952-964.

125. D. S. Ferreira, Y.-A. Lin, H. Cui, J. A. Hubbell, R. L. Reis and H. S. Azevedo, Molecularly Engineered Self-assembling Membranes for Cell-Mediated Degradation, *Advanced Healthcare Materials*, 2014.

126. M. Reches and E. Gazit, Casting Metal Nanowires Within Discrete Self-Assembled Peptide Nanotubes, *Science*, 2003, 300, 625-627.

127. A. Mahler, M. Reches, M. Rechter, S. Cohen and E. Gazit, Rigid, Self-Assembled Hydrogel Composed of a Modified Aromatic Dipeptide, *Advanced Materials*, 2006, 18, 1365-1370.

128. A. M. Smith, R. J. Williams, C. Tang, P. Coppo, R. F. Collins, M. L. Turner, A. Saiani and R. V. Ulijn, Fmoc-Diphenylalanine Self Assembles to a Hydrogel via a Novel Architecture Based on π–π Interlocked β-Sheets, *Advanced Materials*, 2008, 20, 37-41.

129. M. Zhou, A. M. Smith, A. K. Das, N. W. Hodson, R. F. Collins, R. V. Ulijn and J. E. Gough, Self-assembled peptide-based hydrogels as scaffolds for anchorage-dependent cells, *Biomaterials*, 2009, 30, 2523-2530.

130. M. Zhou, R. V. Ulijn and J. E. Gough, Extracellular matrix formation in self-assembled minimalistic bioactive hydrogels based on aromatic peptide amphiphiles, *Journal of Tissue Engineering*, 2014, 5.

131. R. Orbach, I. Mironi-Harpaz, L. Adler-Abramovich, E. Mossou, E. P. Mitchell, V. T. Forsyth, E. Gazit and D. Seliktar, The Rheological and Structural Properties of Fmoc-Peptide-Based Hydrogels: The Effect of Aromatic Molecular Architecture on Self-Assembly and Physical Characteristics, *Langmuir*, 2012, 28, 2015-2022.

132. V. P. Shastri, In vivo Engineering of Tissues: Biological Considerations, Challenges, Strategies, and Future Directions, *Advanced Materials*, 2009, 21, n/a-n/a.

133. A. C. Mendes, K. H. Smith, E. Tejeda-Montes, E. Engel, R. L. Reis, H. S. Azevedo and A. Mata, Co-Assembled and Microfabricated Bioactive Membranes, *Advanced Functional Materials*, 2013, 23, 430-438.

134. L. W. Chow, R. Bitton, M. J. Webber, D. Carvajal, K. R. Shull, A. K. Sharma and S. I. Stupp, A bioactive self-assembled membrane to promote angiogenesis, *Biomaterials*, 2011, 32, 1574-1582.

135. D. S. Ferreira, R. L. Reis and H. S. Azevedo, Peptide-based microcapsules obtained by self-assembly and microfluidics as controlled environments for cell culture, *Soft Matter*, 2013, 9, 9237-9248.

136. D. I. Rozkiewicz, B. D. Myers and S. I. Stupp, Interfacial Self-Assembly of Cell-like Filamentous Microcapsules, *Angew. Chem.-Int. Edit.*, 2011, 50, 6324-6327.

137. H. Hosseinkhani, M. Hosseinkhani, A. Khademhosseini and H. Kobayashi, Bone regeneration through controlled release of bone morphogenetic protein-2 from 3-D tissue engineered nano-scaffold, *J Control Release*, 2007, 117, 380-386.

138. A. Jablonski-Momeni and M. Heinzel-Gutenbrunner, Efficacy of the self-assembling peptide P11-4 in constructing a remineralization scaffold on artificially-induced enamel lesions on smooth surfaces, *J. Orofac. Orthop.*, 2014, 75, 175-190.

139. P. A. Brunton, R. P. W. Davies, J. L. Burke, A. Smith, A. Aggeli, S. J. Brookes and J. Kirkham, Treatment of early caries lesions using biomimetic self-assembling peptides - a clinical safety trial, *Br. Dent. J.*, 2013, 215.

140. R. E. Miller, A. J. Grodzinsky, E. J. Vanderploeg, C. Lee, D. J. Ferris, M. F. Barrett, J. D. Kisiday and D. D. Frisbie, Effect of self-assembling peptide, chondrogenic factors, and bone marrow-derived stromal cells on osteochondral repair, *Osteoarthritis and Cartilage*, 2010, 18, 1608-1619.

141. S. A. Maher, R. L. Mauck, L. Rackwitz and R. S. Tuan, A nanofibrous cell-seeded hydrogel promotes integration in a cartilage gap model, *J. Tissue Eng. Regen. Med.*, 2010, 4, 25-29.

142. A. Schneider, J. A. Garlick and C. Egles, Self-Assembling Peptide Nanofiber Scaffolds Accelerate Wound Healing, *PLoS ONE*, 2008, 3, e1410.

143. B. Kao, K. Kadomatsu and Y. Hosaka, Construction of Synthetic Dermis and Skin Based on a Self-Assembled Peptide Hydrogel Scaffold, *Tissue Engineering Part A*, 2009, 15, 2385-2396.

144. Y. Loo, Y.-C. Wong, E. Z. Cai, C.-H. Ang, A. Raju, A. Lakshmanan, A. G. Koh, H. J. Zhou, T.-C. Lim, S. M. Moochhala and C. A. E. Hauser, Ultrashort peptide nanofibrous hydrogels for the acceleration of healing of burn wounds, *Biomaterials*, 2014, 35, 4805-4814.

145. J. Guo, H. Su, Y. Zeng, Y.-X. Liang, W. M. Wong, R. G. Ellis-Behnke, K.-F. So and W. Wu, Reknitting the injured spinal cord by self-assembling peptide nanofiber scaffold, *Nanomedicine: Nanotechnology, Biology and Medicine*, 2007, 3, 311-321.

146. J. Guo, K. K. G. Leung, H. Su, Q. Yuan, L. Wang, T.-H. Chu, W. Zhang, J. K. S. Pu, G. K. P. Ng, W. M. Wong, X. Dai and W. Wu, Self-assembling peptide nanofiber scaffold promotes the reconstruction of acutely injured brain, *Nanomedicine: Nanotechnology, Biology and Medicine*, 2009, 5, 345-351.

147. F. Gelain, D. Bottai, A. Vescovi and S. Zhang, Designer Self-Assembling Peptide Nanofiber Scaffolds for Adult Mouse Neural Stem Cell 3-Dimensional Cultures, *PLoS ONE*, 2006, 1, e119.

148. S. Koutsopoulos and S. Zhang, Long-term three-dimensional neural tissue cultures in functionalized self-assembling peptide hydrogels, Matrigel and Collagen I, *Acta Biomaterialia*, 2013, 9, 5162-5169.

149. V. M. Tysseling-Mattiace, V. Sahni, K. L. Niece, D. Birch, C. Czeisler, M. G. Fehlings, S. I. Stupp and J. A. Kessler, Self-Assembling Nanofibers Inhibit Glial Scar Formation and Promote Axon Elongation after Spinal Cord Injury, *The Journal of Neuroscience*, 2008, 28, 3814-3823.

150. X. Wang, A. Horii and S. Zhang, Designer functionalized self-assembling peptide nanofiber scaffolds for growth, migration, and tubulogenesis of human umbilical vein endothelial cells, *Soft Matter*, 2008, 4, 2388-2395.

151. Y. D. Lin, C. Y. Luo, Y. N. Hu, M. L. Yeh, Y. C. Hsueh, M. Y. Chang, D. C. Tsai, J. N. Wang, M. J. Tang, E. I. Wei, M. L. Springer and P. C. Hsieh, Instructive nanofiber scaffolds with VEGF create a microenvironment for arteriogenesis and cardiac repair, *Sci Transl Med*, 2012, 4, 146ra109.

152. M. J. Webber, X. Han, S. N. Prasanna Murthy, K. Rajangam, S. I. Stupp and J. W. Lomasney, Capturing the stem cell paracrine effect using heparin-presenting nanofibres to treat cardiovascular diseases, *J. Tissue Eng. Regen. Med.*, 2010, 4, 600-610.

153. L. W. Chow, L.-j. Wang, D. B. Kaufman and S. I. Stupp, Self-assembling nanostructures to deliver angiogenic factors to pancreatic islets, *Biomaterials*, 2010, 31, 6154-6161.

154. J. P. Jung, A. K. Nagaraj, E. K. Fox, J. S. Rudra, J. M. Devgun and J. H. Collier, Co-assembling peptides as defined matrices for endothelial cells, *Biomaterials*, 2009, 30, 2400-2410.

155. H. Misawa, N. Kobayashi, A. Soto-Gutierrez, Y. Chen, A. Yoshida, J. D. Rivas-Carrillo, N. Navarro-Alvarez, K. Tanaka, A. Miki, J. Takei, T. Ueda, M. Tanaka, H. Endo, N. Tanaka and T. Ozaki, PuraMatrix facilitates bone regeneration in bone defects of calvaria in mice, *Cell Transplant*, 2006, 15, 903-910.

156. A. Horii, X. Wang, F. Gelain and S. Zhang, Biological Designer Self-Assembling Peptide Nanofiber Scaffolds Significantly Enhance Osteoblast Proliferation, Differentiation and 3-D Migration, *PLoS ONE*, 2007, 2, e190.

157. A. Firth, A. Aggeli, J. L. Burke, X. Yang and J. Kirkham, Biomimetic self-assembling peptides as injectable scaffolds for hard tissue engineering, *Nanomedicine (Lond)*, 2006, 1, 189-199.

158. P. A. Brunton, R. P. Davies, J. L. Burke, A. Smith, A. Aggeli, S. J. Brookes and J. Kirkham, Treatment of early caries lesions using biomimetic self-assembling peptides–a clinical safety trial, *Br Dent J*, 2013, 215, E6.

159. G. A. Ateshian, Artificial cartilage: Weaving in three dimensions, *Nat Mater*, 2007, 6, 89-90.

160. B. He, X. Yuan, A. Zhou, H. Zhang and D. Jiang, Designer functionalised self-assembling peptide nanofibre scaffolds for cartilage tissue engineering, *Expert Reviews in Molecular Medicine*, 2014, 16, null-null.

161. J. Kisiday, M. Jin, B. Kurz, H. Hung, C. Semino, S. Zhang and A. J. Grodzinsky, Self-assembling peptide hydrogel fosters chondrocyte extracellular matrix production and cell division: Implications for cartilage tissue repair, *Proceedings of the National Academy of Sciences of the United States of America*, 2002, 99, 9996-10001.

162. A. Mujeeb, A. F. Miller, A. Saiani and J. E. Gough, Self-assembled octapeptide scaffolds for in vitro chondrocyte culture, *Acta Biomaterialia*, 2013, 9, 4609-4617.

163. V. G. Shalini, N. J. Eric and S. N. Lakshmi, in *Nanotechnology and Regenerative Engineering*, CRC Press, 2014, pp. 343-366.

164. A. Bikfalvi, Angiogenesis: molecular mechanisms of activation, promotion and maintenance, *J BUON*, 2007, 12 Suppl 1, S59-66.

165. J. Folkman, Fundamental concepts of the angiogenic process, *Curr Mol Med*, 2003, 3, 643-651.

166. M. E. Davis, J. P. Motion, D. A. Narmoneva, T. Takahashi, D. Hakuno, R. D. Kamm, S. Zhang and R. T. Lee, Injectable self-assembling peptide nanofibers create intramyocardial microenvironments for endothelial cells, *Circulation*, 2005, 111, 442-450.

167. N. Ferrara, H. P. Gerber and J. LeCouter, The biology of VEGF and its receptors, *Nat Med*, 2003, 9, 669-676.

168. J. Schlessinger, A. N. Plotnikov, O. A. Ibrahimi, A. V. Eliseenkova, B. K. Yeh, A. Yayon, R. J. Linhardt and M. Mohammadi, Crystal structure of a ternary FGF-FGFR-heparin complex reveals a dual role for heparin in FGFR binding and dimerization, *Mol Cell*, 2000, 6, 743-750.

169. K. Rajangam, H. A. Behanna, M. J. Hui, X. Han, J. F. Hulvat, J. W. Lomasney and S. I. Stupp, Heparin Binding Nanostructures to Promote Growth of Blood Vessels, *Nano Letters*, 2006, 6, 2086-2090.

Section 2

EXPERIMENTAL

Chapter II

Materials and Methods

Chapter II

Materials and Methods

Chapter II – Materials and Methods

Although this thesis is based on published or submitted papers, and chapters III to VII have an own materials and methods section, this chapter aims to provide additional details on the experimental procedures used in the PhD work and on the rationale for the selection of materials and characterization techniques, thus complementing the information given on each experimental chapter.

1. Materials

1.1 General chemicals

The majority of the chemical reagents, unless noted otherwise, were purchased from Sigma (USA) and used as provided. Protected amino acids and resins for peptide synthesis were purchased from Novabiochem (USA). O-(benzotriazol-1-yl)-N,N,N',N'-tetramethyluronium (HBTU) was from Carbosynth (UK). Solvents for high performance liquid chromatography (HPLC) were of HPLC grade and obtained from BDH Prolabo (VWR, Portugal). Details are presented for each chemical when used for the first time in this chapter.

1.2 Hyaluronan

Hyaluronan (HA), also known as hyaluronic acid or hyaluronate, is an extracellular matrix (ECM) anionic polysaccharide found throughout mammalian connective tissues. It is a linear glycosaminoglycan composed of uniformly repetitive disaccharide units of N-acetyl-glucosamine and D-glucuronic acid (Fig. II.1).

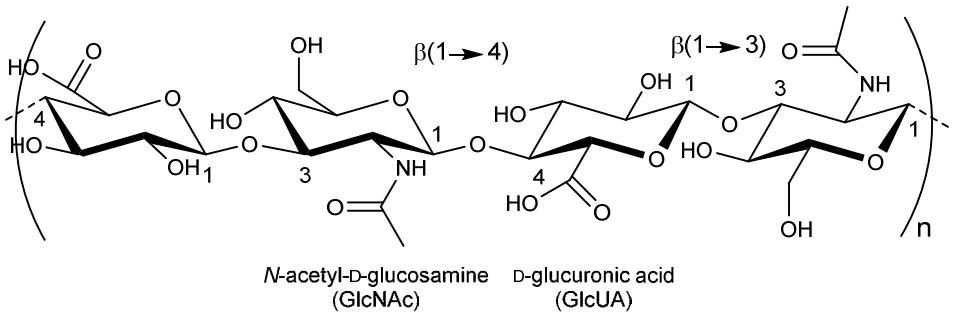

Figure II.1 – Chemical structure of hyaluronan repeating unit.

Depending on the tissue source, HA ranges in relative molecular mass from 10^5–10^7 Da (~2,000-25,000 disaccharides) with polymer lengths of 2–25 μm. In solution, under normal physiological conditions of pH and ionic strength, HA forms a stiffened and expanded random coil due to hydrogen bonding of adjacent sugar units and mutual repulsion between carboxyl groups.[1] HA is known to be involved in essential physiological and pathological processes such as embryological development, migration, adhesion, proliferation and differentiation of cells, immune response, inflammation, angiogenesis and wound healing. The biological functions exhibited by HA depend on the chain length, molecular mass and on the circumstances under which is synthesized.[2] Because of its unique physicochemical properties, and most importantly due its complex interactions with ECM components

and cells, HA is an ideal biomaterial candidate for applications in regenerative medicine and has been chosen as the main polymer used in this work.

The HA used in all experiments had an average molecular mass of 2 MDa (Chapter III), 1.5 MDa (chapter V-VII) 750 and 234 kDa (chapter VI-VII) and was purchased from Lifecore Biomedical, Inc. (Chaska, USA).

1.2.1 HA fluorescent labeling

To evaluate the distribution of HA within the developed membranes (Chapter III), fluorescently labeled HA was synthesized. HA was fluorescently labeled with fluoresceinamine (Fig. II.2) using N-(3-dimethylaminopropyl)-N′-ethylcarbodiimide hydrochloride (EDC, Sigma, USA) chemistry and following the procedure described by Gajewiak et al.[3] Briefly, HA (50 mg) was dissolved in 20 mL of water to give a 0.25% (w/v) solution, which was then mixed with a solution of 5 mg of fluoresceinamine (Sigma, USA) in 20 mL of dimethylformamide. Next, 100 mg of N-hydroxysuccinimide (NHS, Sigma, USA) was added and the solution pH was adjusted to 4.75 with 0.01 M HCl. Finally, 50 mg of EDC (Sigma, USA) was added, maintaining the solution pH at 4.75. After 12 h, the solution was transferred to dialysis tubing (2000 Da MWCO, Sigma, USA) and dialyzed exhaustively against 100 mM NaCl, followed by dialysis against distilled water and lyophilization.

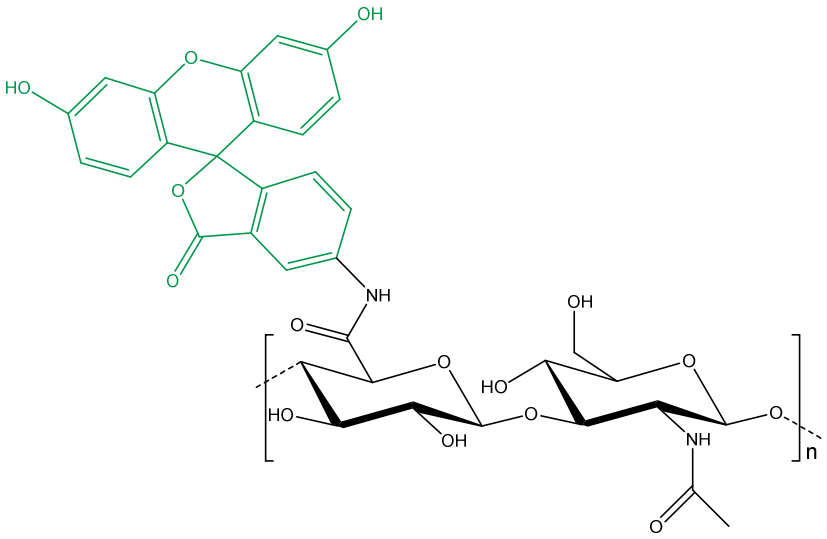

Figure II.2 – Chemical structure of fluorescein-HA repeating unit.

1.3 Alginate

Alginate, also known as alginic acid, is an anionic polysaccharide widely distributed in the cell walls of brown algae. Alginates are linear unbranched polymers containing β (1→4) linked D-manuronic acid (M) and α (1→4) linked L-glucuronic acid (G) residues (Fig. II.3) which vary in amount and sequential

distribution along the polymer chain depending on the source of the alginate.[4] These monomers are arranged in alginate molecules in regions made up exclusively of one unit or the other, or as regions in which monomers alternate in sequence. Divalent cations, like Ca^{2+} or Ba^{2+}, cooperatively bind between the G blocks of adjacent alginate chains, creating ionic interchain bridges which cause gelling of aqueous alginate solutions. Given its anionic behavior and solution viscosity, alginate from brown algae (low viscosity, Sigma, USA), was selected for comparison purposes in Chapter V.

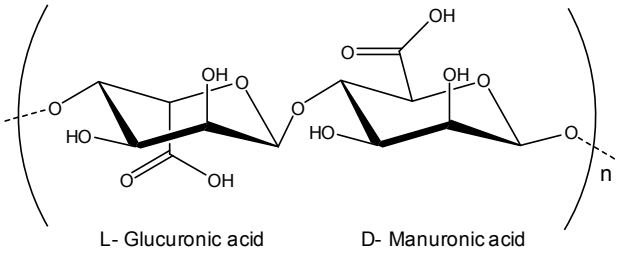

Figure II.3 – Chemical structure of alginate repeating unit.

1.4 Poly(acrylic acid)

Poly(acrylic acid) (PAA) is an anionic synthetic polymer which consists of small repeating units of acrylic acid (Fig. II.4). PAA is easily polymerized and crosslinked into macroscopic hydrogels that have the ability to swell hundreds of times its dry weight. There have been numerous studies on the use of PAA as a biomaterial for biomedical applications, both because of its high swelling capability and because the polyanionic charge allows for easy loading of cationic molecules. Given its hydrophilicity and polyanionic behavior, PAA (450 kDa, Sigma, USA) was selected for comparison purposes in Chapter V.

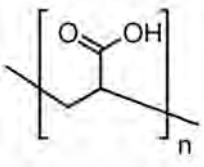

Figure II.4 – Chemical structure of poly(acrylic acid).

1.5 Peptide amphiphiles

Peptide amphiphiles (PAs) used in the present work are characterized by a peptide sequence covalently bond to a hydrophobic alkyl tail of varied length. The peptide sequence includes a β-sheet forming domain (VVVAAA) and a domain with charged amino acids, either positive (KKK) or negative (EEE). In addition, the peptide can also be engineered to undergo enzymatic degradation by the inclusion of an enzyme sensitive site. In aqueous solution, PAs self-assemble into high aspect ratio cylindrical nanofibers, with approximately 6 nm diameter and often several microns in length, if their charge is

screened by addition of (poly)electrolytes or changes in pH.[5] At certain concentrations, these self-assembled nanofibers can form a network that results in the formation of self-supporting gels.[6] In addition, the high density of peptide epitopes present on their surface can result in an acutely potent cellular response. This class of self-assembling peptides was proposed by Stupp's group and has been used for different biomedical applications.[7] The PAs used throughout this thesis consist of a peptide segment covalently linked to a C_{16}-carbon alkyl chain; their sequences and the chemical structure are described in Table II.1.

Table II.1 – Chemical structure of the self-assembling peptides used in this thesis.

PA#	Peptide designation	Structure	Rationale/Application (Chapter)
PA1	K_3	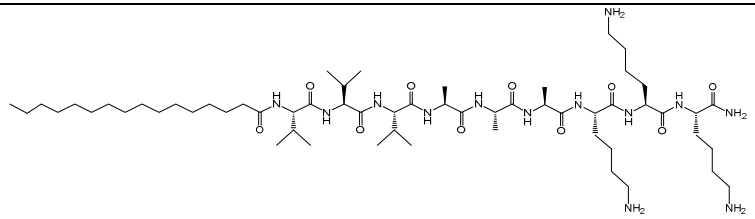	Control PA; used for assembly with HA and E_3 PA (III-VII)
PA2	K_3RGDS	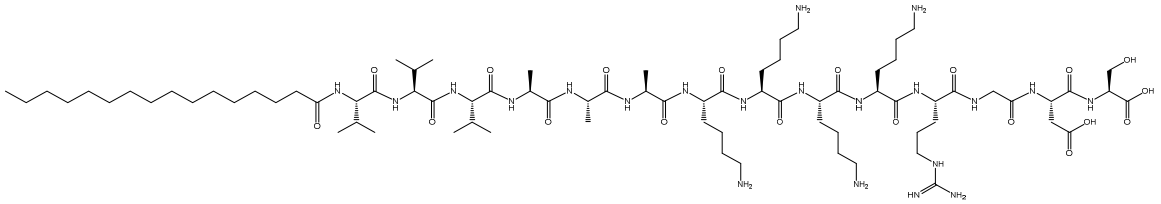	PA containing the cell-adhesion sequence RGDS; membranes for fibroblast adhesion (III)
PA3	K_3DGSR	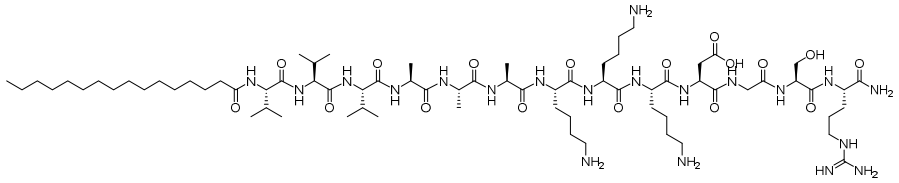	Scrambled RGDS sequence (control in cell adhesion studies) (III)

PA4	$K_{(Rhod)}RGDS$	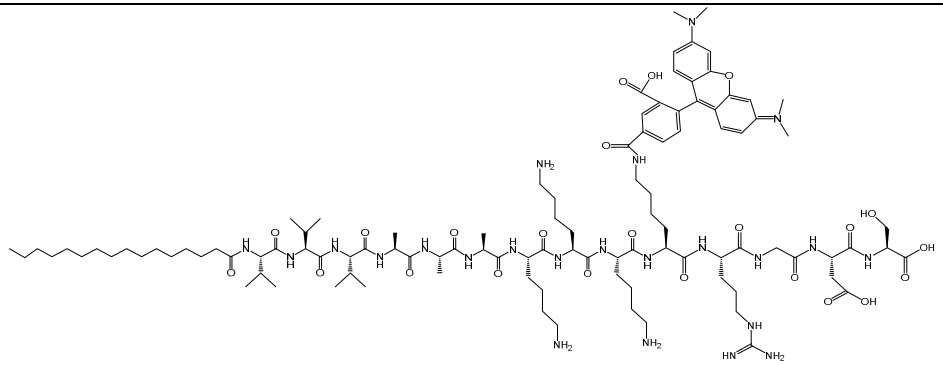	Fluorescent labeled peptide; investigate peptide distribution on self-assembling membranes (III)
PA5	MMP_sK_3	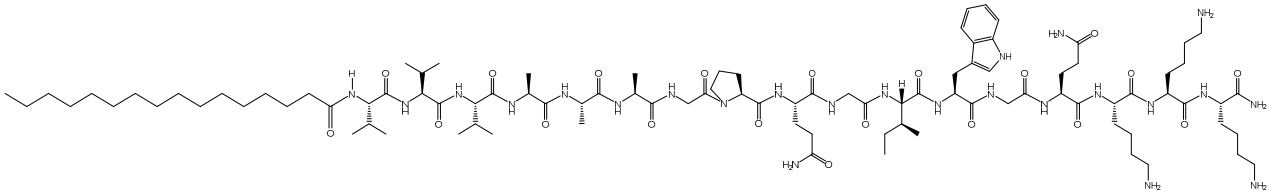	PA containing the MMP sensitive sequence; used to enhance membrane degradation rate (IV-VI)
PA6	MMP_iK_3	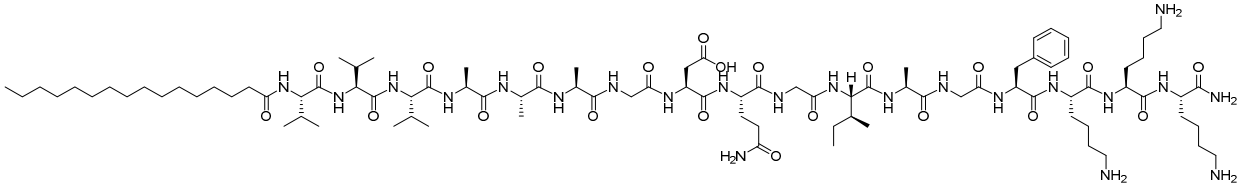	PA containing the MMP insensitive sequence (control in membrane degradation studies with MMP-1) (IV)
PA7	G_8	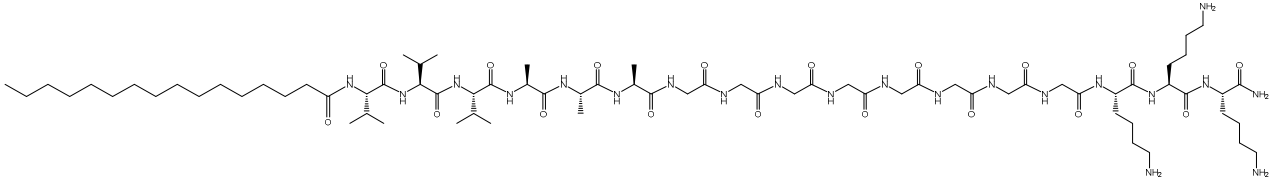	Mutated peptide sequence to determine critical amino acids on the formation of patterned

			membranes. Structural studies (VI)
PA8	P→G	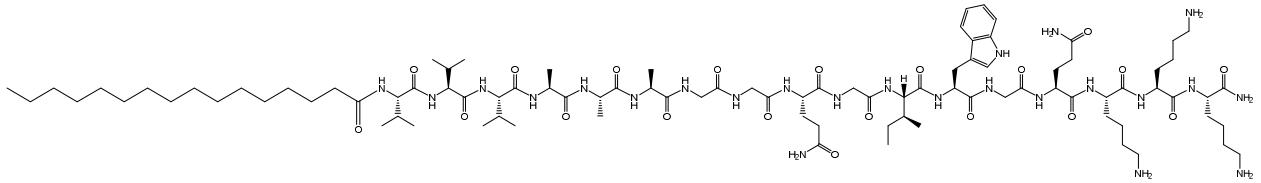	Mutated peptide sequence to determine critical amino acids on the formation of patterned membranes. Structural studies (VI)
PA9	Q→G	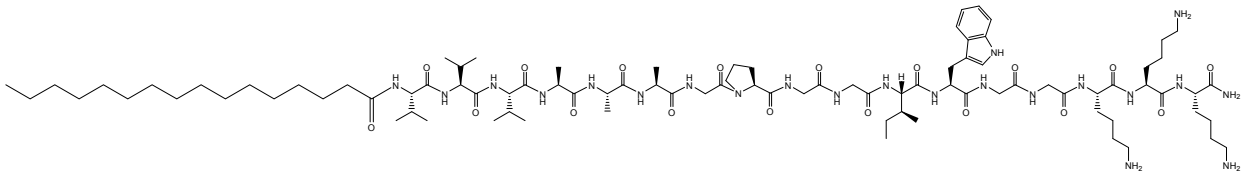	Mutated peptide sequence to determine critical amino acids on the formation of patterned membranes. Structural studies (VI)
PA10	I→G	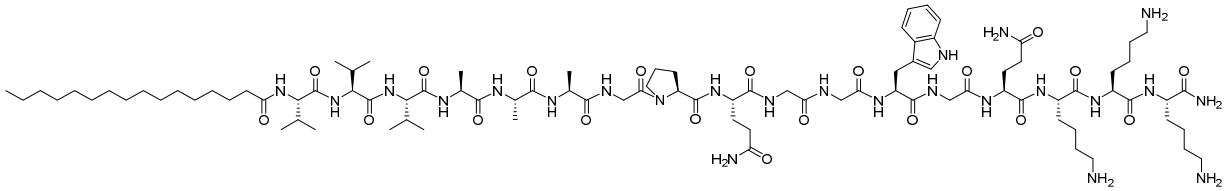	Mutated peptide sequence to determine critical amino acids on the formation of

			patterned membranes. Structural studies (VI)
PA11	W→G	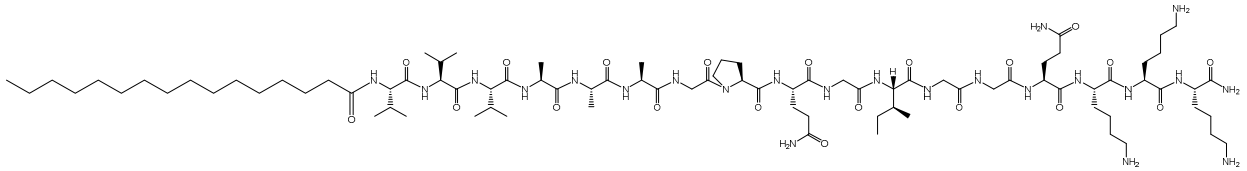	Mutated peptide sequence to determine critical amino acids on the formation of patterned membranes. Structural studies (VI)
PA12	G_4IG_3	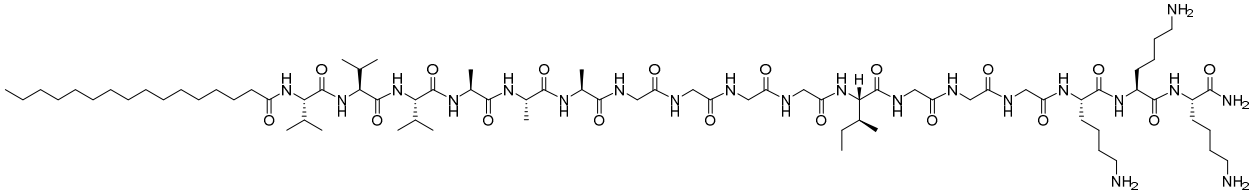	Mutated peptide sequence to determine critical amino acids on the formation of patterned membranes. Structural studies (VI)

PA13	w/ β-sheet	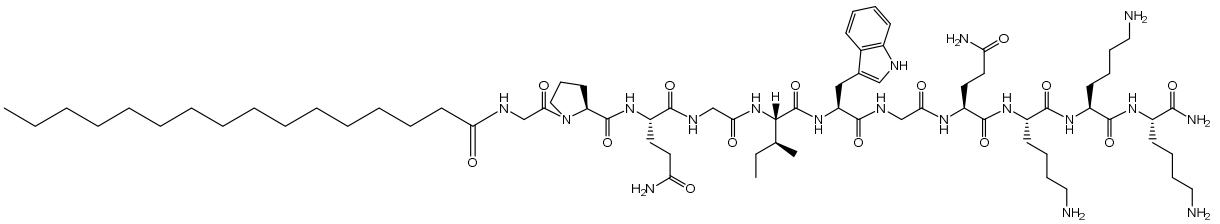	PA without β-sheet to investigate its effect on the formation of patterned membranes. Structural studies (VI)
PA14	IK_3	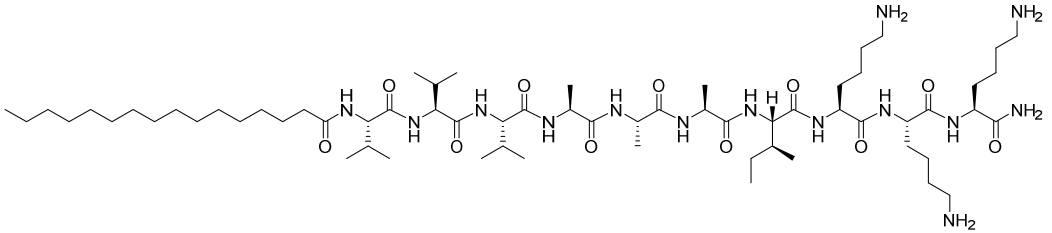	Presence of single Ile on the formation of patterned membranes. Structural studies (VI)
PA15	GIG	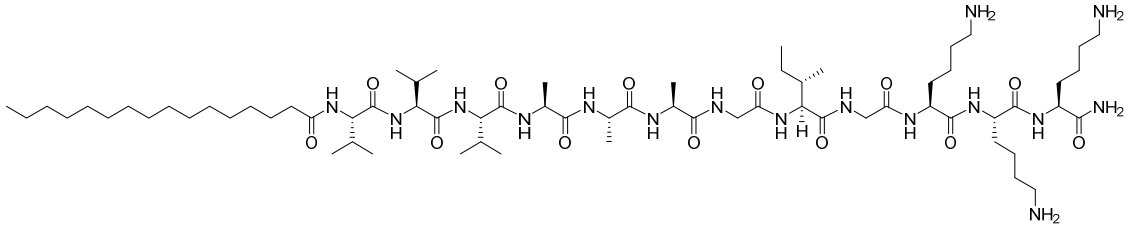	Presence of single Ile spaced with 1 Gly on each side on the formation of patterned membranes. Structural studies (VI)
PA16	G_2IG_2	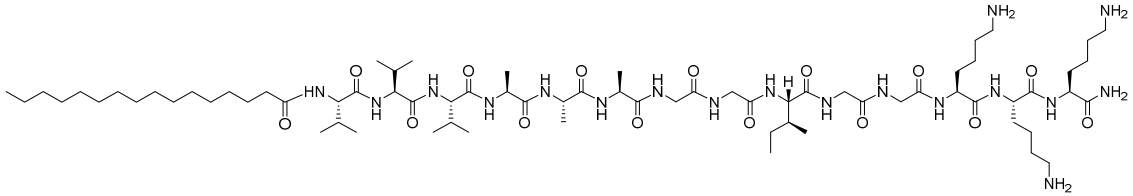	Presence of single Ile spaced with 2 Gly on each side on the formation of patterned

			membrane. Structural studies (VI)
PA17	G_3IG_3	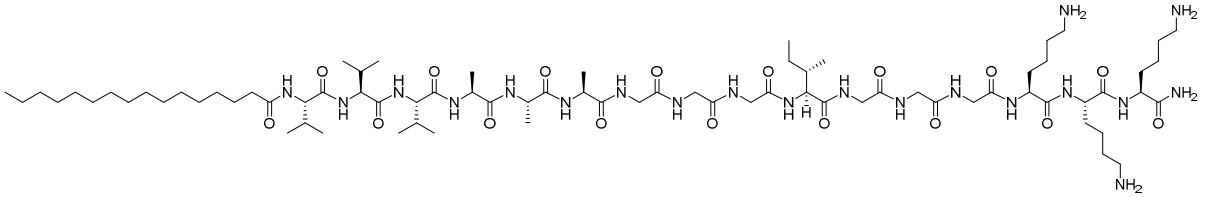	Presence of single Ile spaced with 3 Gly on each side on the formation of patterned membrane. Structural studies (VI)
PA18	G_2IG_5	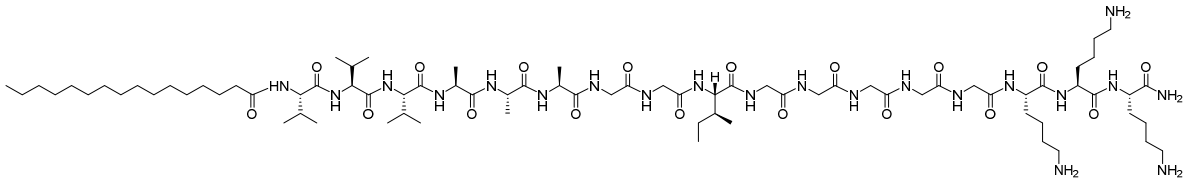	Presence of single Ile spaced with different number of Gly on each side on the formation of patterned membrane. Structural studies (VI)
PA19	GIG_6	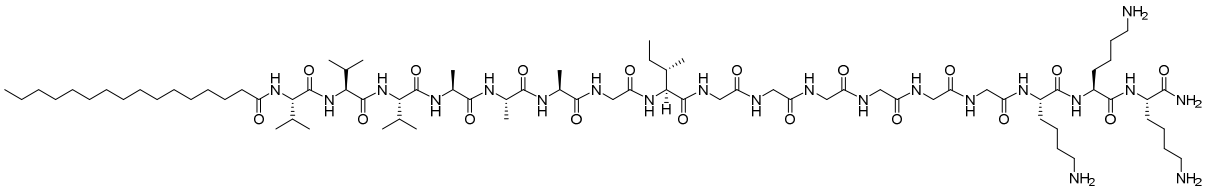	Presence of single Ile spaced with different number of Gly on each side on the formation of patterned

			membrane. Structural studies (VI)
PA20	G_4LG_3	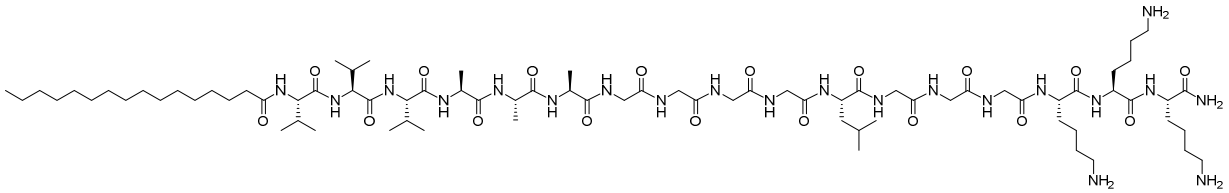	Presence of single Leu spaced with different number of Gly on each side on the formation of patterned membrane. Structural studies (VI)
PA21	G_2LG_5	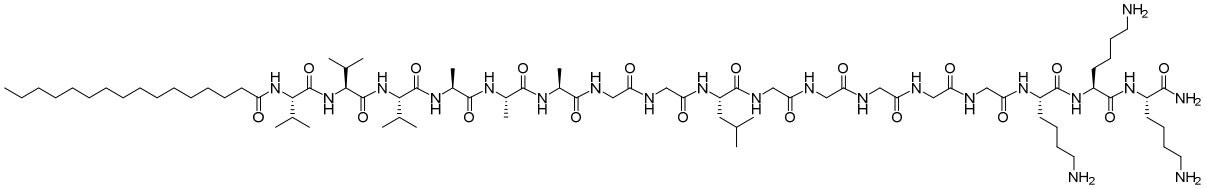	Presence of single Leu spaced with different number of Gly on each side on the formation of patterned membrane. Structural studies (VI)
PA22	GLG_6	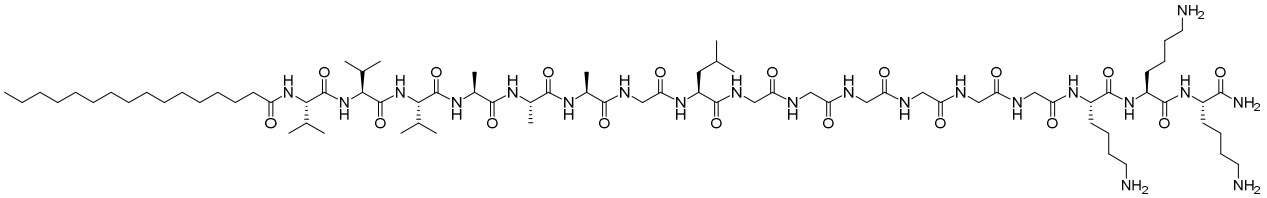	Presence of single Leu spaced with different number of Gly on each side on the formation of

			patterned membrane. Structural studies (VI)
PA23	E3	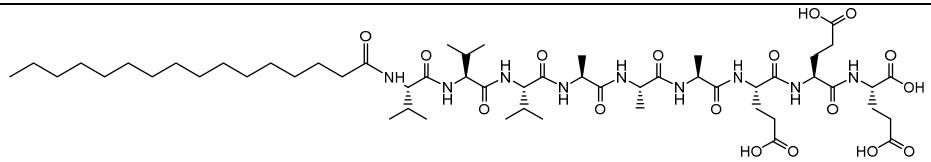	Used for self-assembly with K_3 PA (VII)

1.5.1 Peptide Synthesis

Peptide synthesis includes a large range of techniques and procedures that enable the preparation of materials ranging from small peptides to large proteins. Peptides can be synthesized in solution or by solid phase. Solid phase peptide synthesis (SPPS) has become a method of choice to produce peptides, though solution phase synthesis can still be useful for large-scale production of small peptides.[8] The peptides described in this thesis were synthesized by SPPS using 9-fluorenylmethoxycarbonyl (Fmoc) chemistry.[9] In this protection chemistry, the alpha nitrogen of the amino acids is protected with the base labile Fmoc group and the side chains are protected with acid labile groups based either on the tert-butyl protecting group or the trityl (triphenylmethyl) group. This is an orthogonal protection system, since the side chain protecting groups can be removed without displacing the N-terminal protection. The principles of SPPS are illustrated in Fig. II.5.

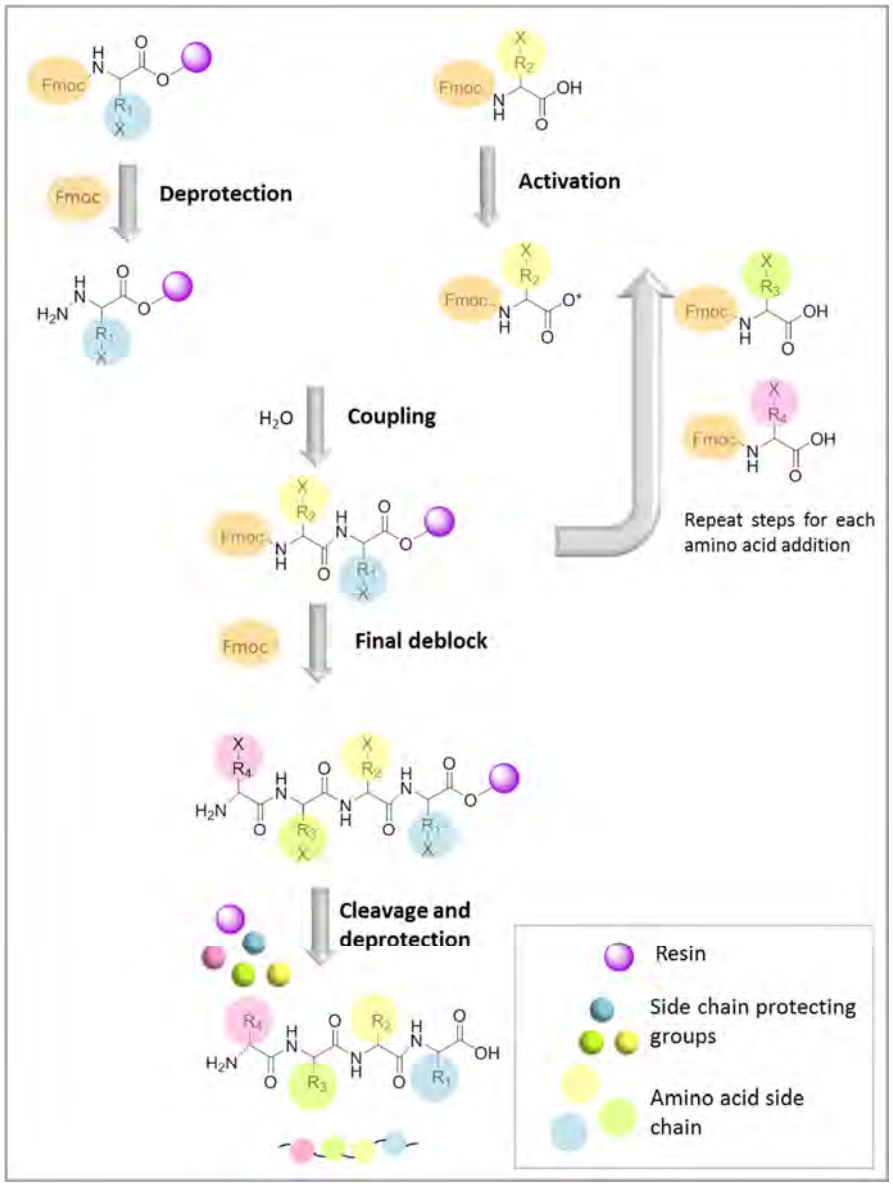

Figure II.5 – Diagram showing the steps in solid phase peptide synthesis (SPPS).

The N-protected amino acid residue is anchored via its carboxyl group to a hydroxyl (Wang) or amino (Rink amide) resin to yield respectively an ester or amide linked peptide that ultimately produce a C-terminal acid or a C-terminal amide peptide. After coupling, the excess of reactants is removed by filtration and washings. The N-terminal protecting group is removed (deprotection) allowing the addition of the next N-protected amino acid by activation of its α-carboxylic acid (coupling). During these processes, side-chain functional groups of amino acids must be masked with protecting groups that are stable in the reaction conditions used during peptide elongation. The peptide is assembled from the C-terminus to the N-terminus (C→N) by repetitive cycles (deprotection/coupling) until the desired sequence of amino acids is obtained. At the end, the peptide is cleaved from the resin and the side-chain protecting groups concomitantly removed. As peptide synthesis involves numerous repetitive steps, the use of a solid support has obvious advantages. Excess reagents and side products can be separated from the growing and insoluble peptide simply by filtration and washings, and all the synthesis steps can be performed in the same vessel without any transfer of material.

The peptides used in the present PhD work were synthesized on a CS Bio 136XT automated peptide synthesizer (CS Bio, USA) using standard Fmoc based solid phase chemistry on a 4-methylbenzhydrylamine (MBHA) rink amide resin or 4-benzyloxybenzylamine Wang resin pre-loaded with the first glutamic acid (Fmoc-Glu(OtBu)-Wang resin). Amino acid couplings were performed using 4 equivalents (4 mmol) of Fmoc protected amino acids (Novabiochem®, USA), 4 equivalents of O-(Benzotriazol-1-yl)-N,N,N′,N′-tetramethyluronium hexafluorophosphate (HBTU, Novabiochem®, USA) and 6 equivalents of N,N-diisopropylethylamine (DIEA, Sigma, USA). Fmoc deprotections were performed with 20% piperidine (Sigma, USA) in dimethylformamide. A palmitic acid ($C_{16}H_{32}O_2$, Calbiochem, USA) tail was manually coupled under the same conditions as the Fmoc-amino acids. Peptide cleavage from the resin and removal of the protecting groups was carried out on a mixture of trifluoroacetic acid (TFA, Sigma, USA)/triisopropylsilane (TIS, Alfa Aesar)/water (95/2.5/2.5)) for 3 h at room temperature. The peptide mixture was collected and excess of TFA was removed by rotary evaporation. The resulting viscous peptide solution was triturated with cold diethyl ether and the white precipitate was collected by filtration, washed with cold ether, and allowed to dry under vacuum overnight. The solid powder was stored at -20 °C for further characterization and purification.

1.5.2 Peptide purification

1.5.2.1 Preparative high performance liquid chromatography

High performance liquid chromatography (HPLC) is a chromatographic technique with ability to identify, quantify and purify the individual compounds of a mixture. In general, chromatography involves moving

a sample through the system over a stationary phase (column). The molecules in the sample will have different affinities and interactions with the stationary support, leading to separation of molecules. Sample components that display stronger interactions with the stationary phase will move slowly through the column than components with weak interactions. Different compounds can be separated from each other as they move through the column. Further, the eluted compound passes through a detector that generates signals that are recorded by a computer. The computer displays the signals graphically as a chromatogram showing the absorbance of the analyte to a pre-established wavelength and their retention time. HPLC has become the central technique in the characterization of compounds due to its reproducibility, ease of selectivity manipulation, and generally high recoveries. The most significant feature is the excellent resolution that can be achieved under a wide range of conditions for very closely related molecules, as well as structurally quite distinct molecules.

Reverse phase high-performance liquid chromatography (RP-HPLC) is the most commonly used mode for peptide characterization and purification. This technique involves the separation of molecules on the basis of hydrophobicity. The separation depends on the hydrophobic binding of the solute molecule from the mobile phase to the immobilized hydrophobic ligands attached to the stationary phase. The peptide mixture is initially injected into the column in the presence of an aqueous solvent, and the peptides are eluted by the addition of organic solvent to the mobile phase. The peptides are, therefore eluted in order of increasing hydrophobicity. RP-HPLC is a very powerful technique for the analysis of peptides and proteins because of the excellent resolution that can be achieved for very closely related molecules as well as structurally quite distinct molecules.

Peptides were purified on a Waters 2545 Binary Gradient (Waters, USA) HPLC system using a preparative reverse-phase C18 columns at a flow rate of 20 mL/min. Peptides with a positive net charge were purified on an Atlantis® Prep OBD T3 column (30 x 150 mm, 5 µm, Waters, USA) with a water/acetonitrile (0.1% TFA) gradient and peptides with a negative net charge on an XBridge® Prep OBD column (430 x 150 mm, 5 µm, Waters, USA) with a water/acetonitrile (0.1% NH_4) gradient. The absorbance of the peptide bond was monitored at 220 nm in a Waters 2489 UV/visible detector (Waters, USA) and fractions were collected on a Fraction Collector III (Waters, USA). The collected fractions were concentrated in a rotary evaporator to remove the acetonitrile and lyophilized. TFA counter-ions were exchanged by sublimation from 0.01 M hydrochloric acid. Finally, the peptides were dialyzed against ultrapure water using 500 MWCO dialysis tubing (Spectrum labs, The Netherlands), lyophilized and stored at -20 °C until further use. Confirmation of mass and purity was done by HPLC and ESI-MS as described in 1.5.3.1 and 1.5.3.2, respectively.

1.5.3 Peptide characterization

1.5.3.1 High performance liquid chromatography

The purity of the peptides used in this PhD work was analyzed by analytical RP-HPLC on a Waters 2545 Binary Gradient (Waters, USA) HPLC system using reverse-phase C18 columns at a flow rate of 1 mL/min. Peptides with a positive net charge were analyzed on an Atlantis® T3 analytic column (4.6 x 150 mm, 5 µm, Waters, USA) with a water/acetonitrile (0.1% TFA) gradient and peptides with a negative net charge on an XBridge® analytic column (4.6 x 150 mm, 5 µm, Waters, USA) with a water/acetonitrile (0.1% NH_4) gradient. The absorbance of the peptide bond was monitored at 220 nm in a Waters 2489 UV/visible detector (Waters, USA).

1.5.3.2 Electrospray ionization mass spectrometry

Mass spectrometry is an analytical technique that can provide both qualitative (structure) and quantitative (molecular mass or concentration) information on analyte molecules after their conversion to ions.[10] Electrospray ionization mass spectrometry (ESI-MS) has emerged as an important technique for the characterization of proteins and peptides. It provides a sensitive, robust, and reliable tool for studying, at femtomole quantities in microliter sample volumes, non-volatile and thermally labile biomolecules that are not amenable to analysis by other conventional techniques. The molecules of interest are first introduced into the ionization source of the mass spectrometer, where they are first ionized to acquire positive or negative charges. The ions then travel through the mass analyzer and arrive at different parts of the detector according to their mass/charge (m/z) ratio. After the ions make contact with the detector, useable signals are generated and recorded by a computer system. The computer displays the signals graphically as a mass spectrum showing the relative abundance of the signals according to their m/z ratio. Peptides were first dissolved in ultrapure water (with 0.1% TFA; positive net charge or 0.1% NH_4; negative net charge) and then diluted (1:1) in acetonitrile. The mass of the synthesized peptides described on Chapters III to VII was determined by ESI-MS (Thermo Electron Corporation Finnigan LXQ MS Waltham, USA).

1.5.3.3 Circular dichroism

Circular dichroism (CD) is an excellent method for analyzing the secondary structure of proteins and peptides in solution.[11] CD is a phenomenon that results when chromophores in an asymmetrical environment interact with polarized light. In proteins, the major optically active groups are the amide bonds of the peptide backbone and the aromatic side chains. CD in the far ultraviolet (UV) region (178–260 nm) arises from the amides of the peptide backbone and is sensitive to the conformation of the

peptide. Thus, CD can determine whether there are changes in the conformation of peptides and proteins when they are in solution. CD bands in the near UV (350–260 nm) and visible regions arise from aromatic and prosthetic groups. Peptides and proteins have regions where the peptide chromophores are in highly ordered arrays, such α-helices or β-sheets. Depending on the orientation of the peptide bonds in the arrays, the optical transitions of the amide bond can be split into multiple transitions, the wavelengths of the transitions can be increased or decreased, and the intensity of the transitions can be enhanced or decreased. As a consequence, many common secondary structure motifs, such as the α-helix β-sheets and β-turns have very characteristic CD spectra. To a first approximation, increases in negative ellipticity at 222 and 208 nm and positive ellipticity at 293 nm usually indicate an increase in α-helical content, while increases in a single negative band near 218 nm and a positive band at 295 nm indicate an increase in β-sheet.

CD spectroscopy was used to evaluate the secondary structure of the synthesized peptides. Peptides were dissolved in ultrapure water to a final concentration of 0.011 mM and the pH was adjusted (with HCl and NH_4OH, 0.1 M) to 5, 7 and 9. The CD measurements were performed in a PiStar-180 spectrometer from Applied Photophysics (Surrey, UK), under a constant flow of nitrogen (8 $L.min^{-1}$) at a constant pressure value of 0.7 MPa. Far-UV spectra were recorded at 25 °C from 190 to 300 nm in a quartz cuvette with 1 mm path-length. All scans were performed in the steady state with a bandwidth of 1 nm and each presented spectrum is an average of 5 spectra. CD measurements were converted to units of molar ellipticity ([θ], $deg.cm^2.dmol^{-1}$). The molar ellipticity [θ] was calculated using equation (II.1).

$$[\theta] = \frac{\theta}{c.l} \qquad \text{(II.1)}$$

were θ is the measured ellipticity in mdeg, c is the concentration of the peptide in dmol L^{-1} and l is the light path length of the cuvette in cm.

1.5.3.4 Transmission electron microscopy

Transmission electron microscopy (TEM) is a microscopy technique that is based on the interaction of a beam of electrons that are transmitted through a thin sample. A micrograph is obtained from the interaction of the electrons with the specimen. TEM uses electrons instead of a light source, their much lower wavelength make it possible to get a higher resolution when compared to optical and scanning electron microscopy (SEM). Thus, this technique allows examining in detail the structure of the specimen at a nano-scale.

To assess the ability of the self-assembling peptides to form nanofibers, they were analyzed by TEM. Samples for TEM analysis were prepared by placing a drop of a 0.1 mM peptide solution directly on the

400 mesh carbon-coated copper TEM grid (Ted Pella, USA). For negative staining, a drop of a 2% (w/v) uranyl acetate (Electron Microscopy Sciences, USA) aqueous solution was placed on the samples. After ca. 3 minutes, the excess solution was wiped away with a piece of filter paper, and the sample was allowed to dry under ambient conditions. Images were collected with a JEOL JEM-1010 transmission electron microscope at 100 kV (JEOL, USA, Chapter III) or with a FEI Tecnai-12 TWIN transmission electron microscope (FEI, USA) equipped with a SIS Megaview III camera (Chapter IV-VI).

1.6 Quartz crystal microbalance with dissipation

Quartz crystal microbalance with dissipation (QCM-D) is a variation of QCM which simultaneously allows monitoring changes of the resonant frequency (Δf) of the adsorbed layers on the sensor surfaces and registering the dissipation (D) of the sensor signal. The D-factor is related to the viscoelastic properties of the adsorbed layer. The QCM instrument operates with a quartz disc in contact with two electrodes. Since the quartz is a piezoelectric material, its excitation by an electric field produces an acoustic wave that propagates and makes the crystal oscillate. The resonance frequency is dependent on the total oscillating mass. The detection principle is based on the resonance frequency shifts due to addition or removal of mass on the crystal surface. Mass adsorption increases the frequency, while mass losses induce decrease of frequency. The mass can be calculated by Sauerbrey equation,[12] that correlates proportionally the frequency change with the mass adsorbed, and is defined as:

$$\Delta f_s = -\frac{2f_0^2 mn}{(\mu_q \rho_q)^{1/2}} \qquad \text{(II.2)}$$

where f_0 is the fundamental frequency of the crystal, m is the mass added, n is the harmonic number, μ_q is the shear modulus and ρ_q is the density.

The present interest in using QCM-D was mainly focused on studying peptide-hyaluronan interactions (Chapter III). Measurements were performed in an instrument with dissipation (QCM-D E4) from Q-Sense (Gothenburg, Sweden). All experiments were performed at 25 °C with a constant flow rate of 50 $\mu L.min^{-1}$ using gold coated crystals (QSX301, Q-Sense, Gothenburg, Sweden) previously cleaned with water and H_2O_2 for 1 h each, and then acetone, ethanol and isopropanol for 3 minutes each at 37 °C with sonication. The system was equilibrated with a 0.15 M sodium chloride (NaCl) solution to obtain a stable frequency and dissipation baseline signal. Once the signal was stable, the NaCl solution was replaced by a solution of K_3-PA (0.2% (w/v) in 0.15 M NaCl) during 30 minutes. To remove weakly bound peptide, the crystals were rinsed with a NaCl solution and then replaced by a solution of HA (0.1% (w/v) in 0.15 M NaCl) for 30 minutes. Again, to remove weakly bound polymer, the system was

rinsed with NaCl. The QCM instrument recorded frequencies up to the 13th overtone, and Δf and ΔD were monitored in real time. In the present study (Chapter III) the results are shown for the 7th overtone; the frequency of this overtone was normalized to the fundamental resonant frequency of the quartz crystal, by dividing it by ν (where ν= 7).

2. Development of self-assembling matrices

2.1. Membrane preparation

Membranes were prepared using cell culture plates as templates (24, 48 and 96 well plates). A 1% (w/v) HA solution was cast on the bottom of the wells and then a 2% (w/v) K_3-PA solution was added on top of the HA solution.[13] A membrane is immediately formed upon contact between the two solutions. The membrane was allowed to grow with time (overnight) and rinsed with sterile ultrapure water to ensure the removal of unreacted HA and PA. To study the effect of RGDS presentation on self-assembled membranes on cell adhesion (Chapter III), PA–HA membranes containing different percentages of the RGDS motif were prepared by mixing the filler peptide (K_3-PA) with 1%, 10% and 50% K_3RGDS-PA and 10% scrambled peptide (K_3DGSR-PA) to give a 2% (w/v) final peptide concentration.

Membranes were also prepared for confocal microscopy to probe the location and retention of fluorescently-labeled HA, as well as to visualize the distribution of RGDS signal on (surface) and within (cross-section) the PA–HA membrane. Membranes were formed as previously described using a fluorescein HA solution (1%, w/v) and a 2% (w/v) peptide mixture containing 0.1% K_3K_{rhod}RGDS-PA and 99.9% K_3-PA. The membranes were incubated overnight at RT protected from light.

To prepare MMP-sensitive membranes (Chapter IV), a 0.017 M solution of MMP_sK_3-PA that contains the MMP substrate (GPQG↓IWGQ) was used. MMP-1 insensitive membranes were also made as control, using the MMP_iK_3-PA (0.017 M) that contains the nonfunctional sequence (GDQGIAGF) and the K_3-PA (0.017 M). The same procedure was used to prepare the membranes used in Chapter V and VI. For comparison purposes (Chapter V), alginate and poly(acrylic) acid (2%, w/v) were used to prepare membranes with MMP_sK_3-PA (0.017 M). In addition, membranes were also prepared by varying the concentration of MMP_sK_3-PA (0.017, 0.0085 and 0.00425 M) and HA molecular weight (234 kDa (1, 2, 3%, w/v) 750 kDa (1, 2%, w/v) and 1.5 MDa (1%, w/v)).

For cell culture studies, membranes were prepared, following the procedure previously described, under sterile conditions. HA sterilization was done by dissolving the polymer, filtering the solution

through a 0.22 μm filter, followed by lyophilization in sterile falcon tubes. Peptide solutions were sterilized by UV exposure for 15 minutes.

2.2. Microcapsule preparation

Microcapsules (Chapter VII) were generated using a microfluidic device developed in our lab that allows the production of stable and size controlled spherical capsules[14]. This system can be conveniently cleaned and sterilized allowing cell encapsulation in a sterile environment, reducing contamination risks during the procedure. A solution of E_3-PA (1 wt%) in 0.15 M NaCl was first injected into one of the microchannels of the microfluidics device using a syringe pump (Aladdin WPI, England). Simultaneously, mineral oil was provided to the oil microchannel from a reservoir using a low speed peristaltic pump (Ismatec, Switzerland). The peptide microdroplets were generated inside the microfluidics device by shear stress when the E_3-PA solution in the horizontal microchannel entered into the stream of mineral oil in the larger vertical microchannel (Fig. II.6). The formed microdroplets were collected from the outlet tubing in a separate vessel containing 1 mL of K_3-PA solution (0.1, 0.2 and 0.5 wt %) in 0.1 M $CaCl_2$. Tween-80 was added as a surface-active agent to prevent aggregation of the capsules. Capsules were incubated in the K_3–$CaCl_2$ solution for 15 minutes and washed three times with 0.15 M NaCl.

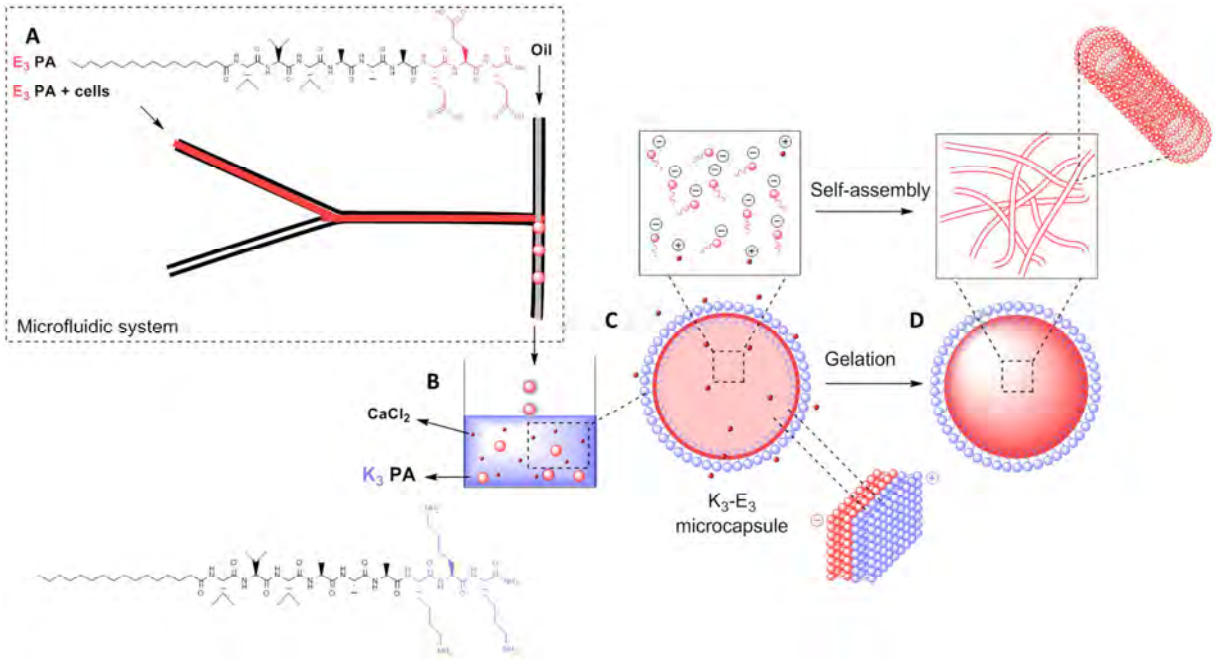

Figure II.6 – Schematic representation of the set-up for capsule generation and cell encapsulation. The E_3-PA microdroplets generated at the T-junction of the microfluidic system (A) were directly extruded into a solution of K_3-PA for electrostatic self-assembly (B). At the interface of the droplets, self-assembly immediately occurs resulting in the formation of a capsular structure (C). The K_3-PA solution was supplemented with 0.1 M $CaCl_2$ to induce the gelation of internal E_3-PA (D).

3. Characterization of the developed self-assembling matrices

3.1. Structural properties

3.1.1. Bright field/phase contrast microscopy

In bright field microscopy, light from an incandescent source is aimed toward a lens beneath the stage called the condenser, through the specimen and the objective lens, and to the eye through a second magnifying lens, the ocular or eyepiece. After passing through the specimen, the light is displayed to the eye with an apparent field that is much larger than the area illuminated. In a light microscope in bright field mode, light from highly refractive structures bends farther away from the center of the lens than light from less refractive structures and arrives about a quarter of a wavelength out of phase. A reduction in brightness of the object is observed, the reduction in brightness will depend on the refractive index of the object. Phase contrast is preferable to bright field microscopy when the specimen is colorless or the details so fine that color does not show up well. In phase contrast a phase plate is placed in the light path. Barely refracted light passes through the center of the plate and is not retarded. Highly refracted light passes through the plate farther from center and is held back another quarter wavelength. To use phase contrast the light path must be aligned.

Bright field and phase microscopy were used to assess size and shape of the microcapsules (Chapter VII). Phase contrast micrographs of the capsules were acquired in an inverted microscope (Axio Observer, Zeiss, Germany). The size of the capsules was then estimated by measuring the diameter of individual capsules.

3.1.2. Polarized light microscopy

The polarized light microscope is designed to observe and photograph specimens that are visible primarily due to their optically anisotropic character. To accomplish this, the microscope must be equipped with both a polarizer, positioned in the light path somewhere before the specimen, and an analyzer (a second polarizer), and placed in the optical pathway between the objective rear aperture and the observation tubes or camera port. Image contrast arises from the interaction of plane-polarized light with a birefringent (or doubly-refracting) specimen to produce two individual wave components that are each polarized in mutually perpendicular planes. The velocities of these components are different and vary with the propagation direction through the specimen. After reaching the specimen, the light components become out of phase, but are recombined with constructive and destructive interference when they pass through the analyzer. Polarized light is a contrast-enhancing technique that improves the quality of the image obtained with birefringent materials.

Polarized light microscopy was used in Chapter V to characterize peptides (K_3-PA and MMPs-PA) and HA individually and together. Drops of concentrated solutions of peptide (20 mg/mL) and HA (10 mg/mL) were placed between a slide and coverslip and observed between crossed polarizers in a polarizing microscope (Olympus BX 60, Olympus, UK). Membranes resulting from the self-assembly of PA and HA were also imaged. Membranes were prepared directly on the glass slide before imaging. A drop of HA was cast on the slide and then a drop of PA was added on the top of HA solution. A membrane is immediately formed upon contact between the two solutions. Samples were covered with a coverslip and examined by polarized optical microscopy.

3.1.3. Fluorescence and laser scanning confocal microscopy

Fluorescence microscopy is based on the phenomenon that certain material emits energy detectable as visible light when irradiated with the light of a specific wavelength. A fluorescence microscope is an optical microscope that uses fluorescence and phosphorescence instead of, or in addition to, reflection and absorption to generate an image. Laser scanning confocal microscopy (LSCM) uses the principle of fluorescence excitation to investigate the structural properties of cells and the location of particular structures or protein populations within those cells in fixed tissue. In confocal microscope, the light source is generally one or more lasers. The laser beam is a narrow beam of light and so, in order to illuminate the whole visual fields, the laser beam has to be rapidly scanned across the area in a series of lines. LSCM increases optical resolution and contrast of a micrograph by using point illumination and a spatial pinhole to eliminate out-of-focus light in specimens that are thicker than the focal plane. It enables the reconstruction of three-dimensional structures from the obtained images.

Confocal microscopy was used to probe the location and retention of fluorescently-labeled HA, to visualize the distribution of RGDS signal on the membranes, as well as cells, in Chapter III. Membranes were imaged by a laser scanning confocal microscope (Olympus FluoView 1000, Japan) with appropriate excitation and emission wavelengths. Optical slices were captured at regular intervals to produce reconstructed z-stacks with 100 μm total thickness. Images of cross sections were compiled from z-stack in the x-direction using FV10-ASW software from Olympus. For examining the morphology of cells cultured on the membranes (Chapter III-VI) or within microcapsules (Chapter VII), cells were stained for F-actin and collagen I and imaged by confocal microscopy. In the co-culture studies (Chapter VII) cells were also characterized using an immunocytochemistry assay with specific markers for each cell type, anti-fibroblast surface protein (fibroblasts) and anti-keratin 5 (keratinocytes). Samples were visualized by CLSM (Olympus FluoView 1000, Olympus, Japan). The background was subtracted and images were processed using FV10-ASW 3.1 software (Olympus, Japan).

3.1.4. Scanning electron microscopy

The scanning electron microscopy (SEM) is a technique that uses a beam of electrons instead of light to form an image. SEM micrographs can be obtained from secondary electrons emitted from the surface of the sample, as a result of the impact of a focused electron beam. Basically, the secondary electrons are collected by an electron detector with a positive potential to have maximum numbers and the detector output is used to modulate the intensity of a display system such as a cathode ray tube. The image is formed pixel by pixel as the beam is scanned across the sample. So, the resolution of the SEM is limited not by the wavelength of the electron beam but by the size of the electron beam spot being scanned. Biomaterials can be imaged at resolutions approaching 0.3 nm at 30 keV using a high-resolution SEM.[15]

SEM was used to evaluate the microstructure of the developed membranes (Chapter III-VI) and microcapsules (Chapter VII). Prior to SEM observation, samples were fixed in a 2% (v/v) glutaraldehyde (Electron Microscopy Sciences, USA)/3% (w/v) sucrose (Sigma, USA) in PBS for 1 h at 4 °C followed by sequential dehydration in graded ethanol concentrations (from 20 to 100%). To remove ethanol, samples were dried in a critical point dryer (Tousimis Autosamdri®-815 series A, USA). Nonconductive samples are usually coated with a thin conductive metal layer in order to minimize charge accumulation. Thus, all specimens were coated with a gold/palladium layer and imaged using an ultra-high resolution field emission gun scanning electron microscope (Nova™ NanoSEM 200) from FEI (Eindhoven, The Netherlands).

SEM was used to evaluate the microstructure on the surface and cross-section of the developed membranes (Chapter II-VI). SEM was also used to evaluate the morphology of the microcapsules (Chapter VII). Microcapsules were cut in half to expose the internal surface. Capsule shell porosity was estimated using SEM micrographs and ImageJ software (NIH, USA) for image analysis and processing.

3.1.5. Small-angle X-ray scattering

Small-angle X-ray scattering (SAXS) is a powerful tool that provides essential information on the structure and dynamics of large molecular assemblies in low ordered environments. The materials can be solid or liquid and they can contain solid, liquid or gaseous domains of the same or another material in any combination. The basic components of all SAXS instruments are a source, a collimation system, a sample holder, a beam stop and a detection system. The source irradiates the sample, and the detector measures the radiation coming from the sample in a certain range of angles. The collimation system makes the beam narrow and defines the zero-angle position. The beam stop prevents the

intensive incident beam hitting the detector, which would overshadow the relatively weak scattering of the sample and would even destroy some of the detectors. Normally, X-rays are sent through the sample (transmission mode) and every particle that happens to be inside the beam will send out its signal. Thus, the average structure of all illuminated particles in bulk material is measured. The SAXS method is accurate, non-destructive and usually requires minimal sample preparation. The particle or structure sizes that can be resolved range from 1 to 100 nm in a typical set-up, but can be extended on both sides by measuring at smaller (ultra small-angle X-ray scattering, USAXS) or larger angles (wide-angle X-ray scattering, WAXS) than the typical 0.1° to 10° of SAXS. When X-rays irradiate a sample, then the atoms inside the sample will scatter the incident radiation into all directions, which gives a background radiation that is almost constant at small angles. The molecules (i.e., clusters of atoms) inside the sample will produce additional scattering (so-called excess scattering) which is due to the fact that the particles are made of a different material or density (to give contrast) and are in the size-range of the X-ray wavelength. By measuring the angle-dependent distribution of the scattered radiation (intensity) it is possible to draw conclusions about the average particle structure.

The SAXS measurements were performed using the SAXSLab Ganesha 300-XL system (Denmark) with Cu Kα radiation generated by a sealed microfocused tube (Genix 3D Cu-source with integrated Monochromator) powered at 50kV and 0.6mA and three pinholes collimation. The scattering patterns were recorded by a Pilatus 300K detector (Dectris, Switzerland). The scattering intensity I(q) was recorded in the interval $0.012 < q < 0.7$ A^{-1} , where q is defined as

$$q = \frac{4\pi}{\lambda}\sin\theta \quad \text{(II.3)}$$

where 2θ is the scattering angle, and λ is the radiation wavelength (1.542A).

The solution under study was sealed in a thin-walled capillary (glass) of about 1.5 mm diameter and 0.01 mm wall thickness. Membrane samples were placed in a customized sample holder where the wet membranes are sandwiched between 2 thin sheets of Mica. Measurements were performed under vacuum at ambient temperature. The 2D SAXS images were azimuthally averaged to produce one-dimensional profiles of intensity, *I* vs. *q*, using the two-dimensional data reduction program SAXSGUI (SAXSLab, Denmark). The scattering spectra of the capillary and solvent were also collected and subtracted from the corresponding solution data using the Irena package for analysis of small-angle scattering data.[16] No attempt was made to convert the data to an absolute scale.

For membrane samples data analysis was based on fitting the scattering curve to an appropriate model by a least-squares method using software provided by NIST[16] (NIST SANS analysis version 7.0 on IGOR).

Modeling of small angle scattering patterns

The scattering intensity of a monodispersed system of particles of identical shape can be described as[17]

$$I(q) = NP(q)S(q) \quad \text{(II.4)}$$

where N is the number of particles per unit volume, P(q) is the form factor revealing the specific size and shape of the scatterers and S(q) is the structure factor that accounts for the interparticle interactions. In dilute solutions, where the interactions between the objects can be neglected, S(q) is equivalent to 1.

A form factor for a simple core-shell cylinder where the core and the shell have a uniform electron density is given by

$$P(q) = \int_0^{\pi/2} \sin\theta \cdot d\theta \cdot \left[V_l(\rho_l - \rho_{solv}) \frac{\sin\left(\frac{qH_l \cos\theta}{2}\right)}{\frac{qH_l \cos\theta}{2}} \frac{2J_1(qR_l \sin\theta)}{qR_l \sin\theta} + V_p(\rho_p - \rho_l) \frac{\sin\left(\frac{qH_p \cos\theta}{2}\right)}{\frac{qH_p \cos\theta}{2}} \frac{2J_1(qR_p \sin\theta)}{qR_p \sin\theta} \right]^2 \quad \text{(II.5)}$$

$$V_x = \pi R_x^2 H_x$$

where $J_1(x)$ is the first order Bessel function. Theta is defined as the angle between the cylinder axis and the scattering vector, q. R_p and R_l are the core and shell radii respectively, H_p and H_l are the core and shell lengths, and is electron density.

3.2 Physical and mechanical properties

3.2.1 Permeability

Capsule permeability is crucial for cell encapsulation to allow the diffusion of oxygen, nutrients and cell metabolites. Additionally, when used for cell delivery therapies, they should also be able to avoid the influx of immune cells and antibodies. To assess the effect of K_3-PA concentration on the permeability of the microcapsules produced in Chapter VII, dextran standards of different molecular weights (20, 40, 155 kDa) were used. Briefly, FITC- and TRITC-labeled dextrans (Sigma, USA) were encapsulated within the capsules and their release followed along the time. Three different solutions were prepared; each solution was a mixture of 0.5 mg mL^{-1} of dextran (20, 40 and 155 kDa) with 1 wt% E3-PA. The mixture was injected into the microfluidic device and capsules were generated as described before in section 2.2. The capsules were then placed in PBS (pH 7.4) at 37 °C in a water bath with agitation. At specific time intervals, the release medium was completely collected for further analysis and replaced with the same amount of fresh PBS solution. The fluorescence was measured at 485/528 nm (FITC-labeled) and 530/590 nm (TRITC-labeled) on a microplate reader (BIO-TEK, Synergy HT, USA). The

concentration of released dextran was measured using a calibration curve using known concentrations of dextran solutions.

3.2.2 Chemical and mechanical stability

A general requirement for using capsules as 3D environments for cell encapsulation and culture includes their mechanical and chemical stability in aqueous media (e.g. buffer, cell culture medium). Microcapsules should be resistant enough to be durable during its production, handling and to resist to the mechanical stress without loss of its membrane integrity[18].

3.2.2.1 Osmotic pressure

To investigate whether capsules were able to maintain their structural integrity when exposed to aqueous solutions, capsules (n=10, in triplicate) were prepared with 0.1, 0.2 and 0.5% K_3-PA and incubated in water or PBS. The capsules were placed at 37 °C and at predetermined time points (1, 2, 3 and 7 days) observed in an inverted microscope (Axio Observer, Zeiss, Germany) and their size was measured using ZEN software (Zeiss, Germany).

3.2.2.2 Mechanical stress

To study the mechanical stability of the different capsules, 10 capsules (in triplicate) were placed in 12-well plates containing 2 mL of PBS and 10 glass beads (3 mm diameter, VWR). The plate was placed in a flat rotator (DSR-2800 V, Digisystem Laboratory Instruments Inc., Taiwan) shaking at about 200 rpm. At predetermined time points (2, 4, 6 and 24 h), the number of intact capsules was counted by observation in an inverted microscope (Axio Observer, Zeiss, Germany). The percentage of intact capsules as a function of time was determined by calculating the ratio between the number of intact capsules at each time point and the initial number

4. Biological evaluation of the developed self-assembling matrices

4.1. Isolation of human dermal fibroblasts and epidermal keratinocytes

Human dermal fibroblasts (hDFb) and epidermal keratinocytes (hKc) were isolated from skin samples discarded from abdominoplasty surgeries of consenting patients at Hospital da Prelada (Porto, Portugal). Briefly, the skin tissue was cut into pieces of 0.5 by 0.5 cm and digested in a dispase solution (2.4 U/mL in PBS) at 4 °C, overnight. After dissociation of the epidermis from the dermis, keratinocytes were isolated by a 5 minutes digestion of the epidermis in 0.25% trypsin/EDTA (Invitrogen, UK) at 37 °C to release the cells. Trypsin was inactivated by the addition of the same

volume of fetal bovine serum (FBS, Gibco, UK), the digestion products were poured through a 100 mm cell strainer and centrifuged at 200 *g* for 5 minutes. The cell pellet was washed with phosphate buffered saline (PBS, Gibco, UK) and centrifuged at 200 *g* for 5 minutes. The pellet was resuspended and the cells were subsequently cultured in Keratinocyte Serum Free Medium (KSFM, Gibco, UK) with L-glutamine and a keratinocyte-SFM supplement (Gibco, UK), in a 37 °C humidified atmosphere with 5% CO_2. Fibroblasts were isolated from the dermis by overnight digestion of the dermal pieces in a collagenase IA solution (125 U/mL in PBS) at 4 °C. The digestion products were poured through a 100 mm cell strainer and centrifuged at 200 *g* for 5 minutes. The pellet was resuspended and the cells were subsequently cultured in Dulbecco's modified Eagle's medium (DMEM) (Sigma, Germany) supplemented with 10% FBS (Gibco, UK) and 1% (v/v) antibiotic/antimycotic solution (A/B) (Gibco, UK) containing 100 units per mL penicillin and 100 mg/mL streptomycin, in a 37 °C humidified atmosphere with 5% CO_2. hDFb were used throughout this thesis in several works (Chapter III-V and VII), hKc were used only in Chapter VII.

4.2. Cell culture

4.2.1. hDFb culture on the PA-HA membranes

Primary human dermal fibroblasts were used on the biological evaluation of the developed self-assembling membranes described in Chapters III to V.

hDFb were expanded in DMEM (Sigma, Germany) supplemented with 10% FBS (Gibco, UK) and 1% (v/v) A/B (Gibco, UK) in a 37 °C humidified atmosphere with 5% CO_2. Confluent hDFbs were harvested from monolayer cultures using trypsin-EDTA (Invitrogen, USA) and used in the different studies.

To study the effect of RGDS signaling on cell adhesion (Chapter III), PA–HA membranes containing different percentages of the RGDS motif were prepared, as described previously (Section 2.1). hDFb were resuspended at a density of 5.0×10^4 cells per mL in serum-free DMEM without phenol red (Sigma, USA) supplemented with 1% (v/v) A/B. Cells (2.5×10^4 cells per well) were cultured on the PA–HA membranes in 48 well plates at 37 °C in a humidified atmosphere of 5% CO_2 for 2, 6, 12 and 24 h. Cells cultured on the membranes were examined under SEM and stained for f-actin to analyze cell morphology and cell–matrix interactions.

To explore whether cell mediated degradation of the membranes would occur in the presence of MMP-1 sensitive sequences, hDFb were seeded on membranes containing the MMP sensitive sequence

(MMPs-HA), the insensitive sequence (MMPi-HA) and the control (K_3-HA) (Chapter IV). Membranes were prepared as described previously (section 2.1). Confluent hDFbs were harvested from monolayer cultures using trypsin-EDTA (Invitrogen, USA). Cells were seeded on the membranes (10^4 cells/cm^2) and cultured in DMEM supplemented with 10% FBS and 1% (v/v) A/B at 37 °C in a humidified atmosphere of 5% CO_2 for 7 days. For inhibition studies, the cell culture media was supplemented with 20 μM of GM6001 MMP-1 inhibitor (Chemicon, USA). Cell culture media was replaced twice a week, and the collected conditioned media was stored frozen (-80 °C) prior to further analysis. At predetermined time points, samples were collected to assess cell proliferation (DNA quantification), morphology and spreading (SEM, F-actin staining) and ECM production (MMP-1, collagen).

To study the effect of the membrane topography on cell morphology and spreading, fibroblasts were cultured on patterned and smooth membranes (Chapter V). Cells were seeded on the membranes (10^4 cells/cm^2) and cultured in DMEM supplemented with 10% FBS and 1% (v/v) A/B at 37 °C in a humidified atmosphere of 5% CO_2. Cell morphology and spreading were assessed by SEM and confocal microscopy.

4.2.2. Encapsulation and culture of hDFb within microcapsules

hDFb were encapsulated on peptide-based microcapsules using a microfluidic device (Chapter VII). Cells were resuspended at a density of $1.0x10^6$ cells per mL in 1 wt% E_3-PA solution. Capsules were generated using a 0.1 wt% K_3-PA solution supplemented with 0.1 M $CaCl_2$. Capsules were transferred to 24-well plates and cultured for up to 14 days in DMEM without phenol red (Sigma, USA) supplemented with 10% FBS (Gibco, UK) and 1% (v/v) A/B (Gibco, UK), in a 37 °C humidified atmosphere with 5% CO_2.

4.2.3. Co-culture studies – seeding of keratinocytes on the surface of capsules with encapsulated hDFb

To validate our peptide capsules for co-culture studies, hDFb and hKc were co-cultured within and on the capsule surface, respectively. Encapsulation of hDFb was processed as described previously. Capsules were transferred to 6-well plates and cultured in DMEM without phenol red, supplemented with 10% FBS and 1% A/B. After 1 day, keratinocytes were seeded on the capsules ($5x10^5$ cells per well) and cultured on a 25:75 mixture (previously optimized in monoculture) of DMEM (containing 10% FBS, 1% A/B) and keratinocyte serum free medium with supplements in a 37 °C humidified atmosphere with 5% CO_2.

4.3. Cell culture assays

The following sections give further details regarding the techniques used in the present thesis for evaluating cells (through analysis of cells viability, proliferation and morphology) after seeding or encapsulation and culture onto the developed matrices.

4.3.1. Live/Dead

Cell viability of encapsulated hDFb (Chapter VII) was assessed through the live/dead assay using calcein-AM (Sigma) and propidium iodide (PI, Molecular Probes, Invitrogen, USA) dyes. This assay provides a two-color fluorescence simultaneous visualization of live and dead cells. It is based on the use of acetomethoxy derivate of calcein (Calcein-AM) that is a non-fluorescent membrane-permeant dye. This dye can be hydrolyzed by endogenous esterase into calcein, a strong green fluorescent dye retained in the cytoplasm (excitation~495 nm/emission~515 nm). On the other hand, dead cells are identified with propidium iodide (PI). This dye passes the membrane of damaged cells and binds to the nucleic acids, increasing up to 40-fold its fluorescence intensity (excitation~495 nm/emission~635 nm). Cells with integrity of plasma membrane will exclude PI. At each time point, the medium was removed and 1 mL of PBS containing 2 µL of calcein-AM and 1 µL of PI was added to each well. Samples were incubated for 10 minutes at 37 °C protected from light followed by three washes in PBS, and were immediately visualized in a fluorescence microscope (Axioimage RZ1M, Zeiss, Germany) as described in section 3.2.

4.3.2. Staining and confocal microcopy

For examining fibroblasts morphology, when cultured either in the self-assembling membranes and microcapsules, staining of F-actin and collagen I was performed (Chapter III-V, VII). Cells were fixed with 10% formalin solution (Sigma-Aldrich, Germany) for 30 minutes at 4 °C. Cells washed once with 0.1 M glycine in PBS and twice with PBS and permeabilized with 2% BSA/0.2% Triton X-100 solution for 1 h at RT. Samples were incubated with the primary antibody, anti-collagen I (ab292, 1 : 500, Abcam, UK), for 1 h at RT and washed three times for 2 minutes with PBS. The samples were then incubated with the secondary antibody, anti-mouse Alexa 488 (1 : 200, Molecular Probes, Invitrogen, USA), for 1 h at RT. To visualize F-actin cytoskeleton fibers, samples were treated with TRITC-conjugated phalloidin (1 U/mL, Sigma-Aldrich, Germany) for 1 h at RT. Cell nuclei were counterstained with 1 mg/mL DAPI (1 : 1000, Sigma-Aldrich, Germany) for 1 min and washed with PBS.

Co-cultured cells in the microcapsules (Chapter VII) were also characterized using an immunocytochemistry assay with specific markers for each cell type. Samples were fixed and prepared as described previously. The primary antibodies and dilutions used in the assay were anti-fibroblast surface protein (F4771, 1 : 500, Sigma, USA) and anti-keratin 5 (PRB-160P, 1 : 500, Covance, Spain). The secondary antibodies and dilutions were anti-rabbit Alexa 488 (1 : 200) and anti-mouse Alexa 594 (1 : 500) (Molecular Probes, Invitrogen, USA).

Samples were visualized by CLSM (Olympus FluoView 1000, Olympus, Japan). The background was subtracted and images were processed using FV10-ASW 3.1 software (Olympus, Japan).

4.3.3. Cell proliferation – DNA quantification assay

Cell proliferation was assessed at different culture times by quantifying the amount of double-stranded DNA (dsDNA). Quantification was performed using a Quant-iT™PicoGreen® dsDNA Assay kit (Invitrogen, Molecular Probes, Oregon, USA) according to the instructions of the manufacturer.

When cells were cultured on membranes (Chapter III and IV), cells were lysed by osmotic and thermal shock and the supernatant was used for DNA quantification. The fluorescent intensity of the dye was measured in a microplate reader (Synergie HT, Bio-Tek, USA) with excitation at 485/20 nm and emission at 528/20 nm. The DNA concentration for each sample was calculated using a standard curve (DNA concentration ranging from 0 to 1.5 $mg.mL^{-1}$) relating the quantity of DNA and fluorescence intensity. Triplicates were made for each time point and for each sample.

Cell proliferation within the microcapsules (Chapter VII) was assessed at different culture times (1, 3, 7 and 14 days). Samples were prepared as described elsewhere[19]. Briefly, the capsules were lyophilized and resuspended in phosphate-buffered EDTA (pH 6.5) supplemented with 0.01 M L-cysteine (Sigma, USA) and 0.5% papain (Sigma, USA). Digestion was performed at 60 °C for 24 h. Following this, quantification was performed using the Quant-iT Pico Green dsDNA Assay Kit (Invitrogen, Molecular Probes, Oregon, USA), according to the instructions of the manufacturer. The DNA concentration for each sample was calculated using a standard curve (0-1.5 mg/mL) by relating the quantity of DNA and fluorescence intensity. The fluorescence signals obtained from blank capsules (i.e. without cells, cultured and processed similarly to those with cells) were used as background values (blanks). Triplicates were made for each time point and for each sample (n=10 capsules per sample).

4.3.4. Scanning electron microscopy

SEM was performed to evaluate cell morphology and cell-matrix interaction when seeded on the membranes (Chapter III-V) or encapsulated in the microcapsules (Chapter VII). After each culture period, samples were washed with PBS and prepared as described in section 3.3 of this chapter.

4.3.5. Statistical analysis

Statistical analysis was performed using GraphPad Prism 5.00 Software (San Diego, USA) and all data were reported as a mean ± standard deviation (SD). Statistical differences between the means of two groups were analyzed with a Student t-test (Chapter III). Although one-way ANOVA measures significant effects of one factor only, two-way ANOVA measures the effect of two factors simultaneously. Thus, the variance among at least three groups was evaluated using two-way analysis of variance (ANOVA) with a Bonferroni's multiple comparisons post-hoc test (Chapter IV, VII). Two-way ANOVA also assesses the interaction between the factors, thus generating three p-values, one for each parameter and one indicating the interaction between both parameters. Post-hoc analysis is commonly used for multiple comparisons among the groups, identifying patterns and limiting the probability of false positive significant differences. The Bonferroni's post-hoc test is one of the most used post-hoc tests and attempts to prevent data from incorrectly appearing statistically significantly. P-values lower than 0.05 were considered statistically significant in all the analysis.

References

1. B. P. Toole, Hyaluronan: From extracellular glue to pericellular cue, *Nat Rev Cancer*, 2004, 4, 528-539.
2. K. S. Girish and K. Kemparaju, The magic glue hyaluronan and its eraser hyaluronidase: A biological overview, *Life Sci*, 2007, 80, 1921-1943.
3. J. Gajewiak, S. S. Cai, X. Z. Shu and G. D. Prestwich, Aminooxy pluronics: Synthesis and preparation of glycosaminoglycan adducts, *Biomacromolecules*, 2006, 7, 1781-1789.
4. J. A. Rowley, G. Madlambayan and D. J. Mooney, Alginate hydrogels as synthetic extracellular matrix materials, *Biomaterials*, 1999, 20, 45-53.
5. N. Stephanopoulos, J. H. Ortony and S. I. Stupp, Self-assembly for the synthesis of functional biomaterials, *Acta Mater*, 2013, 61, 912-930.
6. S. M. Zhang, M. A. Greenfield, A. Mata, L. C. Palmer, R. Bitton, J. R. Mantei, C. Aparicio, M. O. de la Cruz and S. I. Stupp, A self-assembly pathway to aligned monodomain gels, *Nat. Mater.*, 2010, 9, 594-601.
7. H. Cui, M. J. Webber and S. I. Stupp, Self-assembly of peptide amphiphiles: From molecules to nanostructures to biomaterials, *Peptide Science*, 2010, 94, 1-18.
8. M. Amblard, J. A. Fehrentz, J. Martinez and G. Subra, Fundamentals of modern peptide synthesis, *Methods Mol Biol*, 2005, 298, 3-24.
9. R. B. Merrifield, Solid Phase Peptide Synthesis. I. The Synthesis of a Tetrapeptide, *Journal of the American Chemical Society*, 1963, 85, 2149-2154.
10. I. Coin, M. Beyermann and M. Bienert, Solid-phase peptide synthesis: from standard procedures to the synthesis of difficult sequences, *Nat. Protocols*, 2007, 2, 3247-3256.
11. C. S. Ho, C. W. K. Lam, M. H. M. Chan, R. C. K. Cheung, L. K. Law, L. C. W. Lit, K. F. Ng, M. W. M. Suen and H. L. Tai, Electrospray ionisation mass spectrometry: principles and clinical applications, *The Clinical biochemist. Reviews / Australian Association of Clinical Biochemists*, 2003, 24, 3-12.
12. N. J. Greenfield, Methods to Estimate the Conformation of Proteins and Polypeptides from Circular Dichroism Data, *Analytical Biochemistry*, 1996, 235, 1-10.
13. G. Sauerbrey, Verwendung von Schwingquarzen zur Wägung dünner Schichten und zur Mikrowägung, *Zeitschrift für Physik*, 1959, 155, 206-222.
14. R. M. Capito, H. S. Azevedo, Y. S. Velichko, A. Mata and S. I. Stupp, Self-assembly of large and small molecules into hierarchically ordered sacs and membranes, *Science*, 2008, 319, 1812-1816.

15. A. C. Mendes, E. T. Baran, R. L. Reis and H. S. Azevedo, Fabrication of phospholipid–xanthan microcapsules by combining microfluidics with self-assembly, *Acta Biomaterialia*, 2013, 9, 6675-6685.

16. T. S. Sampath Kumar, in *Characterization of Biomaterials*, ed. B. Bose, Elsevier, 1st edn., 2013, ch. 2, pp. 11-47.

17. J. Ilavsky and P. R. Jemian, Irena: tool suite for modeling and analysis of small-angle scattering, *Journal of Applied Crystallography*, 2009, 42, 347-353.

18. O. Glatter, *Small Angle X-Ray Scattering*, Academic Press Inc, 1982.

19. P. de Vos, M. Bucko, P. Gemeiner, M. Navratil, J. Svitel, M. Faas, B. L. Strand, G. Skjak-Braek, Y. A. Morch, A. Vikartovska, I. Lacik, G. Kollarikova, G. Orive, D. Poncelet, J. L. Pedraz and M. B. Ansorge-Schumacher, Multiscale requirements for bioencapsulation in medicine and biotechnology, *Biomaterials*, 2009, 30, 2559-2570.

20. M. J. Webber, J. Tongers, M. A. Renault, J. G. Roncalli, D. W. Losordo and S. I. Stupp, Development of bioactive peptide amphiphiles for therapeutic cell delivery, *Acta Biomater*, 2010, 6, 3-11.

Section 3

RESULTS AND DISCUSSION

Chapter III

Hyaluronan and self-assembling peptides as building blocks to reconstruct the extracellular environment in skin tissue

Chapter III*

Hyaluronan and self-assembling peptides as building blocks to reconstruct the extracellular environment in skin tissue

Abstract

Self-assembling bioactive membranes, incorporating structural components of skin extracellular matrix (ECM), hyaluronan, and biochemical signaling presenting peptide amphiphiles, for recapitulating some aspects of skin tissue microenvironment, are proposed in this work. In the presented strategy, the availability of cell-adhesion ligands (0-50% RGDS epitope) within 2D membranes is controlled aiming at mastering the adhesion of human dermal fibroblasts under serum-free culture conditions. The membranes were characterized with respect to their microstructure by scanning electron microscopy (SEM), degradability and cell behavior regarding adhesion, proliferation, cytoskeleton organization and epitope distribution. SEM of the membrane surface showed a network of nanofibers that are remarkably reminiscent of the filamentous structure found in the ECM. Confocal microscopy images, using a fluorescently labeled RGDS-peptide, showed that the RGDS signal is uniformly distributed on the membranes. Degradation studies indicated that the membranes are susceptible to enzymatic degradation by hyaluronidase. In the presence of the enzyme at physiological concentration, the membranes degrade gradually over time. When grown on membranes with the cell recognition epitope RGDS, fibroblasts had spread out and elongated, exhibiting extended filopodia interacting with fibrillar structure of the membrane surface, thus showing improved adhesion to the substrate. This study demonstrates the positive effect of the RGDS epitope, presented on a self-assembled membrane, in promoting cell-matrix interactions.

* This chapter is based on the following publication:

Daniela S. Ferreira, Alexandra P. Marques, Rui L. Reis, Helena S. Azevedo, Hyaluronan and self-assembling peptides as building blocks to reconstruct the extracellular environment in skin tissue, Biomaterials Science, 1 (9): 952-964, 2013

1. Introduction

The extracellular matrix (ECM) of tissues is a dynamic and hierarchically organized composite structure of various fibrillar proteins and glycosaminoglycans. This network not only has a structural role, providing support and tensile strength for tissues and acting as scaffolds for cell adhesion and organization, but also serves as a storage for growth factors, chemokines and cytokines, and as template for tissue morphogenesis and cell differentiation[1-3].

In skin, the ECM is the largest component of the dermal layer, being composed by structural proteins, like elastin that confers skin elasticity, and collagens, primarily type I and III, which provide structure, strength and integrity[4]. Cell-adhesive proteins like fibronectin, laminin and vitronectin are also present in skin ECM. These glycoproteins have the capacity to bind to cells, via integrins, and to other components of the ECM, namely to glycosaminoglycans, excepting hyaluronan (HA), which is one of the major ECM components in skin[4-5]. HA is an extremely large polymer made up of N-acetylglucosamine and glucuronic acid disaccharide repeating unit (Fig. III.1A). High molecular weight HA acts as an ECM organizer which concentrates and organizes the assembly of other proteins in the ECM by providing a macromolecular template, thus contributing to tissue architecture and function during homeostasis[6-7]. These properties confer HA many unique advantages as a starting material for skin regeneration applications.

Cell adhesion to native ECM is mediated through binding of integrin proteins on the cell surface and specific epitopes present on proteins of the ECM, creating a focal adhesion, responsible for anchoring the cell and the communication between cell cytoskeleton and the surrounding environment[8]. One of ECM cell adhesive proteins, fibronectin, binds to integrins through a domain containing Arg-Gly-Asp-Ser (RGDS)[9]. This sequence, first proposed by Pierschbacher and Rouslahti, functions as a general cell adhesive sequence[10] and has been widely used in biomaterials functionalization, including HA-based hydrogels[11-13], improving cell adhesion and subsequent proliferation[14-17].

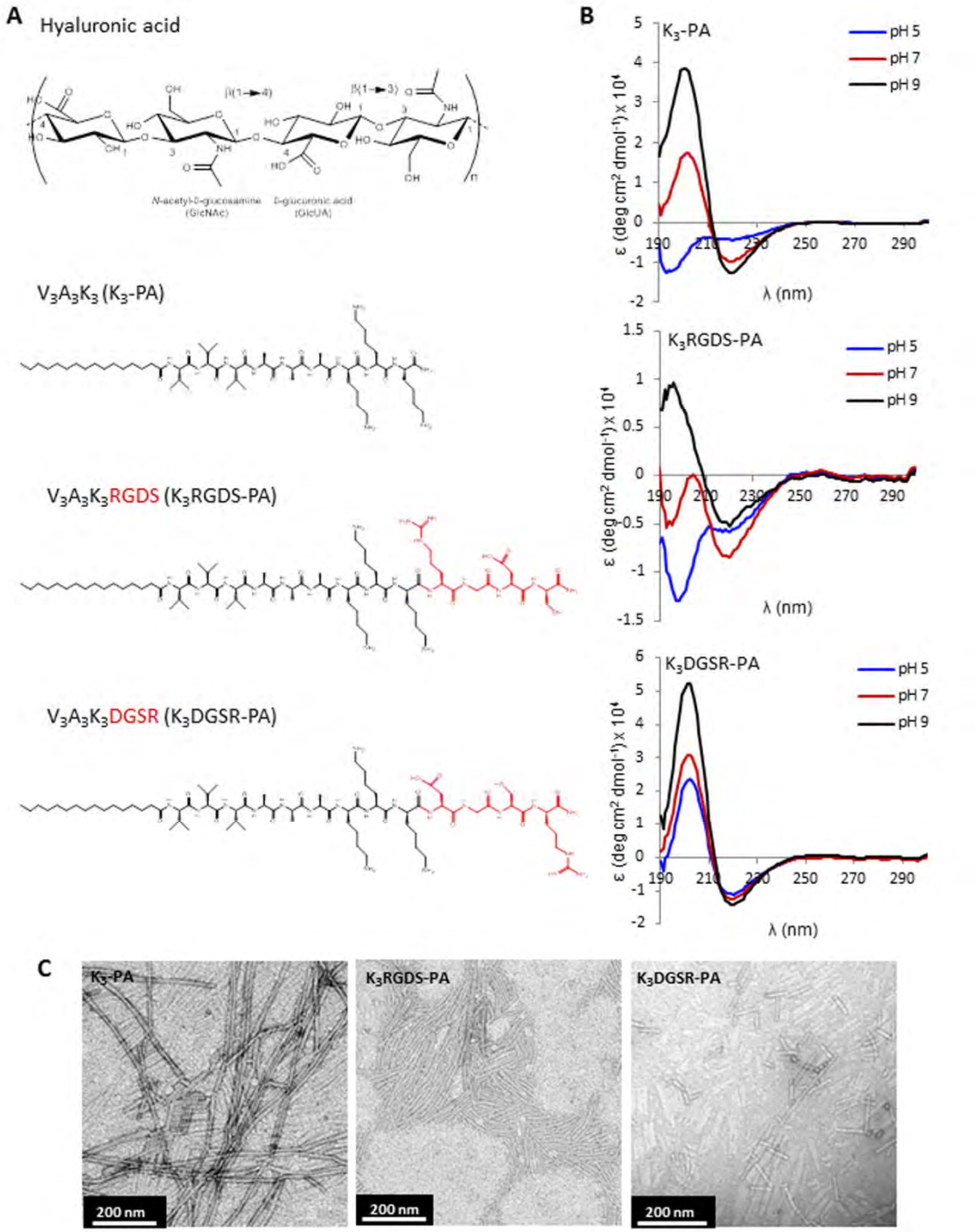

Figure III.1. Peptide design and characterization. A) Chemical structure of the building blocks used for preparing the self-assembled membranes, hyaluronan (HA) and different peptide amphiphiles (PAs): $V_3A_3K_3$ containing positively charged lysines (KKK) to bind the anionic HA, one containing the RGDS epitope (K_3RGDS-PA), a scrambled version (K_3DGSR-PA). B) Circular dichroism spectra of peptide solutions ($3.3x10^{-5}$ M) at pH 5, 7 and 9 showing predominant β-sheet secondary structure. C) TEM images of PA nanostructures formed by deposition of 0.1 mM solutions in water followed by air drying on a carbon-coated TEM grid.

Peptides represent an interesting family of building blocks which can self-assemble to create a large number of nanostructures, such as micelles, vesicles and nanofibers[18-20]. Thus, by self-assembly, structurally simple building blocks can be easily gathered to create functionally complex materials[8].

Bottom-up approaches based on the self-assembly of small molecules provide a unique set of advantages to create biomaterials as they offer the possibility of controlling the architecture, shape and dimensions of the bioactive nanostructures, as well as the spatial display and density of the bioactive signals [21]. The architectural resemblance of self-assembled nanofibers to filamentous structures found in natural ECMs represents an additional feature to attain superior biomimetic scaffolds, and a clear advantage in biomaterials engineering.

The fabrication of artificial ECMs can be used to mimic the properties of native tissues as well as to reconstruct cellular microenvironments *in vitro*. We address this challenge by combining self-assembling peptides (peptide amphiphiles) integrating biochemical signals (RGDS ligand) to permit cell adhesion and spreading, and functional molecules (HA), as components of our matrix. These components were shown to self-assemble in 2D membranes[22-24]. Through self-assembly, epitope spatial organization can be controlled at the micrometer and nanometer scales to guide cellular behavior. Materials that selectively interact with cells may be helpful in improving our understanding of key structural and biochemical ECM components, and ultimately, harnessing the presentation of specific cues to cells. This represents a simplified approach to deconstruct the skin niche and to identify the effect of individual niche components over cell behavior.

2. Materials and methods

Hyaluronan (HA) and fluorescein HA

The hyaluronan used in all experiments had an average molar mass of 2 MDa and was purchased from Lifecore Biomedical, Inc (Chaska, USA). HA was fluorescently labeled with fluoresceinamine (Fig. III.3B) using *N*-(3-dimethylaminopropyl)-*N*'-ethylcarbodiimide hydrochloride (EDC) chemistry and following the procedure described by Gajewiak et al.[25]. Briefly, HA (50 mg) was dissolved in 20 mL of water to give a 0.25% (w/v) solution, which was then mixed with a solution of 5 mg of fluoresceinamine (Sigma, USA) in 20 mL of dimethylformamide. Next, 100 mg of N-hydroxysuccinimide (NHS, Sigma, USA) was added, and the solution pH was adjusted to 4.75 with 0.01 M HCl. Finally, 50 mg of EDC (Sigma, USA) was mixed maintaining the solution pH at 4.75. After 12 h, the solution was transferred to dialysis tubing (2000 Da MWCO, Sigma, USA)) and dialyzed exhaustively against 100 mM NaCl, followed by dialysis against distilled water and lyophilization.

Peptide amphiphiles synthesis and purification

Three different peptide amphiphiles (PAs) were synthesized in this work, consisting of a peptide segment covalently linked to a 16-carbon alkyl chain: $C_{15}H_{31}CO$-$V_3A_3K_3$ (K_3-PA, filler), $C_{15}H_{31}CO$-$V_3A_3K_3$RGDS (K_3RGDS-PA) and $C_{15}H_{31}COV_3A_3K_3$DGSR (K_3DGSR-PA, scrambled) (Fig.III.1). The peptides were synthesized on a CS Bio 136XT automated peptide synthesizer (CS Bio, USA) using standard 9-fluorenylmethoxycarbonyl (Fmoc) based solid phase chemistry on a 4-methylbenzhydrylamine (MBHA) rink amide resin. Amino acid couplings were performed using 4 equivalents (4 mmol) of Fmoc protected amino acids (Novabiochem®), 4 equivalents of O-(Benzotriazol-1-yl)-N,N,N′,N′-tetramethyluronium hexafluorophosphate (HBTU, Novabiochem®) and 6 equivalents of N,N-diisopropylethylamine (DIEA, Sigma, USA). Fmoc deprotections were performed with 20% piperidine (Sigma, USA) in dimethylformamide. A palmitic acid ($C_{16}H_{32}O_2$) tail was manually coupled under the same conditions as the Fmoc-amino acids. Peptide cleavage from the resin and removal of the protecting groups was carried out on a mixture of trifluoroacetic acid (TFA, Sigma, USA)/triisopropylsilane (TIS, Alfa Aesar)/water (95/2.5/2.5)) for 3 h at room temperature. The peptide mixture was collected and excess TFA was removed by rotary evaporation. The resulting viscous peptide solution was triturated with cold diethyl ether. The white precipitate was collected by filtration, washed with cold ether, and allowed to dry under vacuum overnight. The peptide mass was confirmed by electrospray ionization mass spectrometry (ESI-MS, Thermo Electron Corporation Finnigan LXQ MS Waltham, USA). Peptides were then purified on a Waters 2545 Binary Gradient high-performance liquid chromatography (HPLC) system using a preparative reverse-phase C18 column (Atlantis Prep OBD T3 Column, Waters) and a water/acetonitrile (0.1% TFA) gradient. TFA counter-ions were exchanged by sublimation from 0.1 M hydrochloric acid. Finally, the peptides were dialyzed against ultrapure water using 500 MWCO dialysis tubing (Spectrum labs, The Netherlands), and lyophilized. Confirmation of mass and purity was done by ESI-MS and HPLC (Supplementary Information, Fig. III.S1-S3).A fluorescent version of K_3RGDS-PA, $C_{15}H_{31}CO$-$V_3A_3K_3K_{rhod}$RGDS (Fig. III.3B), was also synthesized to allow examining the availability/distribution of the RGDS motif within and on the surface of the membranes. For that, an additional lysine residue, with a 4-Methyl trityl (Mtt) protecting group in the ε amine of the lysine residue (Fmoc-Lys(Mtt)-OH), was introduced in the sequence to which the Rhodamine dye was attached. The peptide was grown on the resin and after coupling the palmitic tail, the Mtt protecting group was selectively removed with a solution of TFA/TIS/DCM (4:4:92) at room temperature. Resin was incubated with deprotection solution for 5 minutes and washed thoroughly with DCM. These steps

were repeated until the resin no longer turned yellow. Then, peptide-resin (150 mg) was swollen in 1150 µL of DMF and 50 µL of DIEA. Ten milligrams of 5-(and 6)-carboxytetramethylrhodamine succinimidyl ester (NHS-rhodamine) were dissolved in the supernatant from the beads swelling step and added to the resin. The reaction took place at room temperature, overnight, and protected from light. After repeatedly washes with DMF and methanol, the peptide was cleaved from the resin following the procedure described above for the other peptides, and purified by HPLC. Mass was confirmed by matrix assisted laser desorption/ionization mass spectrometry (MALDI-MS, 4800 MALDI-TOF/TOF, AbSciex) (Supplementary Information, Fig. III.S4).

Peptide amphiphiles characterization

Circular dichroism (CD) spectroscopy

Peptides were dissolved in deionized water to a final concentration of 0.033 mM and the pH was adjusted to 5, 7 and 9. The CD measurements were performed in a PiStar-180 spectrometer from Applied Photophysics (Surrey, UK), under a constant flow of nitrogen (8 $L.min^{-1}$) at a constant pressure value of 0.7 MPa. Far-UV spectra were recorded at 25 °C from 190 to 300 nm in a quartz cuvette with 1 mm path-length. All scans were performed in the steady state with a bandwidth of 1 nm and each represented spectrum is an average of 5 spectra.

Transmission electron microscopy (TEM)

Samples for TEM analysis were prepared by placing a drop of 0.1 mM peptide solution directly on the 400 mesh carbon-coated copper TEM grid (Ted Pella, USA). For negative staining a drop of 2% (w/v) uranyl acetate aqueous solution was placed on the samples. After ca. 3 minutes, the excess solution was wiped away by a piece of filter paper, and the sample was allowed to dry under ambient conditions. All images were collected with a JEOL JEM-1010 transmission electron microscope at 100 kV (JEOL, USA).

Characterization of PA-HA interactions

Quartz crystal microbalance with dissipation (QCM-D)

Measurements were performed in a quartz crystal microbalance with dissipation monitoring (QCM-D E4) from Q-Sense (Gothenburg, Sweden). All the experiments were performed at 25 °C with a constant flow rate of 50 µl/min using gold coated crystals (QSX301, Q-Sense, Goteborg, Sweden) previously cleaned with water and H_2O_2 for 1 h each, and then acetone, ethanol and isopropanol for 3 minutes

each at 37 °C with sonication. The system was equilibrated with a 0.15 M sodium chloride (NaCl) solution to obtain a stable frequency and dissipation baseline signal. Once the signal was stable, the NaCl solution was replaced by a solution of K_3-PA (0.2% (w/v) in 0.15 M NaCl) during 30 minutes. To remove weakly bound peptide, the crystals were rinsed with a NaCl solution and then replaced by a solution of HA (0.1% (w/v) in 0.15 M NaCl) for 30 minutes. Again, to remove weakly bound polymer, the system was rinsed with NaCl. The QCM instrument recorded frequencies up to the 13th overtone, and Δf and ΔD were monitored in real time. In the present study the results are shown for the 7th overtone, the frequency of this overtone was normalized to the fundamental resonant frequency of the quartz crystal, by dividing it by ν (where $\nu = 7$).

PA-HA membrane preparation

PA-HA membranes were prepared using a 48 well plate as template in a sterile environment. 150 µL of a 1% (w/v) HA solution was cast on the bottom of the wells and then 150 µL of a 2% (w/v) K_3-PA solution was added on top of the HA solution. A membrane is immediately formed upon contact between the two solutions. The membrane was allowed to grow with time (overnight) as reported previously[23]. The membranes were rinsed with sterile ultrapure water to ensure the removal of unreacted HA and PA.

PA-HA membrane characterization

Scanning electron microscopy (SEM)

The microstructure of the membranes was analyzed by SEM. Samples were fixed in a 2% glutaraldehyde/3% sucrose in PBS for 1 h at 4 °C followed by sequential dehydration in graded ethanol concentrations (from 20 to 100%). To remove ethanol, samples were chemically dried in hexamethyldisilazane (HMDS, Electron Microscopy Sciences, USA) 3 times, 15 minutes each, and HMDS excess allowed to evaporate. Prior observation, the samples were coated with a gold/palladium layer and imaged using an ultra-high resolution field emission gun scanning electron microscope (Nova™ NanoSEM 200) from FEI (Eindhoven, The Netherlands).

Confocal microscopy

Confocal microscopy was used to probe the location and retention of fluorescently-labeled HA as well as to visualize the distribution of RGDS signal on (surface) and within (cross-section) the PA-HA membrane. Membranes were formed as previously described using fluorescein HA solution (1%, w/v)

and 2% (w/v) peptide mixture containing 0.1% of K_3K_{rhod}RGDS-PA and 99.9% of K_3-PA. The membranes were incubated overnight at RT protected from light. After washing, membranes were transferred to glass microscopy slides, covered with a glass coverslip, and sealed to prevent dehydration. Membranes were imaged by laser scanning confocal microscope (LSCM, Olympus FluoView 1000, Japan) with the appropriate excitation and emission wavelengths. Optical slices were captured at regular intervals to produce reconstructed z-stacks with 100 μm total thickness. Images of cross sections were compiled from z-stack in the x-direction using FV10-ASW software from Olympus.

In vitro enzymatic degradation

Degradation behavior of the PA-HA membranes in the absence and presence of a HA-degrading enzyme (hyaluronidase, HAase) was analyzed *in vitro*. Bovine testicular HAase (Type IV, EC 3.2.1.35) was obtained from Sigma (USA). This enzyme has the ability to hydrolyze β(1,4) glycosidic bonds between N-acetyl-D-glucosamine and D-glucuronate residues producing HA fragments with a N-acetyl-D-glucosamine at the reducing end. The enzyme activity can thus be measured by the quantification of these reducing ends. Degradation studies were carried out by incubating PA-HA membranes in PBS at 37 °C in the absence (control) or presence of HAase at different concentrations, 2.6 U/mL HAase (to simulate physiological conditions in human plasma) and 50 U/mL HAase, for 14 days. The enzyme solution was replaced every 72 h throughout the study and stored frozen until analysis. At predetermined time points, the solution was completely collected for further quantification of N-acetylamino sugars using the fluorimetric Morgan-Elson assay method[26]. A calibration curve of N-acetyl-D-glucosamine (NAG) standards was used. HA fragments resulting from enzymatic hydrolysis were identified by mass spectrometry in the negative mode (Thermo Electron Corporation Finnigan LXQ MS Waltham, USA). The morphology of the membranes after degradation was analyzed by SEM.

Cell culture studies

Isolation and culture of human primary fibroblasts

Human dermal fibroblasts (hDFb) were isolated from skin samples discarded from abdominoplasty surgeries of consenting patients at Hospital da Prelada (Porto, Portugal). Briefly, the skin tissue was cut in pieces of 0.5 by 0.5 cm and digested in a dispase solution (2.4 U/mL in PBS) at 4 °C, overnight. After removing the epidermis, the fibroblasts were isolated from the dermis by overnight digestion of the dermal pieces in a collagenase IA solution (125 U/mL in PBS) at 4 °C. Digestion products were poured through a 100 μm cell strainer and centrifuged at 200 *g* for 5 minutes. The pellet was resuspended and

the cells were subsequently cultured in Dulbecco's Modified Eagle Medium (DMEM) (Sigma, Germany) supplemented with 10% of fetal bovine serum (FBS, Gibco, UK) and 1% (v/v) antibiotic/antimycotic solution (A/B) (Gibco, UK) containing 100 units/mL penicillin and 100 mg/mL streptomycin, in a 37 °C humidified atmosphere with 5% CO_2.

hDFb culture on the PA-HA membranes

To study the effect of RGDS signaling on cell adhesion, PA-HA membranes containing different percentages of RGDS motif were prepared by mixing the filler peptide (K_3-PA) with 1%, 10% and 50% K_3RGDS-PA and 10% scrambled peptide (K_3DGSR-PA) to give a 2% (w/v) final peptide concentration. HA sterilization for cell studies was done by dissolving the polymer, filtering the solution through a 0.22 μm filter, followed by lyophilization in sterile falcon tubes. Peptide solutions were sterilized by UV exposure for 15 minutes. Membranes were prepared following the procedure previously described under sterile conditions. Confluent hDFbs, at passage 4, were harvested from monolayer cultures using trypsin-EDTA (Invitrogen, USA). Cells were washed in PBS and centrifuged at 200 *g* for 10 minutes in order to remove serum residues. Cell pellet was then resuspended at a density of 5.0 x 10^4 cells/mL in serum-free DMEM without phenol red (Sigma, Germany) supplemented with 1% (v/v) A/B. Cells (2.5 x 10^4cells/well) were cultured on the PA-HA membranes in 48 well plates at 37 °C in a humidified atmosphere of 5% CO_2 for 2, 6, 12 and 24 h. hDFbs cultured on tissue culture polystyrene (TCPS) coverslips were used as control. Cells cultured on the membranes were examined under SEM to analyze cell morphology and cell-matrix interactions. Cell cultured membranes were fixed, dehydrated and prepared as described for SEM analysis.

F-actin staining

Staining for the F-actin cytoskeleton fibers of attached hDFbs was carried out after fixing cells in 10% formalin solution neutral buffer (Sigma-Aldrich, Germany) for 30 minutes at 4 °C. Cells were then washed once with 0.1 M Glycine in PBS and twice with PBS and permeabilized with 2% BSA/ 0.2% Triton X-100 solution for 1 h at RT. Samples were incubated with TRITC-conjugated phalloidin (1U/mL, Sigma-Aldrich, Germany) for 1 h at RT. Cell nuclei were counterstained with 1 mg/mL DAPI (1:1000, Sigma-Aldrich, Germany) for 1 min and washed with PBS. Visualization was performed by CLSM (Olympus FluoView 1000, Olympus, Japan). Background was subtracted and images were processed using ImageJ software (NIH, USA).

dsDNA quantification

The number of cells adherent to the membranes was assessed at different culture times by quantifying the amount of double-stranded DNA (dsDNA). Quantification was performed using the Quant-iT™ PicoGreen® dsDNA Assay Kit (Invitrogen, Molecular Probes, Oregon, USA), according to the instructions of the manufacturer. Briefly, cells on the different membranes were lysed by osmotic and thermal shock and the supernatant used for the DNA quantification. The fluorescent intensity of the dye was measured in a microplate reader (Synergie HT, Bio-Tek, USA) with excitation at 485/20 nm and emission at 528/20 nm. The DNA concentration for each sample was calculated using a standard curve (DNA concentration ranging from 0 to 1.5 mg/mL) relating quantity of DNA and fluorescence intensity. Triplicates were made for each time point and for each sample.

Data analysis and statistics

Statistical analysis for NAG and DNA quantification was performed using the non-parametric Kruskal-Wallis test, after testing the normality of our data with Shapiro-Wilk test. Dunn's post-hoc test were carried out to determine the differences between the various conditions under this study. Values of $p < 0.05$ were considered to determine statistically significant differences between the groups.

3. Results and discussion

Peptide design and formulation in the bioactive membranes

The self-assembling peptides used in this study are amphiphilic peptides consisting in a linear hydrophobic segment coupled to a peptide sequence, that includes a β-sheet forming sequence (VVVAAA) and a domain with positively charged amino lysines (KKK) to bind the anionic HA (K_3-PA). This class of self-assembling peptides, known as peptide amphiphiles (PAs), was proposed by Stupp's group for different biomedical applications[19, 27-28]. The fibronectin-derived RGDS epitope was incorporated into the peptide structure (K_3RGDS-PA) due to its known properties on mediating cell adhesion (Fig. III.1A). Different PA molecules have been co-assembled, allowing for a specific bioactive molecule to be mixed with a non-bioactive diluent molecule[29-32] to vary the epitope density on the assembled structures for optimized cell signaling. For example, Webber and co-workers[29] have investigated the co-assembly of a positively charged PA containing the RGDS sequence (K_3RGDS-PA) with negative diluent PA (E_3-PA) with the aim of producing mixed binary nanofibers. By varying the RGDS composition on surfaces coated with the co-assembled peptide nanofibers, they were able to determine the optimal RGDS density on the adhesion of bone-marrow mononuclear cells. While this co-assembly strategy has been explored by

other groups, using coated surfaces[29, 31] or self-assembled gels[32], the co-assembly of RGDS-containing peptides with HA in self-assembled membranes has been explored by our group[33]. In this configuration, the membranes present different densities of biomolecular signals designed to enhance cell adhesion, but other biochemical functionalities can be incorporated, like growth-factor binding sequences relevant in wound healing.

Previous studies have shown that the formation of stable β-sheet is very important and necessary for peptide self-assembly[20, 34]. Although the formation of β-sheet secondary structure of K_3-PA has been demonstrated previously[35], the inclusion of the RGDS (or DGSR) in the PA sequence could disturb that rearrangement and consequently affect the stability of self-assembled membranes. Therefore, circular dichroism (CD) spectroscopy was performed to evaluate the secondary structure of the synthesized peptides (Fig. III.1B). The CD analysis of the PAs revealed the presence of hydrogen-bonded structures, namely β-sheets or random coil, depending on the pH. At pH 9, a typical spectrum of β-sheet structure was observed for all the molecules, with a minimum in the 210-220 nm range, a crossover from positive to negative above 190 nm, and a positive ellipticity around 200 nm. The scrambled peptide showed this conformation in all the studied pH conditions, with stronger peaks at 205 nm. Below pH 9, the K_3RGDS-PA showed a random coil conformation. K_3-PA presented a β-sheet structure with a minimum at 220 nm and a maximum at 205 nm at pH 7, and a random coil conformation at pH 5. TEM analysis showed the formation of nanofibers for all the peptides, but K_3DGSR-PA formed shorter fibers than the K_3 and K_3RGDS-PAs (Fig. III.1C).

PA-HA interaction

Previous studies have shown the ability of K_3-PA to interact with HA and form macroscopic structures, such sacs and membranes, by self-assembly[22-24]. In the herein presented work, we have investigated, for the first time, the interactions between these two molecules by QCM-D. This technique allows marker-free measurement of specific interactions between immobilized molecules and analytes in solution and has been widely used for studying macromolecular interactions. Due to its sensitivity, allows detecting mass changes of the order of ng.cm^{-2}, and permits to measure the viscoelastic properties of the resulting film[36-37]. Figure III.2 shows the normalized frequency ($\Delta f_v/v$, where v is the overtone) and dissipation (ΔD) variations for the 7th overtone (35 MHz). The first 15 minutes in Figure III.2 show the establishment of the baseline with 0.15 M NaCl. The subsequent 45 minutes correspond to the deposition of K_3-PA, where a decrease in the frequency (of about 23 Hz) and an increase in ΔD were observed. After rinsing with NaCl, the hyaluronan solution was pumped continuously for 45 minutes,

when an adsorption plateau was attained. A decrease in frequency of 38 Hz was registered, and again an increase in dissipation has occurred. After HA deposition, the film was again rinsed with NaCl. During this washing step, the variation in both Δf and ΔD was very small, indicating the formation of a stable film and a strong interaction between both molecules. The frequency variation, Δf, decreases with time, due to the deposition of peptide or hyaluronan on the quartz crystal. On the other hand, the dissipation, ΔD, increases, revealing that the film is not rigid and begins dissipating energy, thus exhibiting the typical viscoelastic behavior. This behavior has been observed before when studying the interaction between poly(L-lysine) and hyaluronan by QCM-D[38]. The QCM-D results demonstrated and confirmed the strong interaction between the K_3-PA and HA and the formation of stable complex.

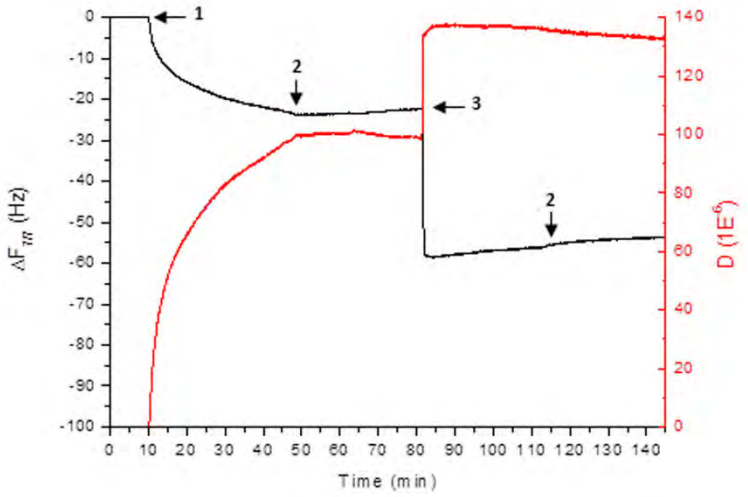

Figure III.2. PA-HA interaction. QCM-D monitoring of frequency (Δf, black) and dissipation (ΔD, red) changes obtained at 7th overtone, during deposition of peptide (step 1) and hyaluronan (step 3) on a bare crystal (step 2 relates to rising). The frequency of this overtone was normalized to the fundamental resonant frequency of the quartz crystal, by dividing it by ν (where ν = 7).

Membrane microstructure and degradation

In this work, we aimed to recreate some aspects of the physical and biochemical environment of skin tissue. It was shown previously that hierarchical membranes can be formed by instant self-assembly between a positively charged PA (K_3-PA) and the megadalton hyaluronan (HA) under certain conditions[22-23]. We thought that these fibrillar membranes, containing components of skin ECM, could provide a starting platform to design complex biomimetic environments of skin ECM (Fig. III.3).

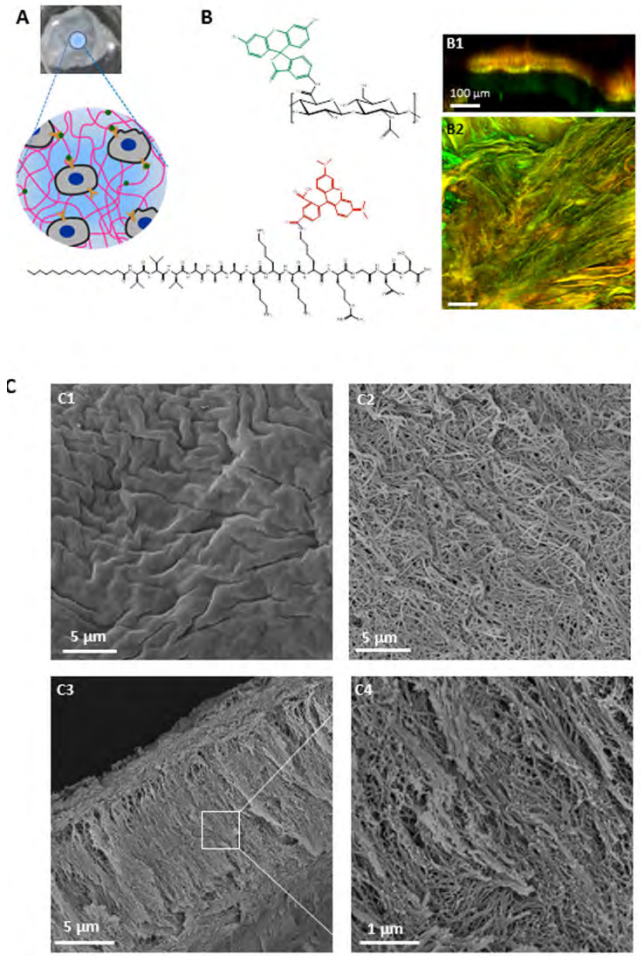

Figure III.3. PA-HA membrane microstructure. A) Schematic representation of PA-HA membranes functionalized with bioactive molecules (green) interacting with cell integrins (yellow). B) Confocal microscopy images of the membranes prepared with 1% (w/v) fluorescein-HA and 2% (w/v) peptide mixture containing 0.1% K_3K(Rhod)RGDS-PA. Images show the localization of HA (green) and PA (red) over the membrane surface (B2) and cross section (B1). Yellow represents the overlaping of both components. C) SEM micrographs of self-assembled membranes with 1% (w/v) HA and 2% (w/v) K_3-PA, showing the surface on the polymer (C1) and peptide (C2) sides and cross section (C3, C4).

SEM analysis of the microstructure of the membranes revealed a very highly organized structure exhibiting two distinct surfaces, as observed previously[22-23, 32]. The surface corresponding to the HA side (Fig. III.3C1) is characterized by a rough and amorphous structure, whereas the peptide side (Fig. III.3C2), exhibit a network of organized nanostructures (nanofibers) randomly distributed, resembling the fibrillar structure of natural ECM. SEM micrographs of the cross section revealed a membrane with around 14 µm in thickness and aligned nanofiber bundles perpendicular to the interface (Fig. III.3C3). To investigate if the addition of the K_3RGDS-PA would affect the membrane microstructure and

morphology, SEM was used to image membranes containing 50% K_3RGDS-PA. Membranes containing 50% of K_3RGDS-PA presented a similar thickness and microstructure to the ones formed with 100% of K_3-PA (Fig. III.S5, supplementary information). Fluorescent micrographs obtained by confocal microscopy, using the fluorescently labeled K_3K_{rhod}RGDS-PA (red) and hyaluronan (green), showed a perfect overlap of the two, in yellow, resulting from the interaction between the peptide and hyaluronan (Fig. III.3B2). This strong yellow region is also seen in a software simulated cross section (Fig. III.3B1), surrounded by a soft area in red or green, that correspond to the peptide and hyaluronan side, respectively. The uniform distribution of the red signal showed that RGDS molecules were well distributed within the membranes although the spatio control of the signal on specific locations of the membrane is yet a major challenge.

The natural ECM is an extremely dynamic network that consists of protein fibers and glycosaminoglycans that support cell fate and provide biophysical and biochemical cues to cells through cell surface receptors, such as integrins[1-2, 39]. Cells degrade the ECM through proteases during their migration. Synthetic ECM matrices that aim to provide an environment for tissue regeneration should recapitulate key features of the natural ECM such as integrin mediated cell binding, cell migration, and cell proliferation, while also allowing their degradation, offering a platform on which cell-triggered remodeling could occur. To mimic the turnover of natural ECM, our matrices were designed to be sensitive to enzymes expressed by surrounding cells (e.g. hyaluronidase). This cell-mediated degradation is a process reminiscent of tissue remodeling. It is well known that the degradation of hyaluronan into large oligosaccharides is mediated by hyaluronidase[40]. Therefore, the degradation behavior of the PA-HA membranes was studied in three different conditions, PBS and PBS containing 2.6 U/mL and 50 U/mL HAase. Degradation was followed by the quantification of N-acetylglucosamine in solution and by SEM analysis (Fig. III.4). Incubation in PBS up to 14 days did not cause degradation of the membranes since the amount of N-acetylamino sugars in the supernatant was significantly lower than the obtained for the membranes incubated in the higher enzyme concentration (50 U/mL). Compared with the physiological concentration (2.6 U/mL), only for the latest time point a statistically difference was observed. In addition, no evident signs of degradation are observed in the SEM images for the membranes incubated in PBS only. This result indicates that the membranes are relatively stable in buffer saline solutions, but are susceptible to enzymatic degradation by HAase. As expected, the membrane degradation was significantly enhanced when incubated with higher enzyme concentration (50 U/mL) than when in presence of the enzyme at physiological conditions (2.6 U/mL), as demonstrated by the higher amount of released N-acetylamino sugars (Fig. III.4A). SEM analysis of

the membranes collected at different time points corroborates these results, showing the appearance of pores on the membrane surface (Fig. III.4B1) and cross-section (Fig. III.4B2), as a result of HA degradation by HAase. At a higher HAase concentration (50 U/mL) the degradation of the membranes is more evident, but progressive along the time (Fig. III.4B1-B2).

The presence of HA oligosaccharides as degradation products was confirmed by mass spectroscopy. ESI-MS analysis of the supernatants after membrane degradation in 2.6 U/mL HAase solution for 7 days showed three main peaks, corresponding to $[HA]_{11}$: $[M-2H]^{2-}$ m/z= 1046.25, $[HA]_{12}$: $[M-2H]^{2-}$ m/z= 1142 and $[HA]_{14}$ $[M-2H]^{2-}$ m/z= 1332.17 (Fig III.4C)[41]. The observed mass for $[HA]_{11}$ is a fragmentation product of ESI-MS since digestion with HAase produces even-numbered oligosaccharides. To confirm that the observed masses are not caused by the technique itself ESI-MS analysis was performed of a HA solution (Fig. III.S6, supplementary information) but no known masses of HA oligosaccharides were identified.

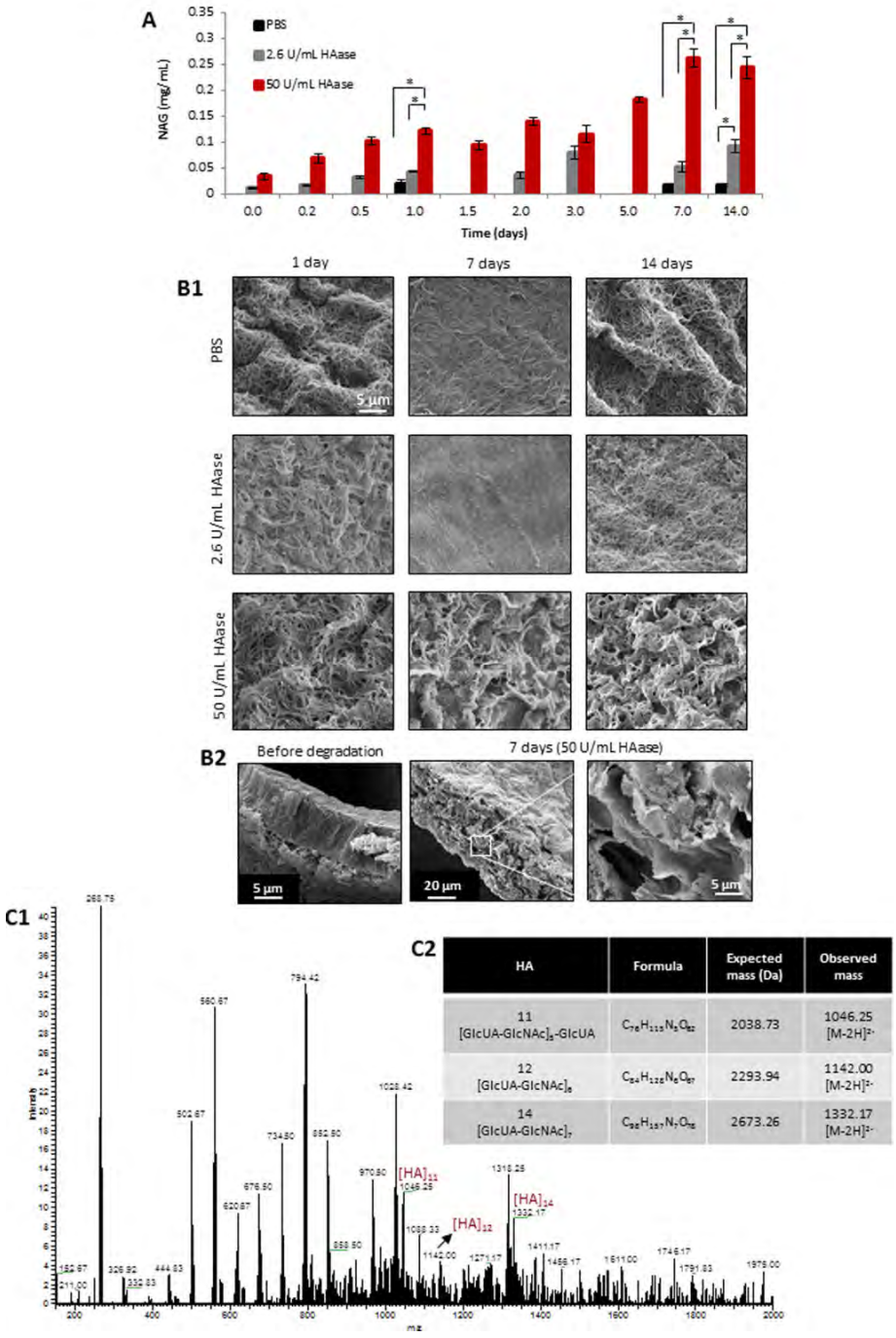

HA	Formula	Expected mass (Da)	Observed mass
11 $[GlcUA\text{-}GlcNAc]_5\text{-}GlcUA$	$C_{76}H_{115}N_5O_{82}$	2038.73	1046.25 $[M\text{-}2H]^{2-}$
12 $[GlcUA\text{-}GlcNAc]_6$	$C_{84}H_{126}N_6O_{87}$	2293.94	1142.00 $[M\text{-}2H]^{2-}$
14 $[GlcUA\text{-}GlcNAc]_7$	$C_{98}H_{147}N_7O_{98}$	2673.26	1332.17 $[M\text{-}2H]^{2-}$

Figure III.4. Degradation of PA-HA membranes. A) Quantification of N-acetylamino sugars released from K_3-HA membranes in PBS and PBS containing 2.6 U/mL and 50 U/mL HAase (*$p < 0.05$, error bars represent standard deviation (n=3)). B1) SEM images showing differences in membrane microstructure when exposed to different hyaluronidase (HAase) concentrations up to 14 days. B2) Cross section of the membranes before and after exposure to 50 U/mL HAase evidencing that degradation is occurring not only on the surface but also inside the membrane. C1) Negative ESI-MS of the supernatant after incubating the membranes in 2.6 U/mL HAase for 7 days showing the presence of HA fragments. C2) Observed and theoretical molecular masses of HA oligosaccharides.

The membranes herein presented were shown to degrade gradually over time in the presence of HAase at physiological concentration. In addition, it is expected that the peptide component of the membrane will degrade overtime by hydrolytic and enzymatic processes into amino acids, which are nontoxic and easily cleared in the body. Peptides can be designed to be susceptible to enzymatic cleavage by incorporating matrix metalloproteases (MMPs)-sensitive peptide sequences[42-43], a strategy that is currently being explored in our lab. By having membranes sensitive to enzymatic activities, we are pursuing the goal of biomimetic matrix degradation. These PA-HA membranes may present an advantage over other systems, once slow degradation will enable the migration of the adhered cells, as well as matrix remodeling and new tissue formation led by the artificial ECM template

Fibroblast response to the PA-HA self-assembled membranes displaying different densities of the RGDS epitope

Preliminary studies were performed with hDFb cultured on K_3PA-HA membranes in DMEM with 10% FBS up to 7 days. These studies indicated that these membranes supported the adherence of fibroblasts, without presenting cytotoxicity (Fig. III.S7, supplementary information).

Understanding the factors that regulate cell behavior is important in many therapeutic applications. In most studies, cell behavior is studied in culture medium supplemented with serum, which is poorly defined in terms of proteins content. To investigate whether the produced PA-HA membranes could integrate cell-adhesive ligands and anchor human dermal fibroblasts, serum-free culture conditions were used to eliminate the complexity of the competing adsorption process of serum proteins on the membrane surface.

It has been shown that fibroblast survival, proliferation and migration are dependent on cell adhesion and that fibronectin (FN) binding domains have significant implications on skin wound healing[4]. These activities require fibroblast attachment to RGD sequence in the tenth FN type III repeat, via cell surface membrane integrin receptors[44]. Several authors reported that inert biomaterials benefit from the presence of the RGDS signaling molecule for optimal cell recognition and adhesion[14-16, 31]. To enhance the adhesion of cells on the developed PA-HA membranes, the RGDS motif (which is a known ligand for integrin receptors) was incorporated into the PA structure creating adhesion points to support integrin-mediated cellular adhesion and migration on the membranes. Previous studies have shown that the density of the RGDS epitope impacts cell recognition and adhesion[45]. Considering this, experiments were performed varying the K_3RGDS-PA composition on the membranes (1, 10 and 50%) to determine the optimal RGDS density. Membranes containing 10% K_3DGSR-PA or only K_3-PA were used as controls.

DNA quantification results (Fig. III.5A) showed that when seeded on 50% K_3RGDS-PA containing membranes, hDFb adhered at significantly higher number than on the ones with lower concentration of RGDS, 1 and 10%, or without RGDS, K_3-PA and K_3DGSR-PA for all time points except at 12h of culture.

Cell morphology and distribution on the membranes was further examined by confocal microscopy analysis (Fig. III.5B). After the first two hours, fibroblasts were uniformly distributed on the membrane surface and a high number of cells was observed on the 50% K_3RGDS-PA containing membranes, as depicted by the higher density of nuclei. These results demonstrate the positive effect of the RGDS epitope on promoting cell adhesion which is mediated by integrins on the cell surface. Considering the presence of HA on the membranes and knowing that CD44, a transmembrane receptor observed in a number of different cell types[46], mediates HA dependent cell adhesion, the expression of this receptor by hDFbs was assessed (Supplementary Information, Fig. III.S8) . Although these cells showed a high expression of CD44 (98.67%), cells cultured on HA-based hydrogels (Supplementary Information, Fig. III.S9) did not show strong adhesion on these substrates. This result suggest that integrins may play a major role, rather than CD44, on cell adhesion on PA-HA membranes.

Staining of cell cytoskeleton (Fig. III.5B) did not reveal strong organized actin fibers. Most of what is known about cell structure and function *in vitro* derives from cells plated on rigid substrates, such as plastic or glass, laminated with a thin film of serum proteins. As a result, some prominent aspects of cell structure, such as the elongated morphology of cultured fibroblasts or the prevalence of large actin fibers that are commonly studied *in vitro*, are rarely if ever seen *in vivo*[47-48]. Furthermore, cells cultured on soft substrates show diffuse adhesion complexes with poor actin cytoskeleton organization[49] and the PA-HA membranes used in this study were shown to have low stiffness (0.9 MPa in the wet state)[23]. Previous findings have also shown that fibronectin fragments containing the RGD cell-binding domain alone cannot sustain cytoskeletal organization of human dermal fibroblasts[50], which might explain our observations.

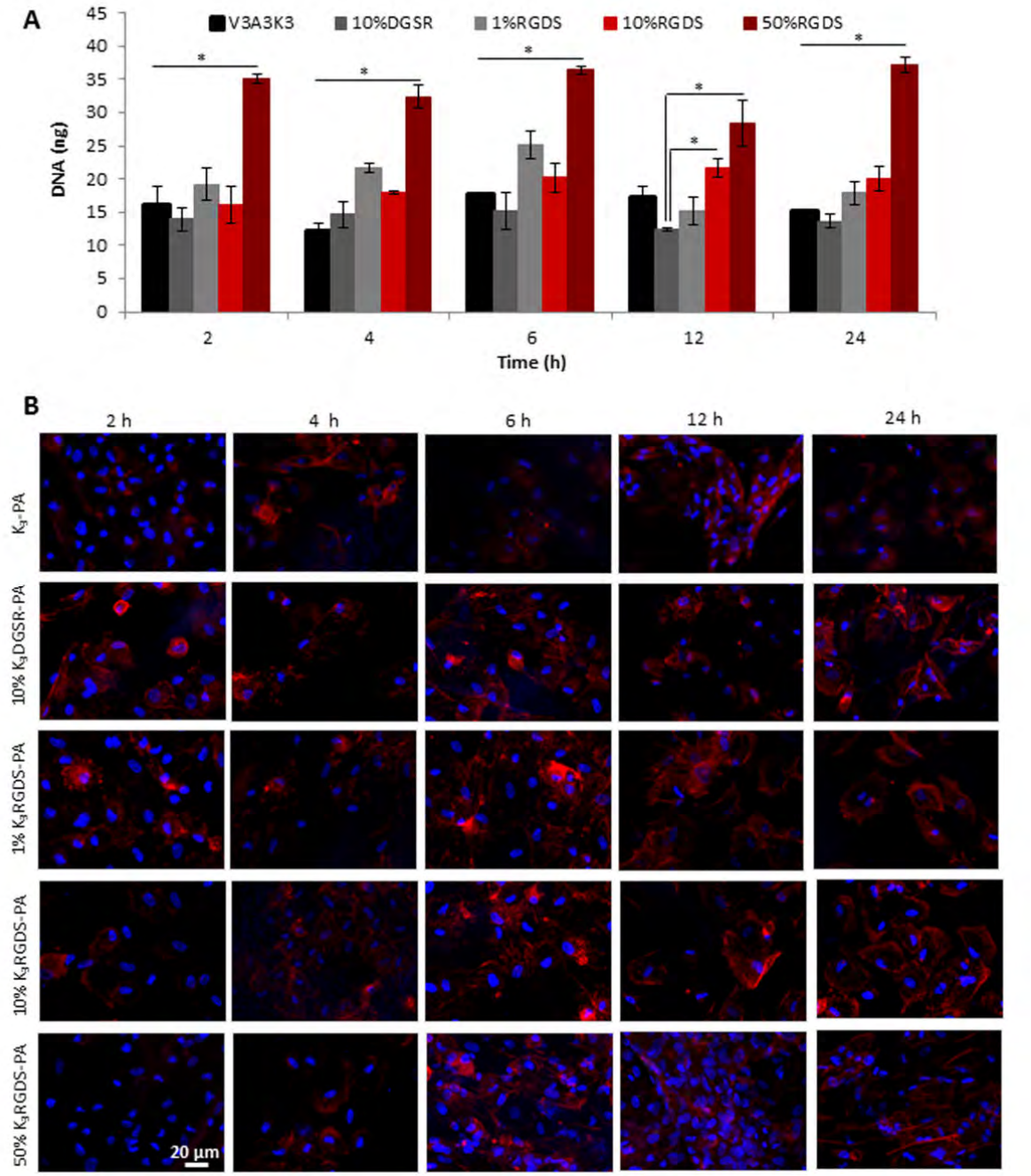

Figure III.5. Cell adhesion on PA-HA membranes. dsDNA quantification (A) (*$p < 0.05$, error bars represent standard deviation (n=3)) and confocal fluorescence images (B) of hDFb cultured on HA-PA membranes containing 1, 10 and 50% K_3RGDS-PA or 10% (w/v) K_3DGSR-PA up to 24 hours of culture. F-actin was labeled with TRITC-phalloidin (red) and nuclei with DAPI (blue).

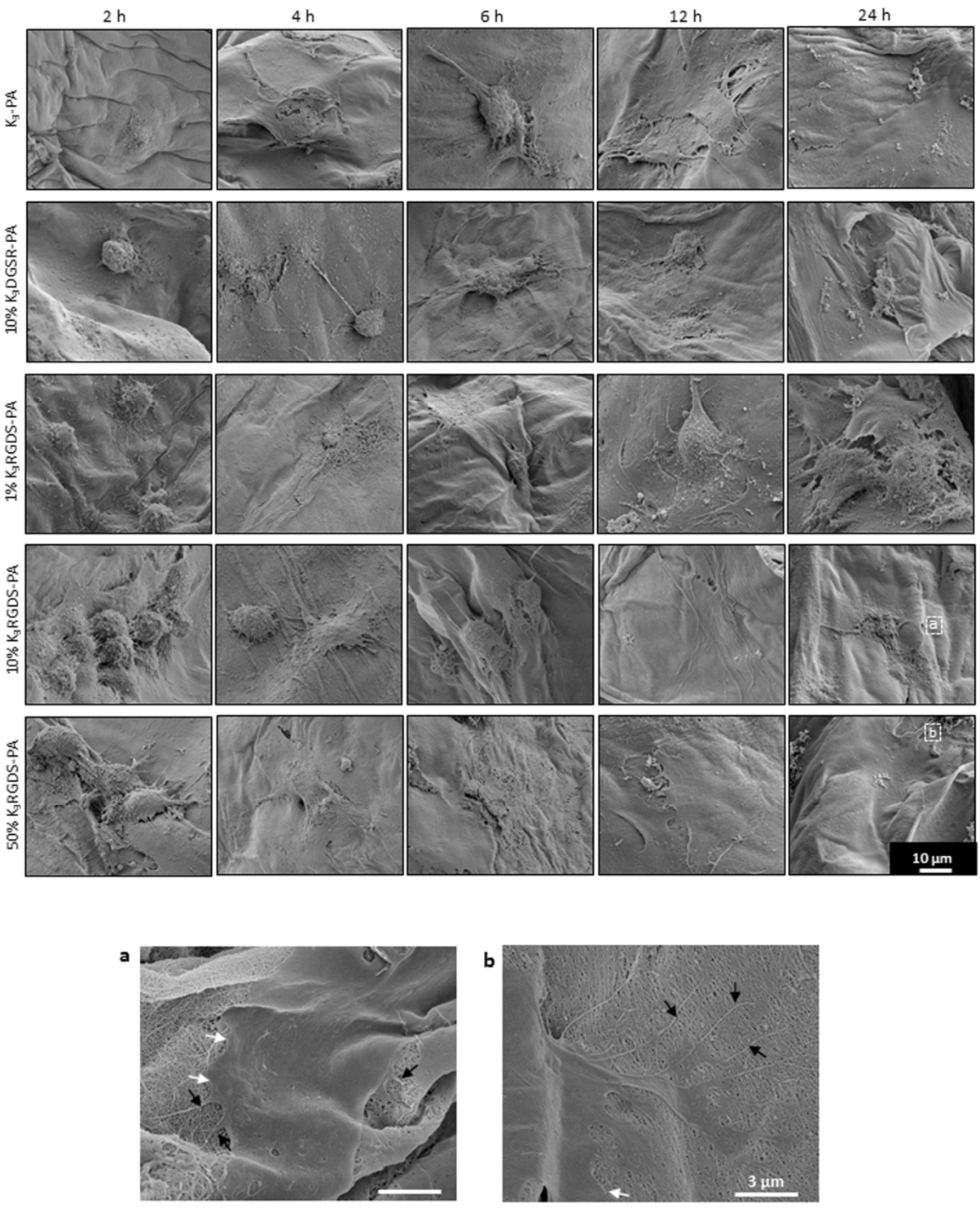

Figure III.6. Cell morphology on PA-HA membranes. A) SEM micrographs of hDFb cultured on HA-PA membranes containing 1, 10 and 50% K_3RGDS-PA or 10% (w/v) K_3DGSR-PA. Cells were cultured on the PA side in medium without FBS up to 24 h. a) and b) show a higher magnification of the surfaces of HA-PA membranes with 10 and 50% (w/v) RGDS, respectively. Black and white arrows indicate the presence of filopodia and lamellipodia, respectively.

Fibroblasts morphology observed in the SEM micrographs is similar to what has been observed previously by others on RGD-coated glass substrates[45]. After 24 hours of culture, only the conditions with 10% and 50% K_3RGDS-PA showed the majority of the cells fully adherent (Fig. III.6). In these conditions, fibroblasts had spread out exhibiting extended lamellipodia and filopodia interacting with fibrillar structure of the membrane surface, thus confirming strong adhesion to the substrate (Fig. III.6a and b). In contrast, cells cultured on the surface of smooth HA hydrogel (Supplementary Information, Fig. III.S9) were completely round, without showing cell protusions (lamellipodia and filopodia) and did not flatten upon contact with the hydrogel surface.

This result highlights the role of the nanofibrillar structure of the self-assembled membranes in controlling cell-matrix interactions. This is in accordance to what was reported in the literature, that fibroblasts in 2D cultures normally exhibit a flat morphology with dorsal-ventral polarity and large lamellipodia[51]. We should highlight that the cell culture experiments were performed in the absence of serum for the entire study and the membranes are displaying the RGDS cell-adhesive domain alone.

Further experiments are yet needed to investigate cell response to HA-PA membranes with higher stiffness and/or with other fibronectin fragment domains in order to be able to make additional considerations regarding the effect of each one of these variables over cell morphology.

4. Conclusion

This study demonstrated that the 2D membranes, formed by self-assembly between hyaluronan and a positively charged peptide amphiphile, are susceptible to enzymatic degradation by hyaluronidase. In the presence of hyaluronidase at physiological concentration, the membranes slowly degrade overtime. The gradual degradation of the membranes is important for allowing the migration of cells and/or the controlled release of bioactive molecules incorporated in the membrane that can control the function of attached cells. Membranes presenting the cell adhesive ligand RGDS showed to increase efficiently the attachment of fibroblasts. This capability to incorporate biochemical signals into 2D self-assembled membranes enables the study of cellular responses to physiologically relevant signal variations. Furthermore, these bioactive matrices permit cell culture studies without serum for short periods. We expect that the proposed biodegradable hybrid membranes could offer significant potential as a biomimetic bioactive supportive matrix for wound healing.

Acknowledgements

Funding for this study was provided by the Portuguese Foundation for Science and Technology (FCT, grant PTDC/EBB-BIO/114523/2009). D.S. Ferreira gratefully acknowledges FCT for the PhD scholarship (SFRH/BD/44977/2008). We also thank Dr A. M. Azevedo from Instituto Superior Técnico (BERG, Lisbon, Portugal) for her support obtaining circular dichroism data, M. T. Cerqueira and I. M. Martins from the 3B's Research Group at the University of Minho (Portugal) for assistance on the isolation of human dermal fibroblasts and FACS analysis, respectively.

References

1. H. K. Kleinman, D. Philp, M. P. Hoffman, Role of the extracellular matrix in morphogenesis, *Curr. Opin. Biotechnol.* 2003, *14*. 526-532

2. W. P. Daley, S. B. Peters, M. Larsen, Extracellular matrix dynamics in development and regenerative medicine, *J. Cell Sci.* 2008, *121*. 255-264

3. F. G. Giancotti, E. Ruoslahti, Integrin Signaling, *Science* 1999, *285*. 1028-1033

4. M. S. Agren, M. Werthen, The Extracellular Matrix in Wound Healing: A Closer Look at Therapeutics for Chronic Wounds, *The International Journal of Lower Extremity Wounds* 2007, *6*. 82-97

5. S. Sakai, R. Yasuda, T. Sayo, O. Ishikawa, S. Inoue, Hyaluronan Exists in the Normal Stratum Corneum, *Journal of Investigative Dermatology* 2000, *114*. 1184-1187.

6. D. Jiang, J. Liang, P. W. Noble, Hyaluronan as an Immune Regulator in Human Diseases, *Physiological Reviews* 2011, *91*. 221-264

7. R. Stern, H. I. Maibach, Hyaluronan in skin: aspects of aging and its pharmacologic modulation, *Clin. Dermatol.* 2008, *26*. 106-122

8. J. H. Collier, J. S. Rudra, J. Z. Gasiorowski, J. P. Jung, Multi-component extracellular matrices based on peptide self-assembly, *Chem. Soc. Rev.* 2010, *39*. 3413-3424

9. E. Ruoslahti, M. D. Pierschbacher, Arg-Gly-Asp: A versatile cell recognition signal, *Cell* 1986, *44*. 517-518.

10. M. D. Pierschbacher, E. Ruoslahti, Cell attachment activity of fibronectin can be duplicated by small synthetic fragments of the molecule, *Nature* 1984, *309*. 30-33.

11. Y. D. Park, N. Tirelli, J. A. Hubbell, Photopolymerized hyaluronic acid-based hydrogels and interpenetrating networks, *Biomaterials* 2003, *24*. 893-900

12. S. Khetan, J. S. Katz, J. A. Burdick, Sequential crosslinking to control cellular spreading in 3-dimensional hydrogels, *Soft Matter* 2009, *5*. 1601-1606

13. J. A. Burdick, G. D. Prestwich, Hyaluronic Acid Hydrogels for Biomedical Applications, *Adv. Mater.* 2011, *23*. H41-H56

14. U. Hersel, C. Dahmen, H. Kessler, RGD modified polymers: biomaterials for stimulated cell adhesion and beyond, *Biomaterials* 2003, *24*. 4385-4415

15. J. P. Jung, A. K. Nagaraj, E. K. Fox, J. S. Rudra, J. M. Devgun, J. H. Collier, Co-assembling peptides as defined matrices for endothelial cells, *Biomaterials* 2009, *30*. 2400-2410

16. L. Perlin, S. MacNeil, S. Rimmer, Production and performance of biomaterials containing RGD peptides, *Soft Matter* 2008, *4*. 2331-2349

17. K. Shroff, E. L. Rexeisen, M. A. Arunagirinathan, E. Kokkoli, Fibronectin-mimetic peptide-amphiphile nanofiber gels support increased cell adhesion and promote ECM production, *Soft Matter* 2010, *6*. 5064-5072

18. X. Zhao, F. Pan, H. Xu, M. Yaseen, H. Shan, C. A. E. Hauser, S. Zhang, J. R. Lu, Molecular self-assembly and applications of designer peptide amphiphiles, *Chem. Soc. Rev.* 2010, *39*. 3480-3498.

19. H. Cui, M. J. Webber, S. I. Stupp, Self-assembly of peptide amphiphiles: From molecules to nanostructures to biomaterials, *Peptide Science* 2010, *94*. 1-18

20. D. W. P. M. Lowik, J. C. M. van Hest, Peptide based amphiphiles, *Chem. Soc. Rev.* 2004, *33*. 234-245.

21. S. G. Zhang, Fabrication of novel biomaterials through molecular self-assembly, *Nat. Biotechnol.* 2003, *21*. 1171-1178

22. D. Carvajal, R. Bitton, J. R. Mantei, Y. S. Velichko, S. I. Stupp, K. R. Shull, Physical properties of hierarchically ordered self-assembled planar and spherical membranes, *Soft Matter* 2010, *6*. 1816-1823

23. R. M. Capito, H. S. Azevedo, Y. S. Velichko, A. Mata, S. I. Stupp, Self-assembly of large and small molecules into hierarchically ordered sacs and membranes, *Science* 2008, *319*. 1812-1816

24. L. W. Chow, R. Bitton, M. J. Webber, D. Carvajal, K. R. Shull, A. K. Sharma, S. I. Stupp, A bioactive self-assembled membrane to promote angiogenesis, *Biomaterials* 2011, *32*. 1574-1582.

25. J. Gajewiak, S. S. Cai, X. Z. Shu, G. D. Prestwich, Aminooxy pluronics: Synthesis and preparation of glycosaminoglycan adducts, *Biomacromolecules* 2006, *7*. 1781-1789

26. T. Takahashi, M. Ikegami-Kawai, R. Okuda, K. Suzuki, A fluorimetric Morgan-Elson assay method for hyaluronidase activity, *Anal Biochem* 2003, *322*. 257-63

27. J. D. Hartgerink, E. Beniash, S. I. Stupp, Peptide-amphiphile nanofibers: A versatile scaffold for the preparation of self-assembling materials, *Proceedings of the National Academy of Sciences* 2002, *99*. 5133-5138

28. M. J. Webber, J. Tongers, C. J. Newcomb, K. T. Marquardt, J. Bauersachs, D. W. Losordo, S. I. Stupp, Supramolecular nanostructures that mimic VEGF as a strategy for ischemic tissue repair, *Proc. Natl. Acad. Sci. U. S. A.* 2012, *109*. 9220-9220

29. M. J. Webber, J. Tongers, M. A. Renault, J. G. Roncalli, D. W. Losordo, S. I. Stupp, Development of bioactive peptide amphiphiles for therapeutic cell delivery, *Acta Biomater.* 2010, *6*. 3-11

30. R. N. Shah, N. A. Shah, M. M. D. Lim, C. Hsieh, G. Nuber, S. I. Stupp, Supramolecular design of self-assembling nanofibers for cartilage regeneration, *Proc. Natl. Acad. Sci. U. S. A.* 2010, *107*. 3293-3298

31. H. Storrie, M. O. Guler, S. N. Abu-Amara, T. Volberg, M. Rao, B. Geiger, S. I. Stupp, Supramolecular crafting of cell adhesion, *Biomaterials* 2007, *28*. 4608-4618

32. R. H. Zha, S. Sur, S. I. Stupp, Self-assembly of Cytotoxic Peptide Amphiphiles into Supramolecular Membranes for Cancer Therapy, *Advanced Healthcare Materials* 2013, *2*. 126-133

33. A. C. Mendes, K. H. Smith, E. Tejeda-Montes, E. Engel, R. L. Reis, H. S. Azevedo, A. Mata, Co-Assembled and Microfabricated Bioactive Membranes, *Adv. Funct. Mater.* 2013, *23*. 430-438

34. X. M. Wang, A. Horii, S. G. Zhang, Designer functionalized self-assembling peptide nanofiber scaffolds for growth, migration, and tubulogenesis of human umbilical vein endothelial cells, *Soft Matter* 2008, *4*. 2388-2395

35. H. A. Behanna, J. Donners, A. C. Gordon, S. I. Stupp, Coassembly of amphiphiles with opposite peptide polarities into nanofibers, *J. Am. Chem. Soc.* 2005, *127*. 1193-1200

36. R. R. Costa, C. A. Custodio, A. M. Testero, F. J. Arias, J. C. Rodriguez-Cabello, N. M. Alves, J. F. Mano, Stimuli-Responsive Thin Coatings Using Elastin-Like Polymers for Biomedical Applications, *Adv. Funct. Mater.* 2009, *19*. 3210-3218

37. L. Y. Shen, P. Chaudouet, J. A. Ji, C. Picart, pH-Amplified Multilayer Films Based on Hyaluronan: Influence of HA Molecular Weight and Concentration on Film Growth and Stability, *Biomacromolecules* 2011, *12*. 1322-1331

38. C. Picart, P. Lavalle, P. Hubert, F. J. G. Cuisinier, G. Decher, P. Schaaf, J. C. Voegel, Buildup mechanism for poly(L-lysine)/hyaluronic acid films onto a solid surface, *Langmuir* 2001, *17*. 7414-7424

39. J. A. Hubbell, Materials as morphogenetic guides in tissue engineering, *Curr. Opin. Biotechnol.* 2003, *14*. 551-558

40. B. Smedsrod, Cellular events in the uptake and degradation of hyaluronan, *Adv. Drug Deliv. Rev.* 1991, *7*. 265-278.

41. D. J. Mahoney, R. T. Aplin, A. Calabro, V. C. Hascall, A. J. Day, Novel methods for the preparation and characterization of hyaluronan oligosaccharides of defined length, *Glycobiology* 2001, *11*. 1025-33.

42. K. M. Galler, L. Aulisa, K. R. Regan, R. N. D'Souza, J. D. Hartgerink, Self-assembling multidomain peptide hydrogels: designed susceptibility to enzymatic cleavage allows enhanced cell migration and spreading, *J Am Chem Soc* 2010, *132*. 3217-23

43. J. Patterson, J. A. Hubbell, Enhanced proteolytic degradation of molecularly engineered PEG hydrogels in response to MMP-1 and MMP-2, *Biomaterials* 2010, *31*. 7836-45

44. F. Lin, X.-D. Ren, Z. Pan, L. Macri, W.-X. Zong, M. G. Tonnesen, M. Rafailovich, D. Bar-Sagi, R. A. F. Clark, Fibronectin Growth Factor-Binding Domains Are Required for Fibroblast Survival, *J Invest Dermatol* 2011, *131*. 84-98.

45. S. P. Massia, J. A. Hubbell, An RGD spacing of 440 nm is sufficient for integrin alpha V beta 3-mediated fibroblast spreading and 140 nm for focal contact and stress fiber formation, *The Journal of Cell Biology* 1991, *114*. 1089-1100

46. A. Aruffo, I. Stamenkovic, M. Melnick, C. B. Underhill, B. Seed, CD44 is the principal cell surface receptor for hyaluronate, *Cell* 1990, *61*. 1303-13

47. T. Yeung, P. C. Georges, L. A. Flanagan, B. Marg, M. Ortiz, M. Funaki, N. Zahir, W. Y. Ming, V. Weaver, P. A. Janmey, Effects of substrate stiffness on cell morphology, cytoskeletal structure, and adhesion, *Cell Motil. Cytoskeleton* 2005, *60*. 24-34

48. D. A. Lauffenburger, A. F. Horwitz, Cell Migration: A Physically Integrated Molecular Process, *Cell* 1996, *84*. 359-369.

49. D. E. Discher, P. Janmey, Y.-l. Wang, Tissue Cells Feel and Respond to the Stiffness of Their Substrate, *Science* 2005, *310*. 1139-1143

50. R. A. F. Clark, J.-Q. An, D. Greiling, A. Khan, J. E. Schwarzbauer, Fibroblast Migration on Fibronectin Requires Three Distinct Functional Domains, *Journal of Investigative Dermatology* 2003, *121*. 695-705.

51. K. M. Yamada, E. Cukierman, Modeling tissue morphogenesis and cancer in 3D, *Cell* 2007, *130*. 601-610

Appendix

Peptide mass and purity

All peptides were synthesized, characterized and purified successfully. ESI and MALDI-MS were used to characterize the mass of the synthesized peptides (Fig. III.S1-S4, A).

The expected mass for $C_{16}V_3A_3K_3$ ($C_{58}H_{111}N_{13}O_{10}$) was 1150.58, three main peaks were found by ESI-MS, corresponding to $[M+H]^+$ m/z = 1151.30, $[M+Na]^+$ m/z= 1173.25 and $[M+2H]^{2+}$ m/z = 576.48 (Fig. III.S1A).

The expected mass for $C_{16}V_3A_3K_3RGDS$ ($C_{73}H_{136}N_{20}O_{17}$) was 1565.98, two mains peaks were found, corresponding to $[M+2H]^{2+}$ m/z = 784.09 and $[M+3H]^{3+}$ m/z = 523.39 (Fig. III.S2A). For $C_{16}V_3A_3K_3DGSR$ ($C_{73}H_{136}N_{20}O_{17}$) the expected mass was 1566.01, two mains peaks were found, corresponding to $[M+2H]^{2+}$ m/z = 784.03 and $[M+3H]^{3+}$ m/z = 523.41 (Fig. III.S3A).

The expected mass for $C_{16}V_3A_3K_3K_{rhod}RGDS$ was 2108.27, two main peaks were found by MALDI-MS, m/z = 2106.54 and m/z = 1694.34, corresponding to the labeled and unlabeled peptide, respectively (Fig. III.S4A).

Analytical HPLC of the collected fractions showed a single peak after purification for all the PAs (Fig. III.S1-S4, B)

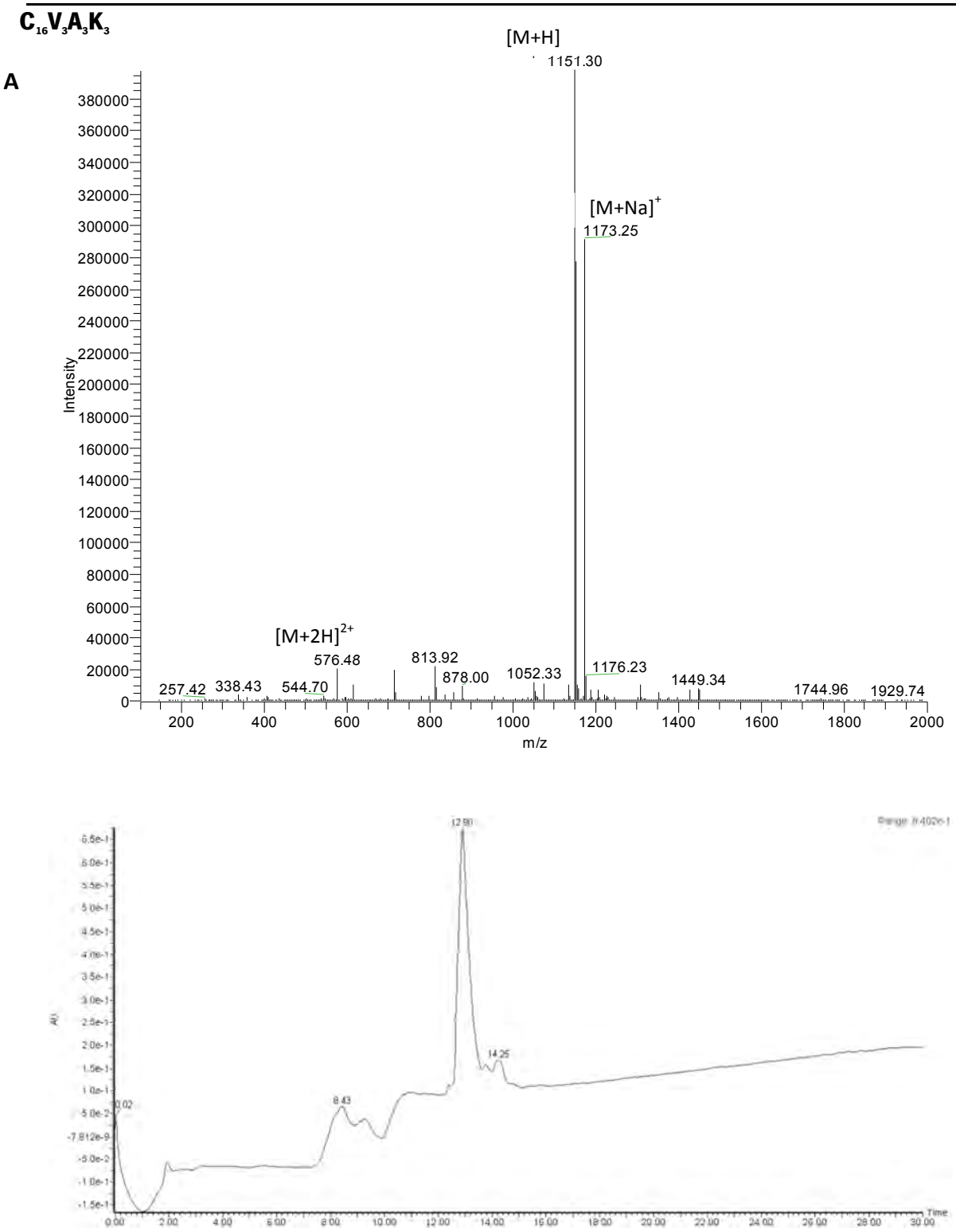

Figure III.S1. Representative ESI-MS data (A) and analytical HPLC trace, detected at 220 nm (B) of $C_{16}V_3A_3K_3$.

A

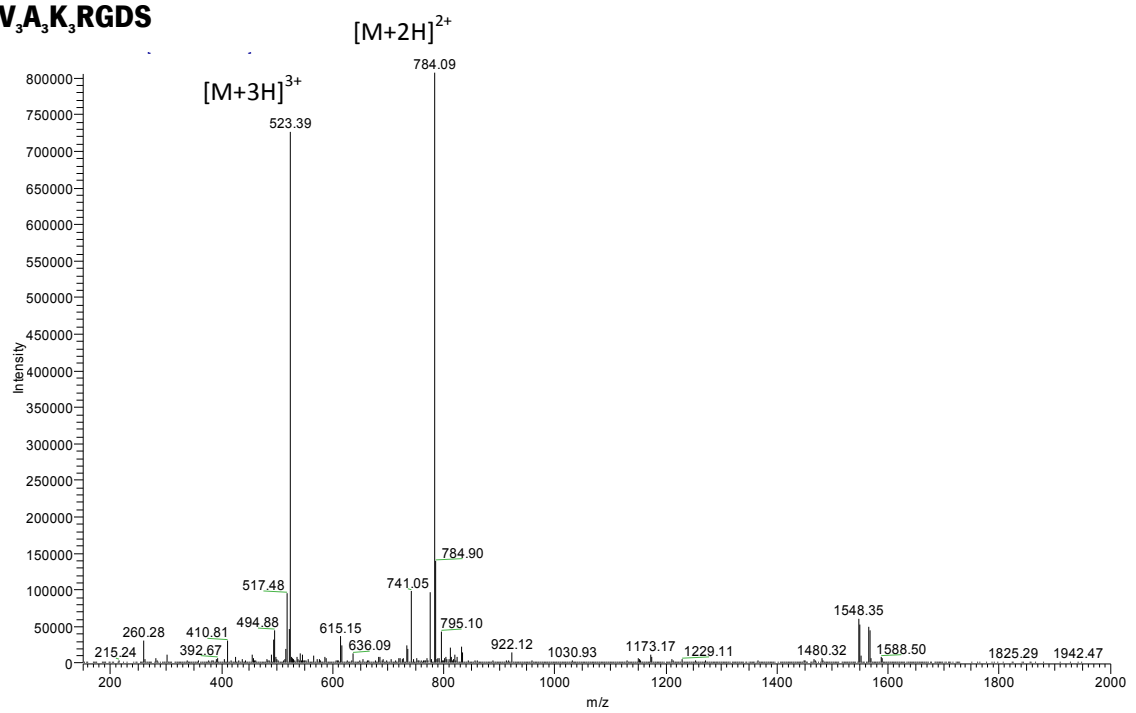

B

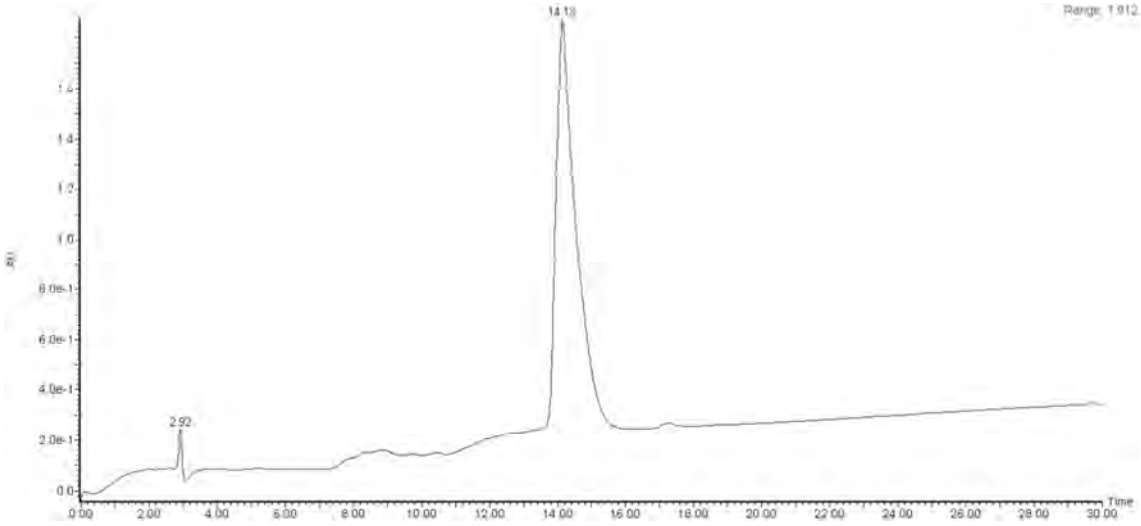

Figure III.S2. Representative ESI-MS data (A) and analytical HPLC trace, detected at 220 nm (B) of $C_{16}V_3A_3K_3RGDS$.

$C_{16}V_3A_3K_3DGSR$

A

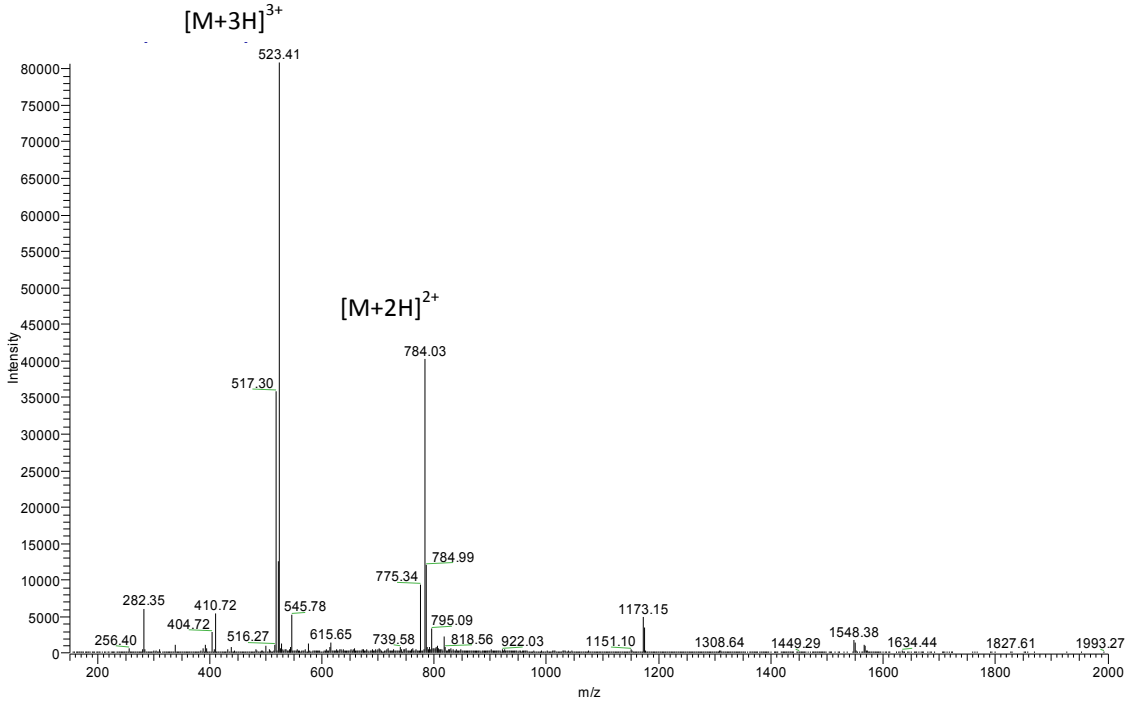

B

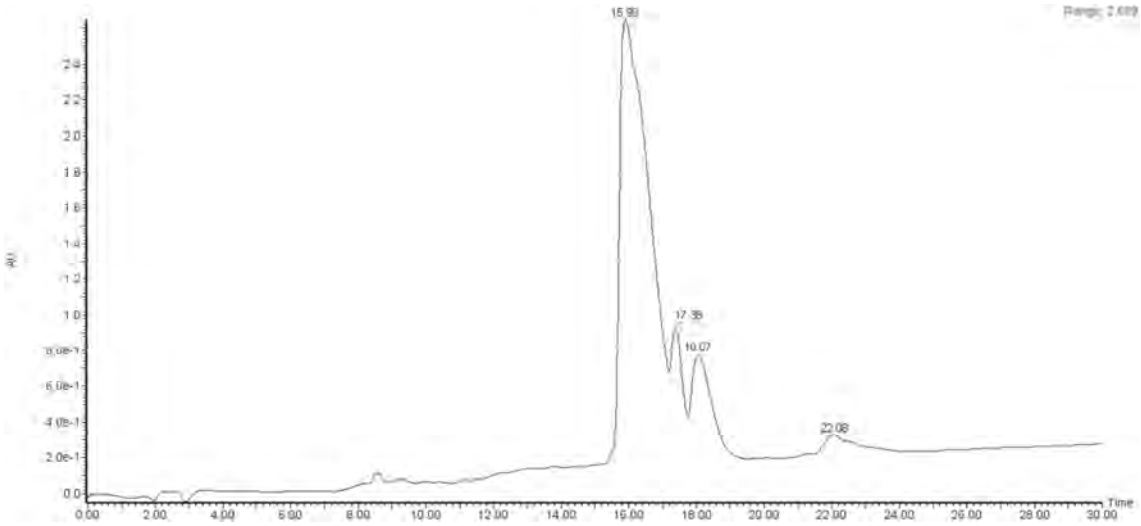

Figure III.S3. Representative ESI-MS data (A) and analytical HPLC trace, detected at 220 nm (B) of $C_{16}V_3A_3K_3DGSR$.

$C_{16}V_3A_3K_3K_{Rhod}$RGDS-PA

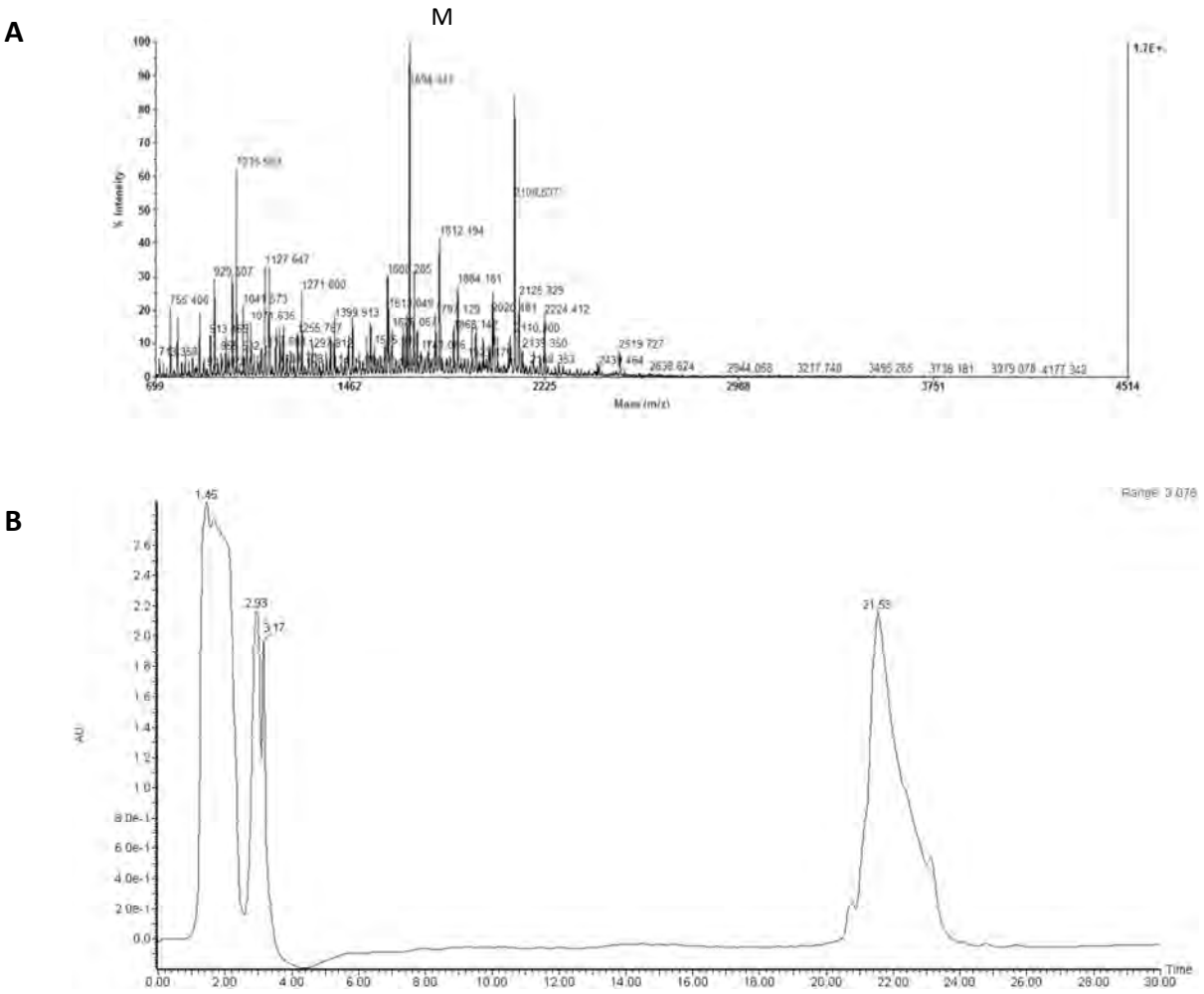

Figure III.S4. Representative MALDI-MS data (A) and analytical HPLC trace, detected at 220 nm (B) of $C_{16}V_3A_3K_3K_{Rhod}$RGDS-PA.

Microstructure of 50% K_3RGDS-PA membrane

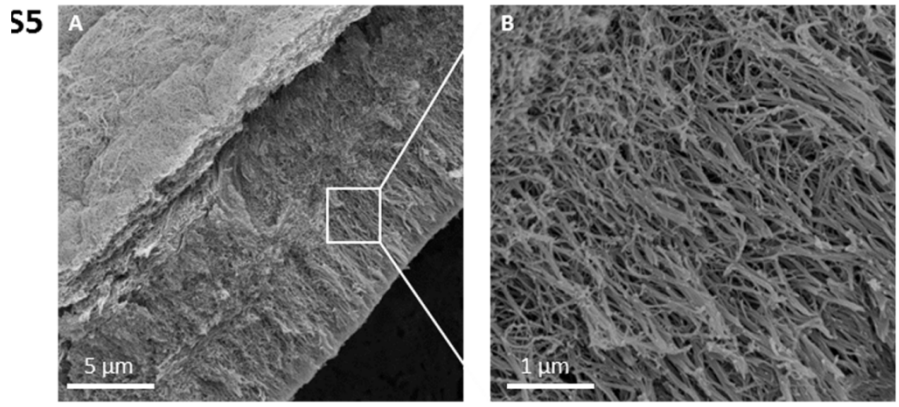

Figure III.S5. SEM micrographs of the cross section of a 50% K_3RGDS-HA membrane.

Identification of HA oligosaccharides from the enzymatic degradation of PA-HA membranes by mass spectrometry

ESI-MS analysis of 0.1% (w/v) HA solution (control) and of the supernatant after incubating the membranes in 50 U/mL HAase for 14 days (Fig. III.S6) showed the presence of HA oligosaccharides only for the samples from degradation solutions. Peaks at 331.8, 389.8 and 411.7 were detected corresponding to the masses of HA oligosaccharides with 7, 4 and 13-mers, respectively, with 4 charges m/z= 331.8 $[M_{HA7}\text{-}4H]^{4-}$; 2 charges m/z= 389.8 $[M_{HA4}\text{-}2H]^{2-}$ and with 6 charges m/z= 411.7 $[M_{HA13}\text{-}6H]^{6-}$.

The observed mass for the odd oligosaccharides are fragmentation products of ESI-MS since digestion with HAase produces even-numbered oligosaccharides. However, these fragments were not observed in the control. Therefore, the oligosaccharides found in the degradation solutions may result from the fragmentation of even oligosaccharides originated from the enzymatic digestion.

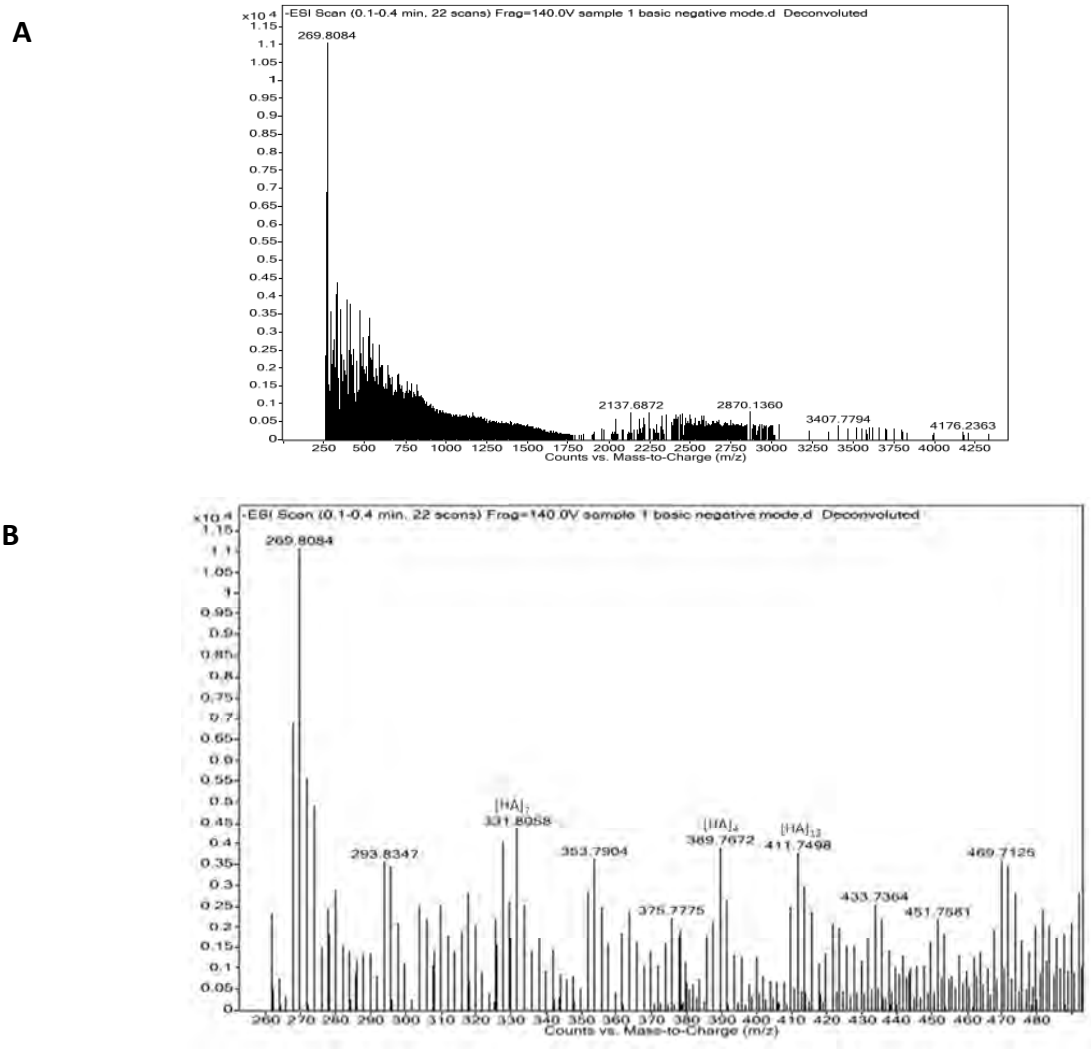

Figure III.S6. Negative ESI-MS of a 0.1% (w/v) hyaluronan solution (A) and of the supernatant after incubating the membranes in 50 U/mL HAase for 14 days (B).

Morphology of hDFbs cultured on PA-HA membranes in serum-containing medium

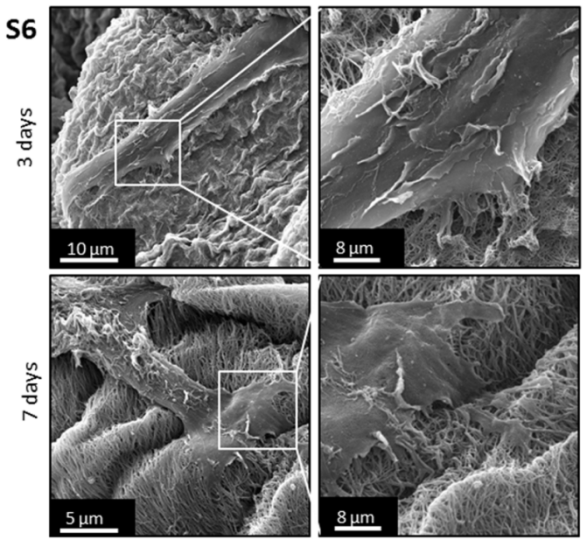

Figure III.S7. SEM micrographs of hDFbs cultured in K_3-HA membranes. Cells were cultured on the PA side in medium containing 10% FBS up to 7 days.

Analysis of the expression of CD44 receptor on hDFbs by flow cytomety

The expression of CD44 receptor on the surface of hDFbs was assessed by flow cytomety. Briefly, harvested cells were incubated with fluorescent monoclonal antibody against CD44, (BD Biosciences Pharmingen, USA) for 20 minutes at room temperature. Cells were then washed in aquisition buffer (0.1% sodium azide, 1% formaldehyde, in phosphate-buffered saline solution). Unlabeled controls were included to evaluate unspecific binding. Samples were analyzed using a FACScalibur(Becton-Dickinson, USA) with CellQuest analysis software (BectonDickinson, USA). FACS analysis confirmed a high expression of CD44 (98.67%) on hDFbs. Similar values were reported in the literature for these cells[S3].

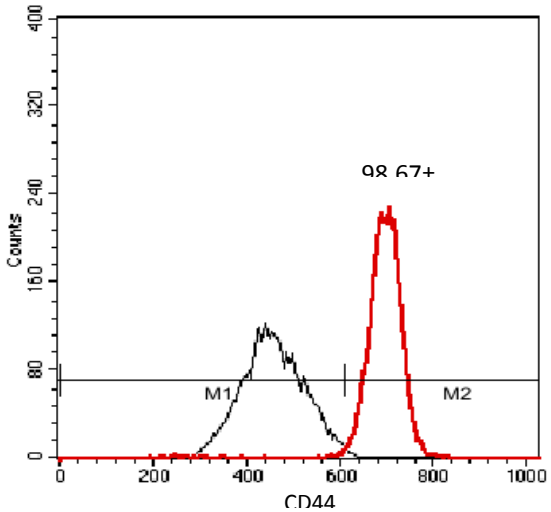

Figure III.S8 - Flow cytometry analysis of the expression of CD44 on the surface of hDFbs used in the cell culture studies.

hDFbs cultured on hyaluronan-based hydrogel film (non self-assembling material)

To demonstrate the role of the self-assembled component, responsible for the nanofibrillar structure of the self-assembled membranes, on the morphology of adhered cells, hDFbs were cultured on the surface of a hyaluronan hydrogel film (non self-assembling film, control). For that, Corgel® BioHydrogel, a tyramine-substituted HA hydrogel (TS-NaHy 1.5% tyramine substitution, Part #85 Corgel® Kit 1%, Lifecore Biomedical, Inc, Chaska, USA) was prepared according with the supplier's instructions and cells were cultured in serum-free conditions as described in Materials and Methods for the PA-HA membranes. The morphology of the cells was examined by SEM. Corgel® BioHydrogel is a patented hyaluronan hydrogel based on di-hydroxyphenyl linkages of tyramine substituted sodium hyaluronate (NaHy)[S1]and was shown to be biocompatible[S1-S2]. SEM images show that the HA hydrogel films presents a smooth surface (Figure III.S9-A) with few adherent cells with a small contact area to the surface (Figure III.S9-B). Furthermore, fibroblasts were completely round, without showing cell protusions (lamellipodia and filopodia) and did not flatten upon contact with the hydrogel surface.

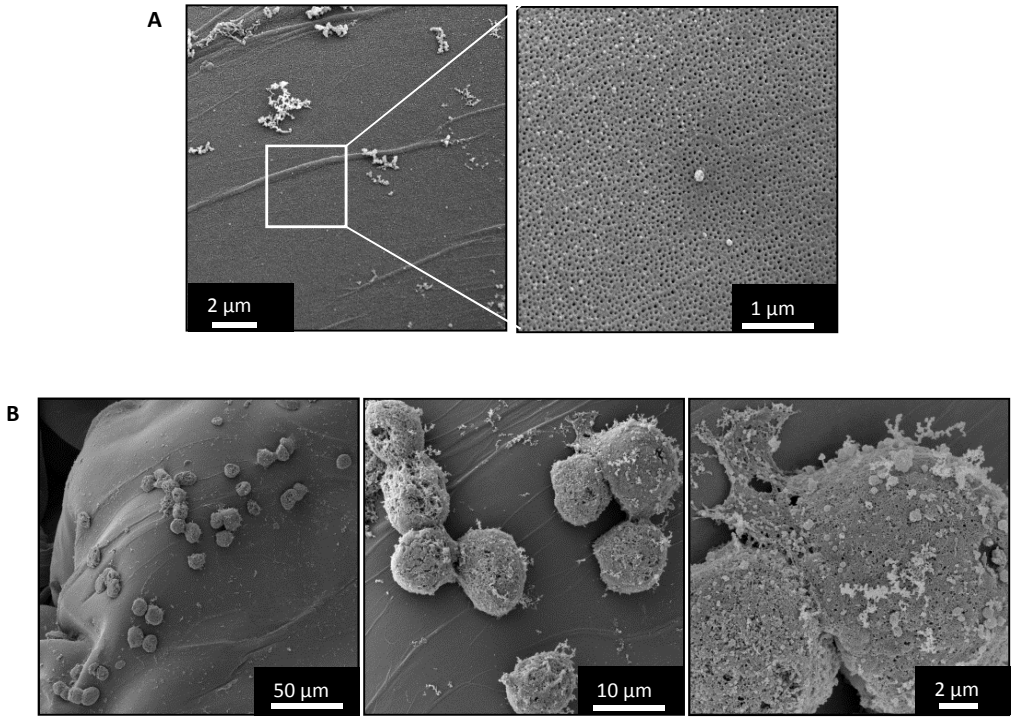

Figure III.S9. SEM micrographs of TS-NaHy hydrogel surface (A) and morphology of hDFbs cultured on their surface in serum-free medium for 24 h.

References

S1. A. Darr, A. Calabro, Synthesis and characterization of tyramine-based hyaluronan hydrogels. J Mater Sci: Mater Med 2009; 20: 33-44

S2. L. Chin, A. Calabro, E. E. Rodriguez, C. D. Tan, E. Walker, K. A. Derwin. Characterization of and host response to tyramine substituted-hyaluronan enriched fascia extracellular matrix. J Mater Sci: Mater Med 2011; 22:1465-1477

S3. A. Blasi, C. Martino, L. Balducci, M. Saldarelli, A. Soleti, S. Navone, L. Canzi, S. Cristini, G. Invernici, E. Parati, G. Alessandri. Dermal fibroblasts display similar phenotypic and differentiation capacity to fat-derived mesenchymal stem cells, but differ in anti-inflammatory and angiogenic potential. Vascular Cell 2011, 3:5

Chapter IV

Molecularly engineered self-assembling membranes for cell-mediated degradation

Chapter IV*

Molecularly engineered self-assembling membranes for cell-mediated degradation

Abstract

Here we report the use of peptide engineering to develop self-assembling membranes that are responsive to cellular activities, in particular to hydrolytic degradation by specific enzymes. The membranes are obtained by combining the matrix polymer hyaluronan (HA) and a rationally designed peptide amphiphile (PA) containing a proteolytic domain (GPQGIWGQ octapeptide) sensitive to matrix metalloproteinase-1 (MMP-1). The self-assembly behavior of the designed MMP-1 sensitive PA was studied by circular dichroism (CD) spectroscopy, transmission electron microscopy (TEM) and ability to form membranes with HA. We found that the insertion of an octapeptide in a typical PA structure does not disturb its self-assembly process into fibrillar nanostructures. CD shows the formation of β-sheet secondary structures in a broad pH range and TEM reveals the presence of filamentous nanostructures. In the presence of high molecular weight HA, this PA forms self-assembling membranes exhibiting a nanofibrillar morphology. Membrane enzymatic degradation was then investigated *in vitro* in presence of exogenous enzymes (hyaluronidase and MMP-1). Our studies reveal that membranes containing the MMP-1 substrate exhibit enhanced enzymatic degradation, compared with control membranes (absence of MMP-1 cleavable peptide or containing a MMP-1 insensitive sequence), being completely degraded after 7 days. Cell culture studies on the developed membranes, using human dermal fibroblasts (hDFbs), show that cell viability and proliferation is minimally affected by the enzymatically cleavable functionality present on the membrane. However, the presence of MMP-1 cleavable sequence does stimulate the secretion of MMP-1 by hDFbs and interfere with matrix deposition, particularly the deposition of collagen. By showing cell-responsiveness to biochemical signals presented on self-assembling membranes, this study highlights the ability of modulating certain cellular activities through matrix engineering. We believe this concept can be further explored to understand the cellular remodeling process in different tissues and could also be used as a strategy to develop artificial matrices with more biomimetic degradation for tissue engineering applications.

* This chapter is based on the following publication:

Daniela S. Ferreira Yi-An Lin, Honggang Cui, Jeffrey A. Hubbell, Rui L. Reis, Helena S. Azevedo, Molecularly Engineered Self-assembling Membranes for Cell-mediated Degradation, Advanced Healthcare Materials, 2014, DOI: 10.1002/adhm.201400586

1. Introduction

The specific and selective activities of enzymes, together with their ability to be controlled by environmental conditions, such as pH, temperature and ionic strength, have been extensively explored in the materials science community with the aim of producing materials with customized functionalities while offering the possibility to perform catalysis reactions very efficiently in mild conditions. According to a recent review published by Ulijn and co-workers on enzyme responsive materials (ERMs),[1] they define ERMs as materials that change their functionality as a result of the direct action of an enzyme on the material. The ubiquitous distribution and great diversity of enzymes present in the human body has motivated biomedical engineers to design biomaterials responsive to enzyme activities and thus translate the enzymatic modification into a suitable materials response. Because the trigger is provided by the biological environment (e.g. cells), with no need to be added exogenously, ERMs offer additional advantages for biomedical applications when compared with other stimuli-responsive (e.g. light, temperature) materials. Enzymes can either be used to form new covalent bonds (e.g. isopeptide bonds between side groups of amino acids in peptides and proteins by transglutaminase, leading to the cross-linking and strengthening of the material), or the cleavage of pre-existing bonds (e.g. hydrolysis of peptide bonds by proteases, leading to the material degradation or disassembly). In the context of 3D biomaterials for cell culture, enzymes have been mainly used to form polymer hydrogels, by incorporating enzyme sensitive cross-links and thus induce gelation *in vivo*, or, conversely, to mimic the degradation process during tissue remodeling and favor cell migration and invasion through enzyme sensitive polymer hydrogels. Both approaches were pioneered by the Hubbell's lab to develop polyethylene glycol (PEG)-based hydrogels with different functionalities.[2-4] These concepts were then applied to other natural[5, 6] and synthetic[7, 8] polymer hydrogels. Similarly, enzyme responsive supramolecular hydrogels were developed, including the formation of gels that are obtained by enzyme-directed self-assembly[9-12] (an enzyme is used to catalyze the synthesis of self-assembling molecules or the removal of a block to trigger the self-assembly), and the degradation[13-16] of supramolecular gels by enzyme mediated disassembly (enzyme converts the self-assembling blocks into non-self-assembling molecules or by degrading the building block directly).[1] Selective enzymatic degradation was also shown to be advantageous in modulating the properties of self-assembled nanostructures, such as nanostructure transitions. For example, Webber and co-workers designed a peptide amphiphile (PA) containing a sequence that is a substrate of a protein kinase A (PKA).[17] Upon treatment with PKA, the PA molecules became phosphorylated causing the disassembly of the original cylindrical structures. Subsequent treatment with alkaline phosphatase enzyme, which cleaves the phosphate groups, resulted in PA reassembly. Seitsonen and co-workers used the model protease α-chymotrypsin to

control the morphologies of peptide self-assemblies (nanotubes/helical ribbons, spherical micelles).[18] In a different approach, Lin and co-workers used a specific proteinase to degrade a cross-linker that stabilizes supramolecular peptide filaments.[19]

Normally during granulation tissue formation, the remodeling of the natural extracellular matrix (ECM) occurs simultaneously with cell invasion. The macromolecular components of the ECM are degraded by cell-secreted proteases, mainly by matrix metalloproteinases (MMPs). The MMPs are a family of protease enzymes that are able to cleave structural components of the ECM, such as collagen types I and IV and fibrin, playing an important role in morphogenesis, wound healing and tissue remodeling.[20, 21] In general, MMPs are not continuously expressed in the skin, but are induced temporarily in response to exogenous signals or pathogenic conditions, such as wound healing.[22] In later stages of dermal wound healing, fibroblasts are the main cell population that produce native ECM[23] and secrete active MMPs (MMP-1, -2, -9 and -13).[22, 24] The action of MMP-1 is essential in the remodeling stage during wound healing.[25] This enzyme is an antagonist to the ECM synthesis and therefore mediates the balance between tissue synthesis and degradation. Several attempts in biomaterial design have been made to mimic this feature of natural ECMs by including protease-sensitive peptides that are cleaved in the presence of cell-secreted enzymes, thus providing further control over cellular responses.[2, 26] The inclusion of MMP-sensitive sequences into PEG gels has been explored by Hubbell's lab to promote cell migration within hydrogels.[2, 27, 28] When the gels come into contact with cells *in vitro* or *in vivo*, they were locally degraded as the cells respond to cues presented by the gels. The inclusion of MMP cleavable sequences into self-assembling peptides has been explored for different biomedical applications, including enzyme responsive hydrogels for controlled matrix degradation and cell migration in tissue engineering,[13, 14, 16, 29] enzyme-triggered drug delivery systems[30, 31] and sensing systems for detecting cell-secreted MMPs overexpressed in various diseases.[32]

Hyaluronan (HA), a major component of the ECM, has attracted considerable interest in a wide range of biomaterials applications.[33, 34] Its unique physicochemical properties[35, 36] (high molecular weight and density of negative charges, inherent biodegradability and biocompatibility), associated with its complex interactions with ECM components and cells,[37, 38] have led us and others to consider this simple polymer as building block for designing biomimetic materials. Moreover, HA has shown to play important roles in wound healing.[39-41]

As bottom-up approach, self-assembly allows the design of biomaterials with specific functionalities and nanoscale organization similar to natural tissues. The formation of hierarchically ordered membranes by self-assembly between high molecular weight HA and positively charged peptide amphiphiles (PAs) was first reported in the seminal work of Stupp and co-workers.[42] We have then used the same approach to

fabricate membranes integrating biochemical signals (RGDS ligand) to enhance the adhesion of fibroblasts in serum-free culture conditions.[43] To further expand the versatility of these self-assembling membranes as temporary matrices for wound healing applications, and recreate some of the aspects of matrix remodeling, an enzymatic cleavable peptide sequence has now been included into the peptide domain. The inclusion of this sequence allows the creation of membranes that are degraded in response to cell-secreted enzyme activities at the wound site during tissue remodeling.

Therefore, the objective of this study was to develop self-assembling membranes made of HA and PAs containing a cleavable site for MMP-1. Since hyaluronidase and MMP-1 enzymes are released by fibroblasts during wound healing, we further examined the ability of these enzymes to degrade the self-assembling membranes. The biological functionality of the membranes was also investigated by culturing human dermal fibroblasts and their effect on cell behavior, like cell adhesion, proliferation and ECM synthesis, evaluated.

2. Experimental Section

Hyaluronan (HA)

Hyaluronan, with an average molar mass of 1.5 MDa (Lifecore Biomedical, Inc, Chaska, USA) was used in this study for self-assembly with the newly designed peptide amphiphiles.

Peptide amphiphiles: design/structure, synthesis and purification

Three different peptide amphiphiles (PAs) were synthesized in this work, all consisting of a peptide segment covalently linked to a 16-carbon alkyl chain: $C_{15}H_{31}CO\text{-}V_3A_3K_3$ (K_3 PA), $C_{15}H_{31}CO\text{-}V_3A_3GPQGIWGQK_3$ (MMP_sK_3 PA) and $C_{15}H_{31}CO\text{-}V_3A_3GDQGIAGFK_3$ (MMP_iK_3 PA) (Figure IV.1A). The peptides were synthesized on a CS Bio 136XT automated peptide synthesizer (CS Bio, USA) using standard 9-fluorenylmethoxycarbonyl (Fmoc) based solid phase chemistry on a 4-methylbenzhydrylamine (MBHA) rink amide resin. Amino acid couplings were performed using 4 equivalents (4 mmol) of Fmoc protected amino acids (Novabiochem, USA), 4 equivalents of O-(Benzotriazol-1-yl)-N,N,N′,N′-tetramethyluronium hexafluorophosphate (HBTU, Carbosynth, UK) and 6 equivalents of N,N-diisopropylethylamine (DIEA, Sigma, USA). Fmoc deprotections were performed with 20% piperidine (Sigma, USA) in dimethylformamide. A palmitic acid ($C_{16}H_{32}O_2$, Calbiochem, USA) tail was manually coupled under the same conditions as the Fmoc-amino acids. Peptide cleavage from the resin, and removal of the protecting groups, was carried out on a mixture of trifluoroacetic acid (TFA, Sigma, USA)/triisopropylsilane (TIS, Alfa Aesar)/water (95/2.5/2.5)) for 3 h at room temperature. The peptide mixture was collected and excess of TFA was removed by rotary evaporation. The resulting viscous

peptide solution was triturated with cold diethyl ether and the white precipitate was collected by filtration, washed with cold ether, and allowed to dry under vacuum overnight. The peptide mass was confirmed by electrospray ionization mass spectrometry (ESI-MS, Agilent, USA).

Peptides were then purified on a Waters 2545 Binary Gradient high-performance liquid chromatography (HPLC) system using a preparative reverse-phase C18 column (Atlantis Prep OBD T3 Column, Waters, USA) and a water/acetonitrile (0.1% TFA) gradient. TFA counter-ions were exchanged by sublimation from 0.01 M hydrochloric acid. Finally, the peptides were dialyzed against ultrapure water using 500 MWCO dialysis tubing (Spectrum labs, The Netherlands), lyophilized and stored at -20 °C until further use. Confirmation of mass and purity was done by ESI-MS and HPLC (Supplementary Information, Figure IV.S1-S3).

Peptide amphiphiles characterization

Circular dichroism (CD) spectroscopy

Peptides were dissolved in deionized water to a final concentration of 0.011 mM and the pH was adjusted to 3, 7 and 9 with hydrochloric acid (0.1 M) or ammonium hydroxide (0.1 M). The CD measurements were performed in a PiStar-180 spectrometer from Applied Photophysics (Surrey, UK), under a constant flow of nitrogen (8 $L.min^{-1}$) at a constant pressure value of 0.7 MPa. Far-UV spectra were recorded at 25 °C from 190 to 300 nm in a quartz cuvette with 1 mm path-length. All scans were performed in the steady state with a bandwidth of 1 nm and each represented spectrum is an average of 5 spectra. The molar ellipticity [θ] was calculated using equation (1).

$$[\theta] = \frac{\theta}{c.l} \quad (1)$$

were θ is the measured ellipticity in mdeg, c is the concentration of the peptide in dmol L^{-1} and l is the light path length of the cuvette in cm.

Transmission electron microscopy (TEM)

Peptides were dissolved in ultrapure water (0.1 wt%) and the solution was aged for 2 days before TEM analysis. Peptide solutions were loaded on carbon-coated copper TEM grid (Electron Microscopy Sciences, USA). For negative staining, a drop of 2 wt% uranyl acetate (Electron Microscopy Sciences, USA) aqueous solution was placed on the samples. The excess solution was wiped away by a piece of filter paper, and the sample was allowed to dry under ambient conditions. All images were collected with a Tecnai 12 TWIN, equipped with SIS Megaview III camera (FEI, USA).

Preparation of self-assembled PA-HA membranes containing different functionalities

Self-assembled membranes were prepared by combining HA with positively charged PAs at optimized conditions, as previously reported.[43] Briefly, 50 µL of a 1 wt% HA solution was cast on the bottom of the wells of a 96 well plate and then 50 µL of 0.017 M K_3PA solution was added on top of the HA solution. Similarly, membranes containing the MMP sensitive and insensitive sequences were prepared using MMP_sK_3 and MMP_iK_3 PAs at 0.017 M concentration. The membranes were allowed to develop overnight and rinsed with sterile ultrapure water to ensure the removal of unreacted HA and PA.

Enzymatic degradation of PA-HA membranes by exogenous enzymes (MMP-1 and hyaluronidase)

Degradation studies were carried out by incubating the different PA-HA membranes in PBS at 37 °C for 14 days without enzymes (control) or containing 10 nM of MMP-1 (human MMP-1, EC 3.4.24.7, Sigma, USA) and 50 $U.mL^{-1}$ of bovine testicular hyaluronidase (Type IV, EC 3.2.1.35, Sigma, USA) isolated or combined. The enzyme solutions were replaced every 72 h throughout the study and collected supernatants were stored at -20 °C for further analysis. At predetermined time points, the membranes were collected and their morphology examined by SEM, as described below. HA degradation on the membranes was assessed by quantification of N-acetylamino sugars in the collected supernatants using the fluorimetric Morgan–Elson assay method[65] and a calibration curve of N-acetyl-D-glucosamine (NAG) standards. Three independent experiments were performed for each degradation condition and incubation time.

Scanning electron microscopy (SEM)

The microstructure of the membranes after degradation was analyzed by SEM. The membranes were first fixed in 2% glutaraldehyde/3% sucrose in PBS for 1 h at 4 °C followed by sequential dehydration in graded ethanol concentrations (from 20 to 100%). To remove ethanol, samples were dried in a critical point dryer (Tousimis Autosandri®-815 series A, USA). Prior observation, the samples were coated with a 15 nm thick layer of gold/palladium and imaged using an ultra-high resolution field emission gun scanning electron microscope (Nova™ NanoSEM 200) from FEI (Eindhoven, The Netherlands).

Cell culture studies

Isolation and culture of primary human dermal fibroblasts (hDFbs)

hDFbs were isolated from skin samples discarded from abdominoplasty surgeries of consenting patients at Hospital da Prelada (Porto, Portugal). Briefly, the skin tissue was cut in pieces of 0.5 by 0.5 cm and

incubated in a dispase solution (2.4 U.mL^{-1} in PBS) at 4 °C overnight. After the tissue digestion, the epidermis was separated from the dermis, and the dermal pieces were digested overnight in a collagenase IA solution (125 U.mL^{-1} in PBS) at 4 °C. Digestion products containing hDFbs were poured through a 100 µm cell strainer and centrifuged at 200 *g* for 5 minutes. The pellet was resuspended and the fibroblasts were subsequently cultured in Dulbecco's Modified Eagle Medium (DMEM) (Sigma, Germany) supplemented with 10% of fetal bovine serum (FBS, Gibco, UK) and 1% (v/v) antibiotic/antimycotic solution (A/B) (Gibco, UK) containing 100 units.mL^{-1} penicillin and 100 mg.mL^{-1} streptomycin, in a 37 °C humidified atmosphere with 5% CO_2.

Culture of hDFbs on the PA-HA membranes

Membranes were prepared under sterile conditions as previously described. HA sterilization for cell studies was done by dissolving the polymer in water, filtering the solution through a 0.22 µm filter, followed by lyophilization in sterile falcon tubes (Sartorius, USA). PA solutions were sterilized by UV exposure for 15 minutes. Confluent hDFbs were harvested from monolayer cultures using TrypLE™ Express (Invitrogen, USA). Cells were seeded on the membranes (10^4 cells.cm^{-2}) and cultured in DMEM supplemented with 10% FBS and 1% (v/v) A/B at 37 °C in a humidified atmosphere of 5% CO_2 for 7 days. For inhibition studies, the cell culture media was supplemented with 20 µM of GM6001 MMP-1 inhibitor (Chemicon, USA). Cell culture media was replaced twice a week, and the collected conditioned media was stored frozen (-80 °C) until further analysis. At predetermined time points, cell-cultured membranes were collected to assess cell proliferation (DNA quantification), morphology and spreading (SEM, F-actin staining) and production of MMP-1, collagen and ECM proteins. Cell culture experiments were performed in triplicate for each condition and time point.

Cell proliferation

Cell proliferation was assessed at different culture times (1, 3 and 7 days) by quantifying the amount of double-stranded DNA (dsDNA). Quantification was performed using the Quant-iT™ PicoGreen® dsDNA Assay Kit (Invitrogen, Molecular Probes, Oregon, USA), according to the instructions of the manufacturer. Briefly, cells on the different membranes/coverslips were lysed by osmotic and thermal shock and the supernatant used for the DNA quantification. The fluorescent intensity of the dye was measured in a microplate reader (Synergie HT, Bio-Tek, USA) with excitation at 485/20 nm and emission at 528/20 nm. The DNA concentration for each sample was calculated using a standard curve (DNA concentration ranging from 0 to 1.5 mg/mL) relating quantity of DNA and fluorescence intensity. Three samples were analyzed per condition and time point.

Staining and confocal microscopy

For examination of cell morphology and MMP-1 production at the protein level, fibroblasts cultured on the different membranes/coverslips were stained for F-actin and MMP-1. Cells were washed in PBS and subsequently fixed in 10% formalin solution (Sigma-Aldrich, Germany) for 30 minutes at 4 °C. Cells were then washed once with 0.1 M glycine in PBS and twice with PBS and permeabilized with 2% BSA/ 0.2% Triton X-100 solution for 1 h at RT. Samples were incubated with primary antibody anti-MMP-1 (ab38929, 1:100, abcam, UK) for 1 h at RT and washed three times for 2 minutes with PBS. Samples were then incubated with the secondary antibody, anti-mouse Alexa 488 (1:200, Molecular Probes, Invitrogen, USA) and TRITC-conjugated phalloidin (1 U/mL, Sigma-Aldrich, Germany) for 1 h at RT. Cell nuclei were counterstained with 1 mg/mL DAPI (1:1000, Sigma-Aldrich, Germany) for 10 min and washed with PBS. Visualization was performed by confocal laser scanning microscopy (CLSM, Olympus FluoView 1000, Olympus, Japan). Background was subtracted and images were processed using FV10-ASW 3.1 software (Olympus, Japan).

Expression of MMP-1

MMP-1 expression by hDFbs was evaluated by analyzing the conditioned medium collected from fibroblast cultures on the PA-HA membranes, or peptide-coated glass coverslips, at different culture times (1, 3 and 7 days). MMP-1 was quantified with a double sandwich enzyme-linked Immunosorbent assay (ELISA) kit (Human Total MMP-1 DuoSet, R&D Systems, USA) according to the instructions of the manufacturer. Optical density (OD) was read at 450 nm and 570 nm in a microplate reader (Synergie HT, Bio-Tek, USA). The MMP-1 concentration for each sample was calculated using a standard curve relating quantity of MMP-1 and OD. Three samples were analyzed per condition and time point.

Quantification of collagen and total ECM proteins

The deposition of ECM proteins by hDFbs cultured on the different membranes was analysed by quantification of collagen and other non-collagenous proteins using a colorimetric analysis (Sirius red/Fast green collagen staining kit, Chondrex, USA) and following the instructions of the manufacturer.[66] Briefly, cells were washed in PBS and subsequently fixed in 10% formalin solution (Sigma-Aldrich, Germany) for 30 minutes at 4 °C. Cells were washed again in PBS and immersed in 200 µL of the dye solution containing Sirius red and fast green. The plates were incubated at RT for 30 minutes in a rotary shaker. The dye solutions were then carefully withdrawn, and the plates were washed repeatedly with distilled water until the solution was colorless. After washing, 1 mL of dye

extraction solution was added to each sample to elute the color. Optical density (OD) was read at 540 nm and 605 nm in a microplate reader (Synergie HT, Bio-Tek, USA). The values of collagen and total ECM proteins were calculated following the manufacturer instructions and normalized to DNA content.

Data analysis and statistics

All data values are presented as mean ± standard deviation (SD). Statistical analysis was performed using GraphPad Prism 5.00 software (San Diego, USA). Statistical differences between the different conditions (NAG, DNA, MMP-1 and collagenous/non-collagenous protein quantifications) were determined using a two-way analysis of variance (ANOVA) with a Bonferroni's multiple comparison post-hoc test (* $p < 0.05$, ** $p < 0.01$ and *** $p < 0.001$).

3. Results and discussion

3.1. Design and self-assembly of PAs with enzymatic cleavable sequences

The self-assembly of HA with positively charged peptides containing the RGDS epitope has previously been explored by our group to generate membranes with different densities of peptide ligands and thus control the adhesion of different cell types.[43, 44] To add different functionalities into our membrane design, such as programmed degradation, a similar molecular engineering approach was pursued in this work by including the matrix metalloproteinase-1 (MMP-1) cleavable site into the peptide building block. The peptide self-assembling blocks used in this study are based on the peptide amphiphile design pioneered by Stupp[45] and are composed of a hydrophobic segment coupled to a peptide segment, that includes a β-sheet forming sequence (V_3A_3) and a domain with positively charged amino acids (K_3) to bind the anionic HA (K_3 PA, Figure IV.1A).[42] A MMP-1-sensitive PA was designed by incorporating the sequence GPQG↓IWGQ[2, 27, 28, 46] (arrow denotes the expected cleavage site by MMP-1) between the β-sheet domain and the lysine residues (MMP_sK_3 PA, MMP sensitive). This peptide is the mutated version of the sequence GPQG↓IAGQ found within the α chain of type I collagen of calf and chick, as well as human.[47] The single substitution of Ala by Trp was shown to enhance enzymatic cleavage.[2, 48] The human α1 type IV collagen sequence, GDQGIAGF, was chosen as a negative control. This sequence has been described to be insensitive to MMP-1 degradation (MMP_iK_3 PA, MMP insensitive).[2, 49] By inserting the GPQG↓IWGQ segment between the HA-binding region and the β-sheet forming segment in the original PA design, instead of adding it to the C-terminus, we aim to promote the breakdown of the peptide at a point that would facilitate the release of the HA-binding motif from the PA nanofibers, hindering binding to HA to remain bound. The lack of interaction between the PA nanofibers and the HA chains would favor the disassembly and dissolution of the membrane components. In addition to MMP-1, hyaluronidase

(HAase) has also been implicated in tissue remodeling during wound healing. The presence of HAase will further contribute for the membrane disassembly and degradation by hydrolyzing HA into smaller fragments.[43] We hypothesize that the incorporation of enzymatic cleavable building blocks in the formulation of our membranes, enables the complete degradation of its components by cell-secreted enzymes and this process would resemble the breakdown of native ECM during tissue remodeling.

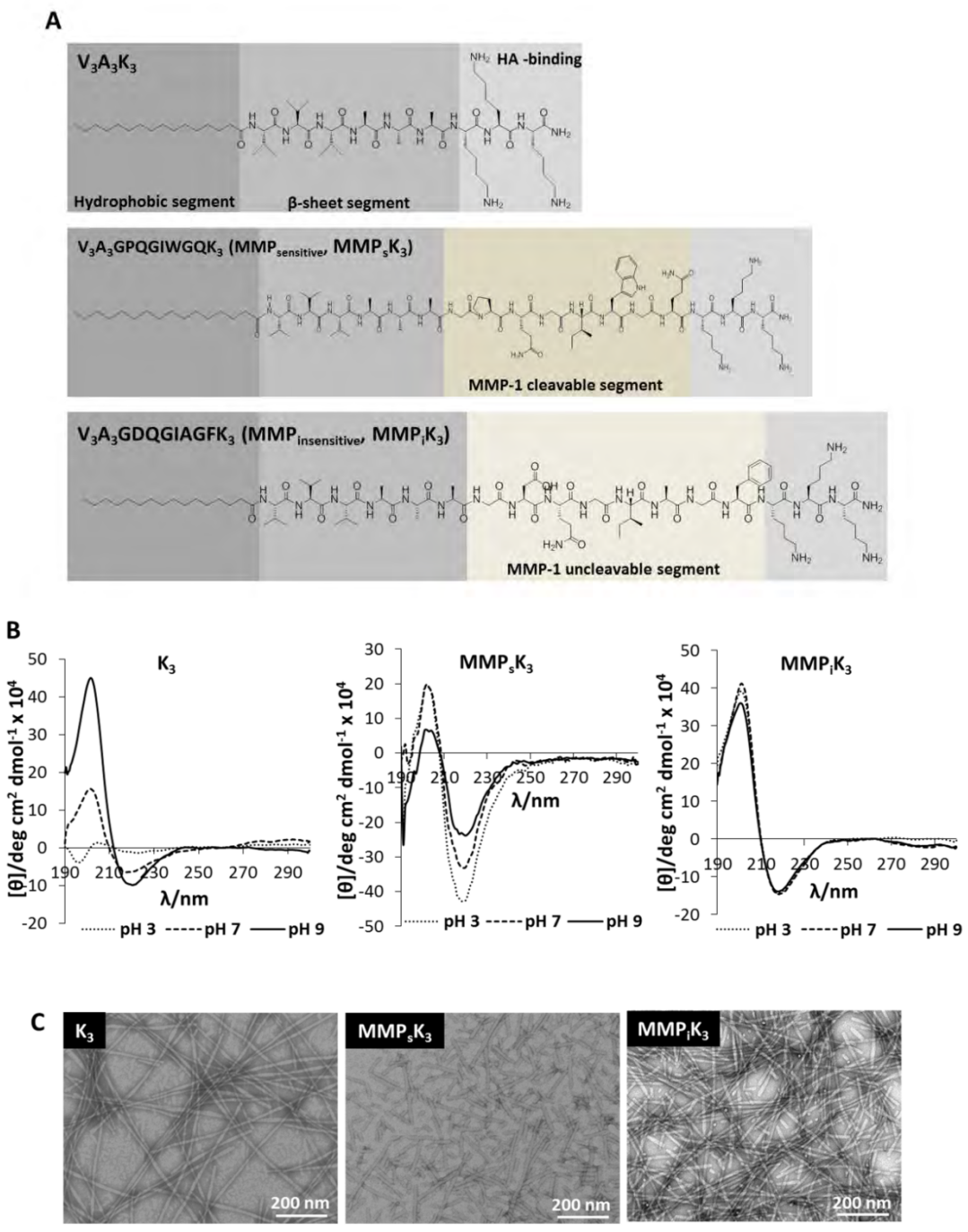

Figure IV.1. Design and characterization of the peptide amphiphiles (PAs) used in this study. (A) Chemical structure of the PAs showing the different functional segments. (B) Circular dichroism spectra of PA solutions (0.011 mM) at pH 3, 7, 9. (C) TEM images of PA nanostructures negatively stained with uranyl acetate (nanofibers were formed by the deposition of 0.1 wt% solutions in water followed by air drying on a carbon-coated TEM grid).

The ability of K_3-PA to form β-sheet secondary structures at certain pHs and to self-assemble into nanofibers was shown previously.[43] However, significant modifications, like the insertion of a sequence containing eight amino acids, may affect the self-assembly properties of the resulting PAs. Profiling the secondary structure of the GPQGIWGQ-containing PA by CD spectroscopy and examining the existence of β-sheets can provide basic information to understand their assembling properties (Figure IV.1B). The CD spectra of β-sheet structures are typically characterized by a minimum at 216 nm and a maximum at 195 nm, while random coils present a maximum at 218 nm and a minimum at 198 nm.[50] The CD spectra obtained for K_3PA at neutral and basic pH were consistent with the known fact that this peptide has a dominant β-sheet content.[43, 51] The inclusion of the sequences GPGIWGQ and GDQGIAGF between the β-sheet domain and the positively charged lysine residues seems to reinforce the β-sheet behavior of the peptides (Figure IV.1B). A typical β-sheet signature was observed for both peptides in all the studied pH conditions, with a minimum in the 210-220 nm range, a crossover from positive to negative above 190 nm, and a positive ellipticity around 200 nm (Figure IV.1B). With exception of proline, all the inserted amino acids are either neutral or β-sheet promoters,[52] thus contributing to the formation of β-sheet structures, independently of the solution pH.

PAs, including these designed in this study, typically self-assemble into high-aspect-ratio filamentous nanostructures. TEM analysis (Figure IV.1C) confirmed the self-assembly of all PAs into nanofiber structures with diameters of between 12 and 16 nm (Table S1) and lengths of from a few hundred nanometers to several micrometers. Interestingly, MMP_sK_3 PA formed shorter nanofibers in comparison with K_3 and MMP_IK_3 PAs. This might be due to the placement of a proline residue next to the β-sheet forming peptide region. The cyclic structure of proline's side chain confers exceptional conformation rigidity. Its unique kink formation may add some steric effect on the molecular packing of the adjacent residues, thus limiting the growth of the nanofiber.

3.2. Membrane self-assembly

Recent advances in biomaterials science have enabled the possibility to develop artificial matrices that recapitulate key features of the natural ECM critical for the process of tissue regeneration.[53-55]

Based on our previous studies,[43] we hypothesize that self-assembling membranes with diverse functionalities can be obtained by self-assembly between HA and positively charged PAs through the incorporation of specific sequences recognized by cell receptors or specific enzymes (Figure IV.1A). Although the insertion of a sequence of eight amino acids into the PA structure did not disturb their self-assembly properties (Figure IV.1B, 1C) the presence of this additional segment could potentially affect the membrane self-assembly. To prepare the membranes (Figure IV.S4), an aqueous solution

containing K_3 PA was added on the top of the HA solution, and left to incubate overnight at the temperature of 37 °C. Similarly, membranes containing the MMP-sensitive (Figure IV.S5) and -insensitive sequences were prepared using MMP_sK_3 PA and MMP_iK_3 PA, respectively. SEM images (Figure IV.3B1) showed that all membranes present a nanofibrillar structure that resulted from the PA self-assembly in presence of the anionic polysaccharide.

3.3. Membrane degradation by exogenous enzymes

Various studies[5, 28] have showed that non-degradable hydrogels limit cellular infiltration. We have demonstrated that self-assembling membranes containing HA and K_3 PA were susceptible to enzymatic degradation by HAase.[43] The incorporation of MMP-sensitive sequences in our membrane design is expected to promote their degradation by proteolytic enzymes and this would lead to enhanced cellular invasion (Figure IV.2). Thus, when implanted *in vivo* both components of the membrane would be susceptible to degradation by enzymes expressed by the surrounding cells (e.g. HAase, MMPs) improving cell migration and tissue morphogenesis.

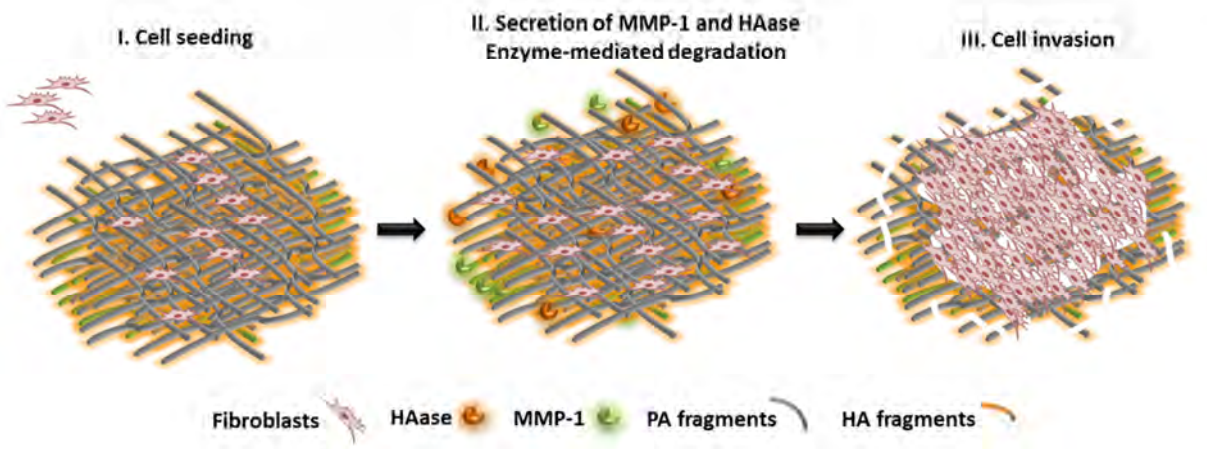

Figure IV.2. Schematic illustration of the proposed enzyme-mediated degradation of self-assembled membranes made of hyaluronan (HA) and peptide nanofibers containing a cleavable site for MMP-1. The incorporation of a MMP-sensitive domain into the membrane design is expected to enhance their degradation by fibroblast secreted enzymes (HAase, MMP-1) and this would lead to enhance cellular invasion.

To assess membrane degradability, membranes containing the MMP sensitive sequence (MMP_sK_3-HA), the insensitive sequence (MMP_iK_3-HA) and the control (K_3-HA) were incubated in PBS in the presence of HAase (50 U mL^{-1}), MMP-1 (10 nM) or both enzymes. HA degradation was followed by quantification of a new reducing N-acetyl-D-glucosamine terminus with each cleavage reaction and membranes were analyzed by SEM (Figure IV.3). Incubation in PBS up to 14 days did not cause degradation of the membranes, as evidenced by the low amount of N-acetylamino sugars in the supernatants (Figure

IV.3A1, A2), and the absence of evident signs of degradation in the SEM micrographs (Figure IV.3B1). When incubated in the presence of HAase, membrane degradation was significantly enhanced in all the conditions, which is in agreement with what we have observed before.[43]

In the presence of MMP-1, only the MMP_sK_3-HA membranes showed signs of degradation, as seen in the SEM micrographs (Figure IV.3B1). From day 5, there is a slightly increase in the released N-acetylamino sugars (Figure IV.3A2). Analyzing the effect of MMP-1 activity on the release of N-acetylamino sugars from MMP_sK_3-HA and MMP_iK_3-HA membranes (Figure IV.3A3), only the MMP_sK_3-HA membranes showed an increase in the amount of N-acetylamino sugars in solution, while in the MMP_iK_3-HA the amount of N-acetylamino sugars was negligible and remained constant along the time. The increase in the amount of N-acetylamino sugars in solution might be due to the release of HA from the membrane, as the peptide being cleaved by MMP-1 (it breaks down the HA-binding region from the main PA sequence) weakens the interaction with HA. The absence of degradation in the K_3-HA and MMP_iK_3-HA membranes in the presence of MMP-1 suggests the specificity of the enzyme for the MMP substrate (GPQG↓IWGQ) and that the control sequence (GDQGIAGF) is not cleaved by the enzymatic actions of MMPs, as reported previously.[2] In the presence of both HAase and MMP-1, the MMP_sK_3-HA membranes were completely degraded after 14 days, demonstrating the additive effect of both enzymes. At this stage, membranes underwent extensive degradation and were difficult to recover for SEM analysis, thus SEM micrograph shows a sample only for day 7 (Figure IV.3B1). SEM analysis of the cross-section of MMP_sK_3-HA membranes in the presence of MMP-1, shows that the degradation was more evident on the surface on the peptide side (Figure IV.3B2).

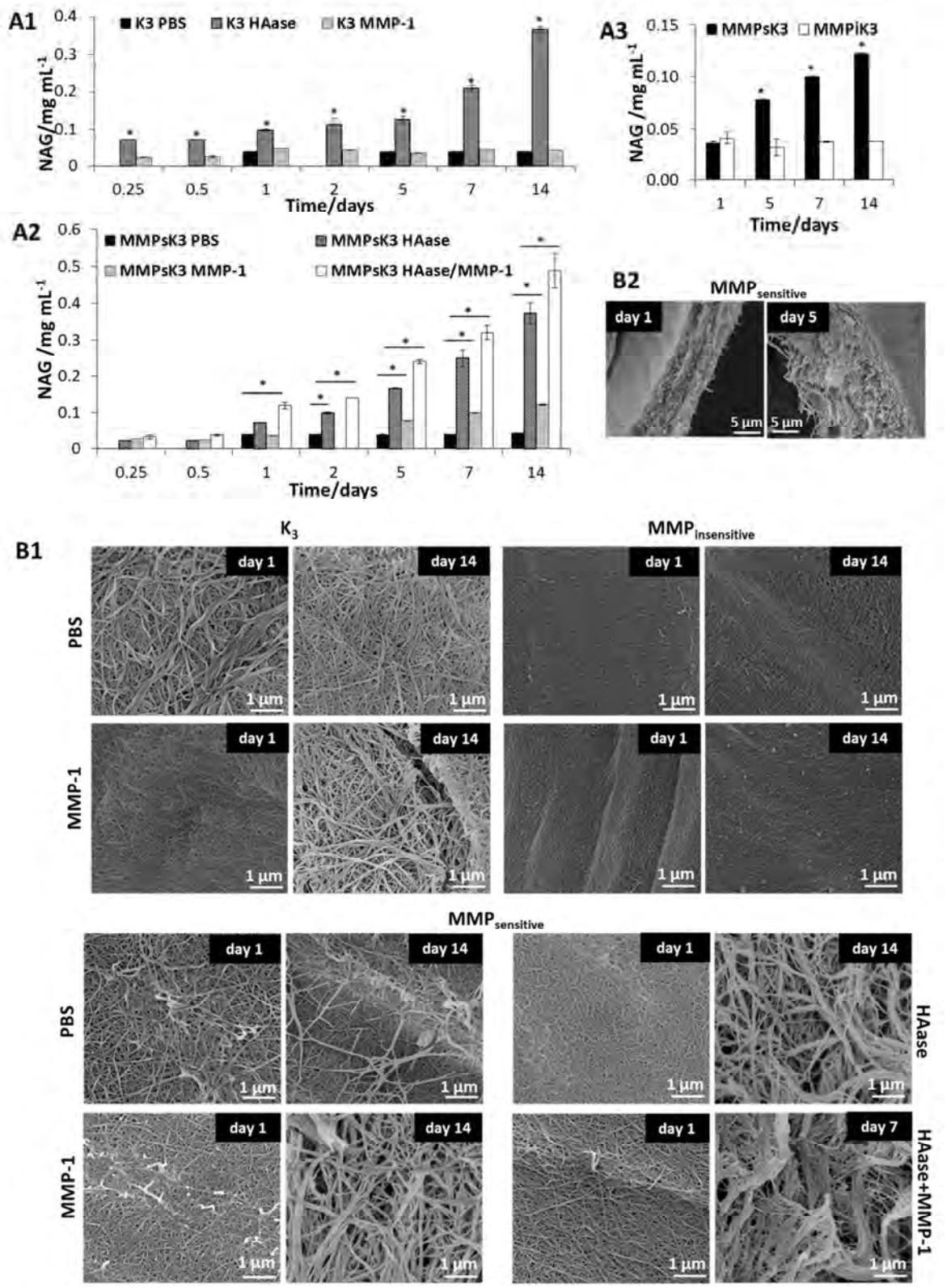

Figure IV.3. Degradation profile of the self-assembled membranes containing different functionalities. (A) Quantification of N-acetylamino sugars released from the membranes when incubated in PBS and in PBS containing 50 U/mL HAase, 10 nM human MMP-1 or both enzymes; Control (K_3-HA, A1), MMP sensitive (MMP_sK_3-HA, A2) and MMP insensitive (MMP_iK_3-HA, A3) (*p< 0.05, error bars represent standard deviation (n=3)). (B1) SEM images showing differences in membrane microstructure when exposed to enzyme solutions up to 14 days. (B2) Cross section of the MMP_sK_3-HA membranes after exposure to 10 nM MMP-1.

3.4. Cell culture studies

Effect of membrane functionalization on fibroblast proliferation

During the early stages of wound healing, fibroblast migration and proliferation into the wound matrix depend on cell-matrix interactions.[25, 56] Previous work suggested that PAs bearing different charges could affect cell viability.[57] To investigate whether some of the sequences could affect fibroblast viability and proliferation, cells were cultured either on glass coverslips coated with different PA molecules or on membranes made with HA and the same PAs. Moreover, the effect of the addition of a broad-spectrum MMP inhibitor (GM6001) in cell proliferation was also investigated, as we intend to use this inhibitor in further experiments. DNA quantification results showed that cells were able to proliferate up to 7 days, either on glass coated coverslips (Figure IV.S4) or on the membranes (Figure IV.4), which indicates that these PA molecules do not affect cell proliferation. Additionally, cell proliferation was greatly decreased in the presence of the MMP-inhibitor (GM6001, 20 μM), which is consistent with what has been observed by other authors that suggest this inhibitor might have a reversible effect on fibroblast proliferation.[28, 58] Contrary to what has been observed when culturing cells in 3D hydrogels,[14, 28] there was no difference on cell proliferation when cells were seeded on MMP_sK_3-HA membranes versus MMP_iK_3-HA.

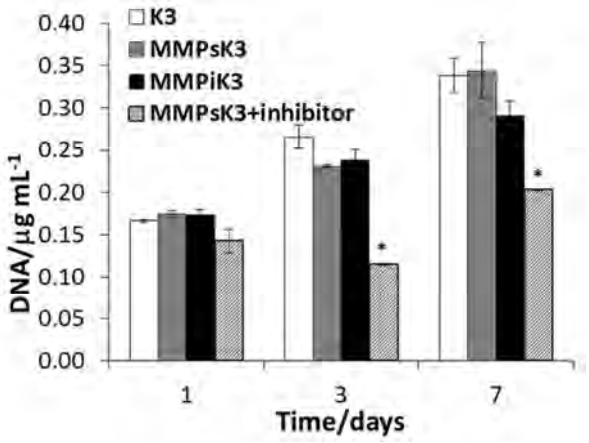

Figure IV.4. Fibroblast proliferation when cultured on membranes with different functionalities. hDFb proliferation assessed by dsDNA quantification. (*p< 0.05, error bars represent standard deviation (n= 3)).

Effect of membrane functionalization on MMP-1 secretion by fibroblasts

In later stages of dermal wound healing, fibroblasts are the main cell population that produces native ECM.[23] Cells normally secrete and activate proteolytic enzymes in order to invade or remodel the extracellular microenvironment.[59] In particular, primary human dermal fibroblasts are known to secrete active MMPs.[24] At this stage, for successful wound healing and prevention of fibrotic tissue, a fine balance between ECM synthesis and degradation is required. The action of MMP-1 is essential during

the remodeling stage of wound healing.[25] Here, MMP-1 expression was examined at the protein level using ELISA. Fibroblasts cultured on the membranes were shown to secrete MMP-1. The amounts of MMP-1 released by the cells cultured on the MMP_sK_3-HA membranes were higher than those of cells cultured on the corresponding MMP-insensitive derivatives and on the control (K_3-HA) (Figure IV.5A), suggesting that the presence of MMP-sensitive motifs in the membrane might have an influence in the secretion of MMP-1. When cultured on peptide coated glass coverslips, however, no differences were observed between different PAs on MMP-1 production (Figure IV.S7). In addition, the values for MMP_sK_3-HA membranes were 2-fold higher than on the coated glass. These findings suggest that the mode of signal presentation to cells may have an influence on their response, a hypothesis that remains to be further investigated. Previous studies have shown the influence of matrices presenting bioactive ligands on the secretion of proteases.[2, 5] As expected, small amount of MMP-1 was detected in the supernatant in the presence of the MMP-inhibitor (Figure IV.5A). Confocal microscopy images showed elongated cells with typical fibroblast morphology (Figure IV.5B). After 24 h, MMP-1 was expressed by the cells in all the conditions but seems more evident for MMP_sK_3-HA membranes, which corroborates the ELISA results (Figure IV.5A).

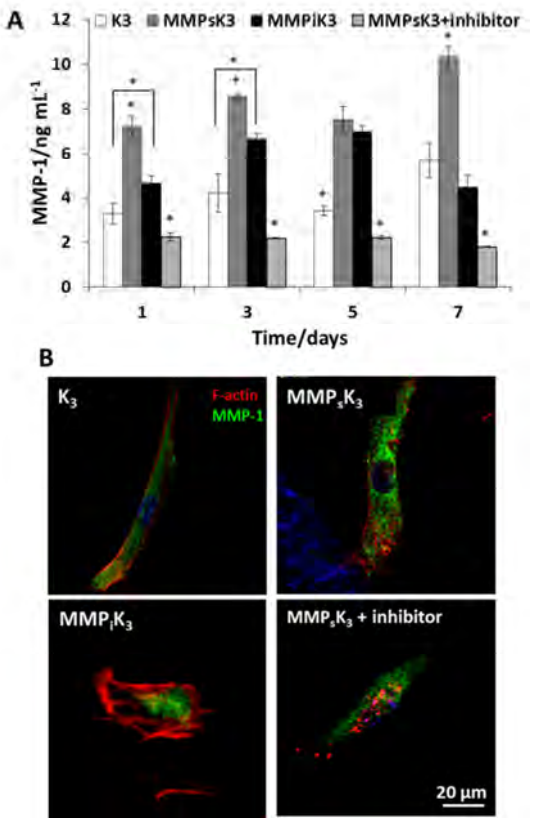

Figure 5. Effect of membrane functionalization on the expression of MMP-1 by fibroblasts (hDFbs). (A) ELISA quantification of MMP-1 in cell culture supernatants (*p< 0.05, error bars represent standard deviation (n= 3)). (B) Confocal microscopy images of fibroblasts stained for MMP-1 (green), F-actin (red) and nuclei (blue) after 24 hours.

Production of ECM proteins by fibroblasts cultured on the membranes with different functionalities

The native ECM of the dermis mainly consists of collagens, proteoglycans and adhesive glycoproteins.[60] In wound healing, fibroblasts are essential for the production of new native ECM.[61, 62] To investigate the ability of hDFbs to synthesize native ECM, we determined the amount of collagen and non-collagenous extracellular matrix proteins produced by the cells when cultured on the different membranes (Figure IV.6). Except for the MMP_sK_3-HA membranes, there was an increase in collagen and non-collagenous proteins production with culture time in all the conditions. The amount of collagen deposited on MMP_sK_3-HA membranes decreased with time (Figure IV.6A) while the amount of non-collagenous proteins increased, as observed for the other conditions (Figure IV.6B). The ECM turnover is controlled by the synthetic rate of matrix proteins, including collagenous and non- collagenous proteins, and their enzymatic degradation by MMPs. In particular, MMP-1 is the only protease able to unwind collagen type I and initiate its degradation.[63] Elevated MMP-1 activity is responsible for an increased turnover of the extracellular collagen matrix.[64] Taken together, the data of collagen and MMP-1 production, suggest that the reduced levels of collagen on MMP_sK_3-HA membranes (Figure IV.6A) could be due to the increased amounts of secreted MMP-1 (Figure IV.5A) observed for these membranes. As previously observed for the production of MMP-1, no differences were shown between conditions on the production of collagen when cells were cultured on peptide coated glass coverslips (Figure IV.S8A), suggesting again the effect of matrix microarchitecture and signal presentation on cell behavior.

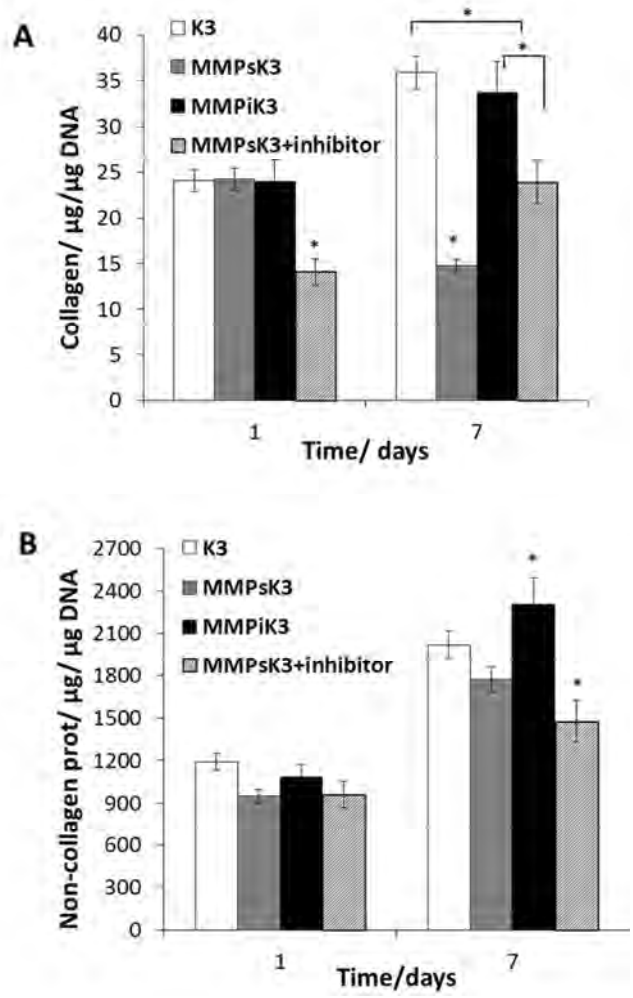

Figure IV.6. Concentration of ECM proteins, collagenous (A) and non-collagenous (B), secreted by hDFbs when cultured on the membranes with different functionalities (*p< 0.05, error bars represent standard deviation (n= 3)).

Membrane microstructure after cell culture

SEM analysis of the membranes after culturing hDFbs showed that cells were able to adhere to and invade the membranes (Figure IV.7). After 14 days of culture, the microstructure of the MMP-sensitive membranes showed a loose network of nanofibers, when compared with the control membranes (K_3 and $MMP_{insensitive}$). Conversely, when adding the MMP inhibitor into the culture medium, the membrane retained its initial morphology. These results suggest that the underlying membrane is responsive to the enzymatic activities produced by the cells. However, the membranes remained intact after 14 days, implying that cell-triggered proteolysis was localized on the surface of the membranes into the cell periphery. The localization of the enzymatic degradation on the surface mimics proteolysis *in vivo*, in which ECM degradation is confined to the immediate pericellular environment.[59] An adequate correlation between the membrane degradation and production of MMP-1 is not possible at this point, because other MMPs are secreted by fibroblasts (MMP-2, MMP-13). In addition, a balance between active MMPs

and their natural inhibitors (tissue inhibitors of metalloproteinases, TIMPs) could also be responsible for the localized degradation behavior in the membranes. Thus, we cannot conclude at the moment which particular molecules are involved in cell proteolysis, but we have an indication that at least MMP-1 is involved.

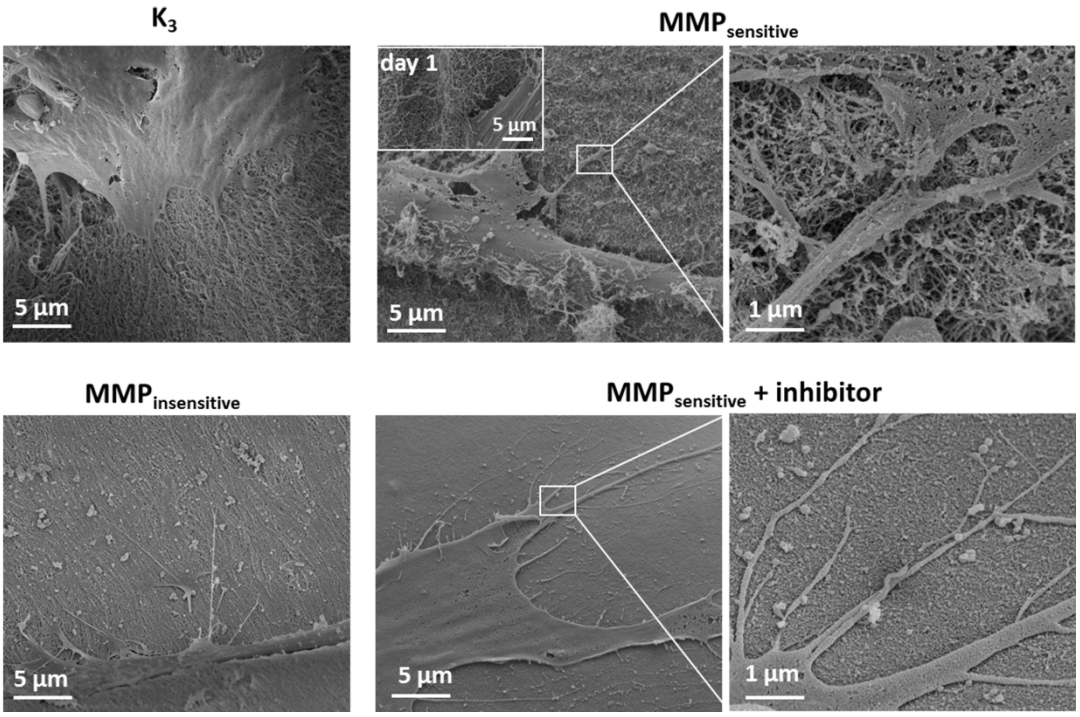

Figure IV.7. SEM micrographs showing differences in membrane microstructure after culturing hDFbs for 14 days, suggesting membrane cell-mediated degradation.

The balanced regulation of fibroblast proliferation and ECM remodeling is essential for optimal wound healing results. Our *in vitro* data suggest that cells responded to the functionalized membranes, and were able to produce ECM proteins without extensive matrix deposition. The inclusion of a MMP-sensitive sequence into the membranes increased matrix proteolytic degradability, which would lead to enhanced cellular invasion when implanted *in vivo*, and thus could be beneficial for an enhanced wound healing response. The mechanisms underlying these observations remain, however, unclear and are worthy to be further investigated.

4. Conclusions

Using a molecular engineering approach, we designed a peptide amphiphile capable of self-assembling with hyaluronan into membranes and containing a proteolytic domain sensitive to matrix metalloproteinase-1 (MMP-1). By pursuing this design, we were able to modulate the degradation rate of the formed self-assembling membranes, as well as certain cellular responses. The membranes were shown to be responsive to enzymes activities, in particular to hyaluronidase and MMP-1, and were

completely degraded after 7 days in presence of exogenous enzymes. Fibroblasts, very active cells in the wound healing process, were used to assess cell-mediated degradation of the membranes and were shown to produce higher amounts of MMP-1 when cultured on MMP-sensitive membranes than when cultured on the MMP-insensitive and on the control (bare membranes without MMP signal). These findings suggest that membranes containing the MMP-1 cleavable sequence stimulate protease secretion, thus leading to cell-mediated degradation process. This hypothesis, however, needs to be further investigated. We expect that by including components sensitive to enzymatic activities in the membrane formulation, their degradation behavior may resemble the process of ECM remodeling, leading to increased cellular infiltration and ultimately more robust healing *in vivo*. Nevertheless, *in vivo* experiments will still be required to verify that the expected remodeling of the ECM actually takes place. These cell-interactive membranes can be further functionalized with other biochemical moieties to study cellular processes *in vitro* and also as temporary matrices in tissue engineering applications.

Acknowledgments

This work was funded by the European Regional Development Fund (ERDF) through the Operational Competitiveness Programme "COMPETE" (FCOMP-01-0124-FEDER-014758) and national funds through the Portuguese Foundation for Science and Technology (FCT) under the project PTDC/EBB-BIO/114523/2009. We also thank a start-up grant provided by the School of Engineering and Materials Science at QMUL. D. S. Ferreira gratefully acknowledges FCT for the PhD scholarship (SFRH/BD/44977/2008).

References

1. M. Zelzer, S. J. Todd, A. R. Hirst, T. O. McDonald and R. V. Ulijn, Enzyme responsive materials: design strategies and future developments, *Biomaterials Science*, 2013, 1, 11-39.
2. M. P. Lutolf, J. L. Lauer-Fields, H. G. Schmoekel, A. T. Metters, F. E. Weber, G. B. Fields and J. A. Hubbell, Synthetic matrix metalloproteinase-sensitive hydrogels for the conduction of tissue regeneration: Engineering cell-invasion characteristics, *Proceedings of the National Academy of Sciences*, 2003, 100, 5413-5418.
3. H. G. Schmoekel, F. E. Weber, J. C. Schense, K. W. Gratz, P. Schawalder and J. A. Hubbell, Bone repair with a form of BMP-2 engineered for incorporation into fibrin cell ingrowth matrices, *Biotechnol Bioeng*, 2005, 89, 253-262.
4. A. H. Zisch, U. Schenk, J. C. Schense, S. E. Sakiyama-Elbert and J. A. Hubbell, Covalently conjugated VEGF–fibrin matrices for endothelialization, *J Control Release*, 2001, 72, 101-113.
5. K. B. Fonseca, F. R. Maia, F. A. Cruz, D. Andrade, M. A. Juliano, P. L. Granja and C. C. Barrias, Enzymatic, physicochemical and biological properties of MMP-sensitive alginate hydrogels, *Soft Matter*, 2013, 9, 3283.
6. S. Khetan, J. S. Katz and J. A. Burdick, Sequential crosslinking to control cellular spreading in 3-dimensional hydrogels, *Soft Matter*, 2009, 5, 1601-1606.
7. S. Kim and K. E. Healy, Synthesis and Characterization of Injectable Poly(N-isopropylacrylamide-co-acrylic acid) Hydrogels with Proteolytically Degradable Cross-Links, *Biomacromolecules*, 2003, 4, 1214-1223.
8. N. S. Khelfallah, G. Decher and P. J. Mésini, Synthesis of a New PHEMA/PEO Enzymatically Biodegradable Hydrogel, *Macromolecular Rapid Communications*, 2006, 27, 1004-1008.
9. P.-F. Caponi, X.-P. Qiu, F. Vilela, F. M. Winnik and R. V. Ulijn, Phosphatase/temperature responsive poly(2-isopropyl-2-oxazoline), *Polymer Chemistry*, 2011, 2, 306-308.
10. J. H. Collier and P. B. Messersmith, Enzymatic Modification of Self-Assembled Peptide Structures with Tissue Transglutaminase, *Bioconjugate Chemistry*, 2003, 14, 748-755.
11. Z. Yang, M. Ma and B. Xu, Using matrix metalloprotease-9 (MMP-9) to trigger supramolecular hydrogelation, *Soft Matter*, 2009, 5, 2546-2548.
12. D. Koda, T. Maruyama, N. Minakuchi, K. Nakashima and M. Goto, Proteinase-mediated drastic morphological change of peptide-amphiphile to induce supramolecular hydrogelation, *Chemical Communications*, 2010, 46, 979-981.
13. H. W. Jun, V. Yuwono, S. E. Paramonov and J. D. Hartgerink, Enzyme-Mediated Degradation of Peptide-Amphiphile Nanofiber Networks, *Advanced Materials*, 2005, 17, 2612-2617.

14. K. M. Galler, L. Aulisa, K. R. Regan, R. N. D'Souza and J. D. Hartgerink, Self-assembling multidomain peptide hydrogels: designed susceptibility to enzymatic cleavage allows enhanced cell migration and spreading, *J Am Chem Soc*, 2010, 132, 3217-3223.

15. Y. Chau, Y. Luo, A. C. Y. Cheung, Y. Nagai, S. Zhang, J. B. Kobler, S. M. Zeitels and R. Langer, Incorporation of a matrix metalloproteinase-sensitive substrate into self-assembling peptides – A model for biofunctional scaffolds, *Biomaterials*, 2008, 29, 1713-1719.

16. M. C. Giano, D. J. Pochan and J. P. Schneider, Controlled biodegradation of Self-assembling β-hairpin Peptide hydrogels by proteolysis with matrix metalloproteinase-13, *Biomaterials*, 2011, 32, 6471-6477.

17. M. J. Webber, C. J. Newcomb, R. Bitton and S. I. Stupp, Switching of self-assembly in a peptide nanostructure with a specific enzyme, *Soft Matter*, 2011, 7, 9665-9672.

18. A. Dehsorkhi, I. W. Hamley, J. Seitsonen and J. Ruokolainen, Tuning Self-Assembled Nanostructures Through Enzymatic Degradation of a Peptide Amphiphile, *Langmuir*, 2013, 29, 6665-6672.

19. Y.-A. Lin, Y.-C. Ou, A. G. Cheetham and H. Cui, Rational Design of MMP Degradable Peptide-Based Supramolecular Filaments, *Biomacromolecules*, 2014, 15, 1419-1427.

20. T. H. Vu and Z. Werb, Matrix metalloproteinases: effectors of development and normal physiology, *Genes & Development*, 2000, 14, 2123-2133.

21. A. Page-McCaw, A. J. Ewald and Z. Werb, Matrix metalloproteinases and the regulation of tissue remodelling, *Nat Rev Mol Cell Biol*, 2007, 8, 221-233.

22. V.-M. Kähäri and U. Saarialho-Kere, Matrix metalloproteinases in skin, *Experimental Dermatology*, 1997, 6, 199-213.

23. S. V. Nolte, W. Xu, H. O. Rennekampff and H. P. Rodemann, Diversity of fibroblasts–a review on implications for skin tissue engineering, *Cells Tissues Organs*, 2008, 187, 165-176.

24. M. P. Lutolf, G. P. Raeber, A. H. Zisch, N. Tirelli and J. A. Hubbell, Cell-Responsive Synthetic Hydrogels, *Advanced Materials*, 2003, 15, 888-892.

25. S. Werner and R. Grose, Regulation of wound healing by growth factors and cytokines, *Physiol Rev*, 2003, 83, 835-870.

26. J. L. West and J. A. Hubbell, Polymeric Biomaterials with Degradation Sites for Proteases Involved in Cell Migration, *Macromolecules*, 1998, 32, 241-244.

27. J. Patterson and J. A. Hubbell, Enhanced proteolytic degradation of molecularly engineered PEG hydrogels in response to MMP-1 and MMP-2, *Biomaterials*, 2010, 31, 7836-7845.

28. K. Bott, Z. Upton, K. Schrobback, M. Ehrbar, J. A. Hubbell, M. P. Lutolf and S. C. Rizzi, The effect of matrix characteristics on fibroblast proliferation in 3D gels, *Biomaterials*, 2010, 31, 8454-8464.

29. K. M. Galler, J. D. Hartgerink, A. C. Cavender, G. Schmalz and R. N. D'Souza, A customized self-assembling peptide hydrogel for dental pulp tissue engineering, *Tissue Eng Part A*, 2012, 18, 176-184.

30. J.-K. Kim, J. Anderson, H.-W. Jun, M. A. Repka and S. Jo, Self-Assembling Peptide Amphiphile-Based Nanofiber Gel for Bioresponsive Cisplatin Delivery, *Molecular Pharmaceutics*, 2009, 6, 978-985.

31. J. Banerjee, A. J. Hanson, B. Gadam, A. I. Elegbede, S. Tobwala, B. Ganguly, A. V. Wagh, W. W. Muhonen, B. Law, J. B. Shabb, D. K. Srivastava and S. Mallik, Release of liposomal contents by cell-secreted matrix metalloproteinase-9, *Bioconjug Chem*, 2009, 20, 1332-1339.

32. J. Banerjee, A. J. Hanson, E. K. Nyren-Erickson, B. Ganguli, A. Wagh, W. W. Muhonen, B. Law, J. B. Shabb, D. K. Srivastava and S. Mallik, Liposome-mediated amplified detection of cell-secreted matrix metalloproteinase-9, *Chem Commun (Camb)*, 2010, 46, 3209-3211.

33. K. T. Dicker, L. A. Gurski, S. Pradhan-Bhatt, R. L. Witt, M. C. Farach-Carson and X. Jia, Hyaluronan: A simple polysaccharide with diverse biological functions, *Acta Biomaterialia*, 2014, 10, 1558-1570.

34. J. A. Burdick and G. D. Prestwich, Hyaluronic Acid Hydrogels for Biomedical Applications, *Advanced Materials*, 2011, 23, H41-H56.

35. A. Almond, Hyaluronan, *Cellular and Molecular Life Sciences*, 2007, 64, 1591-1596.

36. T. C. Laurent and J. R. E. Fraser, Hyaluronan, *Faseb Journal*, 1992, 6, 2397-2404.

37. B. P. Toole, Hyaluronan: From extracellular glue to pericellular cue, *Nature Reviews Cancer*, 2004, 4, 528-539.

38. M. A. Solis, Y.-H. Chen, T. Y. Wong, V. Z. Bittencourt, Y.-C. Lin and L. L. H. Huang, Hyaluronan regulates cell behavior: a potential niche matrix for stem cells, *Biochemistry research international*, 2012, 2012, 346972.

39. M. David-Raoudi, F. Tranchepain, B. Deschrevel, J. C. Vincent, P. Bogdanowicz, K. Boumediene and J. P. Pujol, Differential effects of hyaluronan and its fragments on fibroblasts: relation to wound healing, *Wound Repair Regen*, 2008, 16, 274-287.

40. R. A. Clark, K. Ghosh and M. G. Tonnesen, Tissue engineering for cutaneous wounds, *J Invest Dermatol*, 2007, 127, 1018-1029.

41. W. Y. Chen and G. Abatangelo, Functions of hyaluronan in wound repair, *Wound Repair Regen*, 1999, 7, 79-89.

42. R. M. Capito, H. S. Azevedo, Y. S. Velichko, A. Mata and S. I. Stupp, Self-assembly of large and small molecules into hierarchically ordered sacs and membranes, *Science*, 2008, 319, 1812-1816.

43. D. S. Ferreira, A. P. Marques, R. L. Reis and H. S. Azevedo, Hyaluronan and self-assembling peptides as building blocks to reconstruct the extracellular environment in skin tissue, *Biomaterials Science*, 2013, 1, 952-964.

44. A. C. Mendes, K. H. Smith, E. Tejeda-Montes, E. Engel, R. L. Reis, H. S. Azevedo and A. Mata, Co-Assembled and Microfabricated Bioactive Membranes, *Advanced Functional Materials*, 2013, 23, 430-438.

45. J. D. Hartgerink, E. Beniash and S. I. Stupp, Self-assembly and mineralization of peptide-amphiphile nanofibers, *Science*, 2001, 294, 1684-1688.

46. M. Ehrbar, S. C. Rizzi, R. G. Schoenmakers, B. S. Miguel, J. A. Hubbell, F. E. Weber and M. P. Lutolf, Biomolecular hydrogels formed and degraded via site-specific enzymatic reactions, *Biomacromolecules*, 2007, 8, 3000-3007.

47. R. T. Aimes and J. P. Quigley, Matrix Metalloproteinase-2 Is an Interstitial Collagenase: inhibitor-free enzyme catalyzes the cleavage of collagen fibrils and soluble native type I collagen generating the specific ¾- and ¼-length fragments, *Journal of Biological Chemistry*, 1995, 270, 5872-5876.

48. H. Nagase and G. B. Fields, Human matrix metalloproteinase specificity studies using collagen sequence-based synthetic peptides, *Biopolymers*, 1996, 40, 399-416.

49. W. Babel and R. W. Glanville, Structure of human-basement-membrane (type IV) collagen *European, Journal of Biochemistry*, 1984, 143, 545-556.

50. N. Greenfield and G. D. Fasman, Computed circular dichroism spectra for the evaluation of protein conformation, *Biochemistry*, 1969, 8, 4108-4116.

51. H. A. Behanna, J. J. Donners, A. C. Gordon and S. I. Stupp, Coassembly of amphiphiles with opposite peptide polarities into nanofibers, *J Am Chem Soc*, 2005, 127, 1193-1200.

52. A. C. Mendes, E. T. Baran, R. L. Reis and H. S. Azevedo, Self-assembly in nature: using the principles of nature to create complex nanobiomaterials, *Wiley Interdisciplinary Reviews: Nanomedicine and Nanobiotechnology*, 2013, 5, 582-612.

53. R. Langer and D. A. Tirrell, Designing materials for biology and medicine, *Nature*, 2004, 428, 487-492.

54. L. G. Griffith and M. A. Swartz, Capturing complex 3D tissue physiology in vitro, *Nat Rev Mol Cell Biol*, 2006, 7, 211-224.

55. M. P. Lutolf and J. A. Hubbell, Synthetic biomaterials as instructive extracellular microenvironments for morphogenesis in tissue engineering, *Nature Biotechnology*, 2005, 23, 47-55.

56. T. J. Shaw and P. Martin, Wound repair at a glance, *Journal of Cell Science*, 2009, 122, 3209-3213.

57. M. J. Webber, J. Tongers, M. A. Renault, J. G. Roncalli, D. W. Losordo and S. I. Stupp, Development of bioactive peptide amphiphiles for therapeutic cell delivery, *Acta Biomaterialia*, 2010, 6, 3-11.

58. B. Martin-Martin, V. Tovell, A. H. Dahlmann-Noor, P. T. Khaw and M. Bailly, The effect of MMP inhibitor GM6001 on early fibroblast-mediated collagen matrix contraction is correlated to a decrease in cell protrusive activity, *Eur J Cell Biol*, 2011, 90, 26-36.

59. Z. Werb, ECM and cell surface proteolysis: regulating cellular ecology, *Cell*, 1997, 91, 439-442.

60. A. D. Widgerow, Cellular/extracellular matrix cross-talk in scar evolution and control, *Wound Repair Regen*, 2011, 19, 117-133.

61. S. Werner, T. Krieg and H. Smola, Keratinocyte-fibroblast interactions in wound healing, *J Invest Dermatol*, 2007, 127, 998-1008.

62. B. Hinz, Formation and function of the myofibroblast during tissue repair, *J Invest Dermatol*, 2007, 127, 526-537.

63. O. Langholz, D. Rockel, C. Mauch, E. Kozlowska, I. Bank, T. Krieg and B. Eckes, Collagen and collagenase gene expression in three-dimensional collagen lattices are differentially regulated by alpha 1 beta 1 and alpha 2 beta 1 integrins, *J Cell Biol*, 1995, 131, 1903-1915.

64. J. Varani, Y. Hattori, Y. Chi, T. Schmidt, P. Perone, M. E. Zeigler, D. J. Fader and T. M. Johnson, Collagenolytic and gelatinolytic matrix metalloproteinases and their inhibitors in basal cell carcinoma of skin: comparison with normal skin, *Br J Cancer*, 2000, 82, 657-665.

65. T. Takahashi, M. Ikegami-Kawai, R. Okuda and K. Suzuki, A fluorimetric Morgan-Elson assay method for hyaluronidase activity, *Anal Biochem*, 2003, 322, 257-263.

66. A. López-De León and M. Rojkind, A simple micromethod for collagen and total protein determination in formalin-fixed paraffin-embedded sections, *Journal of Histochemistry & Cytochemistry*, 1985, 33, 737-743.

Appendix

S1. Peptide characterization

S1.1 Mass determination and purity of synthesized peptides

ESI-MS was used to determine the mass of the synthesized peptides (Fig. IV.S1-S3, A). The purity of the peptides was analyzed by reverse-phase analytical high performance liquid chromatography (RP-HPLC). The HPLC traces showed a major peak corresponding to the peptide of interest (Fig. IV.S1-S3, B).

The expected mass for $C_{16}V_3A_3K_3$ ($C_{58}H_{111}N_{13}O_{10}$) was 1150.6, two main peaks were found by ESI-MS, corresponding to $[M+H]^+$ m/z = 1150.8 and $[M+2H]^{2+}$ m/z = 575.9 (Fig. IV.S1A). Purity was 89%, as determined by integration of the peaks shown in the analytical HPLC trace (Fig. IV.S1B).

The expected mass for $C_{16}V_3A_3GPQGIWGQK_3$ ($C_{96}H_{164}N_{24}O_{20}$) was 1974.5, two mains peaks were found, corresponding to $[M+2H]^{2+}$ m/z = 988.0 and $[M+3H]^{3+}$ m/z = 659.0 (Fig. IV.S2A). Purity was 80%, as determined by integration of the peaks shown in the analytical HPLC trace (Fig. IV.S2B).

The expected mass for $C_{16}V_3A_3GDQGIAGFK_3$ ($C_{91}H_{158}N_{22}O_{21}$) was 1895.2, two mains peaks were found, corresponding to $[M+2H]^{2+}$ m/z = 949.0 and $[M+3H]^{3+}$ m/z = 633.0 (Fig. IV.S3A). Purity was 83%, as determined by integration of the peaks shown in the analytical HPLC trace (Fig. IV.S3B).

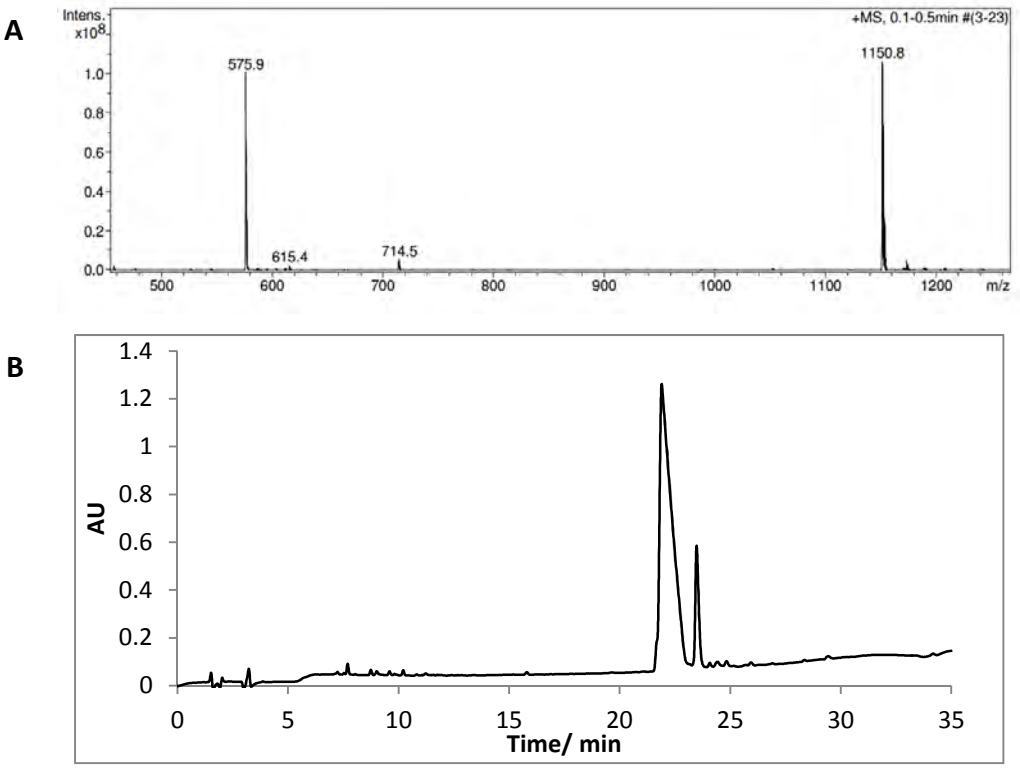

Figure IV.S1. Representative ESI-MS (A) and analytical RP-HPLC trace, detected at 220 nm (B) of $C_{16}V_3A_3K_3$.

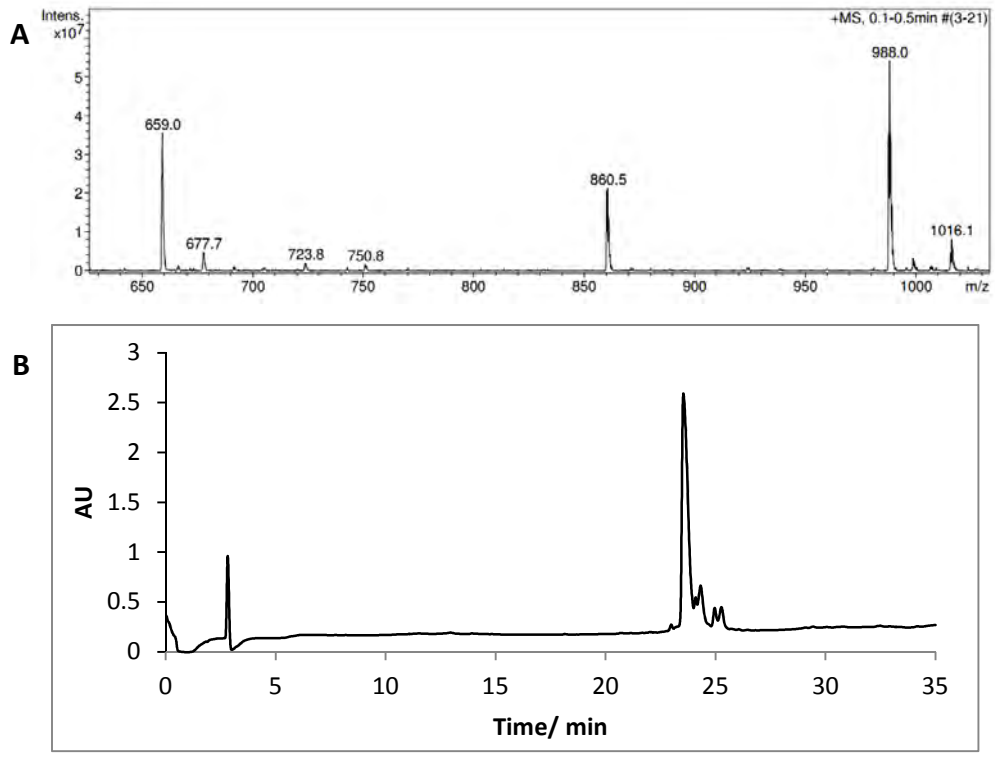

Figure IV.S2. Representative ESI-MS (A) and analytical RP-HPLC trace, detected at 220 nm (B) of $C_{16}V_3A_3GPQGIWGQK_3$.

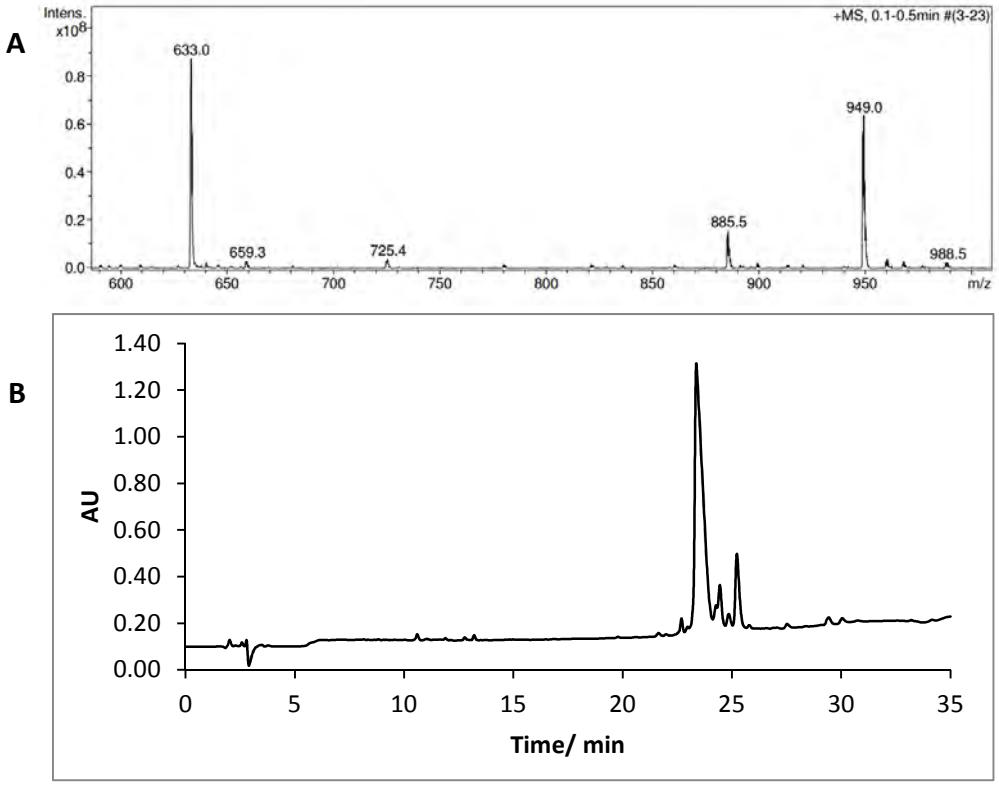

Figure IV.S3. Representative ESI-MS (A) and analytical RP-HPLC trace, detected at 220 nm (B) of $C_{16}V_3A_3GDQGIAGFK_3$.

S1.2 Estimation of nanofiber diameter

The diameter of the PA nanofibers was estimated using TEM micrographs and image analysis. Measurements were done using ImageJ software (NIH, USA).

Table IV.S1 – Estimated PA nanofiber diameter.

PA	Average diameter [nm]
K_3	13.1±2.0
MMP_sK_3	15.8±2.1
MMP_IK_3	12.2±1.9

S2. Membrane characterization

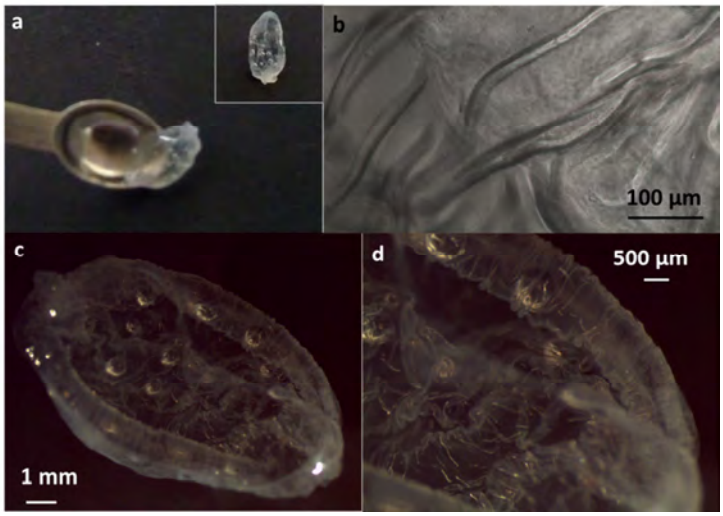

Figure IV.S4. Photographs (a) and bright field microscopy images (b, c, d) of the K_3-HA membranes.

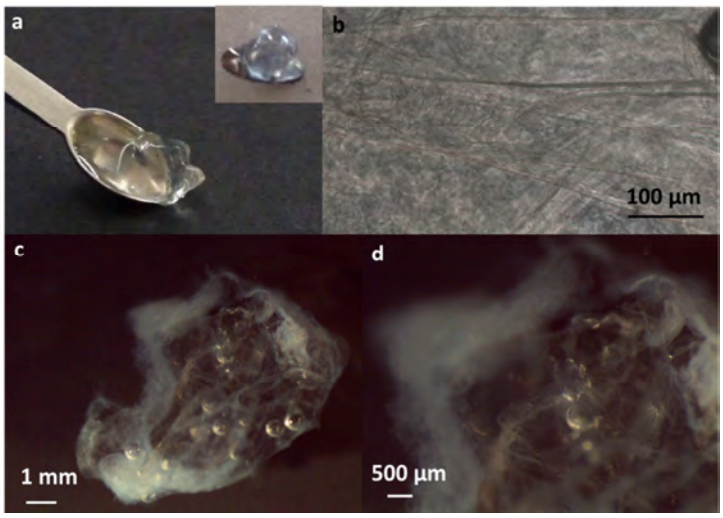

Figure IV.S5. Photographs (a) and bright field microscopy images (b, c, d) of the MMP_s K_3-HA membranes.

S3. Cell culture studies on glass coverslips coated with the synthesized PA molecules

S3.1 Cell proliferation

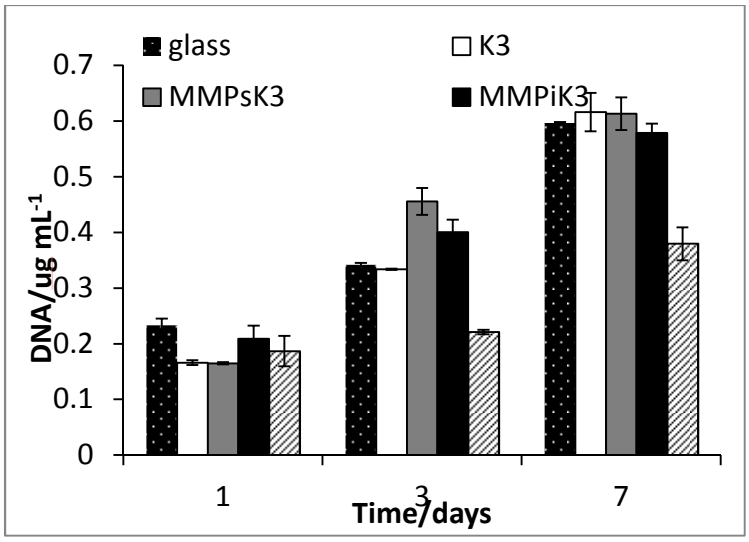

Figure IV.S6. Fibroblast proliferation on PA-coated glass coverslips. hDFb proliferation assessed by dsDNA quantification**.**

S3.2. MMP-1 secretion by fibroblasts

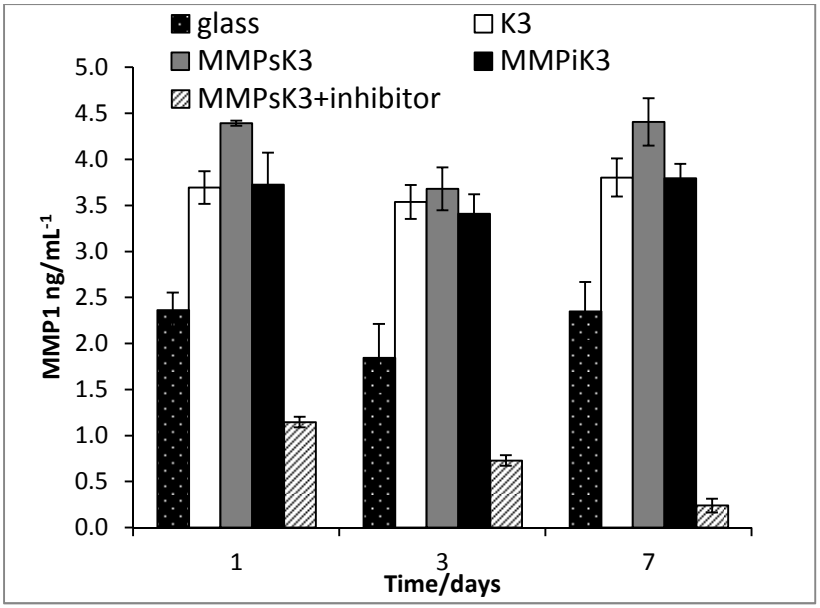

Figure IV.S7. ELISA quantification of MMP-1 in cell culture supernatants from fibroblasts cultured on peptide-coated glass coverslips.

S3.3 Production of ECM proteins by fibroblasts

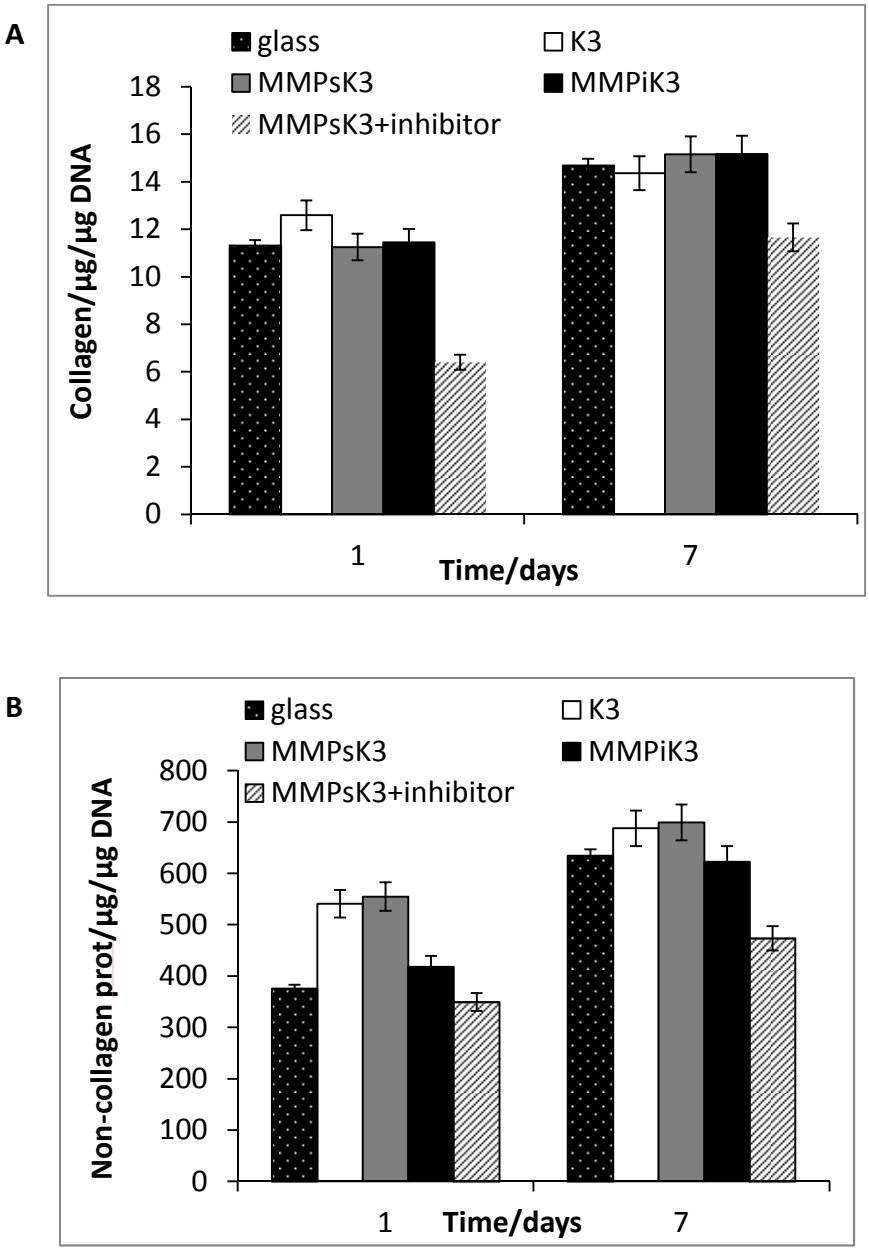

Figure IV.S8 . Concentration of ECM proteins, collagenous (A) and non-collagenous (B) secreted by hDFbs when cultured on peptide-coated glass coverslips.

Chapter V

Single-step self-assembly of micro-patterned membranes: from solution to higher-ordered supramolecular structures

Chapter V*

Single-step self-assembly of micro-patterned membranes: from solution to higher-ordered supramolecular structures

Abstract

This paper describes the fabrication of micro-grooved membranes, which are spontaneously formed by self-assembly in a single step and without the use of a physical template. The micro-patterns are obtained when a positively charged peptide amphiphile (PA), containing an octapeptide domain of alternating hydrophilic and hydrophobic residues, is combined with hyaluronan (HA) at the air-liquid interface. The surface morphology and cross section of the membranes is analyzed by scanning electron microscopy and two-dimensional fast Fourier transform estimates a ~3 μm spacing between ridges. Although small angle X-ray scattering does not reveal nanoscale organization, the micro-pattern formation is further investigated by varying the conditions (experimental set up, incubation time, concentration of the building blocks, HA molecular weight and nature of polyelectrolyte) during self-assembly. In addition to the amino acid sequence in the octapeptide domain, these studies reveal that the presence of an air-liquid interface at the peptide side and the nature of the underneath polyelectrolyte play a key role on the formation of the micro-grooved patterns. Finally, to evaluate the effect of the micro-grooves on cell morphology and orientation, human dermal fibroblasts are cultured on the self-assembled membranes. Cells show adjustable morphology and alignment induced by the surface topography of the membranes. Further development and understanding of this self-patterning system represents an attractive approach for the development of advanced biomaterials for medical applications.

* This chapter is based on the following publication:

Daniela S. Ferreira, Oliver Picot, Yi-An Lin, Honggang Cui, Ronit Bitton, Rui L. Reis, Helena S. Azevedo, Single-step self-assembly of micro-patterned membranes: from solution to higher-ordered supramolecular structures, 2014, submitted

1. Introduction

Human tissues are composed by multiple cell types embedded in the extracellular matrix (ECM) which contains an intricate network of fibrillar structures.[1, 2] Topologically, the ECM is a mixture of heterogeneous pores and fibers having sizes in the nanometer range. ECM structures with nanoscale topography are often folded or bended into secondary microscale topography.[3] The well-defined and specialized ECM of each tissue provides cells with physical (elasticity, topography) and biochemical (adhesion sites, growth factors) signals that influence many cell functions, such as proliferation, migration and differentiation.[4, 5] Nanotopography is also present in individual ECM molecules, such as in collagen, a triple helix of approximately 300 nm long and 1.5 nm wide.[6] Further organization of ECM macromolecules at the different length scales is essential for the integrity and mechanical behavior of tissues, as well as to guide cellular growth and orientation. For example, in tendons, the collagen fiber bundles are arranged parallel to the longitudinal tendon axis. This organization permits tendons to support large tensile forces and cells align between parallel bundles of collagen fibers with elongated nuclei.[7] Another example, is the ECM of small intestine. It folds into a 3D surface comprising three length scales of topography, the centimeter scale mucosal folds, sub-millimeter scale villi and crypts, and nanometer scale topography, which is created by ECM proteins, such as collagen, laminin, and fibronectin.

Currently, advanced nano- and micro-fabrication techniques are being used to fabricate biomaterials with precise patterns to recreate certain ECM topographical features at different length scales or even to replicate the complex hierarchical topography of tissues.[8-10] Techniques such as soft and photolithography, two-photon polymerization, electrospinning, and chemical vapor deposition have been utilized for these purposes, but they are generally limited by the use of exclusive materials and solvents and complicated fabrication process (e.g. multiple steps, expensive equipment).

Molecular self-assembly is a powerful approach for fabricating novel supramolecular biomaterials with designed biochemical functionalities.[11] In addition, by using molecular units as building blocks, self-assembly allows to fabricate materials with structure at the nanometer resolution, the same way as done in nature.[12] Despite displaying structural organization in the nanoscale, most self-assembled materials are macroscopically disordered which can limit their bulk properties and potential uses. One potential method to introduce different levels of organization in supramolecular materials includes the use of external forces. Traditionally, mechanical alignment, electric and magnetic fields have often been used for orientation of materials.[13, 14] On the other hand, patterning on the microscale may extend order in an anticipated manner, dramatically improving performance and enabling new functions.[15, 16] A

number of bottom-up strategies based on self-assembly have been combined with top-down approaches (soft lithography,[17, 18] hierarchical instability patterns of thin films[19] and self-templating assembly[20]) that offer facile control over shape and pattern, to fabricate materials with hierarchical structure.

Through rational molecular design, different self-assembling peptide systems have been developed and shown to assemble into a variety of well-defined nanostructures (micelles, fibers, tapes, vesicles).[21] Peptide amphiphiles (PAs), typically consisting of a hydrophobic linear alkyl tail coupled to peptide block that includes a short peptide sequence with strong propensity to form hydrogen bonding (β-sheet structures) and charged residues for solubility, have gained increased attention in the biomaterials community due to their ability to self-assemble into nanofibrillar structures.[21, 22]In addition to their high degree of order at the nanoscale, PAs can be molecularly designed for specific applications, such as biomineralization,[22] neural regeneration[23] and cell proliferation.[23, 24] Our group has been exploring the self-assembly between peptides and polysaccharides to obtain membranes and micro-capsules for cell culture and encapsulation.[24, 25] To introduce further complexity in our self-assembling systems, we have used a single-step bottom-up (self-assembly) and top-down (soft lithography) fabrication technique to generate membranes with hierarchical structure, consisting of nanofibers and surface micro-topographies.[18] These membranes were obtained by the co-assembly of a positively charged peptide (multi-domain peptide) and the negatively charged polysaccharide hyaluronan (HA).

In an attempt to modulate the degradation properties of self-assembled HA-PA membranes, we discovered that using a specific PA, containing an octapeptide between the β-sheet forming segment and the charged domain, in combination with HA, membranes with well-defined micro-groove patterns were spontaneously formed without the use of any physical template. To our knowledge, the ability to fabricate patterned membranes in a single-step, in which molecules self-assemble from solution into supramolecular films with hierarchical order, has not been reported.

Further development and understanding of this self-patterning system represents an attractive approach for the development of advanced biomaterials for medical applications.

2. Materials and methods

Polymers

Hyaluronan, with an average molar mass of 234 kDa, 750 kDa and 1.5 MDa (Lifecore Biomedical, Inc, Chaska, USA) was used in this study to investigate its self-assembly with a recently designed peptide amphiphile. Alginate from brown algae (low viscosity, Sigma, USA) and poly(acrylic acid) (Mw = 450 kDa, Sigma, USA) were used in this study for comparison with HA.

Peptide amphiphiles: synthesis and purification

The peptides used in this work were synthesized on a CS Bio 136XT automated peptide synthesizer (CS Bio, USA) using standard 9-fluorenylmethoxycarbonyl (Fmoc) based solid phase chemistry on a 4-methylbenzhydrylamine (MBHA) rink amide resin. Amino acid couplings were performed using 4 equivalents (4 mmol) of Fmoc protected amino acids (Novabiochem®, USA), 4 equivalents of O-(Benzotriazol-1-yl)-N,N,N′,N′-tetramethyluronium hexafluorophosphate (HBTU, Carbosynth, UK) and 6 equivalents of N,N-diisopropylethylamine (DIEA, Sigma, USA). Fmoc deprotections were performed with 20% piperidine (Sigma, USA) in dimethylformamide. A palmitic acid ($C_{16}H_{32}O_2$, Calbiochem, USA) tail was manually coupled under the same conditions as the Fmoc-amino acids. Peptide cleavage from the resin and removal of the protecting groups was carried out on a mixture of trifluoroacetic acid (TFA, Sigma, USA)/triisopropylsilane (TIS, Alfa Aesar)/water (95/2.5/2.5)) for 3 h at room temperature. The peptide mixture was collected and excess of TFA was removed by rotary evaporation. The resulting viscous peptide solution was triturated with cold diethyl ether and the white precipitate was collected by filtration, washed with cold ether, and allowed to dry under vacuum overnight. The peptide mass was confirmed by electrospray ionization mass spectrometry (ESI-MS, Agilent, USA).

Peptides were then purified on a Waters 2545 Binary Gradient high-performance liquid chromatography (HPLC) system using a preparative reverse-phase C18 column (Atlantis Prep OBD T3 Column, Waters) and a water/acetonitrile (0.1% TFA) gradient. TFA counter-ions were exchanged by sublimation from 0.01 M hydrochloric acid. Finally, the peptides were dialyzed against ultrapure water using 500 MWCO dialysis tubing (Spectrum labs, The Netherlands), lyophilized and stored at -20 °C until further use. Confirmation of mass and purity was done by ESI-MS and HPLC.

Peptide amphiphiles characterization

Transmission electron microscopy (TEM)

Peptides were dissolved in ultrapure water (0.1 wt%) and the solution was aged for 2 days before TEM analysis. Peptide solutions were loaded on carbon-coated copper TEM grid (Electron Microscopy Sciences, USA). For negative staining a drop of 2 wt% uranyl acetate (Electron Microscopy Sciences, USA) aqueous solution was placed on the samples. The excess solution was wiped away by a piece of filter paper, and the sample was allowed to dry under ambient conditions. All images were collected with a Tecnai 12 TWIN, equipped with SIS Megaview III camera (FEI, USA).

Preparation of micro-grooved membranes by self-assembly

Membranes were prepared by self-assembly using HA (1.5 MDa) and positively charged PAs at optimized conditions, as previously reported.[24] Briefly, 50 µL of a 1 wt% HA solution was cast on the bottom of the wells of a 96 well plate and then 50 µL of PA2 (3.4 wt%, 0.017 M) solution was added on top of the HA solution. A membrane was immediately formed upon contact between the two solutions. HA-PA1 membranes (control membranes) were similarly prepared by combining HA (1 wt%) with PA1 (2 wt%, 0.017 M). To investigate the effect of incubation time on the membrane surface morphology and thickness, the initial formed membrane was allowed to age for either 15, 30 minutes, 1, 4 and 24 hours. After each incubation time, the membrane was rinsed with sterile ultrapure water to ensure the removal of unreacted HA and PA. The effects of peptide (PA2) concentration (8.5 and 4.25 mM), and HA molecular weight (234 and 750 kDa; 1, 2, 3 wt%) were also analyzed. Membranes with alginate from brown algae and poly(acrylic acid) (2 wt%) were also prepared for comparison with HA.

Membrane characterization

Scanning electron microscopy (SEM)

The morphology of the membrane surface and cross-section was analyzed by SEM. Membranes were fixed in 2% glutaraldehyde/3% sucrose in PBS for 1 h at 4 °C followed by sequential dehydration in graded ethanol concentrations (from 20 to 100%). To remove ethanol, samples were dried in a critical point dryer (Tousimis Autosandri®-815 series A, USA). Prior observation, the samples were coated with a gold/palladium layer and imaged using an ultra-high resolution field emission gun scanning electron microscope (Nova™ NanoSEM 200) from FEI (Eindhoven, The Netherlands). The membrane thickness was measured using SEM images from 3 independent membranes. To measure the wavelength of the

ridges, two-dimensional fast Fourier transform (2D FFT) of SEM images of patterned membranes using ImageJ software (NIH, USA).

Polarized light microscopy

Polarized light microscopy was used to characterize PA2 and HA-PA2 membranes. A drop of a concentrated solution of peptide (3.4 wt%) was placed between a slide and coverslip and observed between crossed polarizers in a polarizing microscope (Olympus BX 60, Olympus, UK). Membranes resulting from the self-assembly of PA and HA were also imaged. Membranes were prepared directly on the glass slide before imaging. A drop of HA (1 wt%) was cast on the slide and then a drop of PA2 (3.4 wt%)was added on the top of HA solution. A membrane is immediately formed upon contact between the two solutions. Samples were covered with a coverslip and examined by polarized optical microscopy.

Small angle X-ray scattering (SAXS)

The SAXS measurements were performed using the SAXSLab Ganesha 300-XL system (Denmark) with Cu Kα radiation generated by a sealed microfocused tube (Genix 3D Cu-source with integrated Monochromator) powered at 50kV and 0.6mA and three pinholes collimation. The scattering patterns were recorded by a Pilatus 300K detector (Dectris, Switzerland). The scattering intensity I(q) was recorded in the interval $0.012 < q < 0.7$ A^{-1} , where q is defined as

$$q = \frac{4\pi}{\lambda}\sin\theta$$

where 2θ is the scattering angle, and λ is the radiation wavelength (1.542A).

The solution under study was sealed in a thin-walled capillary (glass) of about 1.5 mm diameter and 0.01 mm wall thickness. Membrane samples were placed in a customized sample holder where the wet membranes are sandwiched between 2 thin sheets of Mica. Measurements were performed under vacuum at ambient temperature. The 2D SAXS images were azimuthally averaged to produce one-dimensional profiles of intensity, *I* vs. *q*, using the two-dimensional data reduction program SAXSGUI (SAXSLab, Denmark). The scattering spectra of the capillary and solvent were also collected and subtracted from the corresponding solution data using the Irena package for analysis of small-angle scattering data.[26] No attempt was made to convert the data to an absolute scale.

For membrane samples data analysis was based on fitting the scattering curve to an appropriate model by a least-squares method using software provided by NIST[26] (NIST SANS analysis version 7.0 on IGOR).

Cell culture studies

Isolation and culture of human primary fibroblasts

Human dermal fibroblasts (hDFbs) were isolated from skin samples discarded from abdominoplasty surgeries of consenting patients at Hospital da Prelada (Porto, Portugal). Briefly, the skin tissue was cut in pieces of 0.5 by 0.5 cm and digested in a dispase solution (2.4 $U.mL^{-1}$ in PBS) at 4 °C overnight. After removing the epidermis, the fibroblasts were isolated from the dermis by overnight digestion of the dermal pieces in a collagenase IA solution (125 $U.mL^{-1}$ in PBS) at 4 °C. Digestion products were poured through a 100 µm cell strainer and centrifuged at 200 *g* for 5 minutes. The pellet was resuspended and the cells were subsequently cultured in Dulbecco's Modified Eagle Medium (DMEM) (Sigma, Germany) supplemented with 10% of fetal bovine serum (FBS, Gibco, UK) and 1% (v/v) antibiotic/antimycotic solution (A/B) (Gibco, UK) containing 100 $units.mL^{-1}$ penicillin and 100 $mg.mL^{-1}$ streptomycin, in a 37 °C humidified atmosphere with 5% CO_2.

Culture of human primary fibroblasts on PA-HA membranes

Membranes were prepared under sterile conditions as previously described. HA sterilization for cell studies was done by dissolving the polymer in water, filtering the solution through a 0.22 µm filter, followed by lyophilization in sterile falcon tubes. PA solutions were sterilized by UV exposure for 15 minutes. Confluent hDFbs were harvested from monolayer cultures using TrypLE™ Express (Invitrogen, USA). Cells were seeded on the membranes (10^4 $cells.cm^{-2}$) and cultured in DMEM supplemented with 10% FBS and 1% (v/v) A/B at 37 °C in a humidified atmosphere of 5% CO_2 for 24 hours. Cells cultured on the membranes were examined under SEM, to analyze cell morphology and spreading. Cell cultured membranes were fixed, dehydrated and prepared as described for SEM analysis.

Staining and confocal microscopy

For examination of cell morphology and spreading, fibroblasts cultured on the membranes were stained for collagen I and F-actin. Cells were washed in PBS and subsequently fixed in 10% formalin solution (Sigma-Aldrich, Germany) for 30 minutes at 4 °C. Cells were then washed once with 0.1 M glycine in PBS and twice with PBS and permeabilized with 2% BSA/ 0.2% Triton X-100 solution for 1 h at RT. Samples were incubated with the primary antibody, anti-collagen I (ab292, 1 : 500, Abcam, UK), for 1 h at RT and washed three times for 2 minutes with PBS. Samples were then incubated with the secondary antibody, anti-mouse Alexa 488 (1:200, Molecular Probes, Invitrogen, USA) and TRITC-conjugated phalloidin (1U/mL, Sigma-Aldrich, Germany) for 1 h at RT. Cell nuclei were counterstained

with 1 mg/mL DAPI (1:1000, Sigma-Aldrich, Germany) for 10 min and washed with PBS. Visualization was performed by CLSM (Olympus FluoView 1000, Olympus, Japan). Background was subtracted and images were processed using FV10-ASW 3.1 software (Olympus, Japan).

Statistics

The results of membrane thickness are expressed as a mean ± standard deviation with $n = 3$ for each condition. Statistical significance of differences was determined using unpaired student's *t*-test multiple comparison procedure at a confidence level of 95% ($p < 0.05$).

3. Results and discussion

3.1. Peptide sequence: design and analysis

The sequences and chemical structures of the peptide amphiphiles (PA1 and PA2) employed in this study are shown in Figure V.1A. Both PAs contain a peptide segment composed of β-sheet forming sequence (VVVAAA) and a domain with positively charged amino acids (KKK) to bind the anionic hyaluronan (HA), coupled to a hydrophobic tail (C16). PA2 contains additionally an octapeptide GPQGIWGQ between the β-sheet domain and the charged domain. This sequence is a mutated version of the sequence found in collagen I (GPQGIAGQ), that has been demonstrated to be cleavable by matrix metalloproteinase 1 (MMP-1)[27] and was used in our previous studies to tailor the degradation of HA-PA membranes.[28] This octapeptide sequence is composed of two hydrophilic (Gln, Q) and two hydrophobic (Ile, I and Trp, W) amino acids separated by one Gly (G) residue.

TEM analysis showed the formation of nanofibers for both peptides, but PA2 formed shorter fibers than PA1 (Figure V.1B).

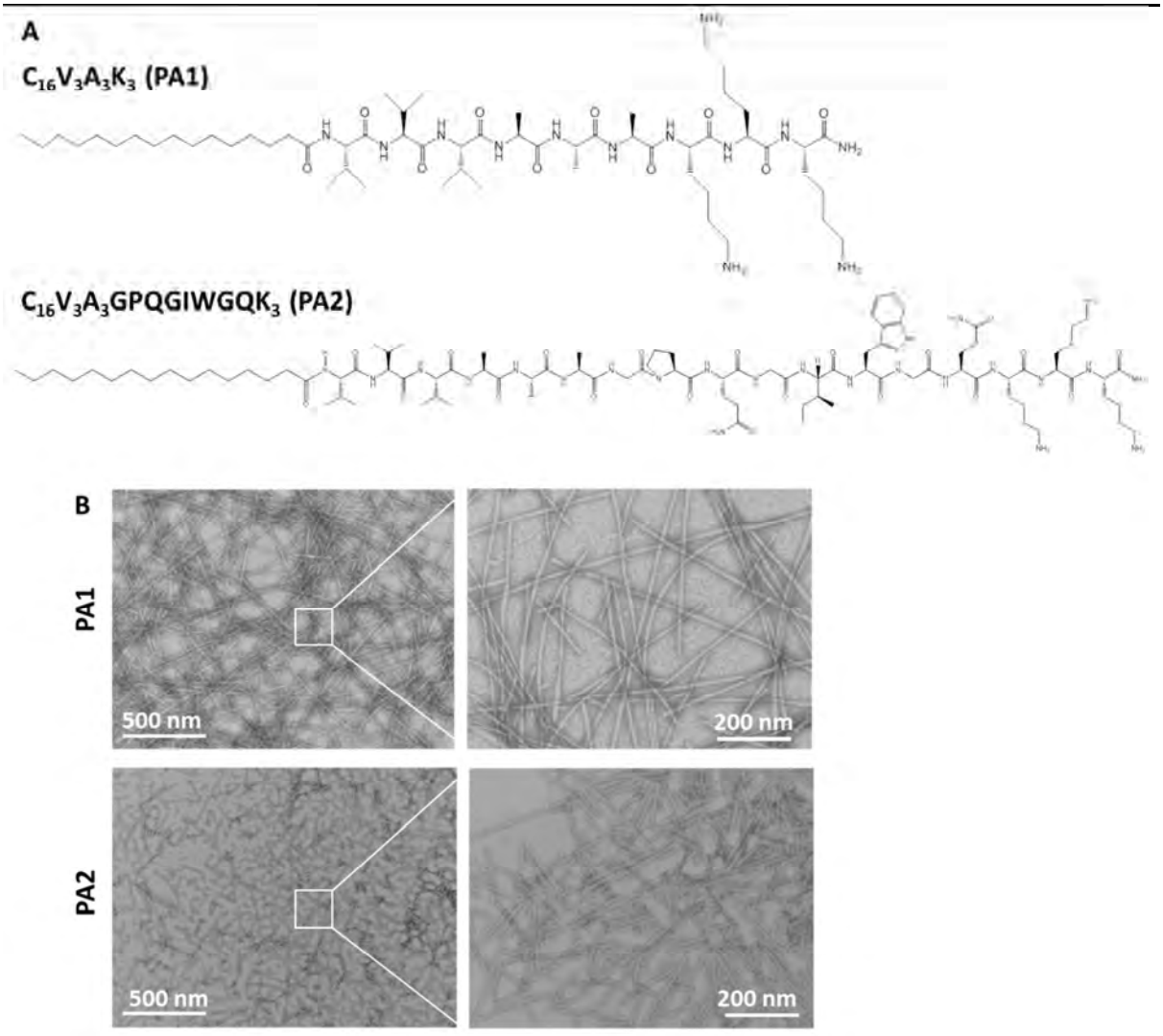

Figure V.1. Chemical structure (A) of the peptide amphiphiles (PAs) investigated in this study and TEM images (B) of PA solutions (0.1 wt% in water) upon drying .

3.2. Membrane fabrication by self-assembly

Previous studies have shown the ability of PA1 to interact with hyaluronan (HA) and form hierarchical sacs and membranes by self-assembly.[24, 29, 30] In addition, our previous findings have shown that the insertion of a sequence of eight amino acids into the PA structure (PA2) did not affect its self-assembly with HA.[28] Here, membranes were prepared by adding a solution of PA1 or PA2 at the same molar concentration (0.017 M) on the top of the HA solution at a 1:1 ratio (v/v). In both conditions, a membrane was immediately formed at the interface between the two solutions, that was then let to react at 37 °C.

3.3. Membrane characterization

3.3.1 SEM

SEM analysis of the microstructure of the membranes showed a highly organized nanofibrillar structure, exhibiting two distinct topographies (Figure V.2A). HA-PA1 membranes presented a flat surface topography with peptide nanofibers randomly distributed, whereas HA-PA2 membranes exhibited folded shapes in a periodic arrangement (Figure V.2A). SEM micrographs of the cross section of HA-PA2 membranes showed well defined micro-scale periodic patterns on the peptide side (Figure V.2B). These remarkable well-organized patterns were formed spontaneously by self-assembly, without the aid of a physical template or mould. This singularity encouraged further experiments to understand the mechanism of pattern formation and identify whether these patterns can be generated under different conditions and using other common anionic polymers.

When the two molecules were combined in the inverse order (HA over the PA2 solution), membranes were still formed. This observation is consistent to what has been reported before by Mendes et al. when mixing HA with a different peptide.[18] However, SEM micrographs, on the PA side, showed flat membranes with random nanofibers and without micro-scale periodic structures (Figure V.2C). These findings suggest that the order in which the components are added influence the ability to form patterns, and that the peptide air-liquid interface may play a role on the pattern formation, a hypothesis that remains to be further investigated. Adsorption of self-assembling peptides (composed of two strands of alternating hydrophoic and hydrophilic residues attached to a β-turn) at the water surface was studied by neutron reflectivity (NR)[31], a technique that determines the scattering length density profile of the surface layer, providing structural information about monolayers formed at the water surface. Based on the obtained results, the authors proposed that the peptide adopted a β-hairpin conformation at the air-water interface, with peptide monolayers almost entirely in the air and with the hydrophobic side chains completely dry and the hydrophilic side chains solvated only at their tips.

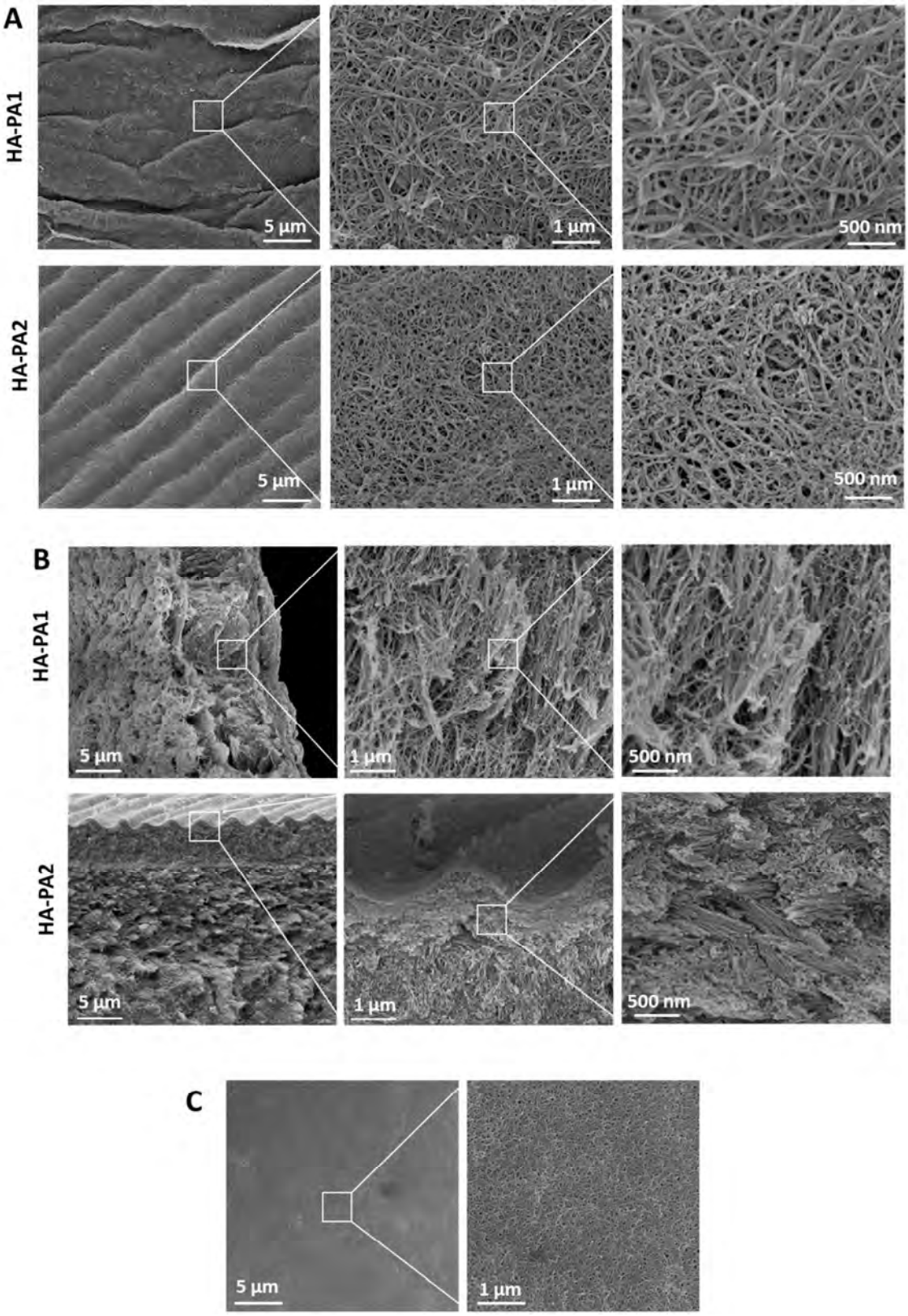

Figure V.2. SEM images of the top surface (A) and cross-section (B) of membranes obtained by self-assembly between HA (1 wt%) and PA1 (2 wt%) (HA-PA1) and PA2 (3.4 wt%) (HA-PA2) and adding PA solutions on top of HA solution. (C) SEM micrographs of the PA side of membranes fabricated with HA on top of the PA2 solution showing the membrane surface.

Based on these findings, and considering the composition of the octapeptide inserted in the PA structure, we may infer that the hydrophobic residue (I and W) will force the peptide to be above the water surface, into the air phase, resulting in a different surface layer and packing density, leading to the ridge formation. NR studies would be helpful for obtaining structural information on the peptide layer at the surface of HA aqueous solution and support the ridge formation caused by the behavior of the octapeptide at the air-liquid interface.

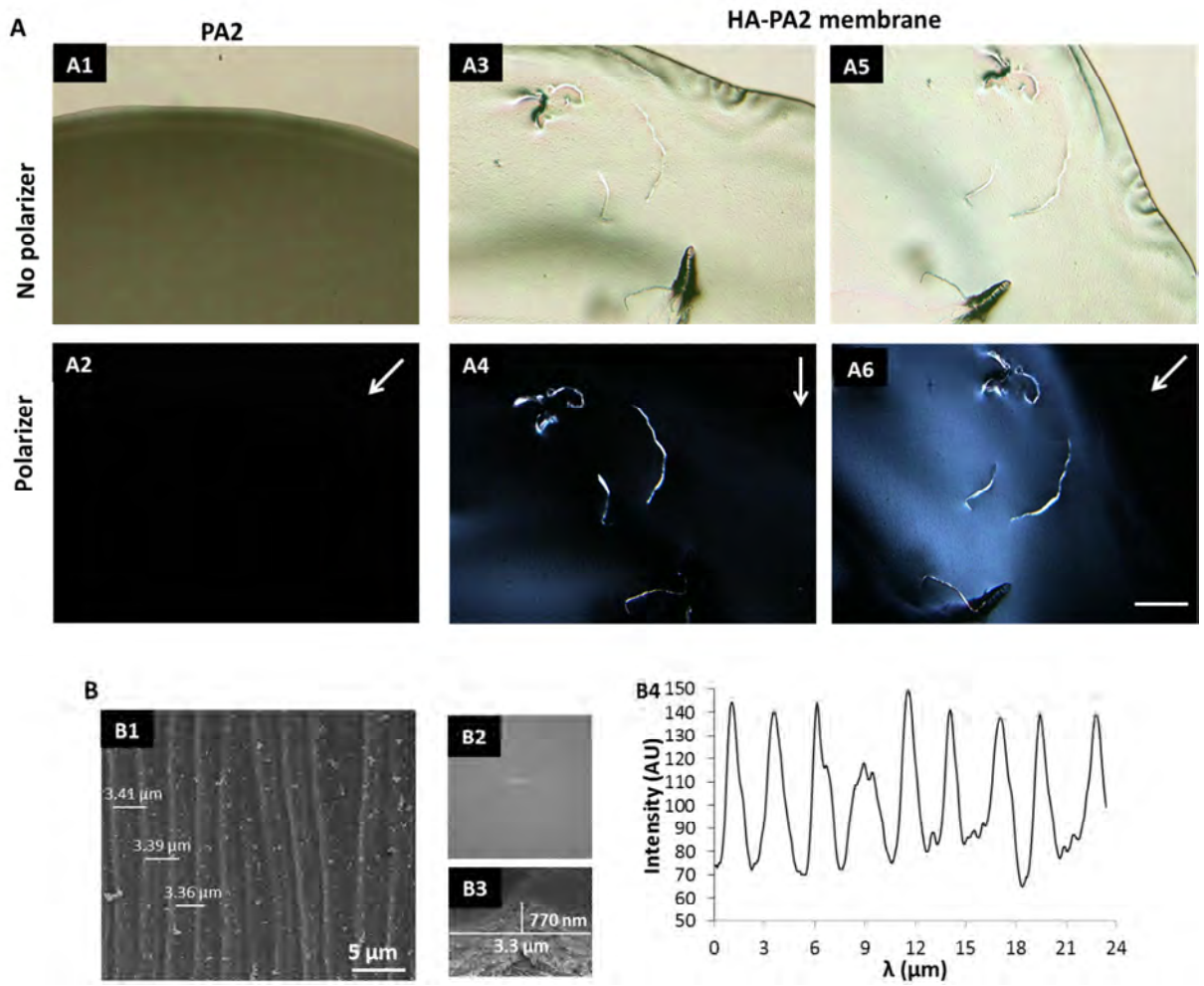

Figure V.3. (A) Polarized light microscopy images of PA2 (3.4 wt%) and HA (1 wt%)-PA2 (3.4 wt%) membrane at the air-liquid interface. Scale bar corresponds to 1mm. (B) Estimation of ridge wavelength (λ) from a plot profile (B4) and two-dimensional fast Fourier transform (B2) of top-down perspective SEM images of HA-PA2 membranes (B1). SEM micrograph of the cross-section of a ridge (B3).

3.3.2 Polarized microscopy

Polarized light microscopy images, taken between two crossed polarizers, showed that when the HA-PA2 membrane is parallel/perpendicular to the polarizer axes (0 degrees), a homogeneous dark state is observed (Figure V.3A4). When the membrane is oriented with approximately 45 degrees to the polarizer axes, a bright state (birefringence) is observed (Figure V.3A6). The same behavior is not observed with the peptide solution alone, visualized under the same conditions (Figure V.3A2). These observations suggest the presence of organized structures with the same orientation as a result of the self-assembly of PA2 with HA. To estimate the wavelength (λ) of the ridges, a plot profile and two-dimensional fast Fourier transform of top-down perspective SEM images of HA-PA2 membranes were performed (Figure V.3B4). The plot profile showed patterns of localized ridges with estimated wavelength of ~3 μm, which corroborates the measurements taken from SEM images of top-down perspective (Figure V.3B1) and cross-section of HA-PA2 membranes (Figure V.3B3). SEM images of a cross-section of HA-PA2 membranes showed ridges with an estimated height of ~770 nm (Figure V.3B3). Figure V.3B2 shows the corresponding 2D Fourier transformation image of the SEM micrograph. Each point in the Fourier domain image represents a particular frequency band in a reciprocal space contained in the spatial image. The brighter spots correspond to specific periodicities and can be used to determine the wavelength of the pattern ridges.

3.3.3 SAXS analysis

To get insight on the possible molecular organization responsible for the micro-pattern formation at the surface, small-angle X-ray scattering (SAXS) experiments were carried out. The 2D scattering patterns of the membranes indicate that no preferred orientation is found in any of the membranes (i.e. the intensity of the peak is uniform along the azimuthal angle) (Figure V.4A1). This result has been observed for HA-PA based membranes,[32] as the incident beam travels through the membrane and the scattering pattern is a result of all three zones within the membrane. The 1D SAXS curves (i.e. the scattered intensity as a function of the wave vector q) of both HA-PA1 and -PA2 membranes exhibit a broad peak (Figure V.4A2). In both cases the peak appears to be split, though the split is more pronounced for the HA-PA1 membrane. This may be attributed to a contribution of two structural features close in size. To interpret the membrane scattering patterns, we analyzed the scattering of the PA solutions alone. The scattering patterns of 2 wt% PA1 and 3.4 wt% PA2 aqueous solutions are presented in Figure V.4B1. Contrary to the expected -1 slope in the low q region, indicative of a cylindrical shape, a slope of -4 is observed for both curves. This suggests the presence of large

structures in the solution. The 2D patterns show the intensity of the peak is not uniform along the azimuthal angle, thus a preferred orientation exists (Figure V.4B2). The scattering patterns of 1 wt% PA1 and 1.7 wt% PA2 aqueous solutions were fitted to a cylindrical core-shell form factor (Figure V.S1) given by Equation S1. The best fit to this model, represented by the solid line in Figure V.S1, yielded a core radii of 11.4 Å and 15.9 Å, and shell thickness of 36.9 Å, and 40.7 Å for PA1 and 2, respectively. These dimensions are approximately in line with the total diameter of PA nanofibers seen previously in literature.[33] The scattering pattern of the higher concentration solution is probably due to bundles of nanofibers. The high viscosity of these solutions and the preferred orientation support this claim. Interestingly, the scattering pattern of 1 wt% PA1 solution is similar to the scattering curve of the HA-PA1 membrane (Figure V.S2A). The similarity between these two scattering curves indicates that PA1 cylindrical structures are the dominant contributors in the membrane scattering profile. The split peak can be attributed to the presence of perpendicular fibers and HA. However, when comparing the scattering of the HA-PA2 membrane to that of 1.7 wt% solution, there is clear difference in the q of the 1st minima (Figure V.S2B). The shift of the minima to lower q's indicates the scattering of the HA-PA2 membranes is not dominant by PA fibers but larger structural features (there is an inverse relationship between the scattering vector and size).

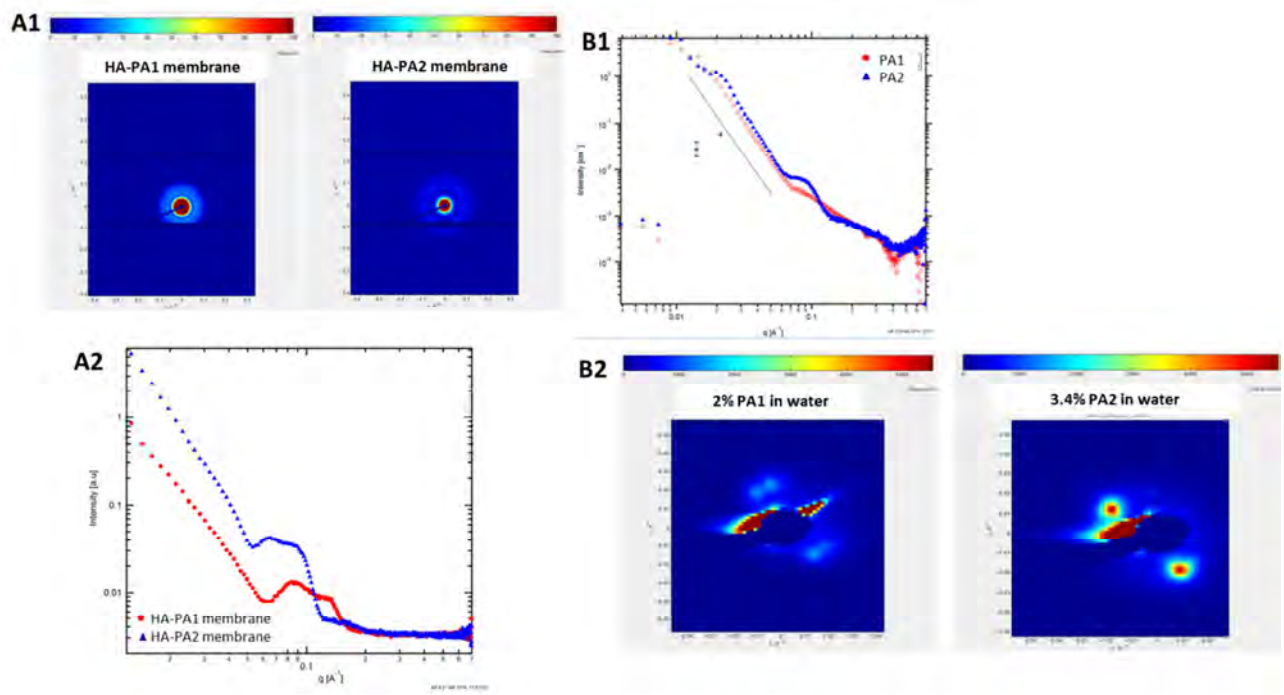

Figure V.4. (A) SAXS analysis of HA(1 wt%)-PA1(2 wt%) and HA(1 wt%)-PA2 (3.4 wt%) membranes: (A1) 2D scattering patterns; (A2) 1D SAXS curves. (B) Scattering patterns of 2 wt% PA1 and 3.4 wt% PA2 aqueous solutions: 1D SAXS curves (B1); 2D scattering patterns (B2).

3.4. Effect of time and building blocks on pattern formation

3.4.1. Incubation time and PA concentration

To better characterize the membranes and understand the pattern formation process, time and PA concentration variations during membrane preparation were investigated.

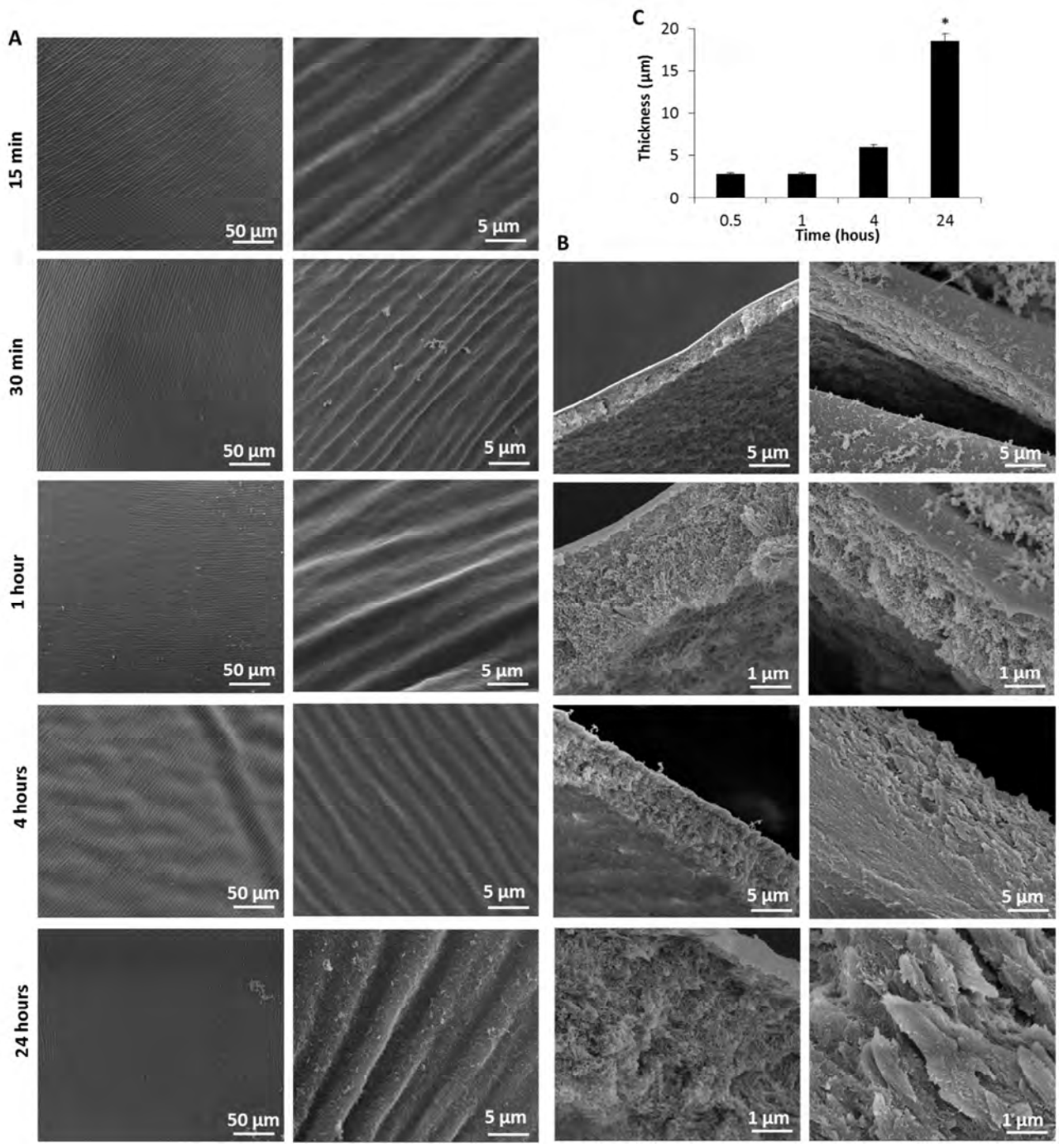

Figure V.5. SEM images of surface morphology (A) and cross-section (B) of HA(1 wt%)-PA2(3.4 wt%) membranes obtained at different incubation times. (C) Evolution of membrane thickness over time (* indicates a significant difference ($p < 0.05$) between conditions).

As observed in the SEM micrographs (Figure V.5A), patterns were formed shortly after 15 minutes of PA2 addition. Further incubation of the membranes at 37 °C, enabled the formation of the patterns with well-defined ridges and grooves and continuous growth of the membranes, with its thickness increasing over time up to 24 hours (Figure V.5B). Membrane thickness increased from 2.53 μm up to 18.51 μm, after 30 minutes and 24 hours of PA2 addition, respectively (Figure V.5C). When the PA2 concentration was decreased (8.5 and 4.25 mM), a thin film was initially formed and let to react up to 24 hours, but the generated membranes were weaker. However, SEM micrographs showed that micro-grooves were formed even at lower peptide concentrations (Figure V.6A). Cross sectional views of the membranes (Figure V.6B) show a thickness of approximately 7 μm, which is lower than the one observed for higher PA2 concentrations (Figure V.2).

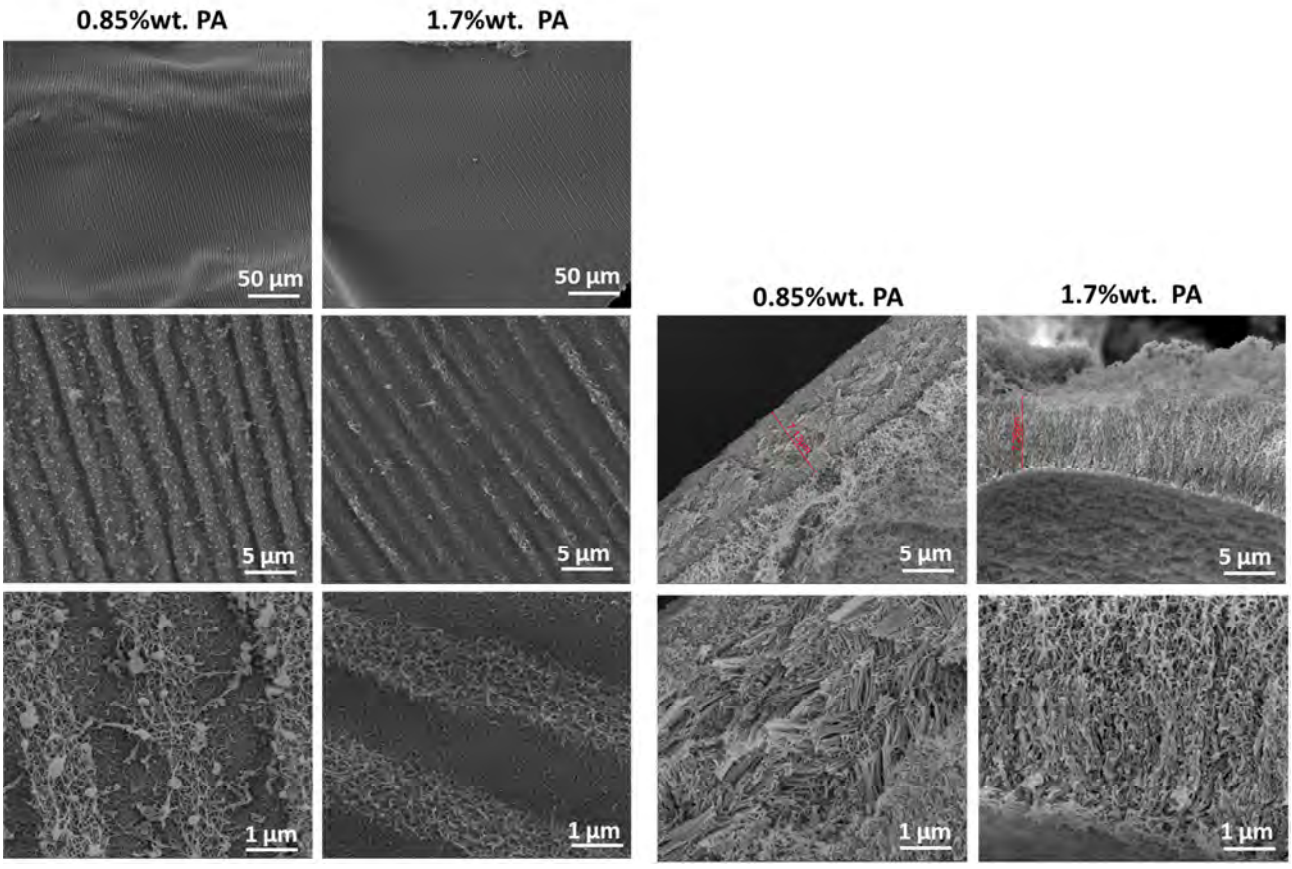

Figure V.6. SEM images of surface morphology (A) and cross-section (B) of HA(1 wt%)-PA2 obtained at with different PA2 concentrations.

3.4.2. HA molecular weight and nature of the polyelectrolyte

In addition to time and PA concentration, HA with different molecular weights and concentrations were also studied. Two molecular weights were investigated (234 and 750 kDa) and to minimize the effect of

solution viscosity, different HA concentrations were used (1, 2 and 3 wt%). Micro-grooved membranes were formed by self-assembly in all the conditions, with slightly topography variations (Figure V.7).

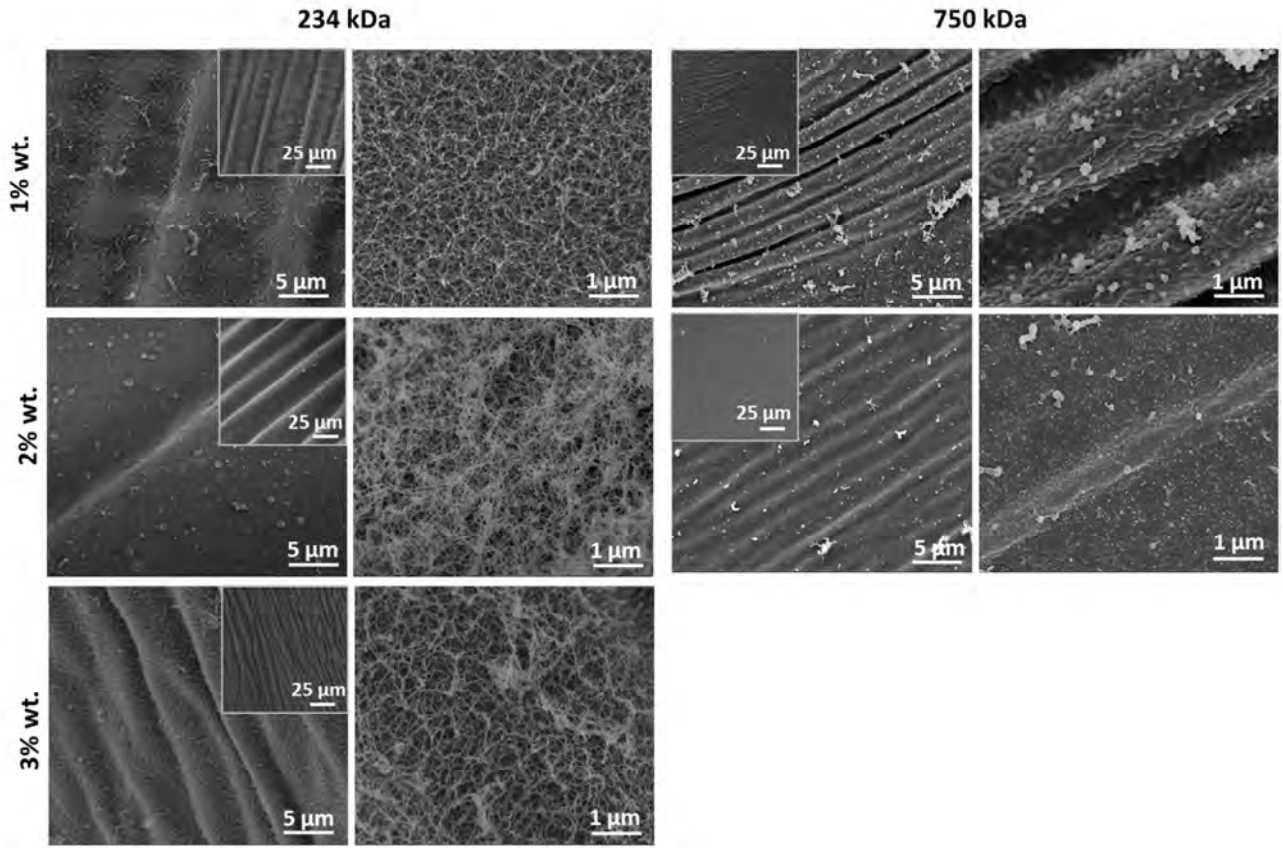

Figure V.7. SEM images of the surface morphology of HA-PA2 membranes obtained with different polymer molecular weights (234, 750 kDa) and concentrations (1, 2 and 3 wt%).

The polyelectrolyte electrostatic charge effect on the self-assembly of membranes has been studied previously, using a positively charged PA with different sequence and polyelectrolytes of different charge density (HA, alginate, carrageenan, poly(acrylic acid)).[32] Authors concluded that the polyelectrolyte charge density can control the micro- and nanostructure of the membrane by affecting diffusion barrier formation during electrostatically-driven self-assembly. To investigate if the electrostatic charge of the polyelectrolyte affects the self-assembly of our system, two anionic polymers, one from natural origin (alginate, twice as charged as HA) and a synthetic one (poly(acrylic acid, similar charge as HA), were tested to self-assemble with PA2. Membranes were formed by self-assembly with both polymers, as seen on the SEM pictures (Figure V.8). However, membranes presented a flat morphology without the presence of evident patterns. Taken together, these results suggest that in conjunction with the PA

sequence, HA may also play a role on pattern formation, not only its electrostatic charge and molecular weight, but also other properties of this polymer, such as viscosity, and chain flexibility.

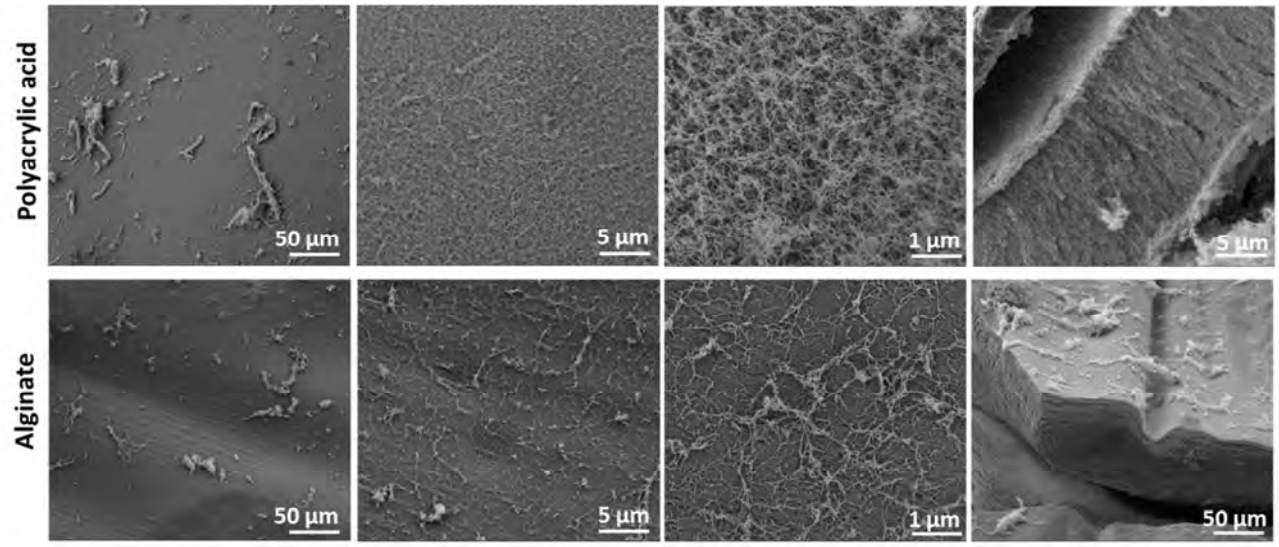

Figure V.8. SEM images of the surface morphology (A) and cross-section (B) of PA2-based membranes obtained with different polyelectrolytes (alginate and polyacrylic acid, 2 wt%).

3.5. Cell culture studies

Research on cell signaling has predominantly focused on the use of soluble chemical cues to influence cell behavior, but now there is mounting evidence that substrate stiffness[34] and topography[35, 36] could potentially be used to generate structured biomaterials for functional tissue engineering. Recent advances in patterning techniques demonstrate a remarkable potential for applications in the fields of biomedical and tissue engineering.[8, 20, 37] The effect of the micro-grooves on the self-assembled membranes on cell morphology was investigated using human dermal fibroblasts (hDFbs). hDFbs were cultured on flat membranes (HA-PA1) presenting random peptide nanofibers and on micro-groove patterned membranes (HA-PA2). After 24 hours of culture, cells showed to interact differently with both surfaces and presented a different morphology and alignment. SEM micrographs showed that, when cultured on the patterned membranes, fibroblasts were oriented in a parallel direction with the channels acting as tissue-guiding matrices (Figure V.9A). In addition, the F-actin of the cells on the patterned membrane also assembled in an orientation that reflected the elongated cell shape (Figure V.9B). In contrast, the cells on flat membranes exhibited a random orientation without strongly defined F-actin filaments. These results are in agreement with previous reports on the ability of fibroblasts to recognize topographical stimuli.[38]

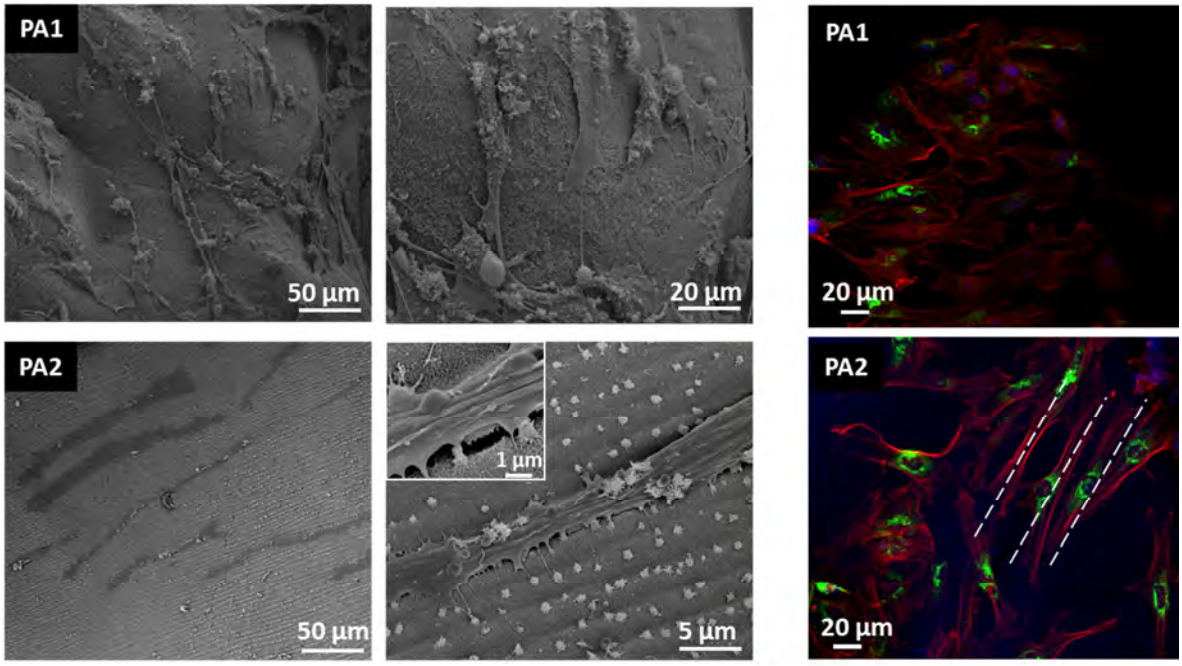

Figure V.9. SEM (A) and confocal microscopy images of human dermal fibroblasts cultured on HA-PA1 vs. HA-PA2 membranes for 24 hours (red: f-actin, green: collagen I, blue: nuclei).

4. Conclusions

Combining the anionic hyaluronan with a peptide amphiphile, containing a specific sequence in its structure, allows the formation micro-grooved membranes by self-assembly in a single step and without the need of a patterned mould. This is a simple method to fabricate membranes with hierarchical structure that can be readily adapted to different membrane formats and does not require multiple and complex steps. A single self-assembly step could facilitate the development of new methods for nano-micro scale fabrication of biomaterials with hierarchical structure. This work also revealed some insights on the main determinants for the formation of micro-grooved membranes, such as nature of the underneath polyelectrolyte and presence of an air-liquid interface at the peptide side. However, further work is necessary to understand the process of micro-groove formation at the membrane surface. Future work will then focus on identifying the key amino acids in the inserted octapeptide responsible for the formation of the particular patterns.

Acknowledgments

This work was funded by the European Regional Development Fund (ERDF) through the Operational Competitiveness Programme "COMPETE" (FCOMP-01-0124-FEDER-014758) and national funds through the Portuguese Foundation for Science and Technology (FCT) under the project PTDC/EBB-BIO/114523/2009. We also thank a start-up grant provided by the School of Engineering and Materials Science at QMUL. D. S. Ferreira gratefully acknowledges FCT for the PhD scholarship (SFRH/BD/44977/2008).

References

1. E. S. Place, N. D. Evans and M. M. Stevens, Complexity in biomaterials for tissue engineering, *Nat Mater*, 2009, 8, 457-470.
2. H. N. Kim, A. Jiao, N. S. Hwang, M. S. Kim, D. H. Kang, D.-H. Kim and K.-Y. Suh, Nanotopography-guided tissue engineering and regenerative medicine, *Advanced Drug Delivery Reviews*, 2013, 65, 536-558.
3. R. G. Flemming, C. J. Murphy, G. A. Abrams, S. L. Goodman and P. F. Nealey, Effects of synthetic micro- and nano-structured surfaces on cell behavior, *Biomaterials*, 1999, 20, 573-588.
4. C.-M. Lo, H.-B. Wang, M. Dembo and Y.-l. Wang, Cell Movement Is Guided by the Rigidity of the Substrate, *Biophysical Journal*, 2000, 79, 144-152.
5. R. J. Petrie, A. D. Doyle and K. M. Yamada, Random versus directionally persistent cell migration, *Nat Rev Mol Cell Biol*, 2009, 10, 538-549.
6. L. Bozec, G. van der Heijden and M. Horton, Collagen Fibrils: Nanoscale Ropes, *Biophysical Journal*, 2007, 92, 70-75.
7. R. James, G. Kesturu, G. Balian and A. B. Chhabra, Tendon: biology, biomechanics, repair, growth factors, and evolving treatment options, *J Hand Surg Am*, 2008, 33, 102-112.
8. D.-H. Kim, H. Lee, Y. K. Lee, J.-M. Nam and A. Levchenko, Biomimetic Nanopatterns as Enabling Tools for Analysis and Control of Live Cells, *Advanced Materials*, 2010, 22, 4551-4566.
9. X. Yao, R. Peng and J. Ding, Cell–Material Interactions Revealed Via Material Techniques of Surface Patterning, *Advanced Materials*, 2013, 25, 5257-5286.
10. P. Zorlutuna, N. Annabi, G. Camci-Unal, M. Nikkhah, J. M. Cha, J. W. Nichol, A. Manbachi, H. Bae, S. Chen and A. Khademhosseini, Microfabricated Biomaterials for Engineering 3D Tissues, *Advanced Materials*, 2012, 24, 1782-1804.
11. S. Zhang, Fabrication of novel biomaterials through molecular self-assembly, *Nat Biotech*, 2003, 21, 1171-1178.
12. C. Sanchez, H. Arribart and M. M. Giraud Guille, Biomimetism and bioinspiration as tools for the design of innovative materials and systems, *Nat Mater*, 2005, 4, 277-288.
13. M. Lescanne, A. Colin, O. Mondain-Monval, K. Heuzé, F. Fages and J.-L. Pozzo, Flow-Induced Alignment of Fiberlike Supramolecular Self-Assemblies during Organogel Formation with

Various Low Molecular Mass Organogelator–Solvent Systems, *Langmuir*, 2002, 18, 7151-7153.

14. H. Jiang and S. I. Stupp, Dip-Pen Patterning and Surface Assembly of Peptide Amphiphiles, *Langmuir*, 2005, 21, 5242-5246.
15. M. Muthukumar, C. K. Ober and E. L. Thomas, Competing Interactions and Levels of Ordering in Self-Organizing Polymeric Materials, *Science*, 1997, 277, 1225-1232.
16. J. Aizenberg, A. J. Black and G. M. Whitesides, Control of crystal nucleation by patterned self-assembled monolayers, *Nature*, 1999, 398, 495-498.
17. A. Mata, L. Hsu, R. Capito, C. Aparicio, K. Henrikson and S. I. Stupp, Micropatterning of bioactive self-assembling gels, *Soft Matter*, 2009, 5, 1228-1236.
18. A. C. Mendes, K. H. Smith, E. Tejeda-Montes, E. Engel, R. L. Reis, H. S. Azevedo and A. Mata, Co-Assembled and Microfabricated Bioactive Membranes, *Advanced Functional Materials*, 2013, 23, 430-438.
19. C. Cao, H. F. Chan, J. Zang, K. W. Leong and X. Zhao, Harnessing Localized Ridges for High-Aspect-Ratio Hierarchical Patterns with Dynamic Tunability and Multifunctionality, *Advanced Materials*, 2014, 26, 1763-1770.
20. W.-J. Chung, J.-W. Oh, K. Kwak, B. Y. Lee, J. Meyer, E. Wang, A. Hexemer and S.-W. Lee, Biomimetic self-templating supramolecular structures, *Nature*, 2011, 478, 364-368.
21. Y.-C. Yu, P. Berndt, M. Tirrell and G. B. Fields, Self-Assembling Amphiphiles for Construction of Protein Molecular Architecture, *Journal of the American Chemical Society*, 1996, 118, 12515-12520.
22. J. D. Hartgerink, E. Beniash and S. I. Stupp, Self-Assembly and Mineralization of Peptide-Amphiphile Nanofibers *Science*, 2001, 294, 1684-1688.
23. G. A. Silva, C. Czeisler, K. L. Niece, E. Beniash, D. A. Harrington, J. A. Kessler and S. I. Stupp, Selective Differentiation of Neural Progenitor Cells by High-Epitope Density Nanofibers, *Science*, 2004, 303, 1352-1355.
24. D. S. Ferreira, A. P. Marques, R. L. Reis and H. S. Azevedo, Hyaluronan and self-assembling peptides as building blocks to reconstruct the extracellular environment in skin tissue, *Biomaterials Science*, 2013, 1, 952-964.
25. A. C. Mendes, E. T. Baran, P. Lisboa, R. L. Reis and H. S. Azevedo, Microfluidic fabrication of self-assembled peptide-polysaccharide microcapsules as 3D environments for cell culture, *Biomacromolecules*, 2012, 13, 4039-4048.

26. J. Ilavsky and P. R. Jemian, Irena: tool suite for modeling and analysis of small-angle scattering, *Journal of Applied Crystallography*, 2009, 42, 347-353.

27. R. T. Aimes and J. P. Quigley, Matrix Metalloproteinase-2 Is an Interstitial Collagenase: Inhibitor-free enzyme catalyzes the cleavage of collagen fibrils and soluble native type I collagen generating the specific ¾- and ¼-length fragments, *Journal of Biological Chemistry*, 1995, 270, 5872-5876.

28. D. S. Ferreira, Y.-A. Lin, H. Cui, J. A. Hubbell, R. L. Reis and H. S. Azevedo, Molecularly engineered self-assembling membranes for cell-mediated degradation, DOI: 10.1002/adhm.201400586

29. R. M. Capito, H. S. Azevedo, Y. S. Velichko, A. Mata and S. I. Stupp, Self-assembly of large and small molecules into hierarchically ordered sacs and membranes, *Science*, 2008, 319, 1812-1816.

30. D. Carvajal, R. Bitton, J. R. Mantei, Y. S. Velichko, S. I. Stupp and K. R. Shull, Physical properties of hierarchically ordered self-assembled planar and spherical membranes, *Soft Matter*, 2010, 6, 1816-1823.

31. J. R. Lu, S. Perumal, E. T. Powers, J. W. Kelly, J. R. P. Webster and J. Penfold, Adsorption of β-Hairpin Peptides on the Surface of Water: A Neutron Reflection Study, *Journal of the American Chemical Society*, 2003, 125, 3751-3757.

32. R. Bitton, L. W. Chow, R. H. Zha, Y. S. Velichko, E. T. Pashuck and S. I. Stupp, Electrostatic Control of Structure in Self-Assembled Membranes, *Small*, 2014, 10, 500-505.

33. D. J. Toft, T. J. Moyer, S. M. Standley, Y. Ruff, A. Ugolkov, S. I. Stupp and V. L. Cryns, Coassembled Cytotoxic and Pegylated Peptide Amphiphiles Form Filamentous Nanostructures with Potent Antitumor Activity in Models of Breast Cancer, *ACS Nano*, 2012, 6, 7956-7965.

34. A. J. Engler, S. Sen, H. L. Sweeney and D. E. Discher, Matrix Elasticity Directs Stem Cell Lineage Specification, *Cell*, 126, 677-689.

35. M. M. Stevens and J. H. George, Exploring and Engineering the Cell Surface Interface, *Science*, 2005, 310, 1135-1138.

36. R. J. McMurray, N. Gadegaard, P. M. Tsimbouri, K. V. Burgess, L. E. McNamara, R. Tare, K. Murawski, E. Kingham, R. O. C. Oreffo and M. J. Dalby, Nanoscale surfaces for the long-term maintenance of mesenchymal stem cell phenotype and multipotency, *Nat Mater*, 2011, 10, 637-644.

37. R. Langer and D. A. Tirrell, Designing materials for biology and medicine, *Nature*, 2004, 428, 487-492.

38. H. N. Kim, Y. Hong, M. S. Kim, S. M. Kim and K. Y. Suh, Effect of orientation and density of nanotopography in dermal wound healing, *Biomaterials*, 2012, 33, 8782-8792.

Appendix

S1. Peptide characterization

S1.1 Mass determination and purity of synthesized peptides

ESI-MS was used to determine the mass of the synthesized peptides (Fig. V.S1-S2, A).

The expected mass for $C_{16}V_3A_3K_3$ ($C_{58}H_{111}N_{13}O_{10}$) was 1150.6, two main peaks were found by ESI-MS, corresponding to $[M+H]^+$ m/z = 1150.8 and $[M+2H]^{2+}$ m/z = 575.9 (Fig. V.S1A).

The expected mass for $C_{16}V_3A_3GPQGIWGQK_3$ ($C_{96}H_{164}N_{24}O_{20}$) was 1974.5, two mains peaks were found, corresponding to $[M+2H]^{2+}$ m/z = 988.0 and $[M+3H]^{3+}$ m/z = 659.0 (Fig. V.S2A).

The purity of the peptides was analyzed by reverse-phase analytical high performance liquid chromatography (RP-HPLC). The HPLC traces showed a major peak corresponding to the peptide of interest (Fig. V.S1-S2, B).

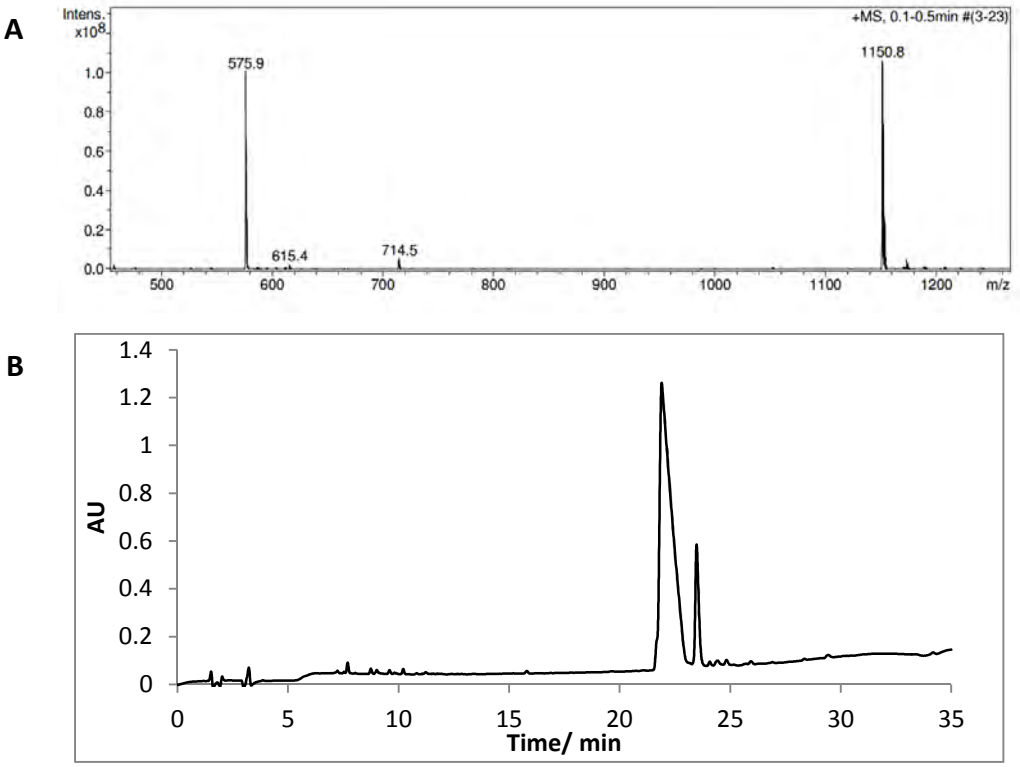

Figure V.S1. Representative ESI-MS (A) and analytical RP-HPLC trace, detected at 220 nm (B) of $C_{16}V_3A_3K_3$.

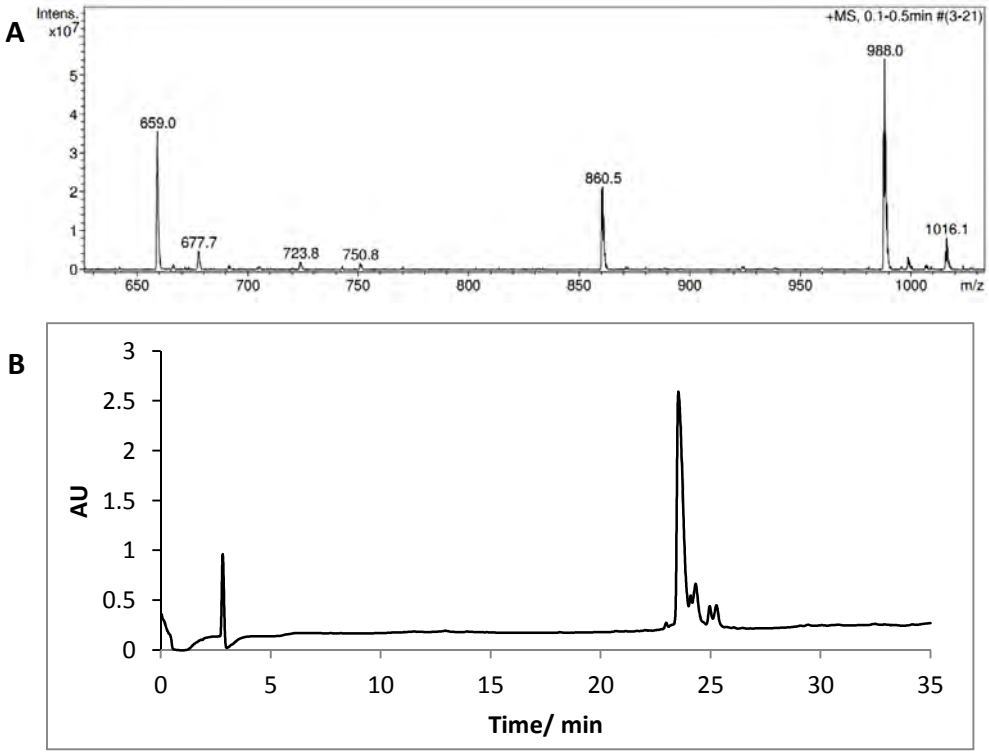

Figure V.S2. Representative ESI-MS (A) and analytical RP-HPLC trace, detected at 220 nm (B) of $C_{16}V_3A_3GPQGIWGQK_3$.

S2.1 Small angle X-ray scattering

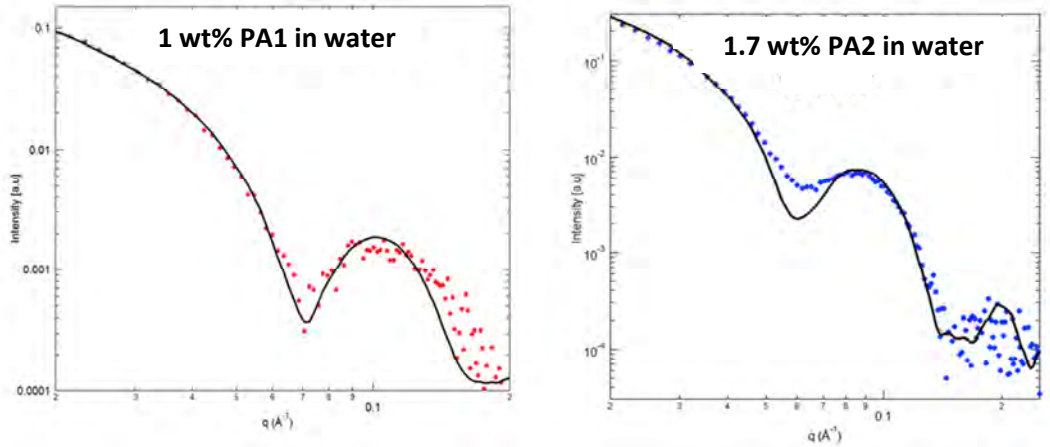

Figure V.S3. Scattering patterns of 1 wt% PA1 and 1.7 wt% PA2 aqueous solutions fitted to a cylindrical core-shell form factor given by equation S1.

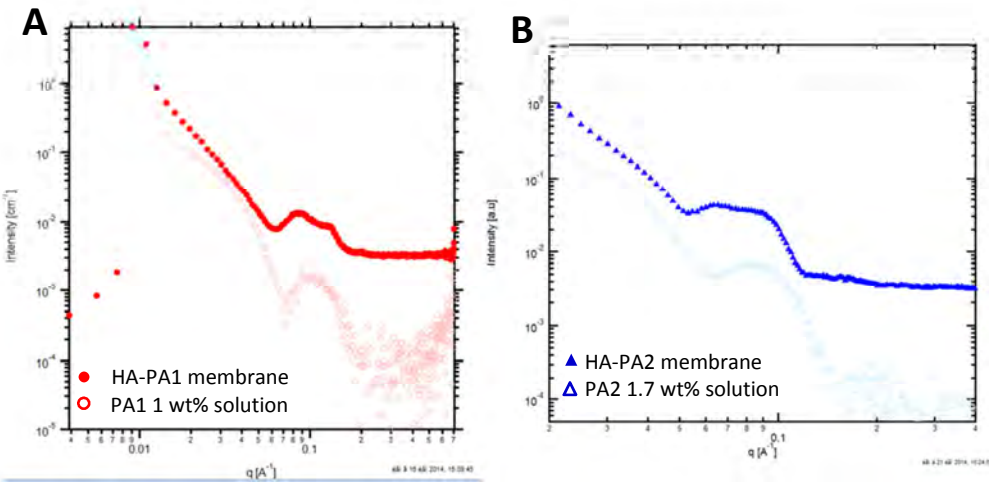

Figure V.S4. Comparison of scattering pattern of HA-PA1 membrane versus 1 wt% PA1 solution and HA-PA2 membrane versus 1.7 wt% PA2 solution.

S2.2 Modeling of small angle scattering patterns

The scattering intensity of a monodispersed system of particles of identical shape can be described by equation S1:

$$I(q) = NP(q)S(q) \qquad (S1)$$

where N is the number of particles per unit volume, P(q) is the form factor revealing the specific size and shape of the scatterers and S(q) is the structure factor that accounts for the interparticle interactions. In dilute solutions, where the interactions between the objects can be neglected, S(q) is equivalent to 1.

A form factor for a simple core-shell cylinder where the core and the shell have a uniform electron density is given by equation S2:

$$P(q) = \int_0^{\pi/2} \sin\theta \cdot d\theta \cdot \left[V_l(\rho_l - \rho_{solv}) \frac{\sin\left(\frac{qH_l\cos\theta}{2}\right)}{\frac{qH_l\cos\theta}{2}} \frac{2J_1(qR_l\sin\theta)}{qR_l\sin\theta} + V_p(\rho_p - \rho_l) \frac{\sin\left(\frac{qH_p\cos\theta}{2}\right)}{\frac{qH_p\cos\theta}{2}} \frac{2J_1(qR_p\sin\theta)}{qR_p\sin\theta} \right]^2 \qquad (S2)$$

$$V_x = \pi R_x^2 H_x$$

where $J_1(x)$ is the first order Bessel function. Theta is defined as the angle between the cylinder axis and the scattering vector, q. R_p and R_l are the core and shell radii respectively, H_p and H_l are the core and shell lengths, and is electron density.

Chapter VI

Specific amino acid sequences and their localization in the structure of peptide amphiphiles modulate the surface topography of self-assembled peptide-hyaluronan membranes

Chapter VI*

Specific amino acid sequences and their localization in the structure of peptide amphiphiles modulate the surface topography of self-assembled peptide-hyaluronan membranes

Abstract

Peptide amphiphiles (PAs), consisting of a hydrophobic alkyl tail (palmitic acid) linked to a peptide segment that includes a β-sheet forming region of six amino acids, a central domain of eight amino acids (octapeptide), a charged block containing three positively charged residues, were designed in this work to self-assemble with anionic hyaluronan (HA) into membranes with specific functionalities. The octapeptide was inserted between the β-sheet segment and the charged block aiming to modulate the structural and biological properties of the resulting assemblies.

A peptide library, containing 15 PAs with variations on the central peptide segment in terms of length and amino acid composition, was synthesized to investigate the role of this central domain on the surface morphology of resulting self-assembled membranes. Membranes with very distinct surface morphologies, from well-defined micro-grooves to micro-sized aggregates, were obtained by simply manipulating the PA structure. The results from site-direct mutations suggest that a sequence of 7-8 amino acids in the central domain, including the presence of isoleucine (Ile) in the middle, and existence of β-sheet structures are determinant for the formation of micro-groove patterns. While we have elucidated some key features on the PA structure responsible for the formation of micro-grooved self-assembled membranes, further experiments and complementary techniques are necessary to confirm the postulated hypothesis.

Nonetheless, the ability of modulating the surface topography of self-assembled membranes, by introducing subtle changes in the PA sequence, offers a simple way to develop patterned substrates with great potential for use in cell culture experiments.

* This chapter is based on the following publication:

Daniela S. Ferreira, Yi-An Lin, Honggang Cui, Rui L. Reis, Helena S. Azevedo, Specific amino acid sequences and their localization in the structure of peptide amphiphiles modulate the surface topography of self-assembled peptide-hyaluronan membranes, 2014, submitted

1. Introduction

Inspired by the structural hierarchy of biological materials, materials engineers are combining micro- and nanoscale fabrication technologies to design and construct synthetic materials with precise spatial patterns and structures.[1] Integration of top-down (e.g. lithography) and bottom-up (e.g. self-assembly) has facilitated construction at relevant length scales.[2, 3] In contrast to top-down techniques, self-assembly provides the possibility of fabricating materials with hierarchical structure,[4, 5] which rely on the interactions of building blocks, such as molecules or particles, that spontaneously assemble into nano-microstructures.[6]

In nature, peptides and proteins interact and self-organize to form well-defined structures that are associated with specific functionality. Based on structure-function relationships displayed by biological molecules, there has been an increased interest in developing self-assembling systems based on peptide molecules. Their small size and facile synthesis, intrinsic bioactivity makes them excellent building blocks for the bottom-up fabrication of hierarchical biomaterials.[7] In fact, peptide-based biomaterials have been investigated in a number of biomedical applications, including scaffolding for tissue repair in regenerative medicine,[8-10] drug delivery[11-13] and biological surface engineering.[14-16]

In attempt to develop self-assembling biomaterials, we have recently found that combining a specific peptide amphiphile (PA) with hyaluronan (HA) resulted in the formation of membranes with a well-defined micro-grooved surface. These hierarchical structures were spontaneously formed without the use of any physical template (unpublished data). The specific PA used in this study differs from the ones previously used[17] by the insertion of an octapeptide between the β-sheet forming domain and the charged block.

Amino acid substitutions are closely related with key changes in protein structure and function.[18] A single amino acid mutation has been shown to be enough to trigger the conformational switch between two different conformations of a protein.[19] Site-directed mutagenesis of protein amino acids has been broadly used to predict the effects of specific amino acid residues on protein function.[18] The same approach has been applied for the redesign of natural peptides to develop structures with enhanced stability and increased biological activity.[20] Site-directed mutagenesis of amino acid residues on peptides, combined with developments on peptide synthesis techniques, offer a great platform for the *de novo* and rational design of peptides with improved properties.

Here, we report a strategy to generate hierarchical self-assembled membranes exhibiting different surface micro-topographies through site-directed mutagenesis of amino acid residues in peptide amphiphiles. The strategy is very versatile, generating various types of hierarchical patterns, most

notably the formation of micro-grooves. This work demonstrates the possibility of controlling membrane surface topography through rational design of peptide structures. By combining specific sequences in PA structures, biomaterials, integrating both physical and biochemical cues, can be easily fabricated for studying how these cues can influence the behavior and function of different cell types.

2. Materials and methods

Peptide amphiphiles: synthesis and purification

The peptides used in this work were synthesized on a CS Bio 136XT automated peptide synthesizer (CS Bio, USA) using standard 9-fluorenylmethoxycarbonyl (Fmoc) based solid phase chemistry on a 4-methylbenzhydrylamine (MBHA) rink amide resin. Amino acid couplings were performed using 4 equivalents (4 mmol) of Fmoc protected amino acids (Novabiochem®, USA), 4 equivalents of O-(Benzotriazol-1-yl)-N,N,N′,N′-tetramethyluronium hexafluorophosphate (HBTU, Carbosynth, UK) and 6 equivalents of N,N-diisopropylethylamine (DIEA, Sigma, USA). Fmoc deprotections were performed with 20% piperidine (Sigma, USA) in dimethylformamide. A palmitic acid ($C_{16}H_{32}O_2$, Calbiochem, USA) tail was manually coupled under the same conditions as the Fmoc-amino acids. Peptide cleavage from the resin and removal of the protecting groups was carried out on a mixture of trifluoroacetic acid (TFA, Sigma, USA)/triisopropylsilane (TIS, Alfa Aesar)/water (95/2.5/2.5)) for 3 h at room temperature. The peptide mixture was collected and excess of TFA was removed by rotary evaporation. The resulting viscous peptide solution was triturated with cold diethyl ether and the white precipitate was collected by filtration, washed with cold ether, and allowed to dry under vacuum overnight. The peptide mass was confirmed by electrospray ionization mass spectrometry (ESI-MS, Agilent, USA).

Peptides were then purified on a Waters 2545 Binary Gradient high-performance liquid chromatography (HPLC) system using a preparative reverse-phase C18 column (Atlantis Prep OBD T3 Column, Waters) and a water/acetonitrile (0.1% TFA) gradient. TFA counter-ions were exchanged by sublimation from 0.01 M hydrochloric acid. Finally, the peptides were dialyzed against ultrapure water using 500 MWCO dialysis tubing (Spectrum labs, The Netherlands), lyophilized and stored at -20 °C until further use. Confirmation of mass and purity was done by ESI-MS and HPLC.

Peptide amphiphiles characterization

Transmission electron microscopy (TEM)

Peptides were dissolved in ultrapure water (0.1 wt%) and the solution was aged for 2 days before TEM analysis. Peptide solutions were loaded on carbon-coated copper TEM grid (Electron Microscopy

Sciences, USA). For negative staining a drop of 2 wt% uranyl acetate (Electron Microscopy Sciences, USA) aqueous solution was placed on the samples. The excess solution was wiped away by a piece of filter paper, and the sample was allowed to dry under ambient conditions. All images were collected with a Tecnai 12 TWIN, equipped with SIS Megaview III camera (FEI, USA).

Circular dichroism (CD) spectroscopy

Peptides were dissolved in deionized water to a final concentration of 0.011 mM and the pH was adjusted to 3, 7 and 9 with hydrochloric acid (0.1 M) or ammonium hydroxide (0.1 M). The CD measurements were performed in a PiStar-180 spectrometer from Applied Photophysics (Surrey, UK), under a constant flow of nitrogen (8 $L.min^{-1}$) at a constant pressure value of 0.7 MPa. Far-UV spectra were recorded at 25 °C from 190 to 300 nm in a quartz cuvette with 1 mm path-length. All scans were performed in the steady state with a bandwidth of 1 nm and each represented spectrum is an average of 5 spectra. The molar ellipticity [θ] was calculated using the following equation:

$$[\theta] = \frac{\theta}{c.l} \qquad (1)$$

were θ is the measured ellipticity in mdeg, c is the concentration of the peptide in dmol L^{-1} and l is the light path length of the cuvette in cm.

Self-assembly of HA with synthesized PAs to prepare membranes

Membranes were formed by self-assembly between HA (1.5 MDa average molar mass, Lifecore Biomedical, Inc, Chaska, USA) and positively charged PAs at optimized conditions as previously reported.[11] Briefly, 50 µL of a 1% (w/v) HA solution was cast on the bottom of the wells of a 96 well plate and then 50 µL of PA (0.017 M) solution was added on top of the HA solution. The membrane was allowed to age for 24 hours and rinsed with sterile ultrapure water to ensure the removal of unreacted HA and PA.

Membrane characterization

Scanning electron microscopy (SEM)

The microstructure of the membranes was analyzed by SEM. Samples were fixed in 2% glutaraldehyde/3% sucrose in PBS for 1 h at 4 °C followed by sequential dehydration in graded ethanol concentrations (from 20 to 100%). To remove ethanol, samples were dried in a critical point dryer (Tousimis Autosandri®-815 series A, USA). Prior observation, the samples were coated with a

gold/palladium layer and imaged using an ultra-high resolution field emission gun scanning electron microscope (Nova™ NanoSEM 200) from FEI (Eindhoven, The Netherlands).

Table VI.1 Chemical structure of PAs used in this study.

Peptide	Mutation	Peptide structure	Observations
PA1	-	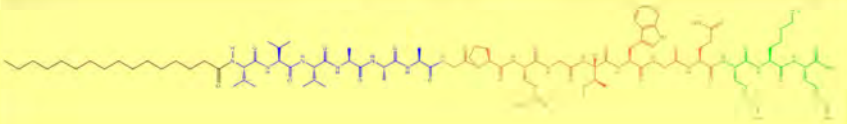	Control
PA2	P→G	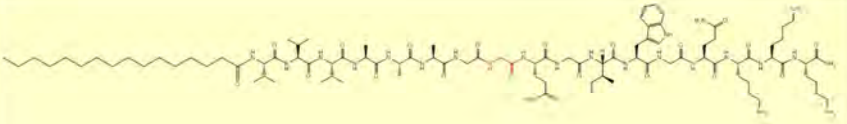	Mutation of single amino acid by glycine
PA3	Q→G	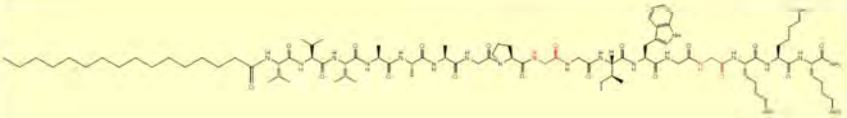	Double mutation of amino acids by glicine
PA4	I→G	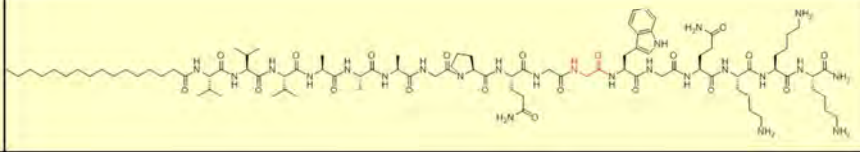	Mutation of single amino acid by glycine
PA5	W→G	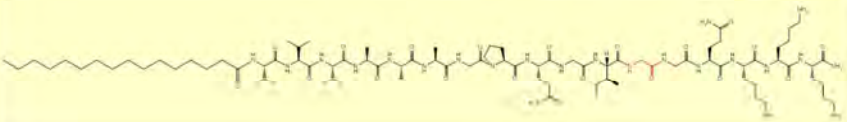	
PA6	G_8	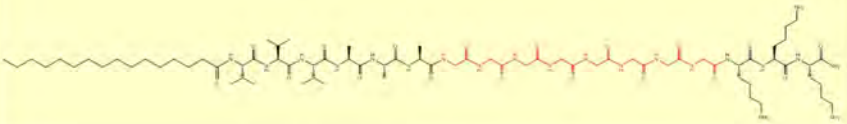	Full mutation of amino acids by glycine
PA7	G_4IG_3	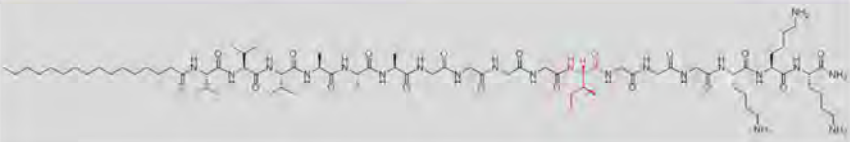	Position of the isoleucine octapeptide
PA8	G_2IG_5	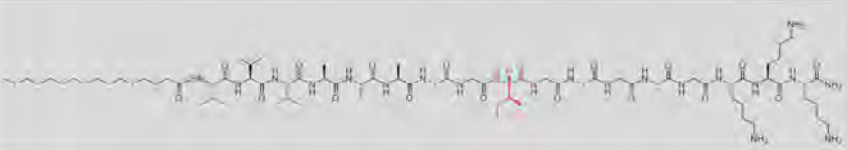	
PA9	GIG_6		

3. Results and discussion

3.1. PAs chemical structure

The molecules used in this study are self-assembling peptide amphiphiles (PAs) consisting in a peptide segment coupled to a palmitic acid ($C_{16}H_{32}O_2$) hydrophobic tail.[12] The peptide segment includes a β-sheet forming sequence and charged amino acids for water solubility and electrostatic screening. In aqueous solution, PAs tend to self-assemble into cylindrical nanofibers as a result of the combined effects of intermolecular hydrogen bonding among the peptide segments and the hydrophobic collapse of the alkyl tails.[13]

Table VI.1 (cont.) Chemical structure of PAs used in this study.

Peptide	Mutation	Peptide structure	Observations
PA10	G_3IG_3	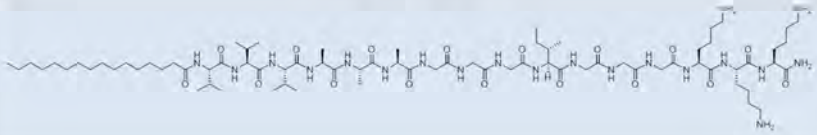	Number of Gly residues flanking the central Ile
PA11	G_2IG_2	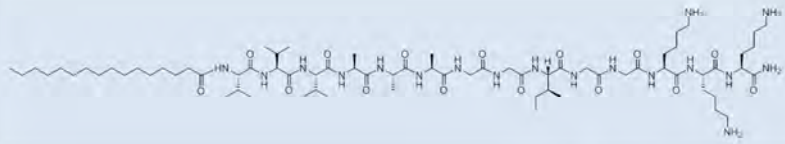	
PA12	GIG	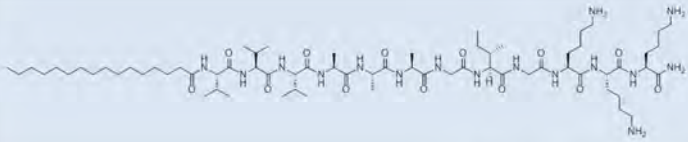	
PA13	IK_3	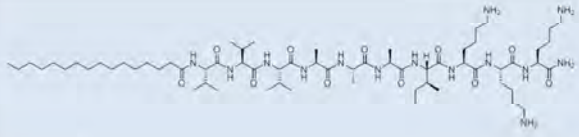	
PA14	G_2LG_5	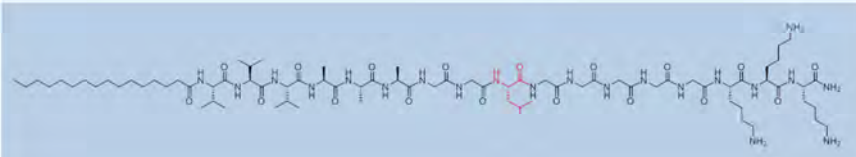	Mutation of isoleucine by leucine
PA15	GLG_6	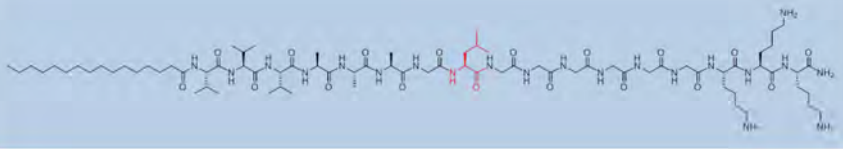	
PA16	w/ β-sheet	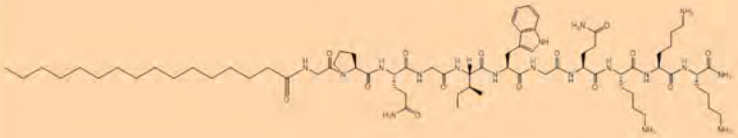	Deletion of β-sheet domain

The ability of these peptides to self-assemble with hyaluronan (HA, a negatively charged polysaccharide) and form membranes has been explored by our group.[11] In addition, we have previously reported that the insertion of the octapeptide Gly-Pro-Gln-Gly-Ile-Trp-Gly-Gln in the PA structure, between the β-sheet sequence and the charged block (Table 1, PA1) induced the formation of patterns with micro-scale periodic ridges on self-assembled membranes (Figure VI.2) when combined with HA solution (unpublished data). Therefore, in this work we have designed a set of PAs that include in their structure, in addition to an alkyl tail of 16 carbons (palmitic acid, brown), a β-sheet forming sequence (V_3A_3, blue), a central domain containing eight amino acids (octapeptide, orange) and a positively charged block containing three lysine (K_3, green) residues (Table 1, PA1-PA9, PA14, PA15) to bind the anionic polymer hyaluronan (HA). Some PAs have less than eight amino acids in the central domain of the peptide sequence (PA10-PA14) or lack the β-sheet domain (PA16) but maintaining the octapeptide sequence of the control PA (PA1).

To get insights on the formation of the previously observed micro-patterns on self-assembled PA-HA membranes, the amino acid sequence of the octapeptide was subjected to site-directed mutations.

3.2 Effect of site directed mutation of the central domain (octapeptide) on PA self-assembly and formation of defined micro-patterns on self-assembled membranes

Single and complete mutation of the octapeptide amino acids by glycine (Gly)

First, PAs were synthesized by replacing a single amino acid in the octapeptide by Gly (G) (X⟶G; PA2: P⟶G; PA3: Q⟶G; PA5: W⟶G). Glycine was chosen due to its minimal size and side chain of only one hydrogen atom.

Transmission electron microscopy (TEM) on these PAs showed the formation of nanofibers with different lengths and diameters, depending on the amino acid composition (Figure VI.1A). PA4 and PA5 form longer fibers, when compared with PA1, PA2, PA3, with chemical structure differing only in one amino acid. PA4 and PA5 represent mutations of Ile (I) and Trp (W) hydrobhobic amino acids. This may indicate that the presence of these amino acids in the PA structure (PA1, PA2, PA3) may disturb the PA self-assembly (less stable PA assemblies) not allowing their growth. TEM of PA6 shows the formation thicker and shorter nanofibers with distinct morphology, resembling open bamboo canes.

Previous studies have shown that the formation of a stable β-sheet is very important and necessary for peptide self-assembly.[14] Pashuck et al. have shown that when β-sheet forming hydrophobic amino acids are included in the molecular design of PAs, the cylindrical shape of the nanofibers is remarkably

tolerant to the choice of the peptide sequence.[15] Changing the number and position of weak and strong β-sheet forming amino acids roughly maintained the overall dimensions of PA molecules, allowing studying the importance of length and sequence in the β-sheet region. Therefore, circular dichroism (CD) spectroscopy was performed to evaluate the secondary structure of the PAs (Figure VI.1B). The CD analysis of the PAs revealed the presence of β-sheet secondary structure for all the PAs, except for PA6 (G_8). For PA1-PA5, a typical spectrum of a β-sheet structure was observed for all studied pHs, with a minimum in the 210-230 nm range, a crossover from positive to negative above 210 nm, and a positive ellipticity around 200 nm, demonstrating that the replacement of a single amino acid by Gly does not affect dramatically the β-sheet conformation. Because Gly has no chiral center, the expected CD signal arising from this amino acid would be relatively weak compared to the other amino acids in the octapeptide. Besides proline, which is a β-sheet blocker, the other amino acids in the octapeptide have a strong propensity to form β-sheets.[16] These properties might explain why when one of these amino acids was mutated and replaced by a glycine, the PAs formed β-sheet secondary structure. Interestingly, PAs (PA4, PA5) exhibiting longer fibers (Figure VI.1A) also present a strong CD signal and β-sheet structure in a broad pH range. PA6 shows a random coil conformation in all the studied pH conditions (Figure VI.1B).

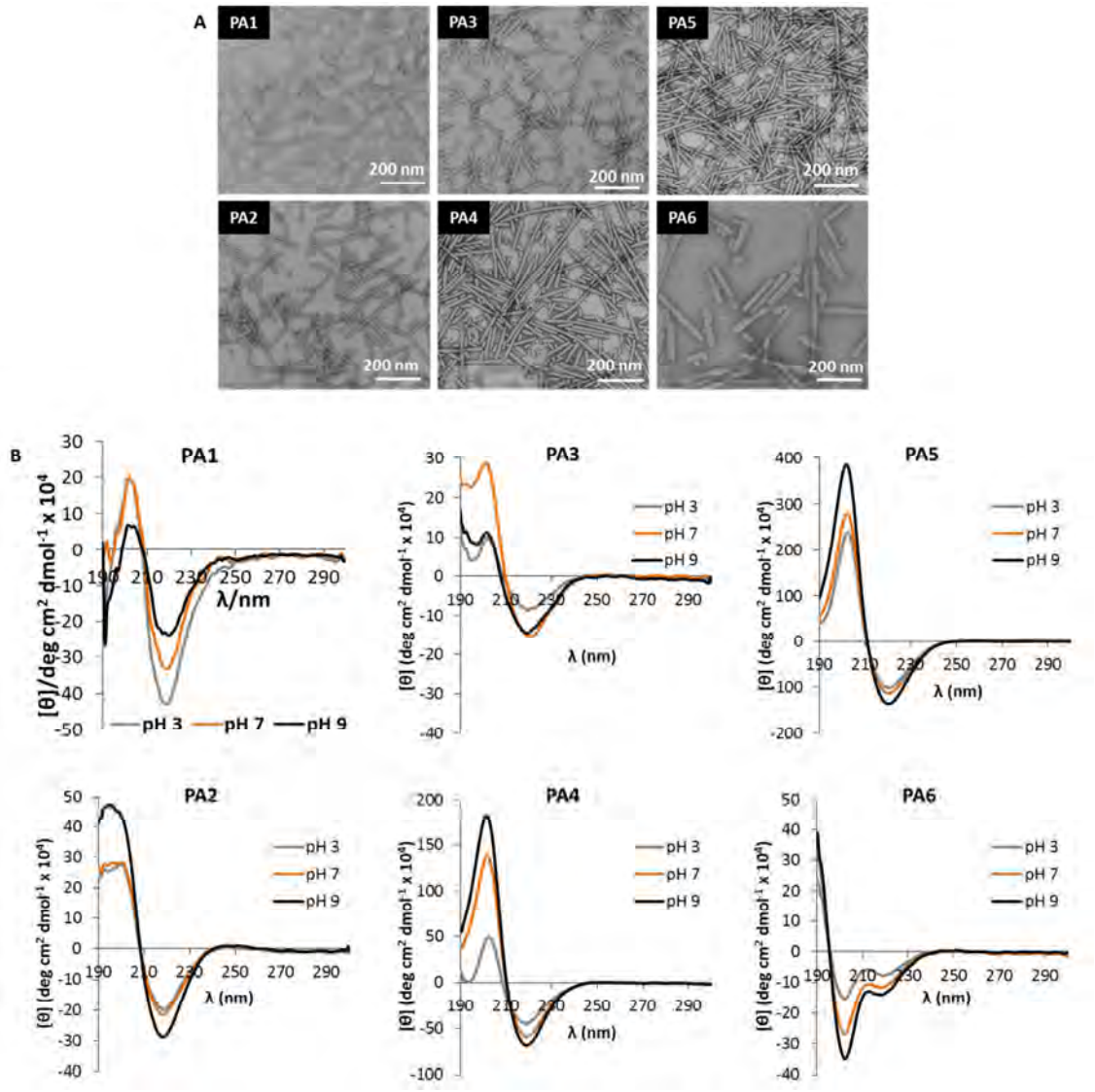

Figure VI.1. Effect of single and complete amino acid mutation of the octapeptide with **Gly (G)** (PA1: control; PA2: **P**→**G**; PA3: **Q**→**G**; PA4: **I**→**G**; PA5: **W**→**G**; PA6: G_8) on PA self-assembly (nanostructure morphology, TEM and secondary structure, CD). (A) TEM images of PA nanostructures negatively stained with uranyl acetate (nanofibers were formed by the deposition of 0.1 wt% solutions in water followed by air drying on a carbon-coated TEM grid). (B) Circular dichroism spectra of PA solutions (0.011 mM) at pH 3, 7, 9.

Analysing the pattern formation on self-assembled membranes using these mutated PA versions (Figure VI.2), patterns are only observed for PA1 (patterned membrane – control), PA2, PA3 and PA5, although the pattern morphology presents slight (PA2, PA5) to major (PA3) variations. Membranes made of PA4 and PA6 were completely flat with a smooth surface and without the presence of visible micro-grooves. These two PAs are lacking the Ile (I) residue in their octapeptide sequence, suggesting that this amino acid may play a critical role on the formation of membranes with micro-grooved patterns. The absence

of patterns on the membrane formed with PA6 also indicate that having a region of eight amino acids inserted between the β-sheet segment and the charged block is not the main driving force for the ridge formation, but the composition of the octapeptide seems to be more important in the generation of micro-grooved patterns.

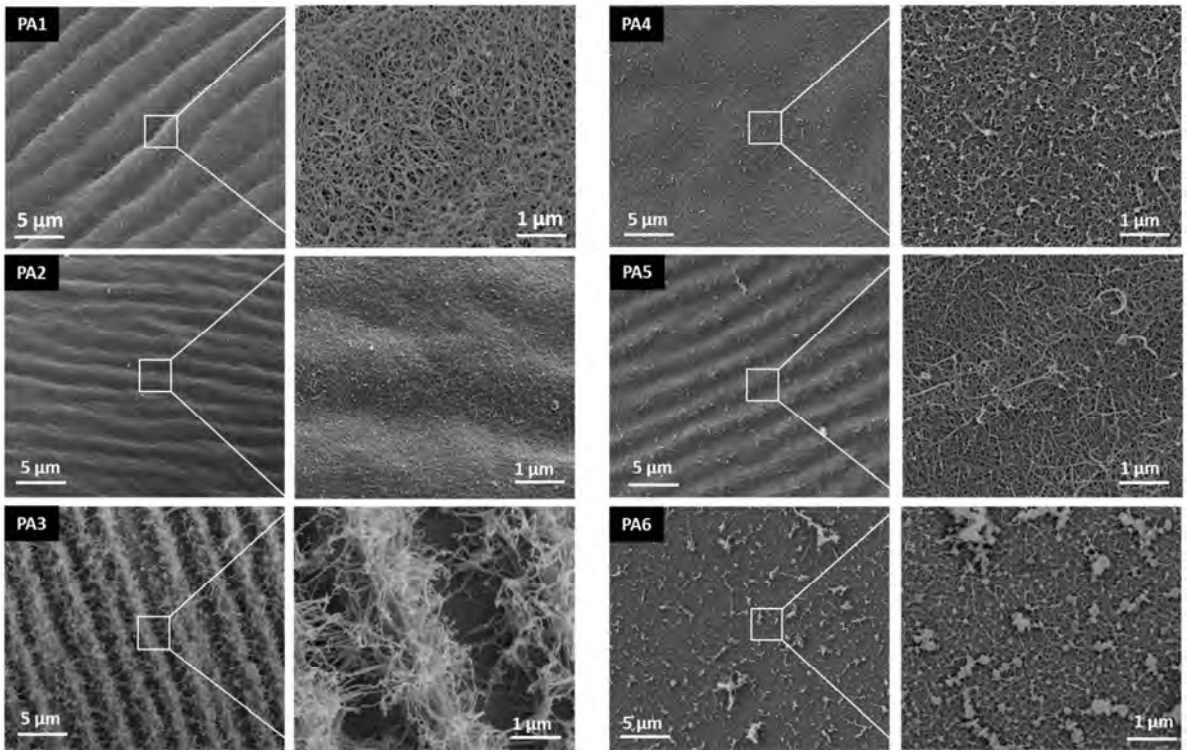

Figure VI.2. SEM images of the top surface of membranes obtained by self-assembly between HA (1 wt%) and PAs (3.4 wt%) having single amino acid mutation in the octapeptide sequence (PA2: P⟶G; PA3: Q⟶G; PA4: I⟶G; PA5: W⟶G) or complete sequence mutation (PA6: G_8) by Gly (PA1: control).

Isoleucine (Ile) position on the octapeptide and length of the glycine (Gly) spacer

Considering the lack of micro-grooves on self-assembled membranes when using PAs lacking the Ile (I) residue (PA4, PA6), we further investigated the importance of the Ile (I) position along the octapeptide sequence (Table 1, PA7-PA9). For that, PAs were synthesized in which all the amino acids, except Ile, were replaced by Gly, to eliminate their influence on PA self-assembly.

TEM analysis showed that all PAs formed nanofibers (Figure VI.3A) but with different diameters. PA8 forms fibers with lower diameter, when compared with PA7 and PA9 fibers. To explore the secondary structure of these PAs, CD studies were performed (Figure VI.3A). The CD spectra revealed that PAs 7 and 8 present higher propensity to form β-sheet structures than PA9, which forms a β-sheet structure only at pH 9, while PA7 and PA8 form at neutral a basic pH. These results suggest that the proximity of

Ile residue to the β-sheet segment and a higher distance from the charged block affects the PA self-assembly when electrostatic repulsion is dominant and the location of Ile towards the middle seems to enhance β-sheet formation.

Micro-grooves (Figure VI.3B) are only observed when Ile is located more centrally in the octapeptide (PA7), having 4 Gly residues before and 3 Gly residues after, indicating that the location of this key amino acid is important for the ridge formation. The other two studied PAs (PA8, PA9) formed membranes with very distinct morphology, showing a very rough surface (Figure VI.3B). Analyzing the surface topography at a higher magnification, the presence of multiple micro-sized aggregates is evident.

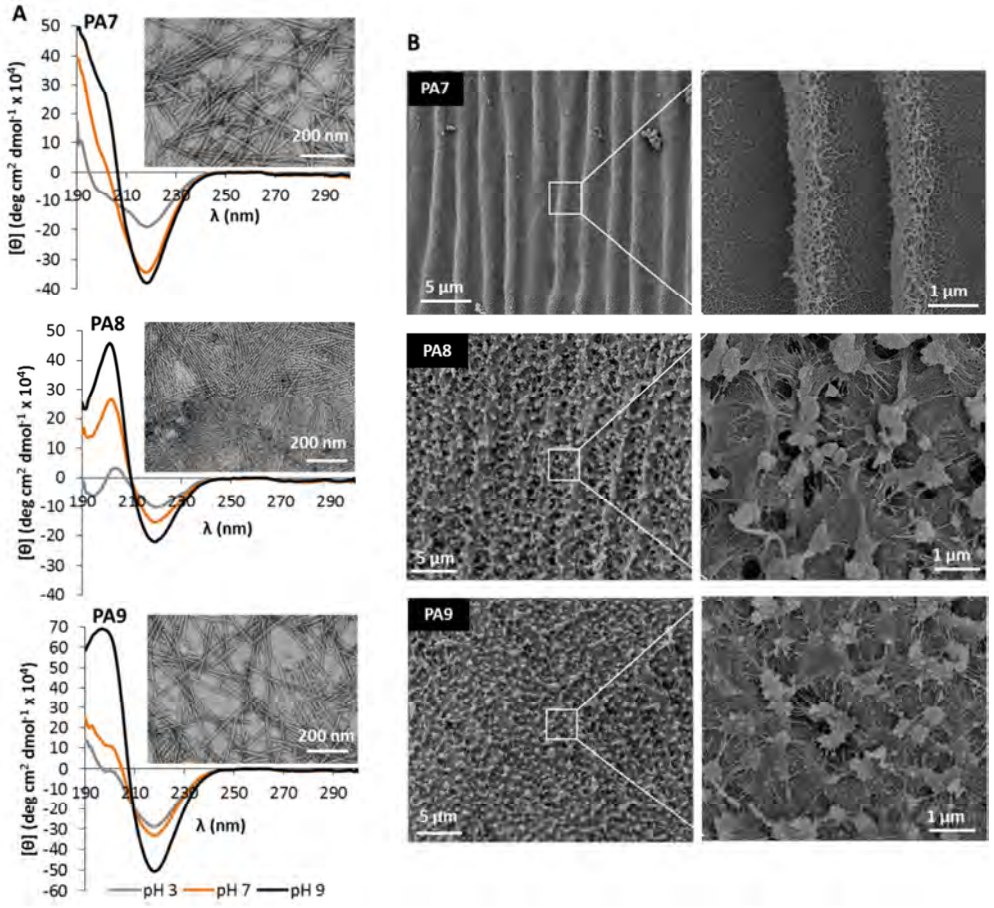

Figure VI.3. Effect of Ile (I) position in the octapeptide domain (PA7: G_4IG_3; PA8: G_2IG_5; PA9: GIG_6) on the PA self-assembly and membrane surface topography. (A) Circular dichroism spectra of PA solutions (0.011 mM) at pH 3, 7, 9 and TEM images of PA nanostructures negatively stained with uranyl acetate (nanofibers were formed by the deposition of 0.1 wt% solutions in water followed by air drying on a carbon-coated TEM grid). (B) SEM images of the top surface of membranes obtained by self-assembly between HA (1 wt%) and the different mutated PA versions (3.4 wt%).

After identifying Ile as key amino acid on the formation of micro-patterned membranes, we next investigated the length of the inserted domain by varying the number of Gly residues, from three to zero, between the Ile residue and the other blocks (Table 1, PA10-PA13). The insertion of Gly residues can infer some flexibility between the β-sheet domain and the charged block.

TEM images show that these PAs tend to form long nanofibers (Figure VI.4A) and they exhibit β-sheet secondary structure in a broad pH range (pH 3-9) as determined by CD analysis (Figure VI.4B).

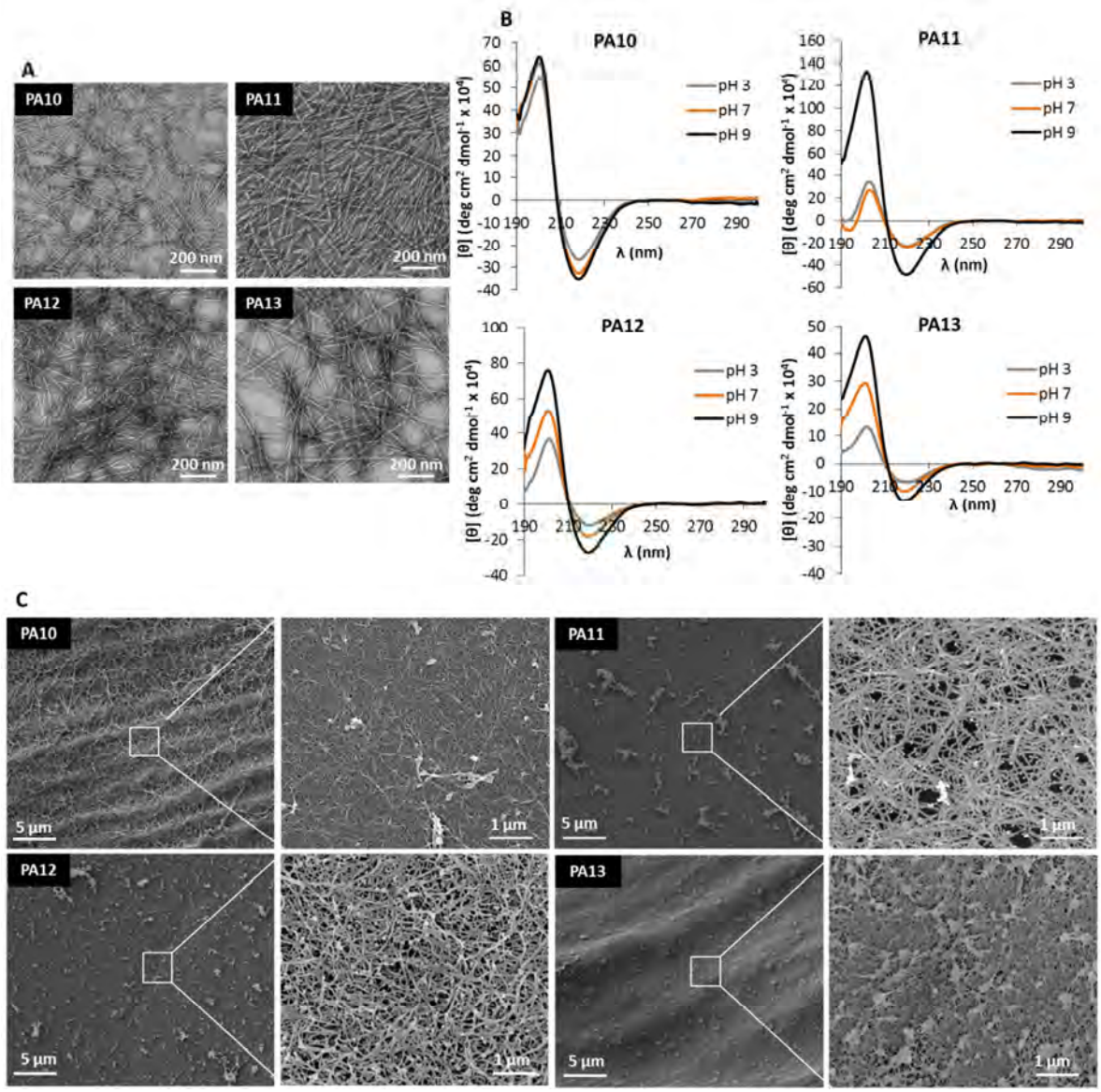

Figure VI.4. Effect of the number of Gly residues (spacer) in the central domain (PA10: G_3IG_3; PA11: G_2IG_2; PA12: GIG; PA13: IK_3) on the PA self-assembly and membrane surface topography. (A) TEM images of PA nanostructures negatively stained with uranyl acetate (nanofibers were formed by the deposition of 0.1 wt% solutions in water followed by air drying on a carbon-coated TEM grid). (B) Circular dichroism spectra of PA solutions (0.011 mM) at pH 3, 7, 9. (C) SEM images of the top surface of membranes obtained by self-assembly between HA (1 wt%) and PAs (3.4 wt%) having different number of Gly residues (0-3) flanking the central Ile.

SEM images of the membranes formed with these PAs revealed membranes with smooth surface without the formation of well-defined patterns (Figure VI.4C), except for PA10 (PA with 3 Gly residues flanking the central Ile residue) that formed membranes with slight micro-grooves. By further decreasing the number of Gly residues, these slight grooves are completely vanished for the membrane surface. These results suggest that the size of the central block also influences the pattern formation and indicate a minimal number of 3-4 Gly residues on each side of a central Ile residue.

Exchange of isoleucine (Ile) for Leucine (Leu)

Isoleucine and leucine are isomeric amino acids, which difference in structure consists on the position of the methyl groups. Due to the similarities between these two amino acids, the ability of Leu (L) to form self-patterned membranes was investigated by replacing Ile (I) in the octapeptide by Leu (I→L). To eliminate the influence of the other amino acids, they were replaced by Gly (Table 1, PA14, PA15).

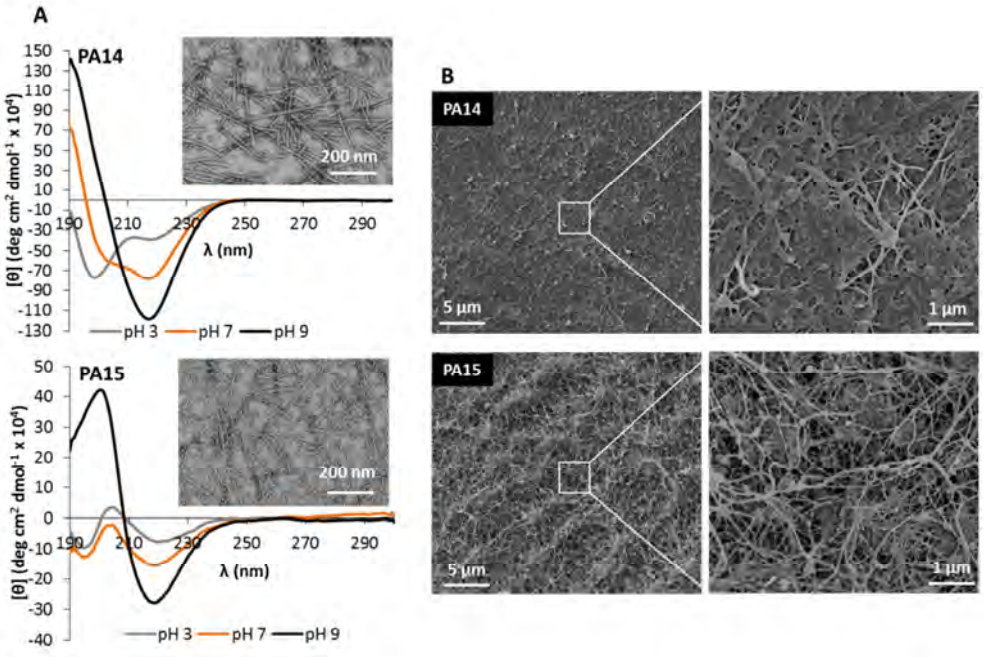

Figure VI.5. Mutation of Ile (I) by its isomer, Leu (**I→L**; PA14: GLG_6; PA15: G_2LG_5). (A) Circular dichroism spectra of PA solutions (0.011 mM) at pH 3, 7, 9 and TEM images of PA nanostructures negatively stained with uranyl acetate (nanofibers were formed by the deposition of 0.1 wt% solutions in water followed by air drying on a carbon-coated TEM grid); (B) SEM images of the top surface of membranes obtained by self-assembly between HA (1 wt%) and mutated PA versions (3.4 wt%).

CD spectra showed significant changes on the secondary structure of the Leu mutated PAs (Figure VI.5A). Like Ile, Leu is a β-sheet promoter, although it also promotes α-helix formation[16] and thus a single mutation could affect the PA overall secondary structure. When Leu was placed in the position 3

of the octapeptide (PA14), the PA no longer formed β-sheet and varied from type I β-turn and random coil (Figure VI.5A). On the other hand, when the mutation occurred in the position 2 of the octapeptide (PA15), the PA was able to form β-sheets at pH 9, but showed type I β-turns at pH 3 and 7. Both PAs form cylindrical nanostructures in the shape of nanofibers, but spherical nanostructures are also observed in the corresponding TEM images (Figure VI.5A).

SEM micrographs of the membranes obtained with PA14 and PA15 (Figure 5B) showed a surface exhibiting nanofibrillar structures, but without evident ridges or grooves and very distinct from the ones observed for similar PAs containing Ile instead of Leu (PA8 and PA9) (Figure VI.3B).

3.2 Effect of the β-sheet segment on PA self-assembly and formation of defined micro-patterns on self-assembled membranes

Previous work on PAs has shown that peptide self-assembly into cylindrical nanofibers and not spherical micelles correlates with a β-sheet signal in CD.[10] All PAs have a β-sheet domain consisting of hydrophobic amino acids (V_3A_3). Valine has the highest propensity of any natural amino acid to form β-sheets and favors forming them over any other secondary structure.[16, 17] Alanine, on the other hand, is a weak β-sheet promoter[17] and has a preference for forming α-helices.[16] Recently, authors have found that this peptide region can be modified to manipulate the shape of their self-assembled nanostructures.[15, 18] Paramonov et al. investigated the role of β-sheet hydrogen bonds and amphiphilic packing in the self-assembly of PAs and found that the disruption of the hydrogen bonds eliminate the ability of a PA to form an elongated, cylindrical nanostructure.[10] To evaluate the effect of the β-sheet region on the PA ability to form nanofibers and interaction with HA, a PA was synthesized without the β-sheet domain (PA16). CD analysis show that PA16 exhibits β-sheet secondary structure only at pH 9, and a random coil at pH 3 and 7 (Figure VI.6A). TEM micrographs show the formation of few nanofibers with 340-380 nm length and also nanofiber with lower length (Figure VI.6B).

When combined with HA, PA16 was able to form very thin membranes. SEM analysis presents membranes with a surface exhibiting a rough topography without the formation of the organized patterns (Figure VI.6C) and without the typical nanofibrillar structure. Membranes were prepared at neutral pH, at which the PA no longer formed β-sheet structures, which can indicate that this domain might have an effect on the nanofiber formation and, consequently, on the self-assembly with HA and pattern formation.

Our preliminary results using site-directed mutation to investigate the effect of amino acid sequence in PAs on the formation of patterned self-assembled membranes suggest that sequence length, presence

of Ile in the sequence at a central position and existence of β-sheet structures are important for the observed patterns. While we have elucidated some key features on the PA structure responsible for the formation of micro-grooved self-assembled membranes, we are certain that further experiments (e.g., synthesis of control peptides, such as octapeptides from PAs in which pattern formation was observed to study their secondary conformation) and complementary techniques are necessary to confirm the postulated hypothesis.

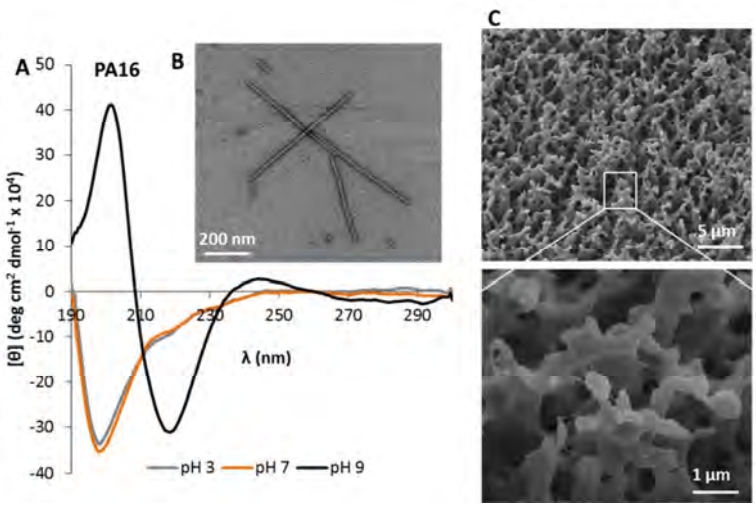

Figure VI.6. Effect of the absence of the β-sheet domain (PA16) on the PA self-assembly and membrane surface topography. (A) Circular dichroism spectra of PA solutions (0.011 mM) at pH 3, 7, 9; (B) TEM images of PA nanostructures negatively stained with uranyl acetate (nanofibers were formed by the deposition of 0.1 wt% solutions in water followed by air drying on a carbon-coated TEM grid). (C) SEM images of the top surface of membrane obtained by self-assembly between HA (1 wt%) and the PA16 (3.4 wt%).

4. Conclusions

Using site-directed mutation on peptide amphiphiles (PAs), a series of modified sequences were prepared to probe the effect of sequence composition and length on their self-assembly behavior and corresponding surface morphology of membranes formed upon their self-assembly with hyaluronan (HA). Membranes with very distinct surface morphologies, from well-defined micro-grooves to micro-sized aggregates, were obtained by simply manipulating the PA structure. This represents an enormous opportunity to manipulate the surface topography of self-assembling membranes by using the 20 amino acids available in nature. It would be now interesting to investigate how different cells would respond to the surface micro- nanotopography of these membranes to assess their potential to control cell adhesion, growth and differentiation and possible applications in regenerative medicine.

References

1. C. Sanchez, H. Arribart and M. M. Giraud Guille, Biomimetism and bioinspiration as tools for the design of innovative materials and systems, *Nat Mater*, 2005, 4, 277-288.

2. B. D. Gates, Q. Xu, M. Stewart, D. Ryan, C. G. Willson and G. M. Whitesides, New Approaches to Nanofabrication: Molding, Printing, and Other Techniques, *Chemical Reviews*, 2005, 105, 1171-1196.
3. G. M. Whitesides, E. Ostuni, S. Takayama, X. Jiang and D. E. Ingber, Soft lithography in biology and biochemistry, *Annu Rev Biomed Eng*, 2001, 3, 335-373.
4. G. Whitesides, J. Mathias and C. Seto, Molecular self-assembly and nanochemistry: a chemical strategy for the synthesis of nanostructures, *Science*, 1991, 254, 1312-1319.
5. M. Geissler and Y. Xia, Patterning: Principles and Some New Developments, *Advanced Materials*, 2004, 16, 1249-1269.
6. S. Zhang, Fabrication of novel biomaterials through molecular self-assembly, *Nat Biotech*, 2003, 21, 1171-1178.
7. Y.-C. Yu, P. Berndt, M. Tirrell and G. B. Fields, Self-Assembling Amphiphiles for Construction of Protein Molecular Architecture, *Journal of the American Chemical Society*, 1996, 118, 12515-12520.
8. S. Maude, E. Ingham and A. Aggeli, Biomimetic self-assembling peptides as scaffolds for soft tissue engineering, *Nanomedicine (Lond)*, 2013, 8, 823-847.
9. M. J. Webber, J. A. Kessler and S. I. Stupp, Emerging peptide nanomedicine to regenerate tissues and organs, *J. Intern. Med.*, 2010, 267, 71-88.
10. H. Hosseinkhani, P. D. Hong and D. S. Yu, Self-Assembled Proteins and Peptides for Regenerative Medicine, *Chemical Reviews*, 2013, 113, 4837-4861.
11. S. Koutsopoulos, L. D. Unsworth, Y. Nagaia and S. G. Zhang, Controlled release of functional proteins through designer self-assembling peptide nanofiber hydrogel scaffold, *Proc. Natl. Acad. Sci. U. S. A.*, 2009, 106, 4623-4628.
12. L. H. Liu, K. J. Xu, H. Y. Wang, P. K. J. Tan, W. M. Fan, S. S. Venkatraman, L. J. Li and Y. Y. Yang, Self-assembled cationic peptide nanoparticles as an efficient antimicrobial agent, *Nat. Nanotechnol.*, 2009, 4, 457-463.

13. S. Y. Fung, H. Yang, P. T. Bhola, P. Sadatmousavi, E. Muzar, M. Liu and P. Chen, Self-Assembling Peptide as a Potential Carrier for Hydrophobic Anticancer Drug Ellipticine: Complexation, Release and In Vitro Delivery, *Advanced Functional Materials*, 2009, 19, 74-83.
14. K. H. Schmedlen, K. S. Masters and J. L. West, Photocrosslinkable polyvinyl alcohol hydrogels that can be modified with cell adhesion peptides for use in tissue engineering, *Biomaterials*, 2002, 23, 4325-4332.
15. B. K. Mann, A. T. Tsai, T. Scott-Burden and J. L. West, Modification of surfaces with cell adhesion peptides alters extracellular matrix deposition, *Biomaterials*, 1999, 20, 2281-2286.
16. S. P. Massia and J. Stark, Immobilized RGD peptides on surface-grafted dextran promote biospecific cell attachment, *J. Biomed. Mater. Res.*, 2001, 56, 390-399.
17. D. S. Ferreira, A. P. Marques, R. L. Reis and H. S. Azevedo, Hyaluronan and self-assembling peptides as building blocks to reconstruct the extracellular environment in skin tissue, *Biomaterials Science*, 2013, 1, 952-964.
18. P. C. Ng and S. Henikoff, Predicting the Effects of Amino Acid Substitutions on Protein Function, *Annual Review of Genomics and Human Genetics*, 2006, 7, 61-80.
19. P. A. Alexander, Y. He, Y. Chen, J. Orban and P. N. Bryan, A minimal sequence code for switching protein structure and function, *Proceedings of the National Academy of Sciences*, 2009, 106, 21149-21154.
20. M. Lakshmanan and A. Dhathathreyan, Amphiphilic laminin peptides at air/water interface—Effect of single amino acid mutations on surface properties, *Journal of Colloid and Interface Science*, 2006, 302, 95-102.
21. Y. S. Velichko, S. I. Stupp and M. O. de la Cruz, Molecular Simulation Study of Peptide Amphiphile Self-Assembly, *The Journal of Physical Chemistry B*, 2008, 112, 2326-2334.
22. D. W. P. M. Lowik and J. C. M. van Hest, Peptide based amphiphiles, *Chemical Society Reviews*, 2004, 33, 234-245.
23. E. T. Pashuck, H. Cui and S. I. Stupp, Tuning Supramolecular Rigidity of Peptide Fibers through Molecular Structure, *Journal of the American Chemical Society*, 2010, 132, 6041-6046.
24. M. Levitt, Conformational preferences of amino acids in globular proteins, *Biochemistry*, 1978, 17, 4277-4285.
25. S. E. Paramonov, H.-W. Jun and J. D. Hartgerink, Self-Assembly of Peptide–Amphiphile Nanofibers: The Roles of Hydrogen Bonding and Amphiphilic Packing, *Journal of the American Chemical Society*, 2006, 128, 7291-7298.

26. C. A. Kim and J. M. Berg, Thermodynamic [beta] -sheet propensities measured using a zinc-finger host peptide, *Nature*, 1993, 362, 267-270.

27. H. Cui, A. G. Cheetham, E. T. Pashuck and S. I. Stupp, Amino Acid Sequence in Constitutionally Isomeric Tetrapeptide Amphiphiles Dictates Architecture of One-Dimensional Nanostructures, *Journal of the American Chemical Society*, 2014.

.

Chapter VII

Peptide-based microcapsules obtained by self-assembly and microfluidics as controlled environments for cell culture

Chapter VII*

Peptide-based microcapsules obtained by self-assembly and microfluidics as controlled environments for cell culture

Abstract

Peptides are excellent building blocks to form precise nanostructures by self-assembly. They can self-assemble into fibril nanostructures, thus recreating some of the architectural features of the natural extracellular matrix. Here, we used a microfluidic approach to drive the self-assembly of peptides of opposite charge into capsular structures for cell encapsulation. The obtained capsules presented a core shell structure made of a network of nanofibers and their properties can be tuned by varying the concentration of each peptide. Capsules were found to be stable in aqueous solutions and their permeability dependent on the capsule composition. Human dermal fibroblasts were encapsulated and remained viable within the capsules and their morphology was shown to be influenced by the matrix density. Additionally, these capsules also supported the co-culture of fibroblasts and keratinocytes. We expect that the developed peptide-based microcapsules can serve as miniaturized environments for cell culture and as biomimetic platforms for in vitro drug screening.

* This chapter is based on the following publication:

Daniela S. Ferreira, Rui L. Reis, Helena S. Azevedo, Peptide-based microcapsules obtained by self-assembly and microfluidics as controlled environments for cell culture, Soft Matter, 9: 9237-9248, 2013

1. Introduction

Molecular self-assembly, the spontaneous organization of molecules into ordered aggregates by noncovalent interactions, is becoming increasingly important in the development of new biomaterials because it offers a great platform for constructing materials with high level of precision and complexity.[1, 2] Although bulk self-assembly of small molecules frequently yields structures that exhibit a high degree of order on the nanometer scale, they exhibit more disordered morphologies at the micrometer scale. However, recent research has demonstrated the feasibility of using electrostatic interactions between small molecules and high molecular weight polymers to drive their assembly into larger assemblies that can extend over multiple length scales.[3] On the other hand, directed self-assembly (DSA) has emerged as strategy to control order in materials across scales by tuning the directionally of self-assembly interactions at the nanoscale.[4] In DSA the positions of self-assembling building blocks are guided by an external input to introduce hierarchical organization in supramolecular materials. Examples of external inputs include mechanical forces, such as shear effects[5], magnetic[6] and electric[7] fields, thermal gradients[8] and chemically[9] or topographically[10] patterned substrates. Although the concept of DSA still remains ambiguous, templated self-assembly (TSA) can be considered as a kind of DSA, in which a prefabricated ''template'' orients and directs the assembling components.[11] Another approach towards DSA is the use of geometric confinement to orient bulk structures or to induce the formation of novel morphologies not found in bulk systems. For example, microfluidics has been used to guide the self-assembly of block copolymers,[12] and in the synthesis of liposomes[13] and microcapsules,[14] thus providing additional control over the size and shape of self-assembled structures.

It is widely understood that in order to encapsulate living cells within an artificial matrix, the encapsulating conditions must not damage the cells and the matrix material must be biocompatible and at the same time provide a natural microenvironment for the cells to sustain their viability, function and growth. The mechanical strength of the encapsulating matrix is also critical for maintaining the matrix integrity and to withstand manipulations associated with *in vitro* culture. Moreover, it is essential that the matrix should have suitable diffusion properties to ensure sufficient access of nutrients, for encapsulated cells to remain viable and functional, and the removal of secreted metabolic waste products. Thus, there is a need for relatively mild cell encapsulation methods, which offers control over properties of the encapsulating matrix. An exciting approach for cell encapsulation is the use of materials that can undergo gelation in cell-compatible conditions. Hydrogels are appealing for cell encapsulation because they are highly hydrated three-dimensional networks that provide an environment for cells to adhere, proliferate, and differentiate and they can often be processed under

relatively mild conditions. Gelation can occur through a change in temperature, or via chemical crosslinking, ionic crosslinking, or formation of an insoluble complex.[15]

Self-assembling materials, not depending on covalent chemistry, enable the direct cell encapsulation under mild conditions. Within self-assembled nanomaterials, peptide nanostructures can present varied geometries (e.g. micelles, nanofibers, vesicles)[16, 17] and chemical diversity for biological recognition. Peptides are, therefore, excellent structural units to form complex nanostructures that can recreate some of the architectural features and functionalities of the natural extracellular matrix (ECM).

Previous work from the Stupp lab demonstrated the self-assembly of peptide-amphiphile (PA) molecules of opposite charges into nanofibers by electrostatic attraction at neutral pH.[18] Mixing solutions of oppositely charged PAs resulted in nanofiber formation and at certain concentration transformed into a 3D gel. Ionic interactions between positively charged and negatively charged moieties within the peptides has been explored as a self-assembly mode.[19-21]

Cell microencapsulation is a technology with enormous clinical potential for the production of biologically important therapeutics and the treatment of a wide range of diseases.[22] The encapsulation of cells in microscopic gel capsules can also be used for exploratory purposes in biology, to study the role of specific microenvironments on cell fate, create cell arrays for single-cell bioassays and for drug screening.[23] To optimize the performance of microgel capsules, it is crucial to control size, shape and the content of encapsulated additives. The use of emulsion droplet as templates for microgel synthesis has been widely explored.[23-25] The principle of this technique is to use micrometer-scale channels to carry a solution of a microgel precursor. The stream of the precursor solution can be broken up by flow focusing with continuous phase of an immiscible fluid, normally an oil phase. When these two fluids meet, droplets are formed, drop-by-drop, due to the interfacial tension and the shear of the continuous phase. By varying the microchannel geometry, the flow rates and viscosities of the fluids, monodisperse droplets with controlled size can be generated. The subsequent droplet gelation allows retaining their morphology. Thus, the main goal of the present study was to produce soft peptide microgel capsules with controlled properties for cell encapsulation and culture. Towards this goal, we used droplet-based microfluidics to guide the electrostatic self-assembly of peptides of opposite charge and generate capsules with controlled spherical shape and monodisperse size. The structure and properties of the obtained peptide capsules are described, as well as their application as 3D matrix for conducting different cell culture studies (e.g. cell-matrix interactions, co-culture).

2. Materials and methods

Peptide synthesis and purification

Two peptide amphiphiles (PAs) with opposite charge were synthesized in this work, consisting of a peptide segment covalently linked to a 16-carbon alkyl chain: C_{16}-$V_3A_3K_3$ (K_3-PA) and C_{16}-$V_3A_3E_3$ (E_3-PA) (Fig. VII.1). The peptides were synthesized on a CS Bio 136XT automated peptide synthesizer (CS Bio, USA) using standard 9-fluorenylmethoxycarbonyl (Fmoc) based solid phase chemistry. K_3-PA was synthesized on a 4-methylbenzhydrylamine (MBHA) rink amide resin (Novabiochem, Germany) and E_3-PA on a 4-benzyloxybenzylamine Wang resin pre-loaded with the first glutamic acid (Fmoc-Glu(OtBu)-Wang resin). Amino acid couplings were performed using 4 equivalents (4 mmol) of Fmoc protected amino acids (Novabiochem, Germany), 4 equivalents of O-(Benzotriazol-1-yl)-N,N,N′,N′-tetramethyluronium hexafluorophosphate (HBTU, Novabiochem®) and 6 equivalents of N,N-diisopropylethylamine (DIEA, Sigma, USA). Fmoc deprotections were performed with 20% piperidine (Sigma, USA) in dimethylformamide. A palmitic acid ($C_{16}H_{32}O_2$, Calbiochem, Germany) tail was manually coupled under the same conditions as the Fmoc-amino acids. Peptide cleavage from the resin and removal of the protecting groups was carried out on a mixture of trifluoroacetic acid (TFA, Sigma, USA)/triisopropylsilane (TIS, Alfa Aesar)/water (95/2.5/2.5)) for 3 h at room temperature. The peptide mixture was collected and excess of TFA was removed by rotary evaporation. The resulting viscous peptide solution was triturated with cold diethyl ether and the white precipitate was collected by filtration, washed with cold ether, and allowed to dry under vacuum overnight. The peptide mass was confirmed by matrix assisted laser desorption/ionization mass spectrometry (MALDI-MS, 4800 MALDI-TOF/TOF, AbSciex). Peptides were then purified on a Waters 2545 Binary Gradient high-performance liquid chromatography (HPLC) system using preparative reverse-phase C_{18} columns. K_3-PA was purified on an Atlantis Prep OBD T3 column (Waters) with a water/acetonitrile (0.1% TFA) gradient and E_3-PA on a Xbridge column (Waters) with a water/acetonitrile (0.1% NH_4) gradient. For K_3-PA, TFA counter-ions were exchanged by sublimation from 0.01 M hydrochloric acid. Finally, the peptides were dialyzed against ultrapure water using 500 MWCO dialysis tubing (Spectrum labs, The Netherlands), lyophilized and stored at -20 °C until further use. Confirmation of mass and purity was done by MALDI-MS and HPLC (Supplementary Information, Fig. VII.S1-S2). Peptide solutions used in cell culture studies were sterilized by UV exposure for 15 minutes.

Preparation of peptide-based capsules

Capsules were generated using a microfluidic device developed in our lab that allows the production of stable and size-controlled spherical capsules.[26] This system can be conveniently cleaned and sterilized allowing cell encapsulation in a sterile environment, reducing contamination risks during the procedure. A solution of E_3-PA (1 wt%) in 0.15 M NaCl was first and injected into one of the microchannels of the microfluidics device using a syringe pump (Alladdin WPI, England). Simultaneously, mineral oil was provided to the oil microchannel from a reservoir using a low speed peristaltic pump (Ismatec, Switzerland). The operation rates of the peristaltic and syringe pumps were set at 50 µL/min and 20 µL/min, respectively. The peptide microdroplets were generated inside the microfluidics device by shear stress when the E_3-PA solution in the horizontal microchannel entered into the stream of mineral oil in the larger vertical microchannel (Fig. VII.1A). The formed microdroplets were collected from the outlet tubing in a separate vessel containing 1 mL of K_3-PA solution (0.1, 0.2 and 0.5 wt%) in 0.1 M $CaCl_2$. 10 µL of Tween-80 was added as a surface-active agent to prevent aggregation of the capsules. Capsules were incubated in the K_3-$CaCl_2$ solution for 15 minutes and washed three times with 0.15 M NaCl.

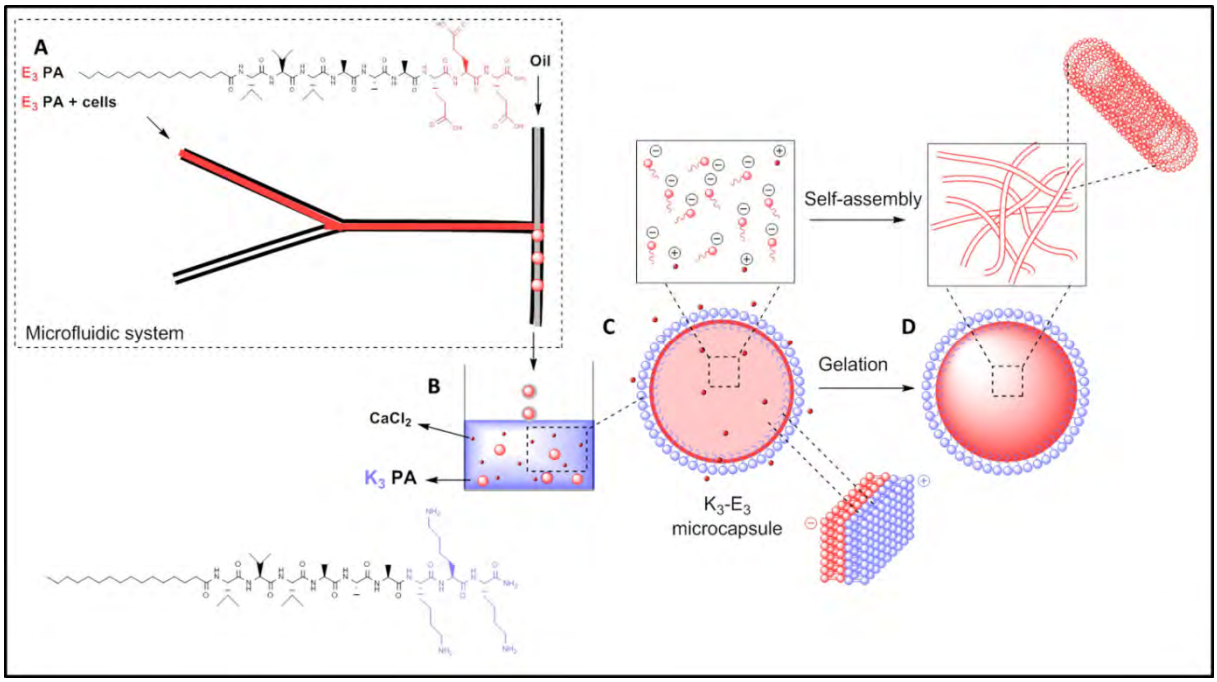

Figure VII.1. Capsule generation by directed self-assembly. Schematic representation of the set-up for capsule generation and cell encapsulation. The E_3-PA microdroplets generated at the T-junction of the microfluidic system (A) were directly extruded into a solution of K_3-PA for electrostatic self-assembly (B). At the droplets interface, self-assembly immediately occurs resulting on the formation of a capsular structure (a wall membrane made of K_3-E_3-PA nanofibers with a liquefied core containing free E_3-PA molecules (C). The K_3-PA solution was supplemented with 0.1 M $CaCl_2$ to induce the gelation of internal E_3-PA (D).

Capsule characterization

Phase contrast microscopy

Microscopic observations of the capsules were carried out to examine their size and shape. Phase contrast micrographs of the capsules were acquired in an inverted microscope (Axio Observer, Zeiss, Germany). The size of the capsules was then estimated by measuring the diameter of individual capsules (n=30).

Scanning electron microscopy (SEM)

The microstructure of the capsules was analyzed by SEM. Samples were fixed in a 2% glutaraldehyde/3% sucrose in PBS for 1 h at 4 °C followed by sequential dehydration in graded ethanol concentrations (from 20 to 100%). To remove ethanol, samples were dried in a Tousimis Autosandri®-815 (series A) critical point dryer. To expose the internal surface of the capsules, they were cut into half with a sharp blade. Prior observation, the samples were coated with a gold/palladium layer and imaged using an ultra-high resolution field emission gun scanning electron microscope (Nova™ NanoSEM 200) from FEI (Eindhoven, The Netherlands).

Swelling

The stability of the capsules in aqueous environment was studied by incubating them in water and PBS. Capsules (n=10/well, in triplicate) prepared with 0.1, 0.2 and 0.5% K_3-PA were distributed in a 24 well plate and 1 mL of ultrapure water or PBS was added to each well. Samples were incubated at 37 °C and at predetermined time points (1, 2, 3 and 7 days) capsules were observed in an inverted microscope (Axio Observer, Zeiss, Germany) and their size was measured using ZEN software (Zeiss, Germany) .

Mechanical stability

To study the mechanical stability of the different capsules, 10 capsules (in triplicate) were placed in 12 well plates containing 2 mL of PBS and 10 glass beads (3 mm diameter, VWR) . The plate was placed in a flat rotator (DSR-2800 V, Digisystem Laboratory Instruments Inc., Taiwan) shaking at about 200 rpm. At predetermined time points (2, 4 6 and 24 h), the number of intact capsules was counted by observation in an inverted microscope (Axio Observer, Zeiss, Germany). The percentage of intact capsules as a function of time was determined by calculating the ratio between the number of intact capsules at each time point and the initial number.

Permeability

The capsule permeability was investigated by using dextran standards of different molecular weights (20, 40 and 155 kDa). For that, FITC- and TRITC-labeled dextrans (Sigma, USA) were encapsulated within the capsules and their release followed along the time. Three different solutions were prepared; each solution was a mixture of 0.5 mg/mL of dextran (20, 40 and 155 kDa) with 1 wt% E_3-PA. The mixture was injected into the microfluidic device and capsules were generated as described before. The capsules were then placed in PBS (pH 7.4) at 37 °C in a water bath with agitation. At specific time intervals, the release medium was completely collected for further analysis and replaced with the same amount of fresh PBS solution. The fluorescence was measured at 485/528 nm (FITC-labeled) and 530/590 nm (TRITC-labeled) on a microplate reader (BIO-TEK, Synergie HT, USA). The concentration of released dextran was measured using a calibration curve using known concentrations of dextran solutions.

Cell culture and encapsulation

Isolation and culture of human dermal fibroblasts and epidermal keratinocytes

Human dermal fibroblasts (hDFb) and epidermal keratinocytes (hKc) were isolated from skin samples discarded from abdominoplasty surgeries of consenting patients at Hospital da Prelada (Porto, Portugal). Briefly, the skin tissue was cut in pieces of 0.5 by 0.5 cm and digested in a dispase solution (2.4 U/mL in PBS) at 4 °C, overnight. After dissociation of the epidermis from the dermis, keratinocytes were isolated by a 5 minute digestion of the epidermis in 0.25% trypsin/EDTA (Invitrogen, UK) at 37 °C to release the cells. Trypsin was inactivated by the addition of the same volume of fetal bovine serum (FBS, Gibco, UK), the digestion products were poured through a 100 µm cell strainer and centrifuged at 200 *g* for 5 minutes. Cell pellet was washed with phosphate buffered saline (PBS, Gibco, UK)) and centrifuged at 200 *g* for 5 minutes. The pellet was resuspended and the cells were subsequently cultured in Keratinocyte Serum Free Medium (KSFM, Gibco, UK) with L-glutamine and keratinocyte-SFM supplement (Gibco, UK), in a 37 °C humidified atmosphere with 5% CO_2. Fibroblasts were isolated from the dermis by overnight digestion of the dermal pieces in a collagenase IA solution (125 U/mL in PBS) at 4 °C. Digestion products were poured through a 100 µm cell strainer and centrifuged at 200 *g* for 5 minutes. The pellet was resuspended and the cells were subsequently cultured in Dulbecco's Modified Eagle Medium (DMEM) (Sigma, Germany) supplemented with 10% FBS (Gibco, UK) and 1% (v/v) antibiotic/antimycotic solution (A/B) (Gibco, UK) containing 100 units/mL penicillin and 100 mg/mL

streptomycin, in a 37 °C humidified atmosphere with 5% CO_2. Cells used in this study were between passage 2 and 4 (hDFb) and passage 1 and 2 (hKc).

Encapsulation and culture of hDFb within capsules

Confluent hDFb were harvested from monolayer cultures using trypsin-EDTA (Invitrogen, USA). Cells were washed in PBS and centrifuged at 200 *g* for 10 minutes to remove calcium residues from the medium. Cell pellet was then resuspended at a density of 1.0 x 10^6 cells/mL in 1 wt% E_3-PA solution. Capsules were generated as described before, using a 0.1 wt% K_3-PA solution supplemented with 0.1 M $CaCl_2$. Capsules were transferred to 24-well plates and cultured up to 14 days in DMEM without phenol red (Sigma) supplemented with 10% FBS (Gibco, UK) and 1% (v/v) A/B (Gibco, UK), in a 37 °C humidified atmosphere with 5% CO_2. Fibroblast morphology and interaction with the artificial matrix were also investigated as a function of matrix composition by varying E_3-PA concentration. Cell pellet was resuspended at a density of 1.0x10^6 cells/mL in E_3-PA solutions (0.5, 1 and 2 wt%) in NaCl. At predetermined time points, samples were collected to assess cell viability (live/dead assay), morphology and spreading (SEM, F-actin and collagen I staining).

Live/Dead staining

Cell viability was assessed through live/dead assay using calcein-AM (Sigma) and propidium iodide (PI, Molecular Probes, Invitrogen, USA) dyes. Calcein-AM is a membrane-permeant dye, which is hydrolyzed by endogenous esterase into the highly negatively charged green fluorescent cell marker calcein retained in the cytoplasm. Propidium iodide is a membrane impermeant, thus binding to DNA of dead cells. At each time point, medium was removed and 1 mL of PBS containing 2 µL of calcein-AM and 1 µL of PI was added to each well. Samples were incubated for 10 minutes at 37 °C protected from light followed by three washes in PBS, and were immediately visualized in a fluorescence microscope (Axioimage RZ1M, Zeiss, Germany).

Staining and confocal microscopy

For examining the morphology of encapsulated hDFbs within the different capsules, staining for collagen I and e F-actin was carried out after fixing cells in 10% formalin solution (Sigma-Aldrich, Germany) for 30 minutes at 4 °C. Cells were then washed once with 0.1 M Glycine in PBS and twice with PBS and permeabilized with 2% BSA/ 0.2% Triton X-100 solution for 1 h at RT. Samples were incubated with primary antibody anti-collagen I (ab292, 1:500, abcam, UK) for 1 h at RT and washed

three times for 2 minutes with PBS. Samples were then incubated with the secondary antibody, anti-mouse Alexa 488 (1:200, Molecular Probes, Invitrogen, USA) for 1 h at RT. In some cases, samples were treated with TRITC-conjugated phalloidin (1 U/mL, Sigma-Aldrich, Germany) for 1 h at RT. Cell nuclei were counterstained with 1 mg/mL DAPI (1:1000, Sigma-Aldrich, Germany) for 1 min and washed with PBS. Visualization was performed by confocal laser scanning microscopy (CLSM,Olympus FluoView 1000, Olympus, Japan). Background was subtracted and images were processed using FV10-ASW 3.1 software (Olympus, Japan).

Cell proliferation

Cell proliferation within the capsules was assessed at different culture times (1, 3, 7 and 14 days) by quantifying the amount of double-stranded DNA (dsDNA). Samples were prepared as described elsewhere[27]. Briefly, capsules were lyophilized and resuspended in phosphate-buffered EDTA (pH 6.5) supplemented with 0.01 M L-cysteine (Sigma, USA) and 0.5% papain (Sigma, USA). Digestion was performed at 60 °C for 24 h. Following this, quantification was performed using the Quant-iT™ PicoGreen® dsDNA Assay Kit (Invitrogen, Molecular Probes, Oregon, USA), according to the instructions of the manufacturer. The fluorescent intensity of the dye was measured in a microplate reader (Synergie HT, Bio-Tek, USA) with excitation at 485/20 nm and emission at 528/20 nm. The DNA concentration for each sample was calculated using a standard curve (DNA concentration ranging from 0 to 1.5 mg/mL) relating quantity of DNA and fluorescence intensity. The fluorescence signals obtained from blank capsules (i.e. without cells, cultured and processed similarly to those with cells) were used as background values (blanks). Triplicates were made for each time point and for each sample (n=10 capsules/sample).

Co-culture studies - seeding of keratinocytes on the surface of the capsules with encapsulated fibroblasts

To validate our peptide capsules for co-culture studies, hDFb and hKc were co-cultured within and on the capsule surface, respectively. Encapsulation of hDFb capsules was processed as described previously. Capsules were transferred to 6-well plates and cultured in DMEM without phenol red, supplemented with 10% FBS and 1% A/B. After 1 day, keratinocytes were seeded on the capsules ($5x10^5$ cells/well) and cultured on a 25:75 mixture (previously optimized in monoculture) of DMEM (containing 10% FBS, 1% A/B) and keratinocyte serum free medium with supplements in a 37 °C humidified atmosphere with 5% CO_2. Cells were examined under SEM to analyze cell morphology and

cell-matrix interactions. Samples were fixed, dehydrated and prepared as described for SEM analysis. Co-cultured cells were also characterized using an immunocytochemistry assay with specific markers for each cell type. Samples were fixed and prepared as described previously. The primary antibodies and dilutions used in the assay were anti-fibroblast surface protein (F4771, 1:500, Sigma, USA) and anti-keratin 5 (PRB-160P, 1:500, Covance, Spain). The secondary antibodies and dilutions were anti-rabbit Alexa 488 (1:200) and anti-mouse Alexa 594 (1:500) (Molecular Probes, Invitrogen, USA). Samples were visualized by CLSM (Olympus FluoView 1000, Olympus, Japan). Background was subtracted and images were processed using FV10-ASW 3.1 software (Olympus, Japan).

Data analysis and statistics

All data values are presented as mean ± standard deviation (SD). Statistical analysis was performed using GraphPad Prism 5.00 software (San Diego, USA). Statistical differences were determined using one-way analysis of variance (ANOVA) with a Bonferroni's multiple comparisons post-hoc test (Permeability, DNA quantification). Differences between groups in the mechanical stability study were determined using a two-way analysis of variance (ANOVA) with a Bonferroni's multiple comparisons post-hoc test. ($*$ $p < 0.05$, $**$ $p < 0.01$ and $***$ $p < 0.001$)

3. Results and discussion

Building blocks for electrostatic driven-self-assembly

The self-assembling peptides used in this study are amphiphilic molecules, composed of a hydrophobic segment coupled to a peptide sequence, that includes a β-sheet forming sequence (VVVAAA) and a domain with charged amino acids, either positive (KKK, K_3-PA, Fig. VII.1B) or negative (EEE, E_3-PA, Fig. VII.1A).[27]

The negatively charged peptide (E_3-PA) was chosen by its known ability to undergo self-assembly into nanofribrillar structures in the presence of divalent cations, such as Ca^{2+}, and form stable gels at certain concentrations.[8, 27, 28] It has been shown that self-assembling peptide gels present a nanofibrillar network that resemble de structural architecture of extracellular matrix, making them attractive for studying cell-matrix interactions on a 3D environment.[29-31] Electrostatic-driven self-assembly between PAs of opposite charge was demonstrated by the formation of nanofibers with subsequent formation of self-supporting gels.[18] Based on these findings, we hypothesized that microfluidic technology could be used to control the size and microscopic shape of nanostructures generated by electrostatic self-assembly. Peptide droplets generated in the microfluidic device would serve as templates to produce spherical capsular structures by self-assembly (Fig. VII.1). The core and shell of the proposed capsules can be further tailored by changing the peptide concentration and/or the conditions during the self-assembly process, for example the pH, as it is known that pH affects the charge of peptides. For example, Savin and Doyle[19] studied the effect of pH on the kinetics of self-assembly of a model peptide containing positively charged and negatively charged residues. Using multiple particle tracking, they found that increasing the pH of the peptide solution from 3.5 to 4.0, the gelation time decreased by almost hundredfold. By incorporating bioactive moieties in the peptide sequences, these peptide capsules can offer a versatile artificial matrix to encapsulate cells and study their behavior under different physical and biochemical signals.

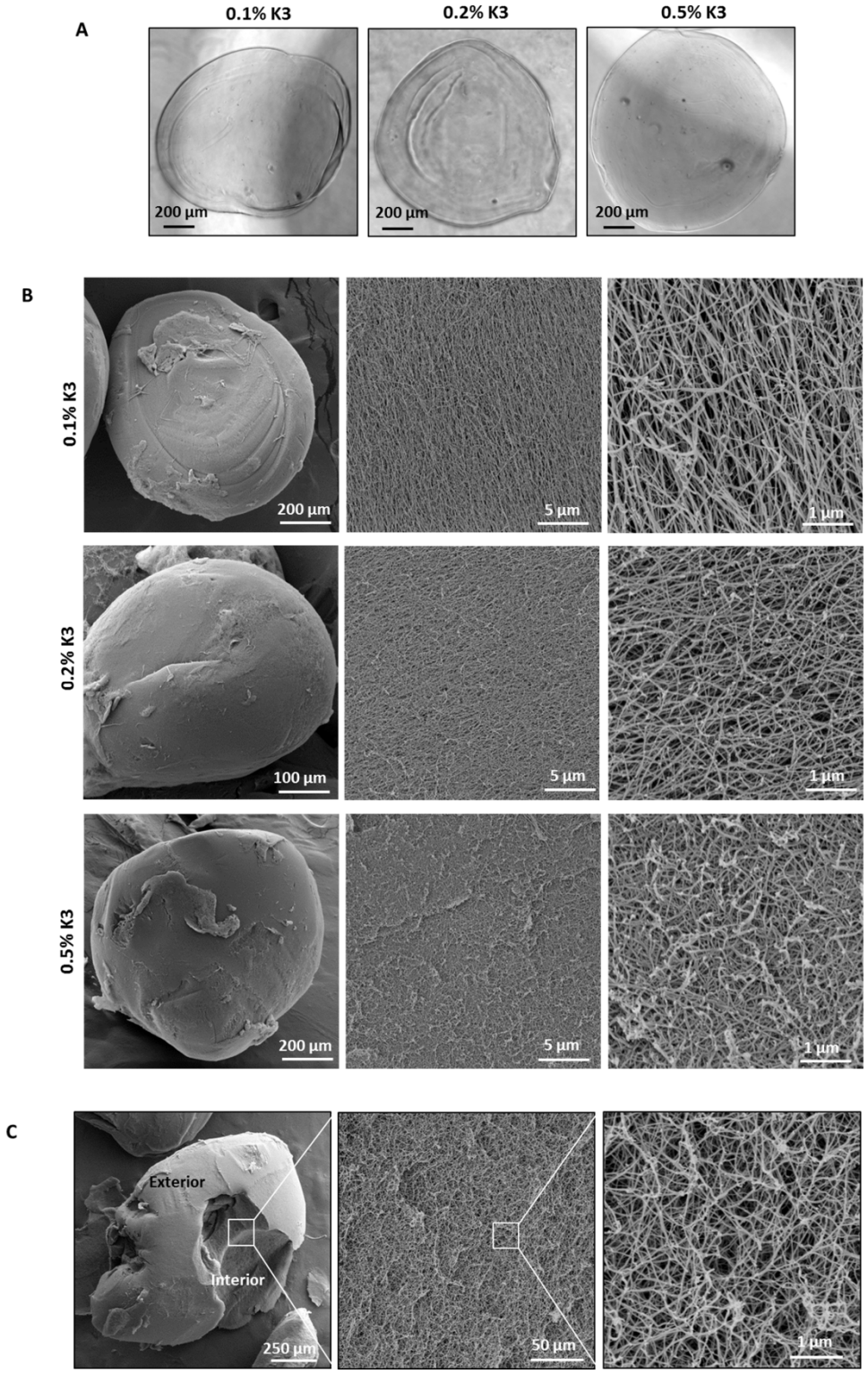

Figure VII.2. Capsules morphology and microstructure. Phase contrast microscopy images (A) and SEM micrographs (B) showing the size and overall structure of peptide-based capsules. SEM micrographs of capsule shell at higher magnification show a network of nanofibers randomly distributed with higher density for the capsules with higher concentration of K_3-PA. SEM micrographs of capsule interior show a dense core with a random fibrillar structure (C).

Capsule generation by directed self-assembly

In the present work, we have used a microfluidic method to generate spherical capsular structures by self-assembly between oppositely charged peptides for the encapsulation of human dermal fibroblasts.

The first step in capsule preparation requires the formation of microdroplets of an aqueous solution of a negatively charged peptide (E_3-PA, 1 wt%) in the microfluidic device through emulsification in the oil phase (Fig. VII.1A). The E_3-PA microdroplets were then directly extruded into a solution of a similar peptide with opposite charge (Fig. VII.1B). The peptide microdroplets formed in the oil phase served as templates for the formation of stable spherical capsules by electrostatic self-assembly between the E_3 and K_3PAs. The microfluidics device was used to control/guide the interfacial self-assembly between the two peptides to obtain a final microstructure with a spherical shape, instead their "chaotic" self-assembly in solution. Here, the shape and size of the peptide droplet, formed in the microfluidic device, determines the final morphology of the assembly. At the droplet interface, self-assembly immediately occurs resulting on the formation of a capsular structure (a wall membrane made of K_3-E_3-PA nanofibers with a liquefied core containing free E_3-PA molecules – Fig. VII.1C). The oil phase separates from the K_3-PA solution and floats to the surface because of the difference in densities. This phase separation allows the aqueous peptide droplets to be dispersed in the K_3-PA solution (below the oil phase). The mineral oil is removed from the collection vessel by pipetting out the upper layer. The K_3-PA solution was supplemented with 0.1 M $CaCl_2$ to induce the gelation of internal E_3-PA (Fig. VII.1D). To further control the microstructure and permeability of the capsule wall, the concentration of K_3-PA was varied (0.1, 0.2, 0.5 wt%).

The morphology and microstructure of the generated capsules were analyzed with phase contrast microscopy and SEM. Their stability, mechanical resistance, permeability and ability to support the encapsulation and survival of human dermal fibroblasts were also studied.

Capsule characterization

Size, morphology and microstructure

Images obtained by phase contrast microscopy showed spherical shaped capsules with uniform size and a diameter of around 1000 μm (Fig. VII.2A). Higher concentrations of K_3-PA (> 1 wt%) generated larger capsules with a dense shell that would difficult the diffusion of nutrients and cell metabolites, leading to the formation of necrotic centers and cell death. On the other hand, lower concentrations, ranging from 0.1 to 0.5 wt%, resulted in stable capsules. SEM micrographs of the capsules showed a shell with a nanofibrillar structure (Fig. VII.2B) as a result from the self-assembly between the peptides.

The external surface of the capsules exhibit a network of nanofibers randomly distributed but the nanofiber density was higher for the capsules formed at higher concentration of K_3-PA. This observation showed that we were able to modulate capsule shell microstructure by varying K_3-PA concentration, which may have implications on the capsule permeability. Furthermore, this external membrane enables the protection of encapsulated species from the external environment. The capsules can have either a liquid (Fig. VII.1C) or gel core after gelation with Ca^{2+} ions (Fig. VII.1D), allowing to create different cellular microenvironments, either for culturing cells in suspension or anchorage-dependent cells. Liquid core capsules were less stable and more susceptible to burst, whereas core gelation generates robust capsules using concentrations of E_3-PA from 0.5 to 2 wt%. To assess the internal surface, capsules were fractured before SEM imaging. SEM micrographs showed a dense core with a random fibrillar structure (Fig. VII.2C).

Swelling, mechanical stability and permeability

A general requirement for capsules as 3D environments for cell encapsulation and culture include their mechanical and chemical stability in aqueous media (e.g. buffer, cell culture medium). To investigate whether capsules were able to maintain their structural integrity when exposed to aqueous solutions, capsules were incubated in water or PBS and their size variation was followed for 7 days. Capsules were shown to be very stable in both solutions, without relevant size variation along time (Fig. VII.3A). Capsules with lower swelling rate are less prone to rupture and to induce an inflammatory response when implanted *in vivo*.[32] To evaluate capsules mechanical stability, an additional study was performed. Capsules were incubated in PBS with glass beads under agitation and their membrane integrity was followed for 24 h. As expected, capsules formed at higher concentration of K_3-PA (0.5 wt%), with a denser outer shell, showed to be less prone to damage (Fig. VII.3B), although the difference between conditions is more notorious only after 24 h.

Capsules permeability is crucial for cell encapsulation to allow the diffusion of oxygen, nutrients and cell metabolites. Additionally, when used for cell delivery therapies, they should also be able to avoid the influx of immune cells and antibodies. To assess the effect of K_3-PA concentration on the permeability of the capsules, dextran standards of different molecular weights (20, 40, 155 kDa) were encapsulated within the capsules and their release followed with time. The release profile of 20 kDa dextran was similar for all the conditions and faster than the dextran with higher MW, as expected, and after 24 h about 60% of the encapsulated dextran was released from the capsules (Fig.VII. 3C). For the 40 kDa dextran, a similar behavior was observed for the capsules with 0.1 and 0.2 wt% K_3-PA. After 24 h, about

50% of the encapsulated dextran was released. The percentage of dextran released from the capsules formed with 0.5 wt% K_3-PA was lower (40%) as expected (Fig. VII.3C). The diffusion of the higher MW dextran (155 kDa) was slower. After 24 h, only 20-25% of the encapsulated dextran was released in all the conditions (Fig. VII.3C). These results indicate that capsules formed in higher peptide concentration exhibit a controlled diffusion of high molecular weight molecules.

This difference in the capsule permeability may be related to their microstructure observed by SEM (Fig. VII.3C, Fig. VII.S3). Capsules formed with higher concentration of K_3-PA showed a shell structure with a much denser nanofibrillar organization which may hamper the diffusion of larger molecules. Estimation of the porosity of the capsule external surface also confirmed higher porosity for the capsules prepared with lower peptide concentrations (Supplementary Information, Fig. VII.S4). By varying the concentration of one of the components (K_3-PA) we were able to modulate the capsule wall porosity and permeability.

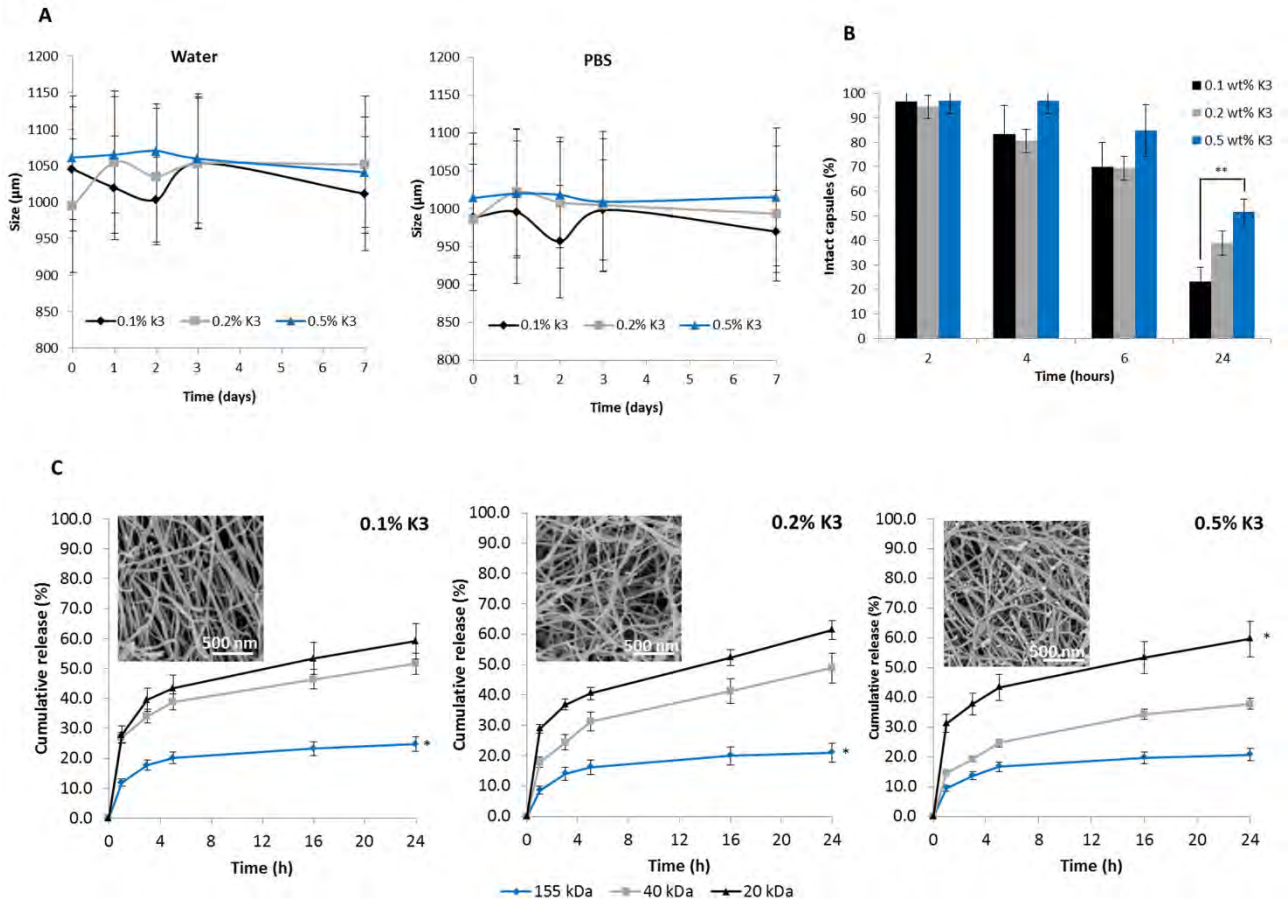

Figure VII.3. Capsules stability and permeability. Capsules stability in aqueous solutions (A) and mechanical resistance (B) as a function of K_3-PA concentration. Capsule permeability assessed by the release of encapsulated dextran (fluorescently labeled) with different molecular weights (20, 40 and 155 kDa) (C). Scanning electron micrographs shows differences in network morphology and fiber density that depend on K3-PA concentration. (**) $p< 0.01$, (*) $p< 0.05$, error bars represent standard deviation.

Encapsulation and culture of hDFb within capsules

Most of cell-matrix interactions *in vivo* occur in 3D environments, with the cells normally embedded within an ECM that is constantly undergoing remodelling by the cells themselves. The potential of the developed capsules as 3D scaffolds for anchorage-dependent cells was investigated by the encapsulation of human dermal fibroblasts.

Cell viability and proliferation

A fluorescence live/dead assay was performed to assess the viability of encapsulated cells. Living (green) cells with well-defined round contours were visualized and no dead cells (shown as red nuclei) were detected within the capsules. Furthermore, cells remained viable and well distributed within the capsules throughout the 14 days of culture (Fig. VII.4B).

The quantification of DNA (Fig. VII.4A) revealed a gradual increase in DNA as a result of fibroblast proliferation over time. These results demonstrate that the capsule composition and the method to obtain them did not affect cell viability.

Expression of collagen I

Fibroblasts have the natural ability to remodel their extracellular microenvironment by either expressing proteolytic enzymes or synthesizing ECM proteins, such as collagen I.[33] The ability of fibroblasts to synthesize collagen I was assessed by immunofluorescence, as an indirect way to evaluate encapsulated fibroblasts functionality. Confocal microscopy images showed that cells maintained the ability to produce collagen I during the culture time (Fig. VII.4C2,C3).

Cell morphology

The morphology of fibroblasts within the capsules was assessed by SEM. Micrographs showed round-shaped cells in the capsules inside cavities, that reflect the living spaces preserved by the cells (Fig. VII.4D). In the SEM images, cell size can be estimated to be around 10 μm. A thin fiber-like matrix secreted by the cells was visible shortly after one day. The presence of these protrusions was more evident after 14 days of culture, showing the interaction of the fibroblasts with the nanofibrillar structure of the gelled E_3-PA. Although fibroblasts were still interacting with the fibrillar matrix of the self-assembled peptide, cells still remained round after 14 days of culture. Based on this observation, and previous findings on the effect of matrix properties on fibroblast proliferation in 3D gels,[34] which showed that at higher stiffness the matrix acts as physical barrier for cells in 3D, impeding their proliferation

and migration, we have further investigated the influence of peptide concentration inside the capsules on the morphology of encapsulated fibroblasts.

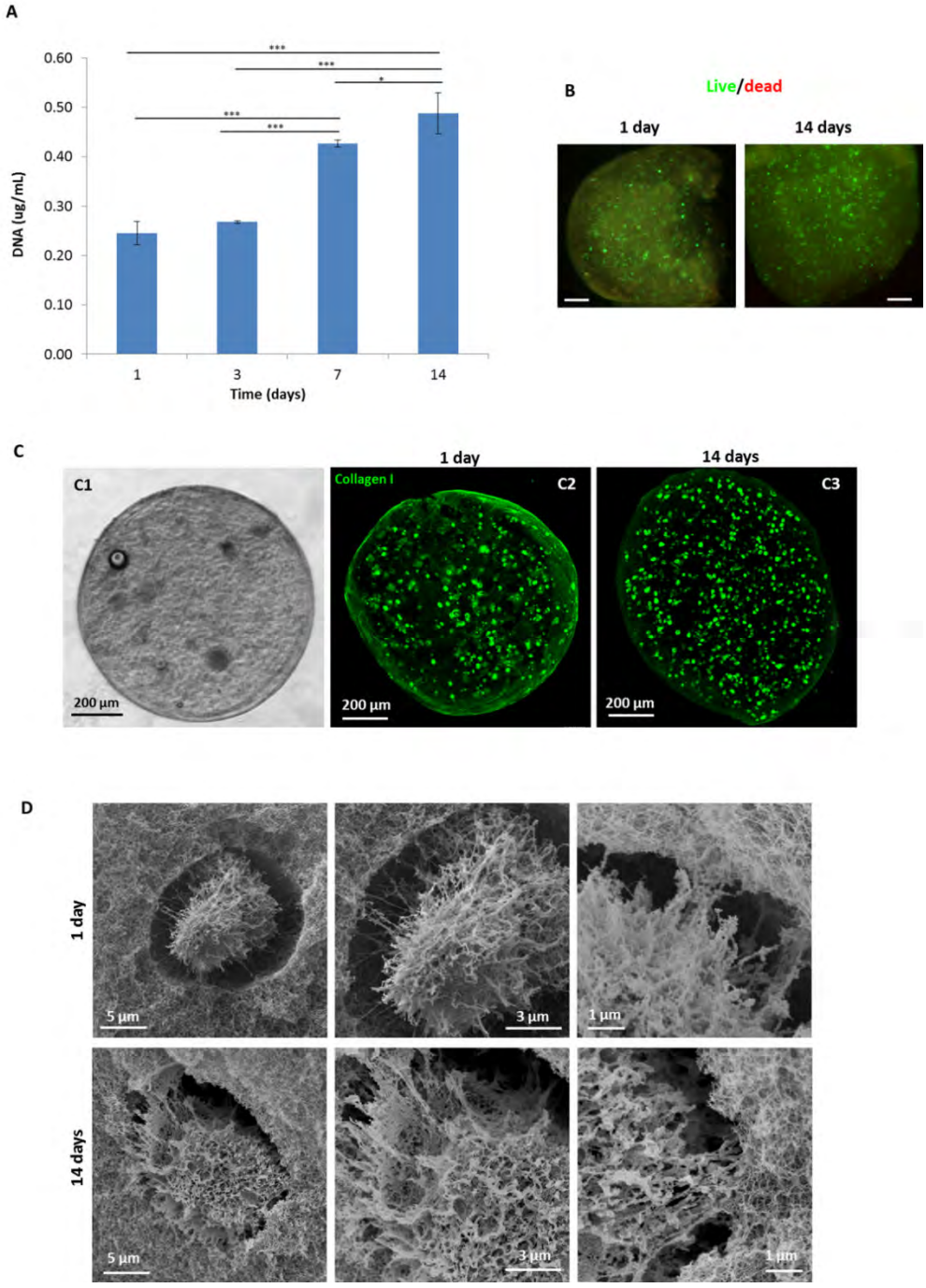

Figure VII.4. *In* vitro viability and proliferation of hDFb encapsulated within peptide-based capsules. Cell proliferation assessed by dsDNA quantification (A) ((***) $p < 0.001$, (*) $p < 0.05$, error bars represent standard deviation (n=3)) and fluorescence microscopy images of live/dead assay on encapsulated fibroblasts (B). Living cells were stained by calcein (green) and dead cells by propidium iodide (red). Scale bar represents 200 µm. Phase contrast microscopy of encapsulated fibroblasts in the capsules (C1) and confocal microscopy images of stained collagen I produced by hDFb during culture time (C2, C3). SEM micrographs of encapsulated cells show round-shaped cells inside cavities (D).

Influence of matrix composition on fibroblast morphology

Fibroblast morphology and cell-matrix interactions were investigated by varying the percentage of E_3-PA (0.5, 1 and 2 wt%) inside the capsule. Previous studies using collagen matrices prepared under diverse conditions showed that matrix stiffness increases with matrix density.[35] Here, we intended to modulate the matrix density in the capsules core by varying peptide concentration.

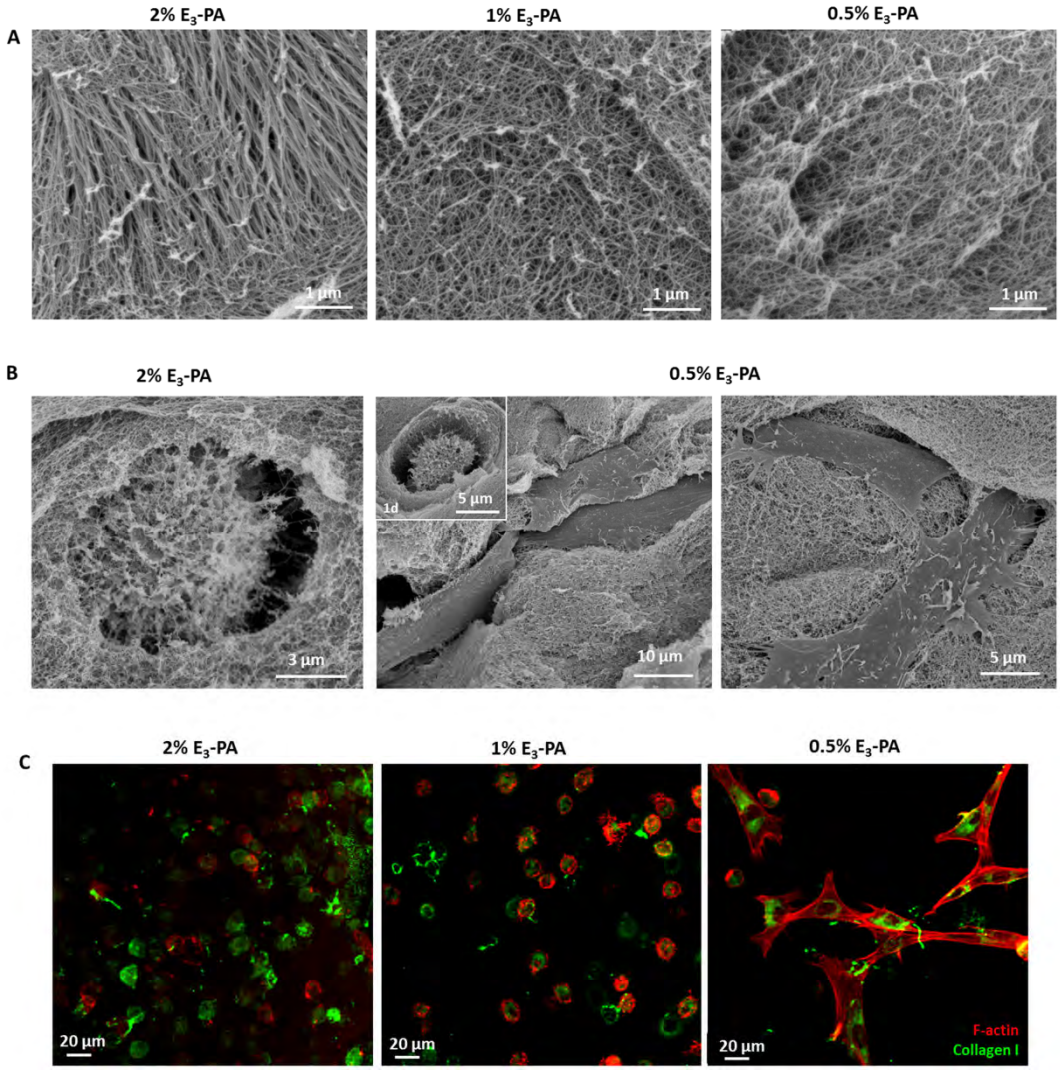

Figure VII.5. Influence of matrix composition on fibroblast morphology. SEM micrographs of the capsules interior revealed a higher density of fibrillar nanostructures with increasing concentration of E_3-PA (A). Morphology of hDFb cultured within the peptide capsules revealed by SEM at day 14 (inset image shows the morphology of the cells at day 1) (B). Confocal microscopy images of stained collagen I (green) and f-actin (red) after 14 days, showed spread cells that formed a 3D-network with highly elongated cells in 0.5% E3-PA capsules (C). Cells cultured in 1 and 2 wt% E_3-PA capsules maintained a spherical shape, with peripheral deposition or poorly organized F-actin that followed the cell contours.

SEM micrographs of the capsules interior confirmed our hypothesis revealing a higher density of fibrillar nanostructures with increasing concentration of E_3-PA (Fig. VII.5A). SEM micrographs of encapsulated fibroblasts within 1 and 2 wt% E_3-PA showed round shaped cells interacting with the nanofibrillar structure of the gelled peptide, similar to what we have observed before (Fig. VII.5B). In contrast, within 0.5 wt% E_3-PA capsules, cells remained round after 1 day, but after 7 days, fibroblasts had spread out exhibiting extended protrusions interacting with fibrillar structure of E_3-PA. When cultured in 0.5 wt% E_3-PA, cells adopted a spindle shape with fine filopodia. After 14 days, the spread cells formed a 3D-network and phalloidin-stained F-actin showed highly elongated cells with clearly-defined stress fibers (Fig. VII.5C). In contrast, cells cultured in 1 and 2 wt% E_3-PA capsules maintained a spherical shape, and phalloidin staining showed peripheral deposition or poorly organized F-actin that followed the cell contours. As previously observed, fibroblasts maintained their ability to synthesize collagen I. Within 0.5 wt% E3-PA capsules, collagen I has a strong signal and was well distributed in the cytosol, whereas in 1 and 2 wt% E_3-PA the signal was weaker and collagen distribution was more peripheral. These results show a similar trend to what has been observed by Bott and co-authors,[34] when studying the effect of matrix stiffness on fibroblast proliferation in 3D gels. It has been shown that fibroblasts normally exhibit a flat morphology with dorsal-ventral polarity and extended protrusions when cultured in 2D[36, 37] because when they migrate and proliferate they do not experience major physical barriers.[38] However, when encapsulated in a 3D matrix, fibroblasts need to overcome barriers posed by the surrounding environment to proliferate and migrate, re-acquiring a natural spindle-shaped morphology.[36-38] These results highlight the role of the core matrix density/stiffness in controlling cell morphology and cell-matrix interaction.

Co-culture studies – culture of hKC over the surface of the peptide capsules encapsulating hDFb

In vitro co-culture systems, using relevant cell types, can serve as mimics of tissue niches found *in vivo* and be used as valuable tools for probing and manipulating cell-cell interactions. Since interactions between cells can occur through soluble factors via paracrine signaling, co-culture studies should be performed in interactive microenvironments to permit the exchange of soluble factors between neighboring cells, while maintaining the different cells physically separated. In addition, these microenvironments should recreate the composition and structure of native ECMs. By using gelled core peptide capsules with a fibrillar structure, we have demonstrated that hDFb could be encapsulated within the capsules and were able to survive for 14 days. To further demonstrate the ability of these

capsular structures for conducting more complex cellular studies (e.g. co- culture) we investigated their ability to support the co-culture of hDFb and hKc, within and on the capsule surface, respectively (Fig. VII.6A). The hKc gradually adhered to the capsule surface and covered it after 24 h, resulting in hDFb-hKC co-cultured capsules, as seen in phase contrast microscopy images (Fig. VII.6B1).

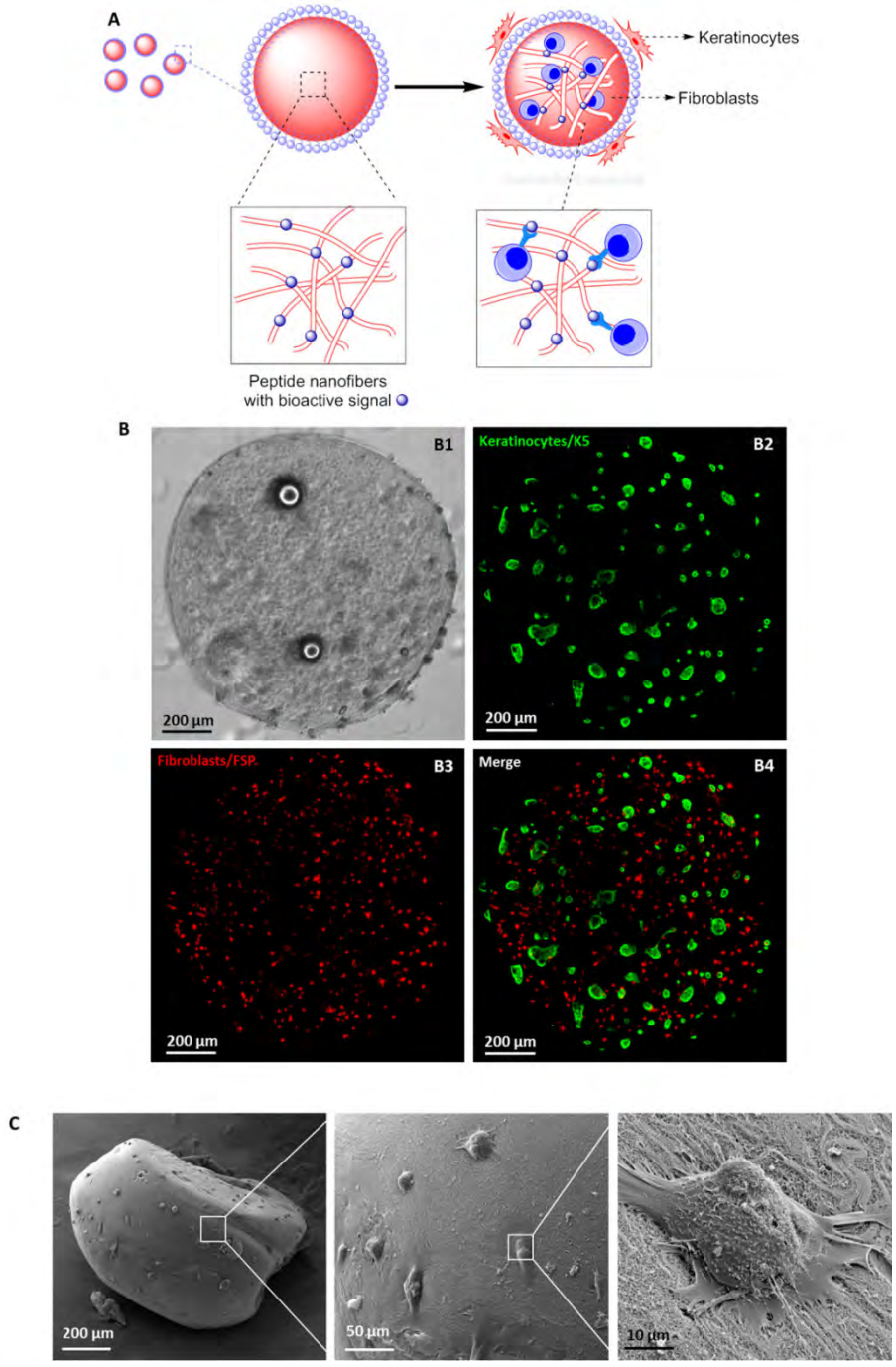

Figure VII.6. Co-culture studies. Concept of co-culturing skin cells within and on the peptide-based capsules (A). Phase contrast image showing keratinocytes on the capsule surface (B1). Immunostaining of specific markers for each cell type confirmed the localization of the fibroblasts in the capsule interior (B3) and keratinocytes on the surface (B2). SEM micrographs show keratinocytes fully adhered to the capsule shell, exhibiting extended filopodia and lamellipodia and interacting with the fibrillar surface (C).

Confocal microscopy images of the capsules stained with antibodies specific for each cell type (Fig. VII.6B2-B4), showed that co-cultured capsules consisted of encapsulated fibroblasts within the E_3-PA fibrillar matrix (Fig.VII. 6B3), confined by a layer of keratinocytes on the outer shell (Fig. VII.6B2). SEM micrographs showed that keratinocytes were fully adhered to the capsule shell, exhibiting extended filopodia and lamellipodia and interacting with the fibrillar surface of K_3-PA (Fig. VII.6C). Our results showed that these capsules represent a good model to resemble the three-dimensional architecture of *in vivo* tissues carrying different cell types. In addition, these peptide-based capsules can be tailored in a highly controlled manner to mimic ECM properties and functions. For example, the peptides in the capsule outer shell and core can be customized for other cell types by incorporating specific peptide sequences and their composition can be tuned to obtain matrices with defined structure and stiffness for 3D cell culture.

4. Conclusions

Here we demonstrate the application of electrostatic self-assembly, between peptide amphiphiles, combined with microfluidics to guide the assembly into spherical capsules. These capsules present a core shell structure and their properties (nanofibrillar density, permeability, stiffness) can be tuned by varying the concentration of each peptide. By controlling the capsules properties, cell-matrix interactions can be studied in a 3D environment. Capsules composed of a simple negatively charged peptide, without any cell-adhesive sequence, were shown to support the survival of encapsulated human dermal fibroblasts. Another application of these capsules is demonstrated by co-culturing two cell types within and on their surface. The versatility of the selected building blocks to present bioactive ligands provides the opportunity to mimic other functionalities of the natural ECM, which can find numerous applications in cell biology and regenerative medicine.

Acknowledgements

Funding for this study was provided by the Portuguese Foundation for Science and Technology (FCT, grant PTDC/EBB-BIO/114523/2009). D.S. Ferreira gratefully acknowledges FCT for the PhD scholarship (SFRH/BD/44977/2008). We also thank Dr A. C. Mendes from the 3B's Research Group at the University of Minho (Portugal) for her assistance with the microfluidics device.

References

1. T. Aida, E. W. Meijer and S. I. Stupp, Functional Supramolecular Polymers, *Science*, 2012, 335, 813-817.
2. S. I. Stupp, Self-Assembly and Biomaterials, *Nano Lett*, 2010, 10, 4783-4786.
3. R. M. Capito, H. S. Azevedo, Y. S. Velichko, A. Mata and S. I. Stupp, Self-assembly of large and small molecules into hierarchically ordered sacs and membranes, *Science*, 2008, 319, 1812-1816.
4. R. Haghgooie and P. S. Doyle, Directed self-assembly of field-responsive fluids in confined geometries, *Soft Matter*, 2009, 5, 1192-1197.
5. C. W. Wang, D. Sinton and M. G. Moffitt, Morphological Control via Chemical and Shear Forces in Block Copolymer Self-Assembly in the Lab-on-Chip, *Acs Nano*, 2013, 7, 1424-1436.
6. D. W. P. M. Lowik, I. O. Shklyarevskiy, L. Ruizendaal, P. C. M. Christianen, J. C. Maan and J. C. M. van Hest, A highly ordered material from magnetically aligned peptide amphiphile nanofiber assemblies, *Adv Mater*, 2007, 19, 1191-+.
7. Y. S. Velichko, J. R. Mantei, R. Bitton, D. Carvajal, K. R. Shull and S. I. Stupp, Electric Field Controlled Self-Assembly of Hierarchically Ordered Membranes, *Adv Funct Mater*, 2012, 22, 369-377.
8. S. M. Zhang, M. A. Greenfield, A. Mata, L. C. Palmer, R. Bitton, J. R. Mantei, C. Aparicio, M. O. de la Cruz and S. I. Stupp, A self-assembly pathway to aligned monodomain gels, *Nat Mater*, 2010, 9, 594-601.
9. K. Sugihara, M. Chami, I. Derenyi, J. Voros and T. Zambelli, Directed Self-Assembly of Lipid Nanotubes from Inverted Hexagonal Structures, *Acs Nano*, 2012, 6, 6626-6632.
10. A. C. Mendes, K. H. Smith, E. Tejeda-Montes, E. Engel, R. L. Reis, H. S. Azevedo and A. Mata, Co-Assembled and Microfabricated Bioactive Membranes, *Adv Funct Mater*, 2013, 23, 430-438.
11. B. A. Grzybowski, C. E. Wilmer, J. Kim, K. P. Browne and K. J. M. Bishop, Self-assembly: from crystals to cells, *Soft Matter*, 2009, 5, 1110-1128.
12. R. Karnik, F. Gu, P. Basto, C. Cannizzaro, L. Dean, W. Kyei-Manu, R. Langer and O. C. Farokhzad, Microfluidic platform for controlled synthesis of polymeric nanoparticles, *Nano Lett*, 2008, 8, 2906-2912.
13. A. Jahn, S. M. Stavis, J. S. Hong, W. N. Vreeland, D. L. DeVoe and M. Gaitan, Microfluidic mixing and the formation of nanoscale lipid vesicles, *Acs Nano*, 2010, 4, 2077-2087.

14. A. C. Mendes, E. T. Baran, P. Lisboa, R. L. Reis and H. S. Azevedo, Microfluidic Fabrication of Self-Assembled Peptide-Polysaccharide Microcapsules as 3D Environments for Cell Culture, *Biomacromolecules*, 2012, 13, 4039-4048.
15. D. Seliktar, Designing cell-compatible hydrogels for biomedical applications, *Science*, 2012, 336, 1124-1128.
16. E. Gazit, Bioinspired chemistry diversity for self-assembly, *Nat Chem*, 2010, 2, 1010-1011.
17. E. Gazit, Self-assembled peptide nanostructures: the design of molecular building blocks and their technological utilization, *Chem Soc Rev*, 2007, 36, 1263-1269.
18. K. L. Niece, J. D. Hartgerink, J. J. J. M. Donners and S. I. Stupp, Self-assembly combining two bioactive peptide-amphiphile molecules into nanofibers by electrostatic attraction, *J. Am. Chem. Soc.*, 2003, 125, 7146-7147.
19. T. Savin and P. S. Doyle, Electrostatically tuned rate of peptide self-assembly resolved by multiple particle tracking, *Soft Matter*, 2007, 3, 1194-1202.
20. M. R. Caplan, P. N. Moore, S. G. Zhang, R. D. Kamm and D. A. Lauffenburger, Self-assembly of a beta-sheet protein governed by relief of electrostatic repulsion relative to van der Waals attraction, *Biomacromolecules*, 2000, 1, 627-631.
21. S. G. Zhang, T. Holmes, C. Lockshin and A. Rich, Spontaneous assembly of a self-complementary oligopeptide to form a stable macroscopic membrane, *Proc. Natl. Acad. Sci. U. S. A.*, 1993, 90, 3334-3338.
22. T. M. S. Chang, Therapeutic applications of polymeric artificial cells, *Nat Rev Drug Discov*, 2005, 4, 221-235.
23. D. Velasco, E. Tumarkin and E. Kumacheva, Microfluidic Encapsulation of Cells in Polymer Microgels, *Small*, 2012, 8, 1633-1642.
24. S. Allazetta, T. C. Hausherr and M. P. Lutolf, Microfluidic Synthesis of Cell-Type-Specific Artificial Extracellular Matrix Hydrogels, *Biomacromolecules*, 2013.
25. S. Seiffert, Microgel capsules tailored by droplet-based microfluidics, *Chemphyschem*, 2013, 14, 295-304.
26. A. C. Mendes, E. T. Baran, R. L. Reis and H. S. Azevedo, Fabrication of phospholipid–xanthan microcapsules by combining microfluidics with self-assembly, *Acta Biomater.*, 2013, 9, 6675-6685.

27. M. J. Webber, J. Tongers, M.-A. Renault, J. G. Roncalli, D. W. Losordo and S. I. Stupp, Development of bioactive peptide amphiphiles for therapeutic cell delivery, *Acta Biomater.*, 2010, 6, 3-11.

28. E. T. Pashuck, H. G. Cui and S. I. Stupp, Tuning Supramolecular Rigidity of Peptide Fibers through Molecular Structure, *J. Am. Chem. Soc.*, 2010, 132, 6041-6046.

29. E. Beniash, J. D. Hartgerink, H. Storrie, J. C. Stendahl and S. I. Stupp, Self-assembling peptide amphiphile nanofiber matrices for cell entrapment, *Acta Biomater.*, 2005, 1, 387-397.

30. S. G. Zhang, Fabrication of novel biomaterials through molecular self-assembly, *Nature Biotechnology*, 2003, 21, 1171-1178.

31. M. Zhou, A. M. Smith, A. K. Das, N. W. Hodson, R. F. Collins, R. V. Ulijn and J. E. Gough, Self-assembled peptide-based hydrogels as scaffolds for anchorage-dependent cells, *Biomaterials*, 2009, 30, 2523-2530.

32. M. D. Darrabie, W. F. Kendall Jr and E. C. Opara, Characteristics of Poly-l-Ornithine-coated alginate microcapsules, *Biomaterials*, 2005, 26, 6846-6852.

33. A. D. Metcalfe and M. W. Ferguson, Tissue engineering of replacement skin: the crossroads of biomaterials, wound healing, embryonic development, stem cells and regeneration, *J R Soc Interface*, 2007, 4, 413-437.

34. K. Bott, Z. Upton, K. Schrobback, M. Ehrbar, J. A. Hubbell, M. P. Lutolf and S. C. Rizzi, The effect of matrix characteristics on fibroblast proliferation in 3D gels, *Biomaterials*, 2010, 31, 8454-8464.

35. B. A. Roeder, K. Kokini, J. E. Sturgis, J. P. Robinson and S. L. Voytik-Harbin, Tensile mechanical properties of three-dimensional type I collagen extracellular matrices with varied microstructure, *J Biomech Eng*, 2002, 124, 214-222.

36. K. M. Yamada and E. Cukierman, Modeling Tissue Morphogenesis and Cancer in 3D, *Cell*, 2007, 130, 601-610.

37. E. Cukierman, R. Pankov, D. R. Stevens and K. M. Yamada, Taking cell-matrix adhesions to the third dimension, *Science*, 2001, 294, 1708-1712.

38. P. Friedl and E. B. Bröcker, The biology of cell locomotion within three-dimensional extracellular matrix, *CMLS, Cell. Mol. Life Sci.*, 2000, 57, 41-64.

Appendix

All peptides were synthesized, characterized and purified successfully. MALDI-MS was used to characterize the mass of the synthesized peptides (Fig. VII.S1-S2, A).

The expected mass for $C_{16}V_3A_3K_3$ ($C_{58}H_{111}N_{13}O_{10}$) was 1150.58, two main peaks were found by MALDI-MS, corresponding to [M] m/z = 1150.84, and $[M+Na]^+$ m/z= 1172.83 (Fig. VII.S1A).

The expected mass for $C_{16}V_3A_3E_3$ ($C_{55}H_{95}N_9O_{17}$) was 1152.68, one main peak was found by MALDI-MS, m/z = 1152.80(Fig. VII.S2A).

Analytical HPLC of the collected fractions showed a single peak after purification for all the PAs (Fig. VIIS1-S2, B)

$C_{16}V_3A_3K_3$

A

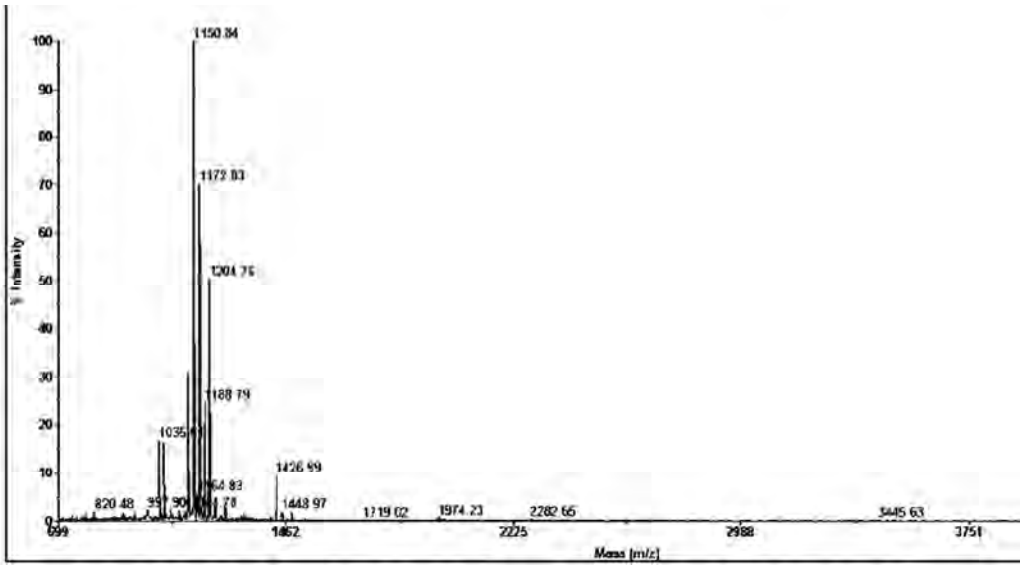

B

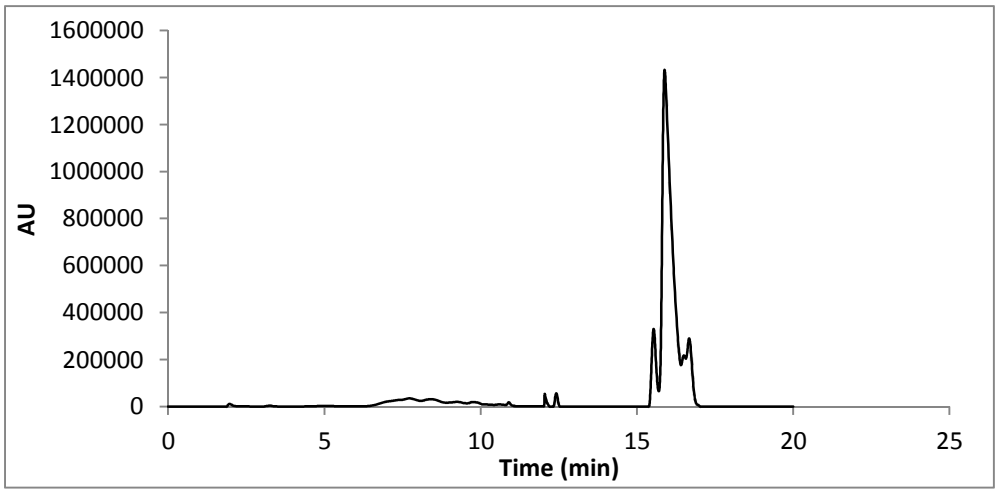

Figure VII.S1. Representative MALDI-MS data (A) and analytical HPLC trace, detected at 220 nm (B) of $C_{16}V_3A_3K_3$.

$C_{16}V_3A_3E_3$

A

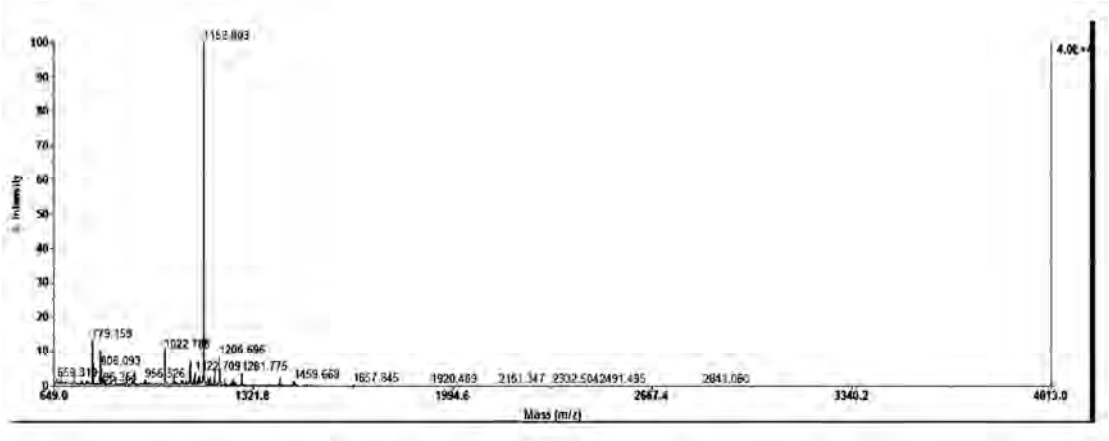

B

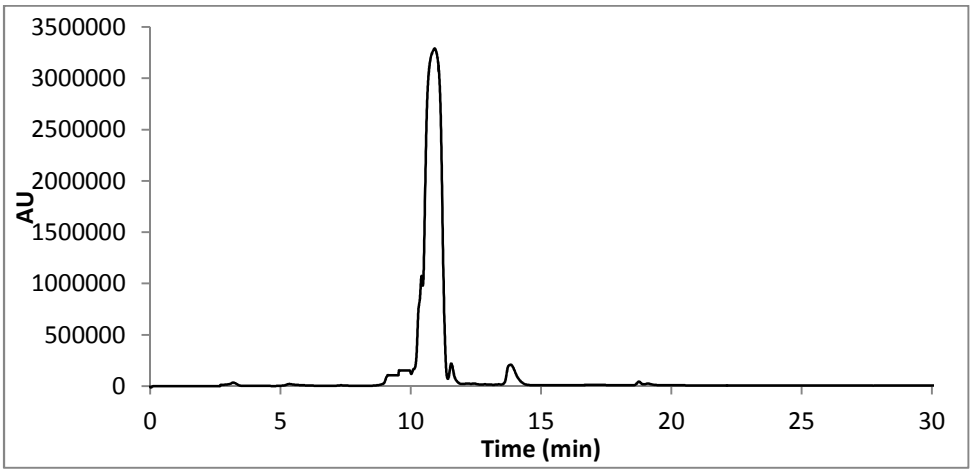

Figure VII.S2. Representative MALDI-MS data (A) and analytical HPLC trace, detected at 220 nm (B) of $C_{16}V_3A_3E_3$.

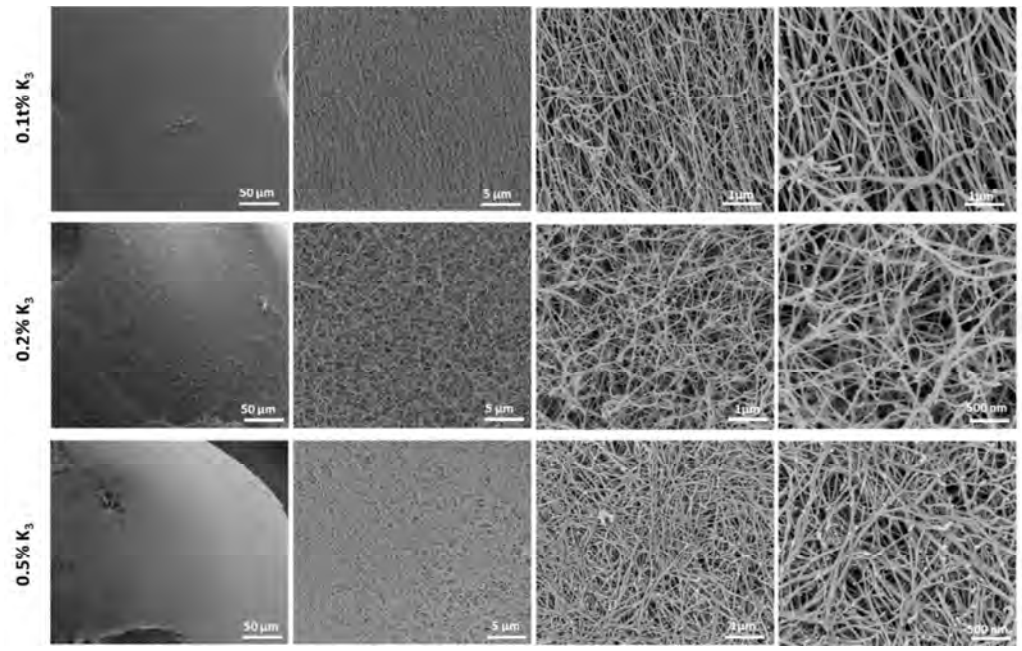

Figure VII.S3. SEM micrographs of capsule external surface at different magnifications and as function of K3-PA concentration.

Capsule shell porosity was estimated using SEM micrographs and ImageJ sotware (NIH, USA) for image analysis and processing.[S1] To separate the nanofibers from the background, a threshold was set to the image by assigning the pixels in the image as either completely white or black. Once the range was selected a binary image was created (Fig. VII.S4) by the software in which objects (nanofibers) are white and background is black. The measurement tool was then used to quantify the area covered by the pores or by the nanofibers. Since the image area was known, the area fraction filled by the pores was calculated giving an estimated value of porosity.

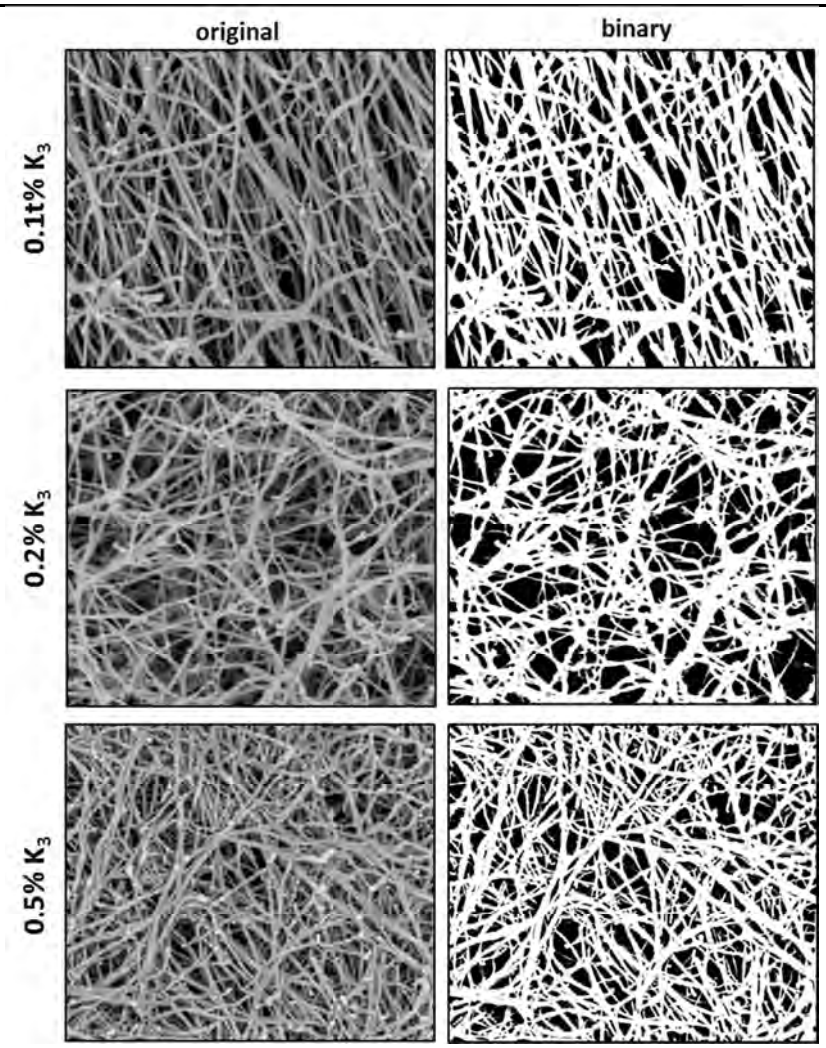

%K3	Estimated Porosity (%)
0.1	64.4
0.2	41.6
0.5	23.1

Figure VII.S4. SEM micrographs of external surface of capsules prepared at different K_3-PA concentrations and images processed with ImageJ software (A). Estimated porosity of capsule shell as function of K_3-PA concentrations.

References

S1. J. Farmer, B. Duong, S. Seraphin, S. Shimpalee, M. J. Martinez-Rodriguez, J. W. Van Zee, *J. Power Sources*, 2012, **197**,1-11.

Section 4

CONCLUSIONS

Chapter VIII

Summary and outlook

Chapter VIII

Summary and outlook

It is object of the present chapter to summarize the significant findings in the experiments presented in the preceding chapters and describe how the conclusions address the aforementioned hypotheses.

Bottom-up approaches based on peptide self-assembly provide a unique set of advantages to create novel biomaterials, as they offer the possibility of controlling the architecture, shape and dimensions of bioactive nanostructures, as well as the spatial display and density of bioactive signals. The architectural resemblance of self-assembled nanofibers to filamentous structures found in natural extracellular matrix (ECM) represents an additional feature to attain superior biomimetic scaffolds, and a clear advantage in biomaterials engineering.
In this thesis, molecular engineering was used to design peptide molecules with self-assembling properties and specific biofunctionalities. Then, self-assembly was applied to generate biomaterials (membranes and capsules) with hierarchical structure integrating physical and biochemical features of the ECM microenvironment. By pursuing this approach, artificial ECMs can be developed and used in regenerative medicine applications to mimic the properties of native tissues as well as to reconstruct cellular microenvironments *in vitro*.

Hierarchical membranes were obtained by self-assembly between hyaluronan (HA) and a positively charged peptide integrating biochemical signals (RGDS) to permit cell adhesion and spreading. HA was chosen due to its remarkable physicochemical properties (high molecular weight and density of negative charges, inherent biodegradability and biocompatibility), associated with its complex interactions with ECM components and cells. In the presence of hyaluronidase at physiological concentration, the membranes slowly degraded overtime. Membranes presenting the cell adhesive ligand RGDS were shown to increase efficiently the attachment of fibroblasts in serum-free conditions. Although this represents a simplified approach to deconstruct the ECM microenvironment, the capability to incorporate biochemical signals into 2D self-assembled membranes enables the study of cellular responses to physiologically relevant signal variations and to identify the effect of individual components over cell behavior.

The remodeling process of the natural ECM, in which the macromolecular components of the ECM are degraded by cell-secreted proteases (metalloproteinases, MMPs), occurs simultaneously with cell invasion. The recreation of these features in the previously developed self-assembled membranes would represent a valuable strategy as ECM mimetics. Thus, an enzymatic cleavable site (GPQGIWGQ, octapeptide) sensitive to matrix metalloproteinase-1 (MMP-1) was incorporated into the peptide sequence. Self-assembled membranes were shown to be responsive to enzymes activities, in particular to hyaluronidase and MMP-1. This design enabled to modulate the degradation rate of the membranes. Fibroblasts cultured on the MMP-sensitive membranes were shown to produce higher amounts of MMP-1 and lower deposition of collagen. We expect that by including components sensitive to enzymatic activities in the membrane formulation, their degradation behavior may resemble the process of ECM remodeling, leading to increased cellular infiltration and ultimately more robust healing *in vivo*. Nevertheless, *in vivo* experiments will still be required to verify that the expected remodeling of the ECM actually takes place.

The ECM of each tissue provides cells with not only biochemical (adhesion sites, growth factors) but also physical (elasticity, topography) signals that influence many cell functions, such as proliferation, migration and differentiation. Nanotopography, resulting from the organization of the ECM macromolecules, is essential for the integrity and mechanical behavior of tissues, as well as to guide cellular growth and orientation. In this thesis, the fabrication of micro-grooved membranes, which are spontaneously formed by self-assembly, was reported. The micro-patterns were obtained when a positively charged PA, containing an octapeptide domain of alternating hydrophilic and hydrophobic residues, was combined with HA at the air-liquid interface.

Fibroblasts were shown to sense the membrane topography, by adjusting their morphology and alignment, according with the surface where cells were cultured. Membranes with very distinct surface topographies, from well-defined micro-grooves to micro-sized aggregates, were obtained by simply manipulating the PA amino acid composition. Although further knowledge is needed to understand this process, this represents a promising strategy to create customized patterned biomaterials with minimal steps.

Soft peptide based microcapsules were developed, combining electrostatic self-assembly of PAs of opposite charge with microfluidics. The resulting capsules exhibited a core shell structure made of a nanofibrillar network, resembling the architecture of the native ECM. The properties of the microcapsules (nanofibrillar density, permeability, stiffness) were controlled by changing the peptide

concentration. Microcapsules were shown to support the growth and proliferation of encapsulated fibroblasts in mono-culture and also to support the co-culture of two cell types (fibroblasts and keratinocytes) within and on their surface. The versatility of the selected building blocks to present bioactive ligands provides the opportunity to mimic other functionalities of the natural ECM, which can find numerous applications in cell biology and regenerative medicine.

The work presented in this thesis has contributed to expand the use of peptide amphiphiles and self-assembly approaches to engineer biomaterials with both biophysical and biochemical cues. These biomaterials proved to be useful for culturing cells and modulating different aspects of cell behavior (adhesion, morphology, spreading, growth and matrix deposition). By integrating specific functionalities during peptide design, biomaterials with precise chemistry and complex structure can be obtained simply by self-assembly. This represents an huge advantage for biomaterials fabrication when compared with alternative techniques that require complex equipment and additional chemical reactions. Further development and understanding of these self-assembling systems, as well as *in vivo* experiments will still be required to fully explore their potential.

Sebastião Salgado – *Genesis*

Fim – o que resta é sempre o princípio feliz de alguma coisa.

Agustina Bessa-Luís